A computational study on the molecular recognition in water using endo-functionalized molecular tubes and uses of these receptors as drug delivery vehicles

A thesis submitted

in partial fulfillment of the requirements

for the degree of

DOCTOR OF PHILOSOPHY

by

Rabindranath Paul

to the

Department of Chemistry

Indian Institute of Technology Guwahati, India

2021

Dedicated to
my beloved parents and family members

Declaration

I hereby declare that the matter manifested in this thesis entitled "*A computational study on the molecular recognition in water using endo-functionalized molecular tubes and uses of these receptors as drug delivery vehicles*" is the result of research carried out by me in the Department of Chemistry, Indian Institute of Technology Guwahati, India under the supervision of Prof. Sandip Paul.

In keeping with the general practice of reporting scientific observations, due acknowledgement has been made wherever the work described is based on the findings of other investigators.

Rabindranath Paul
IIT Guwahati

Certificate

It is certified that the work contained in this thesis entitled, "*A computational study on the molecular recognition in water using endo-functionalized molecular tubes and uses of these receptors as drug delivery vehicles*" has been carried out by Mr. Rabindranath Paul for the degree of Doctor of Philosophy under my supervision and the same has not been submitted elsewhere for a degree.

Prof. Sandip Paul
Thesis Supervisor
Department of Chemistry
Indian Institute of Technology Guwahati
Guwahati-781039, India

Preface

On accomplishing of my doctorate studies, it is a true-hearted pleasure to express my gratitude to the people who made this journey an ineffaceable and wonderful experience for me. First and foremost, I would like to express my deep gratitude to my supervisor, Prof. Sandip Paul, for his lucid and excellent guidance. I have been extremely lucky to have a supervisor who kept his door always open for the myriad discussion sessions. He provided me with continuous support, constant encouragement, and instructive advice, which taught me how the science and its challenges could be more fascinating to ease a solution. I am thankful to him for giving me the freedom to pursue my ideas and respond to my questions and queries so promptly during the whole Ph.D. process.

Besides my supervisor, I am highly obliged to the doctoral committee members, Prof. Gopal Das, Prof. Aditya Narayan Panda, and Dr. Shankar Prasad Kanaujia, for periodically assessing my work and providing valuable suggestions for its improvement. My sincere thanks go to all other faculty members in the chemistry department for their kind help at various stages of my doctoral work. I gratefully acknowledge the Ministry of Human Resource and Development (MHRD), India, for financial support and IIT Guwahati for providing the research facilities to carry out my research work. I would like to appreciate the IIT Guwahati super-computing facility PARAM-ISHAN, without which the completion of my dissertation was not possible within this time period.

Here, I want to thank my lab mates Rituparna, Aritra, Madhusmita, Rimjhim, Sanjib, Monoj, and Mira for their support, efficient discussions, and building a pleasant working ambiance in the lab. A heartfelt thank to my seniors Dr. Rahul Sarma, Dr. Subrata Paul, Dr. Bhanita Sharma, Dr. Gargi Borgohain, Dr. Shubhadip Das, Dr. Srijita Paul, Dr. Saikat Pal, and Dr. Krishna Gopal Chattaraj for sharing their valuable suggestions and experiences during my Ph.D. days. Also, I would like to acknowledge the project students Dipisha, Siddhartha, and Triasha, whose contributions should be mentioned.

I extend my sincere gratitude and respect to all my teachers in school, college, and university days to make me academically and non-academically capable in various aspects of life. All the learning from the days will be an asset in every walk of my life.

I take this opportunity to thank my friends for their love and helping hand throughout my journey. I am also grateful to my friends Shyam, Somnath, Partha, and Monoj for their assistance, encouragement and for listening to me at every moment to lend their support. I owe a lot to my IITG friends for making my Ph.D. journey joyful and memorable.

Last but not the least, this dream could not have been fulfilled without the love, support, and blessings from my family members. I extend my sincere gratitude to my father and mother for always being the best guide and philosopher. They are the biggest of all the blessings in my life. My words will be insufficient to pen their unconditional support and auspicious encouragement. I am blessed to have my sisters and brothers as one of the best supporters of my life. I am truly grateful to Joyshree for being my inspiration and strength. Her constant support, encouragement, and academic assistance enrich me a lot to achieve this goal. I am genuinely obliged to my brother Dr. Amal Kumar Saha, for the constant motivation and for helping me to be a better human being.

Rabindranath Paul

2021

"Science is not only a disciple of reason but, also, one of romance and passion."

— Stephen Hawking

Outline of the thesis

Chapter 1

Introduction

"Research is what I'm doing when I don't know what I'm doing."

– Wernher von Braun

■ SUPRAMOLECULAR CHEMISTRY

Supramolecular chemistry is the study of noncovalent binding interactions that lead to assemblies between molecules and/or ions. It covers the chemical, physical and biological characteristics of substances, which are strongly interdisciplinary. Thus, research begins in organic chemistry to synthesize molecules, moves to coordination and physical chemistry to investigate noncovalent interactions, eventually, biochemistry to analyze the binding characteristics of substrates or materials to suggest novel uses. Supramolecular chemistry is a perfect stimulus for chemists who are keen to gather information and expertise in various fields of study [1].

In 1894, Emil Fischer developed the fundamental principles in the field of supramolecular chemistry. He studied the fermentation mechanism of many sugars with yeasts with Hans Thierfelder and discovered that several sugar molecules were fermented while some were not. To promote fermentation, they proposed that the active site of the yeast cell must have a structure that is analogous to the geometrical shape of the sugar molecule [2]. Fischer conducted additional research using enzymes that cleave glycosides (invertase and beta-glucosidase) and discovered that the previous theory was right. As a result, he came up with his famous remark, *"...the enzyme and glycoside have to fit like a lock and key to initiate a chemical reaction"* [3]. This lock and key concept in supramolecular chemistry is schematically presented in Figure 1-1. Though Johannes D. van der Waals postulated intermolecular forces only in 1873 [4], improved knowledge of noncovalent interactions was not developed until the early twentieth century to provide chemists a more comprehensive analysis of molecules. This also articulates the deoxyribonucleic acid (DNA) structure by James D. Watson and Francis H. C. Crick in 1953. They proposed a two-stranded double-helical conformation bound by intermolecular interactions [5]. The seminal work of Charles J. Pedersen [6, 7], Jean-Marie Lehn [8], and Donald J. Cram [9, 10] on noncovalent interactions in synthetic host-guest systems in the late 1960s marked a watershed moment in supramolecular chemistry. These three chemists were awarded the Nobel Prize in Chemistry in 1987, which significantly boosted the supramolecular chemistry field. Jean-Marie Lehn described supramolecular chemistry as *"...chemistry of molecular assemblies and of the intermolecular bond"* or *"the chemistry beyond the molecule"* [1].

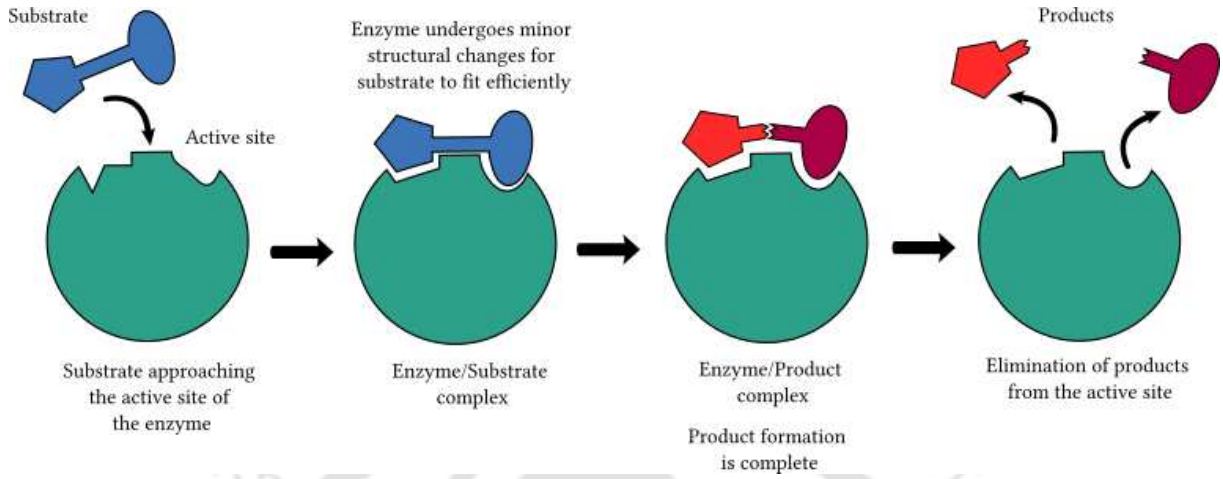

Figure 1-1. *Lock and key concept in supramolecular chemistry is schematically presented here.*

Supramolecular Chemistry in Nature: Enzyme enantioselectivity is attributed to the enzymes' chiral structure, reflecting the three-dimensional folding in the polypeptide backbone and alignment of the amino acid side chains in the folded molecule, which is a property in enzymes to identify and metabolize only one of two enantiomers of chiral molecules. The arrangement of the enzyme structure can be classified into primary, secondary, tertiary, and quaternary classes [11]. Tertiary and quaternary enzyme architectures are responsible for the arrangement of binding sites; they form the most stable part of the configuration of the enzyme, enabling the binding site to deform as a result of guest binding. The supramolecular interactions of enzymes with coenzymes, substrates, and inhibitors necessarily accompany substantial dehydration and conformational change of both the enzymes and ligands [11]. Antibody-antigen-specific supramolecular interactions are also allowed by weak cooperative interactions. The antibody, made up of similar components (amino acids), acts as an enzyme when interacted with its particular antigen. Hence, in an aqueous medium, antigen binding to the curved hydrophobic pocket of antibody causes significant structural changes, as well as extensive dehydration of both components around the receptor site. The most sophisticated supramolecular structures that perform critical, important roles in living organisms are DNA, ribonucleic acid (RNA), and polynucleotides [12]. DNA performs many roles, including genetic information transfer, transcription, and replication, as well as protein synthesis, all of these properties rely on the equilibrium of single and double-stranded DNA. Although the hydrophilic phosphates, the carbonyl, and the amino

groups of nucleic acid bases are exposed to aqueous solvent and thus, highly hydrated, the hydrophobic domains of nucleic acid bases in single-stranded DNA, on the other hand, are known to associate together in aqueous solutions. Consequently, DNA duplex formation eventually involves the initial separation of single-strand aggregation and a bimolecular interaction, which unquestionably lead to dramatic changes in formulation and substantial dehydration [12]. Artificial enzymes, enzyme mimics, and protein-protein interactions, all inspired by nature, are the newest challenge in supramolecular chemistry.

Molecular Recognition and Host-Guest Chemistry: The selection of a substrate (or substrates) by a particular receptor (or host) molecule through the development of noncovalent interactions between them is characterized as molecular recognition, and it lies at the heart of all aspects of supramolecular chemistry [1]. The receptor molecule is a molecular entity with convergent binding sites at crucial locations throughout its structure, each of which has a well-defined size and shape. Charge, polarity, polarisability, size, shape, quantity, and placement of the electronic properties in the receptor architecture are all characteristics of binding sites. The substrate (or guest) might be considered as a species (cationic, anionic, or neutral), complementarily to the receptor molecule with different binding sites. They combine to produce a supermolecule, which has its own thermodynamic and structural characteristics [1]. It is important to note, however, that binding is not the same as recognition. Molecular recognition necessitates a high degree of geometrical and interactional complementarity between the receptor and the substrate, allowing the latter to be chosen even in the presence of additional competitors, such as the solvent. Several factors must be considered to accomplish selective binding between receptor and substrate: (a) steric complementarity – receptor and substrate must be the same size and shape; (b) interactional complementarity – the presence of complementary binding sites in the correct configuration on the receptor and substrate, such as positive/negative charge, charge/dipole, dipole/dipole, hydrogen bond donor/acceptor, etc.; (c) multiple interaction sites – the weak nature of noncovalent interactions necessitates the use of several interaction sites; (d) the medium – due to its interactions with both binding partners and the supermolecule itself, the solvent in which the recognition takes place plays a critical role.

Preorganization and Macrocyclic Effects: Almost all supramolecular host-guest complexes are much more stable than would otherwise be assumed based on cooperative/chelate effects. In these species, the receptors are typically macrocyclic (large ring) ligands that

chelate their guests through various binding sites. These compounds are indeed stabilized by what is known as the *macrocyclic effect* [13]. One such aspect relates to both the chelation of the guest by multiple binding sites and the spatial arrangement of those binding sites leading up to guest binding (*i.e., preorganization*). During the reorganization of macrocyclic host and guest molecules' binding sites, the entropic and enthalpic penalty are involved due to unfavorable repulsion and desolvation effects. This energy penalty is paid in advance during the macrocycle synthesis procedure. As a result, macrocycles are more difficult to synthesize but more effective complexing agents than similar nonmacrocyclic hosts (podands). Cabbiness and Margerum discovered the macrocyclic effect in 1969 [14]. Macrocyclic stabilization due to preorganization contributes both enthalpically and entropically. The enthalpic contribution arises due to the macrocyclic hosts are often less well solvated than their acyclic counterparts. This may be because they have less amount of solvent-accessible surface area. Thus, unlike the extended acyclic counterpart, there are fewer solvent-ligand bonds to break. Macrocycles are less conformationally flexible, resulting in fewer degrees of freedom lost during complexation. Thus, entropic contribution loss are less for macrocycles compared to their acyclic counterparts. The relative relevance of the entropic and enthalpic components varies depending on the system being examined, though enthalpy is typically dominating. The receptor molecule is preorganized if it does not experience a major conformational change upon guest interaction. The idea of host preorganization is important because it represents a significant (and in some circumstances decisive) increase in the overall free energy of host-guest complexation. Without considering the effects of solvation, the host-guest binding process may be separated into two steps. The activation step begins with the host undergoing conformational realignment; its binding sites must complement to the guest while also minimizing unfavorable interactions between binding sites. This is inefficient in terms of energy, and because the host must maintain this binding posture throughout the complexes' lifespan, this energy is never repaid. Binding occurs in the second stage, which is advantageous energetically due to the enthalpically stabilizing attraction between mutually compatible binding sites of the host and guest molecule. The difference between the unfavorable reorganization energy and the favorable binding energy is the total free energy of complexation. The overall free energy is diminished when the reorganization energy is high, destabilizing the complex. This rearrangement energy is low if the host is preorganized [15].

Interactions Playing Role in Supramolecular Chemistry: The construction of non-

covalent interaction between the receptor and the substrate is required to develop of supramolecular complexes. Some of the important noncovalent interaction in supramolecular chemistry are [16, 17]: electrostatic, van der Waals (vdW), hydrogen bond, solvophobic/hydrophobic, $\pi\cdots\pi$, cation$\cdots\pi$, anion$\cdots\pi$, C–H$\cdots\pi$, N–H$\cdots\pi$, S$\cdots\pi$, ion-ion, ion-dipole, and dipole-dipole interactions. These interactions are schematically presented in Figure 1-2. Noncovalent interactions are far weaker than covalent interactions. Thus, numerous different interactions must work together to produce durable supramolecular complexes. Designing effective molecular recognition systems requires finding the right combinations of molecular interactions.

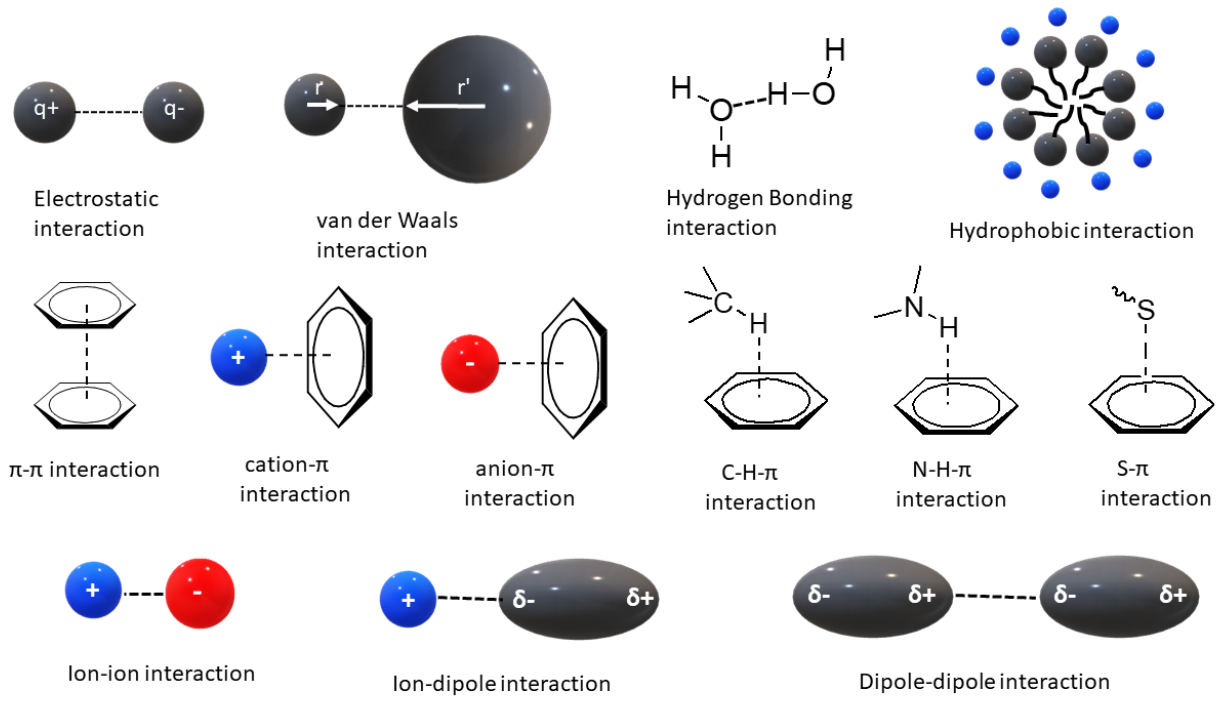

Figure 1-2. *Different types of interactions that have a significant role in supramolecular chemistry are schematically represented here.*

The Role of Solvent Molecules in Supramolecular Chemistry: Complementarity and preorganization characteristics itself are inadequate to capture the complexities of host-guest interactions. The lock and key approach is more simplified, which characterizes the interaction of two individuals based purely on enthalpic binding, without regard to the solvents' almost all function [18]. The solvent itself can interact with both the receptor

and the substrate in several noncovalent manners. Consequently, the solvent is in a significantly larger amount than both the host and the guest at diluted circumstances when binding procedures generally occur. The number and placement of solvent molecules, or the degree of solvation, as well as the intensity of host-solvent and guest-solvent interactions, all have a significant impact on the dynamics and energetics of the association process and are greatly influenced by the kind of solvent molecule used. Polar solvents may form strong connections with host and guest molecules (ion-dipole, dipole-dipole, and hydrogen bonding interaction), making it more difficult for charged species to bind by increasing the amount of energy required to break host-solvent and guest-solvent interactions. Host-guest interaction in the presence of solvent molecules is schematically presented in Figure 1-3.

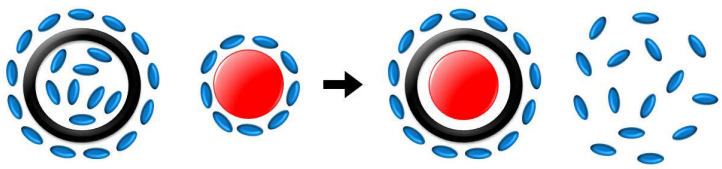

Figure 1-3. *The association process of host and guest molecules in water medium is schematically presented here. The receptor is shown by the black circle, the red circle represents the substrate, and the solvent molecules are represented by the blue ellipsoids.*

Host and guest molecules are surrounded by solvent molecules and interacted with them in a solution. Maximum of these interactions must be disrupted and new ones generated between the host and the guest throughout the association process. Enthalpic energy must be consumed to break the host-solvent and guest-solvent contacts, but the enthalpic gain will arise from the newly created host-guest contacts. The importance of complementarity and preorganization in extending the enthalpic contribution cannot be overstated. The removal of solvent molecules from the host and guest, on the other hand, releases them into the bulk region, where they have more degree of freedom, raising entropy while also raising the enthalpic term due to increased solvent-solvent interactions. Moreover, host-guest binding is accompanied by binding partner conformational constraints, which leads to entropy loss. The affinity of a host molecule for a guest molecule in a particular solvent is determined by the ultimate balancing of all these potential enthalpic and entropic losses, gains, and compensations.

■ SUPRAMOLECULAR RECEPTOR MOLECULES

A host molecule provides a cavity to encapsulate a guest molecule through noncovalent interactions in a typical host-guest inclusion complex. Host molecules are organic structures linked together by covalent bonds that can bind ionic or neutral substrates through a series of intermolecular interactions, resulting in a supermolecule composed of two or more species [1]. The characteristics listed above must be considered in the receptor design in order to obtain high affinity and recognition. A well-defined three-dimensional architecture demands the proper arrangement of binding sites that may include their guests to produce many noncovalent binding interactions. As a result, molecules with cavities, clefts, or pockets into which the substrate can fit are useful. The interior of these cavities, clefts, or pockets should be decorated with multiple binding sites. Structures that are macrocyclic or macropolycyclic are particularly well suited for this. These compounds have cavities that can be tailored to the right size and shape, allowing for the strategic spatial arrangement of the binding sites. In addition, an appropriate choice of building composites that make up the receptor molecule can help to balance rigidity and flexibility and is of particular importance to the binding and dynamic properties of the setup. The brilliance of the supramolecular chemists has envisioned molecular receptors that range from acyclic to macropolycyclic compounds, of significantly different structural kinds. From the earlier synthetic macrocycles crown ethers [19,20] to cyclodextrins [21–23], calixarenes [24,25], and cucurbiturils [26], the elevation of every new macrocyclic receptor impulse onward the uplift of supramolecular chemistry. The supramolecular host-guest complexation is an immensely obligated process in chemistry. A large class of synthetic macrocyclic arene receptors, namely, calixarenes [27], resorcinarenes [28], cyclotriveratrylenes [29], pillararenes [30,31], or modified receptors thereof blending pyrrole [32], pyridine [33], and imidazolium heterocycles [34] in place of phenyl moieties in their structures have been modified and distinguished by using X-ray diffraction and other spectroscopic methods. At present, naphthalene flourished molecular receptors possessing identical structural properties such as water-soluble cyclic tetramer cyclotetrachromotropylene (CTCT) in which methylene bridges connects the four naphthyl units have been synthesized [35–37]. These macrocyclic receptors are short methylene bridged, and the use of these receptors has been restricted due to steric hindrance from the two naphthalene rings and their harsh cavities. As a result, they have very weak complexation capabilities. The scope of binding capabilities of such receptors can be enhanced by introducing larger bridging functional groups in their architectures. Jiang et al. [38]

synthesized a naphthol-based host wherein a couple of progressive imine-flourished isomers are interconnected via covalent bonds. In light of this, recently manifested oxatub[4]arene receptor has conformational isomers, which put an exclusive partiality for specific guest binding [39, 40].

Supramolecular Receptors as Drug Delivery Vehicles: Supramolecular chemists have developed and found various artificial receptors, such as calixarenes, cyclodextrins, cucurbit[n]urils, and their acyclic compounds, pliiar[n]arenes, deep cavitands, and molecular tweezers and found the permeation and interaction properties with model membranes [41–50]. These receptors can act as drug delivery system and deliver drugs or many other important components through lipid bilayers by encapsulating these molecules into their cavities [50, 51]. Nanocarriers can alter the physicochemical characteristics of the integrated molecules; they influence the cytotoxic effect of inserted drugs and can resolve physiological barriers of the integrated molecules. Therefore, nanovesicles are now utilized to improve drug efficacy, reduce serious complications, and shield drugs from chemical modification, undermining the efficacy or result of producing harmful secondary compounds [52].

Endo-Functionslized Molecular Tubes as Artificial Receptors and Drug Delivery Vehicles: It may be simple to decorate a functional group at the cavitys' rim, but positioning the functional group within a deep, well-defined cavity is difficult. Glass and coworkers [53–55] reported a pair of molecular tubes (the acid form of molecular tubes 1a and 1b) with bisnaphthalene cleft [56–58] architecture. When both the bisnaphthalene clefts are in parallel orientations (syn), it is labeled as host-1a, and when they are in antiparallel orientations (anti), it is referred to as host-1b. Host-1a and host-1b are presented in Figure 1-4. A deep look into the host-1a and host-1b revealed that the amide 'N-H' bonds are directed towards the cavity. For this reason, they are referred to as endo-functionalized molecular tubes. During macrocyclization, the inward-directed amide groups and the deep cavity were built concurrently by amide bond formation. The cavity shape of the macrocycles that arise is comparable to that of bioreceptors. Furthermore, to strengthen the hydrophobic action, the amide protons were substituted with allyl groups later [54]. These molecular tubes were used to recognize lipid molecules in water through hydrophobic effects [53, 54]. The binding pockets of host-1a and host-1b are neutral since the charged carboxylate groups only provide water solubility. Further, Jiang. et al. synthesized similar types of macrocyclic receptors with different types of functional groups in their architecture. These functional groups are ester, amine, urea, thiourea, imine, ether, and amide [38, 59].

These types of receptor molecules are formed from naphthols and have a tubular cavity. Thus these are also called naphthotubes [60].

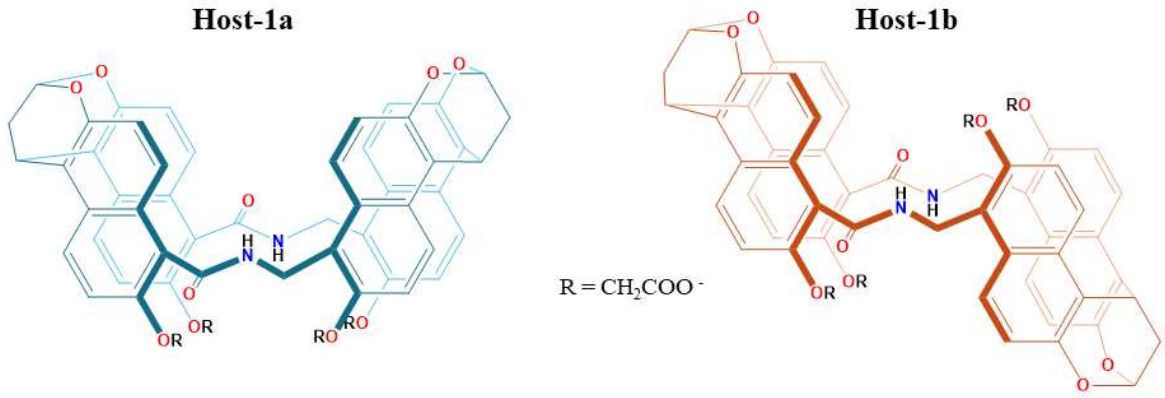

Figure 1-4. *Chemdraw representation of the chemical structure of both the receptors, host-1a and host-1b.*

Throughout my doctoral thesis, my focus will be on the molecular recognition of these two receptors (host-1a and host-1b) and the uses of these two receptors as drug delivery vehicles following the drug delivery property of some other previously synthesized receptor molecules [41–50].

■ METHODOLOGY

Despite the theoretical basis for computing the time evolution of a molecular system using a complete quantum mechanical approach exists, the computational cost for any system size of biological relevance is immense. As a result, classical molecular dynamics (MD) simulation techniques have been devised, which ignore electronic motion and may be used to analyze systems with up to a million atoms on the nanosecond (ns) to millisecond (ms) timescales [61]. In MD approaches one choses to model the Born-Oppenheimer potential in terms of classical forces. The classical MD simulation technique has been used to perform this thesis work. This MD method is extensively used to study the structure and dynamics of biomolecular systems, including proteins, nucleic acids, and small molecules like amino acids, carbohydrates, and pharmaceutical drug molecules.

MD approaches are also known as force field methodologies because they use a mathematical function, or force field, comprising several components representing bonded and nonbonded interactions between the atoms to characterize the potential energy function

(U) of a system. The force field formulation governs how particles interact with one another [62]. There are several MD packages available, each with somewhat different force fields. The molecular dynamics force fields from Assisted Model Building with Energy Refinement (AMBER) were employed entirely in this thesis, and the functional form of these force fields will be presented [63]. In such a formulation, atoms are generally portrayed as hard and charged spheres in the presence of point charges centered on them. Types of atomic interactions acted between atoms are schematically presented in Figure 1-5. In this figure, the top three (bond, angle, and torsion/dihedral) are the bonded, which describe the bond stretching, angle bending, torsion rotation, and the bottom two (electrostatic/Coulomb and van der Waals) are the nonbonded interaction.

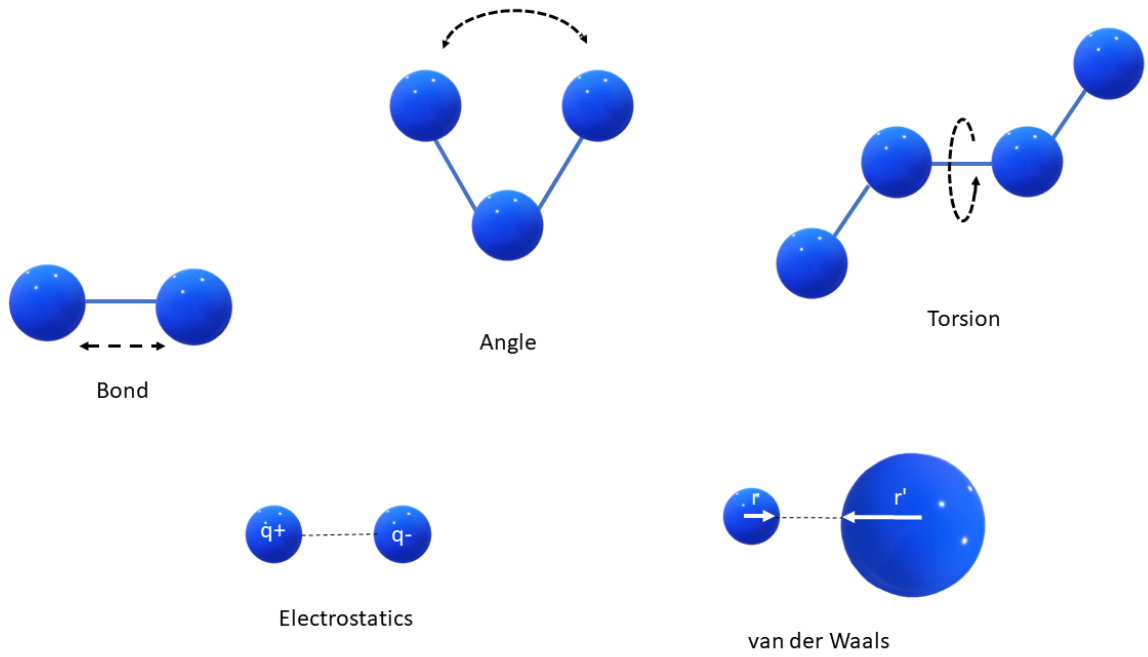

Figure 1-5. *Different types of atomic interactions acted between atoms in a system. The top three are the bonded, and the bottom two are the nonbonded interaction.*

This potential energy function for the AMBER set of force fields is represented as a sum of bonded and nonbonded components, as [64]:

$$U = U_{bond} + U_{angle} + U_{dihedral} + U_{vdW} + U_{Coulomb} \tag{1.1}$$

In bonded terms (U_{bond}, U_{angle}, and $U_{dihedral}$), potentials terms described the bond and angle contributions, and these interactions are between immediately connected atoms (1-2

interactions), angles (1-3 interactions, where two atoms bonded to a common atom), and torsion (interactions between pairs of 1-4 atoms) are mathematically described as:

$$U_{bond} = \sum_{bonds} K_b(b_{ac} - b_{eq})^2 \tag{1.2}$$

$$U_{angle} = \sum_{angles} K_\theta(\theta_{ac} - \theta_{eq})^2 \tag{1.3}$$

$$U_{dihedral} = \sum_{dihedrals} \frac{V_n}{2}(1 + cos(n\phi - \delta)) \tag{1.4}$$

The symbols b, θ, ϕ, and δ represents the bond length, bond angle, dihedral angle, and phase angle. The phase angle is the phase difference or phase shift as it is also called of a Sinusoidal Waveform is the angle δ, in degrees or radians that the waveform has shifted from a certain reference point along the horizontal zero axis. The subscripts ac and eq are for actual and equilibrium, respectively. The variables K_b, K_θ, and V_n are the force constants for bond, bond angle, and dihedral angle, respectively. Periodicity is represented by n. The nonbonded potentials are computed using two terms, the Lennard-Jones term (U_{vdW}) [65] for the van der Waals interaction [4] and the Coulomb term ($U_{coulomb}$) [66] for the electrostatic interactions between particles' partial charges. These nonbonding interaction terms are mathematically described as:

$$U_{vdW} = \sum_i \sum_{i<j} 4\epsilon_{ij}\left[\left(\frac{\sigma_{ij}}{r_{ij}}\right)^{12} - \left(\frac{\sigma_{ij}}{r_{ij}}\right)^{6}\right] \tag{1.5}$$

$$U_{coulomb} = \sum_i \sum_{i<j} [\frac{q_i q_j}{4\pi\epsilon_o r_{ij}}] \tag{1.6}$$

where the total value is calculated across all atom pairs i and j. Lennard-Jones parameters σ and ϵ are the diameter of atomic sites and well depth energy, respectively. r_{ij} is the inter-atomic separation. q_i and q_j are the partial charges on interaction sites i and j, and ϵ_o is the free space permittivity. The bond and angle terms K_b, b_{eq}, K_θ, and θ_{eq} in the AMBER force field are fitted to reproduce experimental normal mode vibrational frequencies, whereas the torsion barrier heights V_n are fitted to quantum mechanical energy profiles for rotation around a given torsion. The atomic partial charges are derived from quantum mechanical calculations of molecular electrostatic potential (MEP) via the restrained electrostatic potential (RESP) charge fitting method [67], and the r_{ij} and ϵ are fitted to reproduce experimental liquid phase properties [68]. The MEP surrounding a molecule is computed at a suitable level of theory using quantum mechanics (QM) to obtain partial charges using the RESP fitting technique; for the AMBER force field, this is often the

HF/6-31+G** level. This level of theory has been found to overestimate molecule polarization, resulting in charges in the gas phase that is close to charges in the solution phase. The MEP is sampled at many locations around the molecule, and partial charges are fitted to match the MEP produced from QM. Used least-squares fitting has two steps: partial charges are first fitted to atom centered points with weak hyperbolic restraints on non-hydrogen atoms, and then charges for methyl and methylene carbon and hydrogen atoms are refitted with a higher hyperbolic penalty, the hydrogen atoms in the same methyl or methylene group constrained to have an equivalent charge (as they are rotationally degenerate). All other atoms keep their charges from the first stage of the fit during the second step. This method guarantees that buried atoms are not subjected to an excessively high partial charge [63].

The force field determines bonded and nonbonded interactions between all atoms in the system, with each atom having a radius, mass, partial charge, and vdWs parameters. As a result, MD may be used to determine the energy state of a group of atoms or molecules. The system coordinates can be changed until a minimum is attained on the potential energy surface because the first energy derivative is zero regarding all the coordinates and the second energy derivatives are all positive. To prepare a system for future simulation, the steepest descent and conjugate gradient energy minimization methods are widely utilized. The steepest descent method descends in the opposite direction of the gradient until it reaches a minimum. After then, the minimum is utilized as a starting point for the following stage. The steepest descent approach, on the other hand, exhibits oscillating behavior in tiny valleys. Thus, the conjugate gradient approach is typically employed for the latter stages of energy minimization, as it uses the current gradient and previous search direction to predict the next line search direction, resulting in higher performance when the search direction is close to the minimum.

MD simulation provides the time evolution of atomic coordinates. The following Hamiltonian characterizes one N-particle system as:

$$H = \sum_{i=1}^{N} \frac{p_i^2}{2m} + U(\mathbf{r}^N) \tag{1.7}$$

where m, p_i, and $U(\mathbf{r}^N)$ represent the mass of each particle, the momentum of the i-th particle, and the total potential energy of the system, which includes all particle-particle interactions. The coordinates of the atoms are defined by $\mathbf{r}^N = \{\mathbf{r}_1, \cdots, \mathbf{r}_N\}$. $\mathbf{r}_i$ and $\mathbf{v}_i$ are the position and velocity of the i-th atom, respectively. The molecular dynamics approach

entails solving the equation:

$$a_i = \frac{\mathbf{F_i}}{m_i} \tag{1.8}$$

where $i = 1, 2, ...N$, m_i is the mass of i-th particle and $\mathbf{F}_i$ is the force acting on particle i. This equation can be obtained easily from the Lagrangian:

$$L = \frac{1}{2}\sum_{i=1}^{N} m_i \mathbf{v_i}.\mathbf{v_i} - \frac{1}{2}\sum_{i=1}^{N}\sum_{j\neq i}^{N} u(r_{ij}) \tag{1.9}$$

where the sum of pair potentials u_{ij} is the potential U. The Lagrangian equation of motion is ascribed as:

$$\frac{d}{dt}(\frac{\partial L}{\partial \dot{q}_i}) - \frac{\partial L}{\partial \dot{q}_i} = 0 \tag{1.10}$$

Eq. 1.10 indicates that the dynamics of particles are described by a 3N number of second-order differential equations. The Hamiltonian (H) for the system may also be written down, and the Hamiltonian equations of motion may be solved, as:

$$\dot{\mathbf{q}}_k = \frac{\partial H}{\partial p_k} \tag{1.11}$$

$$\dot{\mathbf{p}}_k = -\frac{\partial H}{\partial q_k} \tag{1.12}$$

where generalized coordinates and momenta are represented by $\mathbf{q}_k$ and $\mathbf{p}_k$, respectively. The Hamiltonian is for a system with pair-wise interaction potential is:

$$H = \frac{1}{2}\sum_{i=1}^{N} m_i \mathbf{v_i}.\mathbf{v_i} + \frac{1}{2}\sum_{i=1}^{N}\sum_{j\neq i}^{N} u(r_{ij}) \tag{1.13}$$

and Eqs. 1.11 and 1.12 yield

$$\frac{dr_i}{dt} = \frac{\mathbf{p_i}}{m_i} \tag{1.14}$$

$$-\dot{\mathbf{p}}_i = -\nabla \mathbf{u} = \mathbf{F_i} \tag{1.15}$$

where i=1,2,....N. Now, it has $6N$ first-order differential equations to be solved. Particle velocities and positions as a function of time are obtained by numerically solving the equation of motion. The finite difference method is generally used to integrate it. One of the most often used algorithms for this purpose is the Verlet algorithm [69]. The usage of the Verlet method has the benefit of being simple to implement and has low storage needs. However, it has the disadvantage of modest precision during computation, and velocity does not appear directly in the Verlet integration. The leap-frog algorithm [70] was created as an upgrade to the Verlet algorithm. However, the positions and velocities are not synchronized, which is a disadvantage of the leap-frog algorithm. The Velocity Verlet method

has been designed as an alternative to Verlet or the leap-frog method, and the following equations are utilized to compute new position and velocity at the same time:

$$r(t+dt) = r(t) + v(t)dt + \frac{1}{2}a(t)dt^2 \tag{1.16}$$

$$v(t+dt) = v(t) + \frac{1}{2}[a(t) + a(t+dt)]dt \tag{1.17}$$

This approach needs acceleration at time t and $t+dt$ to determine velocities at time $t+dt$. We used the Velocity Verlet algorithm in this thesis work. The time step dt defines the time between MD steps; normally, this quantity is such determined that the maximum frequency vibration in the system is at least ten times higher than dt to ensure that atoms are not unduly closer to each step since this might lead to instabilities in the system. As the number of steps performed multiplied by the time step determines the length of time of a simulation, a time step that is too short will restrict the amount of phase space that may be sampled in any particular simulation. A compromise must thus be reached, and simulations using AMBER usually utilize a time step of 2 femtosecond (fs). Even though the highest frequency motion in a system is on the order of 10 fs (bond stretching involving hydrogen atoms) technically limits the integration time step to 1 fs, limitations imposed by these motions, such as the SHAKE algorithm [71], allow for a larger time step.

Constraint on every hydrogen-containing covalent bond is ensured by applying the SHAKE algorithm [71]. Lagrange multipliers, which are obtained by estimating the solution of a linear system of constraint equations, are the indeterminate forces needed to fulfill position constraints. This technique is performed repeatedly with each MD step until all requirements are met to a set tolerance (the AMBER default is 1×10^{-5}). Following that, the constraint contribution to the virial is added.

MD simulations of physiologically relevant systems need solvation, which may be accomplished either implicitly or explicitly by adding water to the system. All simulations in this thesis employed explicit solvation by using the three-point transferable interaction potential (TIP3P) waters [72], a common water model for MD simulations that have been parameterized to replicate experimental water parameters such as dipole moment, self-diffusion, density, and expansion coefficient. A single oxygen atom is connected to two hydrogen atoms in the TIP3P water model, which is a three-point rigid water model. A hydrogen-hydrogen connection is also formed between the hydrogens. Each of the three atoms has a partial charge, but only the oxygen atom possesses Lennard-Jones (L-J) pa-

rameters and a vdW radius that also covers the hydrogens. Because of its stiffness, the TIP3P model may be employed with constraint approaches like the SHAKE algorithm.

A method known as periodic boundary conditions is frequently used to reduce the number of explicit waters necessary and avoid discontinuities at the simulation box boundary. This method can also be used to simulate a systems' bulk phase. The system is contained within a three-dimensional periodic box, whose pictures are infinitely reproduced in all directions. When a molecule passes through one side of the box, it is mapped to the opposing side. This approach restricts that the box size must be bigger than twice the nonbonded cut-off value to avoid atoms interacting with their own images.

The assessment of the nonbonded interactions, which determines the electrostatic and vdWs forces and scales as N^2, where N is the number of particles in the system, is the most time-intensive step in assessing the energy of a system using a potential energy function of the force field. Although vdWs interactions quickly fall to zero due to their $1/r^6$ dependence, but electrostatic interactions remain important over longer distances which dropping as 1/r, so a nonbonded cut-off length r_c is typically used to improve computational efficiency, meaning that nonbonded interactions are only calculated for particles with separation distance artifacts. As a result, a range of methodologies is used to recover nonbonded energy and forces that exist beyond the cut-off distance. The particle mesh Ewald (PME) approach [73] is used in several MD codes, including AMBER, to restore the electrostatic interactions lost owing to this truncation. A 'PME grid', which normally has a side of 1 Å, is used to map atomic partial charges beyond the cut-off distance. A Fast Fourier Transform (FFT) of the Poisson equation in reciprocal space is then used to estimate the charge distribution. This approach is computationally efficient and allows for the comprehensive evaluation of electrostatic interaction energy in a system scaled as $N\ln(N)$.

Here, we discussed all the simulation protocols which we used through this thesis work. At first, the PACKMOL [74] program is used to pack the systems' components with a tolerance value of 2.0 Å. The parameters and the starting coordinates of these packed systems are prepared with the LEaP module of AMBER14 [63], and the generated configurations are simulated with the SANDER implementation of AMBER14. A cubic simulation box with periodic boundary conditions (PBC) in all three directions is applied for each of the simulations. Initially, some steps of energy minimization (among which some

initial steps are in steepest descent method and conjugate gradient method for the rest of the steps) are performed for every simulation to eliminate erroneous contacts among the atoms in the systems. All the systems are then subjected to heating in a canonical (NVT) ensemble from 0 K to the desired temperature for some time. Following the heating step, equilibration of every simulation for a sufficient amount of time (at desired temperature and pressure) is attained in an isothermal-isobaric (NPT) ensemble. The temperature and pressure are retained using the Berendsen barostat [75] with 2 ps pressure relaxation time and the Langevin thermostat [76] with 1 ps^{-1} collision frequency, respectively. A sufficient amount of NPT production run is accomplished for every system to ensure convergence. CPPTRAJ program [77] of AMBER14 and Visual Molecular Dynamics (VMD) [78] package are used for analysis and visualization of the obtained simulation trajectories.

The stability of encapsulated guest molecules into the host cavity is quantitatively determined by determining the binding free energy (ΔG^0_{bind}) values. Lately, several methods are available to compute the ΔG^0_{bind} of a system. Some suitable techniques are Molecular-Mechanics-Poisson-Boltzmann (or generalized Born) surface area (MM-PBSA or MM-GBSA) method [79, 80], the linear response approximation (LRA) method [81, 82] (it is a microscopic all-atom method), the linear interaction energy (LIE) method [83, 84], and the double-coupling method [85]. Among all these methods, MM-PBSA/GBSA is the most efficient and widely used one. Molecular Mechanics-Poisson Boltzmann Surface Area (MM-PBSA) [79, 80] procedure was employed for obtaining the binding free energy (ΔG^0_{bind}) of host-guest complexes. Obtained binding free energy values from this technique correlate with the free energy values obtained experimentally. MM-PBSA (and MM-GBSA method) primarily measures the difference in the free energy values between a bound and an unbound state of two solvated molecules or two different solvated states of a single molecule. From this method, ΔG^0_{bind} is evaluated as:

$$\Delta G^0_{bind} = \left\langle G^{HG} \right\rangle - \left\langle G^{H} \right\rangle - \left\langle G^{G} \right\rangle \tag{1.18}$$

HG, H, and G represent host-guest complex, host, and guest molecule, respectively. The bracket signifies ensemble averages over all the trajectories. Components of ΔG^0_{bind} are estimated as follows:

$$\Delta G^0_{bind} = \Delta E_{vac} + \Delta G_{solv} - T\Delta S \tag{1.19}$$

Here ΔE_{vac}, ΔG_{solv}, and $T\Delta S$ represent the gas phase host-guest interaction energy, free energy of solvation, and solute entropy variation during complexation. ΔE_{vac} is computed

as:

$$\Delta E_{vac} = \Delta E_{ele} + \Delta E_{vdw} \tag{1.20}$$

Here electrostatic and van der Waals interaction energies are represented by ΔE_{ele} and ΔE_{vdw}, respectively. Besides, ΔG_{solv} [86, 87] energy term also splits into two, as:

$$\Delta G_{solv} = \Delta G_{PB} + \Delta G_{NP} \tag{1.21}$$

where ΔG_{NP} and ΔG_{PB} represent the nonpolar solvation energy and polar (electrostatic) solvation energy, respectively. The continuum solvent method of the PBSA module of AMBER14 is used to obtain the ΔG_{PB} value. Solvent-accessible surface area (SASA) value is utilized during the computation of the ΔG_{NP} value. SASA value in AMBER14 package is computed with the help of MSMS [88] module and ΔG_{NP} from SASA value as:

$$\Delta G_{NP} = \gamma(SASA) + \beta \tag{1.22}$$

here, $\gamma = 0.005$ kcal/Å^2 and $\beta = 0.0$. NMODE program of AMBER14 package is used to compute TΔS value for all the simulated systems.

Free energy change as a function of reaction coordinate ξ is the potential of mean force (PMF). PMFs of these host-guest complexes were computed by biased umbrella sampling (US) simulation [89] technique. In the current work, Z-direction distance (r) between the center of mass (COM) of the host and COM of the guest molecule [90, 91] is considered as the reaction coordinate (ξ). In the US simulation technique, a biased window potential $w(\xi)$ is employed to improve the sampling in the adjacent window of a selected value of ξ. The various number of biased simulations are undertaken at i = 0, 1, $\cdots$, n (n is a positive number), in which ξ is obstructed to the value of $\xi_i = i \times 0.25$ Å in the phase space configurations X by a harmonic potential defined by:

$$w_i(\xi) = 1/2K(\xi(X) - \xi_i)^2 \tag{1.23}$$

where K is designated as the harmonic restraint force constant. The used restraint force constant is 6 kcal/mol/Å^2 for most of the work. Guest inserted host (i.e., guest molecule initially fixed inside the host cavity) is used as the initial configuration for each US simulation. The host-guest distance is then enhanced by pulling the guest molecule from inside the host cavity (towards Z-direction). The configuration at the last step of the MD production (NPT) stage is considered the starting configuration for each US simulation. The simulation procedure followed for US simulation is identical to the previous NPT run. Each

US simulation window is introduced to some steps of minimization (some initial steps follow the steepest descent method followed by the conjugate gradient minimization for the rest of the steps), followed by sufficient time of equilibration and production run simulation. The unbiased probability distribution P(ξ) of each window position is computed with the Weighted Histogram Analysis Method (WHAM) [92, 93] program. From here, we get the PMF values as,

$$PMF = -k_B T \ln P(\xi) \tag{1.24}$$

where k_B represents the Boltzmann constant, and T represents the absolute temperature of the system.

■ PRESENT WORK

My doctoral dissertation is directed towards the scientists working in supramolecular chemistry and intending to advance their knowledge about artificial receptors, molecular recognition, and uses of these artificial receptors as drug delivery vehicles. The design and synthesis of new molecules with outstanding complexity and versatility is a major accomplishment of modern physical organic chemistry, after which chemists gain more knowledge about natures' working mechanisms. The endo-functionalized molecular tubes or naphthotubes (host-1a and host-1b in Figure 1-4) mentioned in this thesis are an important class of supramolecular receptors for mimicking natural recognition processes due to their willingness to bind small molecules reversibly. These two receptor molecules are exclusively used throughout this thesis. Host-guest coupling investigations indicate the driving factors behind complexation and offer insight into noncovalent interactions between the host and guest moiety. This study also provides interaction between these receptors and different model lipid bilayers to find the possibility of using these receptors as drug delivery vehicles. The expertise accumulated leads to the design of therapeutic functional compounds, such as molecular reactors for catalysis, or the advancement of structure-based drug design and their delivery in medicinal chemistry.

The present chapter (**Chapter 1**) of this thesis includes a review of related experimental and theoretical works in the literature and the basic methodology of MD simulations, MM-PBSA, and umbrella sampling simulation. This chapter introduces the endo-functionalized molecular tubes or naphthotubes (host-1a and host-1b in Figure 1-4) as an important class of supramolecular receptors for mimicking natural recognition processes due to their willingness to bind small molecules reversibly. We have also discussed how these receptors can be used as drug delivery vehicles following the drug delivery property

of some other previously synthesized receptor molecules. **Chapter 2** manifests the fundamental mechanism of the possibility of how these two synthetic macrocyclic receptors can separate the epoxide enantiomers (five pairs of enantiomers) in water. The present study showcases with atomistic details the main stabilizing factors in these recognition processes, structural stability of molecular tubes in water, and how we can use these molecular tubes as a CSP in chiral chromatography. In **Chapter 3**, we have shown the structural aspects and the energetics involved in the chiral separation of two model dipeptides, namely, (d, l)-asparagine and (d, l)-phenylalanine with the help of the two synthetic supramolecular receptors (mentioned above) in solvent water. We have studied the interactions operating in the host-peptide complexes and the associated structural changes to better understand the chiral segregation process. We have also investigated the dynamics and the changes in the water structure for selected host-guest complexes close to the receptor surface. **Chapter 4** deals with the solubility enhancement of sparingly soluble drug molecules (seven class II drug molecules) by these two synthetic macrocyclic host molecules, as enhancement of drug solubilization, is the need of modern time. Biomedical engagements of supramolecular receptors commence with the formation of stable host-drug complexes with the drug molecules. As host-drug complexation enhances drug molecules' water solubility and sustained the release rate and bioavailability of drug molecules. Thus, in the present work, we focus on forming stable host-drug complexes in water medium. **Chapter 5** presents the role of water molecules in the guest binding process of these two small miniature endo-functionalized molecular tubes. We have portrayed this using classical MD simulation and grid inhomogeneous solvation theory (GIST) methodology. Trajectories from MD simulation have been utilized in GIST methodology to estimate different localized thermodynamic parameters at different regions of these receptors. From this work, we get the idea that host-1b is a better complexing agent than host-1a. **Chapter 6** illustrates the complexation of host-1b with different strongly neutral hydrophilic guest molecules in water and the concentration dependency of these complexes. This chapter is divided into two parts, **Part A** and **Part B**. **Part A** describes the encapsulation of four different strongly neutral hydrophilic guest molecules, namely 1,4-dioxane (14D), acetone, DMSO, and DMF, by host-1b in an aqueous solution. **Part B** includes the findings on how this type of complexation ability depends on the concentration of guest molecules? **Chapter 7** elaborates the effect of both the receptors (host-1a and host-1b) on seven different types of model lipid bilayers. Lipid types include six model lipid bilayers (POPC, POPE, DOPC, POPG, DPPE, POPE/POPG) and one realistic membrane (Yeast). Here, we have focused on the insertion

and permeation of these receptors into these model bilayers using unbiased MD simulation and the effects of an external force on the translocation of these receptors through these model lipid bilayers using biased MD simulation (umbrella sampling) techniques. In the last chapter (**Chapter 8**), we have summarized the overall conclusions to agitate the molecular recognition in water using endo-functionalized molecular tubes or naphthotubes (host-1a and host-1b in Figure 1-4) and uses of these receptors as drug delivery vehicles.

Chapter 2

Tuning the trapping of epoxides by endo-functionalized molecular tubes in an aqueous medium

"We cannot solve our problems with the same thinking we used when we created them."

— Albert Einstein

Overview: In biological and pharmaceutical industries, the production of pure enantiomeric compounds is incredibly essential. In chemistry and biology, chiral epoxides are essential intermediates. It is, therefore, of interest to have a simple procedure to detect and separate epoxide enantiomers. In recent times, several varieties of chiral stationary phases (CSPs), based on supramolecular receptors, such as crown ether, cyclodextrin, calixarene, among others available for the separation of chiral molecules. Inspired by this, we have used two already synthesized supramolecular receptor molecules (host-1a and host-1b) (known as endo-functionalized molecular tube), which may be used to separate the epoxide enantiomer. We present an elaborate description of the structure and the energetics of the chiral separation of epoxide enantiomers. Complexes of epoxide enantiomers having a larger hydrophobic surface area with host-1a and host-1b show a significant amount of difference in binding energy and potential of mean force values. This indicates, these water-soluble host molecules may be used as CSP in chiral chromatography for epoxide chiral enantiomer separation. Host-guest hydrophobic and hydrogen bonding interaction is the main stabilizing factor for these stable host-guest complexes. We hope, this work may be an excellent pole star for several enantiomeric separations.

■ INTRODUCTION

At first, we begin with some application of these receptors (host-1a and host-1b, Figure 1-4 of Chapter 1) at various important fields like chiral or enantiomeric separation and drug solubilization. This chapter describes the chiral separation properties of these receptors in the aqueous medium.

Two molecules with the same molecular weights, same atomic connectivity, similar chemical and physical properties, but the only difference in their optical activities are known as enantiomeric pair of molecules. Two enantiomers interact with a chiral system with different affinity [94]. The human body contains many important chiral systems such as amino acids, proteins, peptides, carbohydrates, sugars, and nucleic acids. Interestingly, all of these bio-macromolecules commonly exist in one of the two possible enantiomeric forms. Thus, only one enantiomer of the desired drug molecules possess the intended biological activity; the other one could show nil biological activity, or even toxic (show unintended side effects) to the human body [95]. So, chiral drugs with an individual enantiomer are intended and more fruitful to a patient [95, 96]. Pharmaceutical industries acknowledge the worth of the chirality of a particular drug molecule for many decades. US Food and Drug Agency (FDA) has also acknowledged this and published a resolution regarding this in the year of 1992, which states that if the final product molecule contains both the isomers, then probing the pharmaceutical properties of each of the enantiomer is imperative [97]. The importance of particular enantiomer is also acknowledged in different areas, such as analytical chemistry, medical science, forensic toxicology, synthetic chemistry, food additives, and agrochemical developments etc [95, 98]. Thus, the design, synthesis, and separation of a particular enantiomer of a molecule is the core interest of synthetic chemists [97]. Also, there is an increasing demand from the industrial sector to prepare, purify, and analyze chiral compounds. A particular stereoisomer of an organic molecule is used to develop biologically active drugs. Chiral molecules are the backbone for pharmaceutical and biomedical industries [99]. But, the two stereoisomers of a particular chiral organic molecule remain as a mixture (with the different quantity of contributions), and separation of this mixture is a tenacious work. Chiral separations are mainly the separation of stereoisomers or enantiomers. Generally used separation techniques such as liquid-liquid extraction, chromatography, and distillation (these methods are mainly based on differences in boiling points or solubilities) are less effective due to the similar chemical and physical properties of enantiomers in the achiral environment [100,101]. In the last few

decades, various techniques are developed for chiral separation such as gas chromatography (GC), high-performance liquid chromatography (HPLC), and capillary electrophoresis (CE) chromatography [100,101]. In these chromatographic techniques, separation is mainly controlled by the analyte interaction with both mobile and stationary phases of the system. Chiral separation by using chromatographic techniques depends mostly on the action of 'R' and 'S' enantiomers. Different enantiomers must be present for the measurement of the two chromatographic centers for either enantiomer [102]. The stationary phase as a chiral stationary phase (CSP) in HPLC has become faster and less expensive separation of chiral substances. The choice of CSP is the fundamental and obligate issue for profoundly impact the separation of enantiomers. In recent times, several varieties of CSPs, based on supramolecular receptors, such as protein, macrocyclic antibiotic, polysaccharide, crown ether, cyclodextrin, calixarene, and synthetic polymer among others are available for enantiomeric separation [97]. These types of separation techniques are based on molecular recognition [101]. Different isomers have a different interaction with these CSPs. This molecular recognition based chiral separation has gained significant attention due to the excellent selectivity for target molecules [102]. Receptors as CSP will barely effective when they are soluble in water and stable in solution. Chiral recognition firmly depends on the capability of a molecular receptor to form a complex using higher interaction with one of the enantiomers than others [95]. Effectiveness and capability of the chiral separations are based on the difference of complexation ability or affinity with different isomers; higher the difference, better will be the separation efficiency. Macrocyclic motifs are the main building blocks of the receptors employed for chiral separation techniques. An essential prerequisite is that chiral macrocycles form evocatively stable complexes with the guest enantiomers to effectively lower the stability of the complex of an enantiomer by repelling interaction [102].

In chemistry and biology, chiral epoxides or oxiranes are essential intermediates [103]. These epoxides can be transformed into several functional groups during chemical reactions and biosynthetic pathways. Epoxide compounds are candidates for insect control agents, which function as a juvenile hormone mimic and are a photoproduct or pharmaceutical chemicals of a variety of pesticides and drug products [104]. In particular, in the field of polymers, epoxides showed increasing industrial importance. The metabolic destiny of the oxirane group is essential because some polyvinyl chloride (PVC) food packaging films are plasticated with epoxidized glyceride generated via hydroperoxides in heated fats [104]. It is, therefore, of interest to have simple procedures to detect and separate epoxide enantiomers effectively.

This chapter is devoted to the possibility of separation of the enantiomers of epoxides with the help of two synthetic molecular receptors from the aqueous medium [105]. These synthetic receptors are also known as the endo-functionalized molecular tube [59,60]. Here we have used both the water-soluble syn (host-1a) and anti (host-1b) form of molecular tube receptors (Figure 1-4 of Chapter 1). All the used model epoxide guest molecules are presented in Figure 2-1. As mentioned above, although rather briefly, some experimental research works have been dedicated to deducing the mechanism by which these molecular tubes may be used to separates organic epoxide enantiomers in water but without much achievement. MD simulation and quantum chemical calculation could provide a thorough knowledge of these separation and encapsulation properties that can often not be achieved from standard experiments. In this work, we have used MD simulation along with quantum chemical analysis to deduce the actual mechanism behind the epoxide separation process.

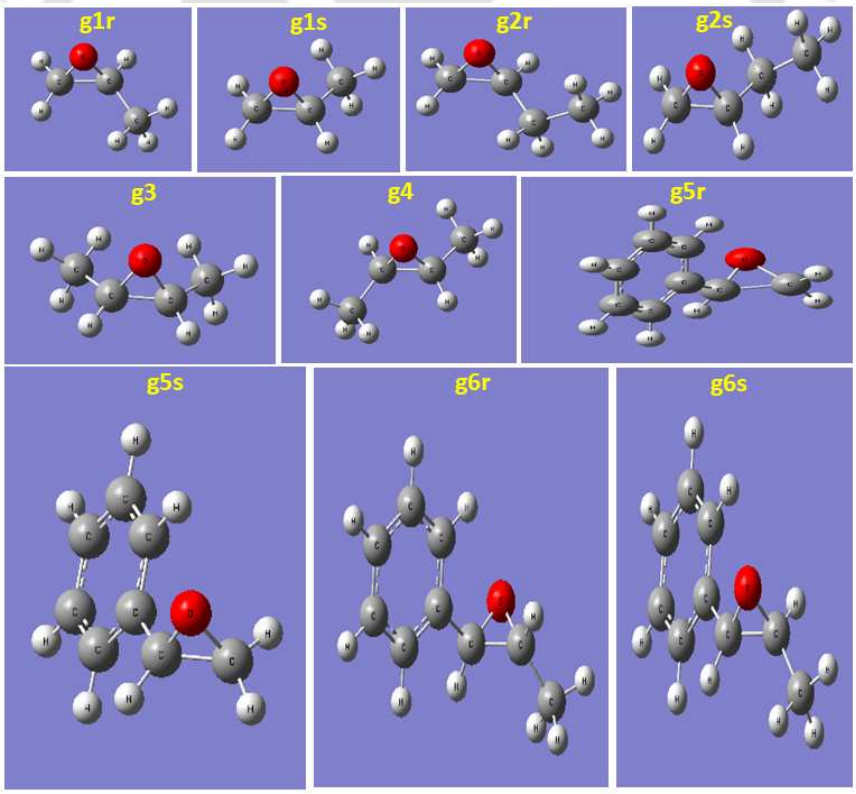

Figure 2-1. *All the guest molecules used for this work. g1 to g6 represents the guests 1 to 6. 'R' and 'S' isomer of the guest molecule is represented by 'r' and 's', respectively.*

In this regard, we would like to mention that, for this kind of separation technique of epoxide enantiomers with the help of synthetic molecular receptors in the aqueous medium,

no such MD simulation work has been carried out so far. In this work, we highlight the encapsulation of epoxide enantiomers by endo-functionalized molecular tubes and how these epoxide enantiomers may be separated.

The remaining chapter is arranged in this way. The models of endo-functionalized molecular tubes, ammonium ion, epoxide enantiomers, and water molecules used in this study, as well as computational details, are discussed in 'COMPUTATIONAL DETAILS' section. The findings are provided and discussed in 'RESULTS AND DISCUSSIONS' section. Our results are summarized in 'SUMMARY AND CONCLUSIONS' section.

■ COMPUTATIONAL DETAILS

Table 2-1. Partial charges of all the atomic sites of host-1a[a]

host-1a					
Atom	Charge (e)	Atom	Charge (e)	Atom	Charge (e)
O1, O62	-0.5823	C41	0.6477	H37, H79	0.1771
C61	0.8341	C97	0.0211	H87, H88	0.0203
C10	-0.7799	H98, H99	0.0191	O90, O89	-0.7196
H11, H12	0.1558	C100, C108	1.0341	H73, H78	0.1737
C13	0.7208	O109, O110	-0.9125	H77	-0.0661
H14	-0.0346	O2, O5	-0.4183	H81, H82	0.1462
C56, C26	-0.4491	C42, C29	-0.2864	H83	-0.0432
C55, C25	0.1818	H43, H72	0.2007	H48, H74	0.0203
C53, C23	-0.3292	C44, C30	-0.2970	C57, C18	0.0776
C51, C21	0.2322	C45, C31	0.1471	C59, C17	-0.2162
C50, C20	0.4397	C63, C38	0.1321	C60, C16	-0.3960
C101, C91	-0.0935	C67, C36	-0.1179	C58, C15	0.5560
O3, O4	-0.3124	C66, C34	-0.4062	H85, H75	0.1879
H102, H105	0.0441	C65, C33	0.5554	H86, H76	0.2138
H92, H93	0.0441	O69, O68	-0.5962	H52, H22	0.1870
C94, C106	1.0770	C70	0.8723	H54, H24	0.1734
O113, O114	-0.9252	C64	-0.7891	H84	-0.0358
O111, O112	-0.9252	C39	0.8470	C40, C27	-0.5248
N6, N8	-0.6500	C32, C103	-0.5007	H35, H80	0.1750
C49, C19	-0.3002	O115, O116	-0.9125	C46, C104	0.9067
C47, C71	0.3091	C28	0.6477	H96, H107	0.0191
H7, H9	0.2978	C95	0.0211		

[a] e is the elementary charge.

Two host molecules (host-1a and host-1b), ammonium ion, and all ten guest molecules are optimized by using HF/6-31+G** basis set of Gaussian 09 [106]. Partial

charges of every atomic site of all these molecules are calculated by RESP (restrained electrostatic potential) [67] module of AMBER14 [63].

Table 2-2. Partial charges of all the atomic sites of host-1b[a]

host-1b							
Atom	Charge (e)	Atom	Charge (e)	Atom	Charge (e)	Atom	Charge (e)
O5, O6	-0.6651	C85	-0.6899	C68	0.5877	H97, H98	0.0123
C20	0.5716	C84	0.5877	C66	-0.6117	H81	0.1708
C13	1.0925	C82	-0.6117	C65	-0.2608	O101, O102	-0.5940
C99, C100	-0.6651	C80	-0.2608	H103	0.1708	H14	-0.0695
C36	0.5716	C79	0.4658	H67	0.3942	C15	-1.0468
C37	-0.3272	O9, O10	-0.5802	H59	0.1657	H16, H17	0.1888
H38	0.1814	C72	0.8542	H61, H90	0.1740	H54, H55	0.0123
C39	-0.2464	C29	-0.2464	C77	0.9714	C18	1.0382
H40	0.1632	C64	0.4658	C74	-0.7070	H19	-0.1261
C41	0.2421	C63	-0.4062	H75, H76	0.0996	C21, C49	-0.5908
C42	-0.6232	C62	-0.0491	H32	0.1814	C22	0.1891
C43	0.4809	C60	-0.2565	H78	-0.1762	C23	-0.2887
O7, O8	-0.1990	C58	-0.2864	C92	-0.4062	H24	0.1635
C50	-0.2490	C57	0.5118	C91	-0.0491	C25	-0.2642
H51, H52	0.0636	O11, O12	-0.3156	C89	-0.2565	H104	0.1653
C96	0.5277	C69	0.0133	C87	-0.2864	C26	0.4809
C111	1.1483	H70, H71	-0.0031	C86	0.5118	H2	0.5133
O114, O116	-0.9397	H83	0.3942	H88	0.1657	C33	-0.2490
N1, N3	-1.1261	C112	1.0887	C93	0.0133	H34, H35	0.0636
C44	-0.2642	O113, O115	-0.9441	H94, H95	-0.0031	H4	0.5133
H45	0.1653	H73	-0.0469	C31	-0.3272	C105	1.1483
C46	-0.2887	C56	-0.6899	C106	1.0887	O107	-0.9397
H47	0.1635	C53	0.5277	O108, O110	-0.9441	O109	-0.9397
C48	0.1891	H30	0.1632	C28	0.2421	C27	-0.6232

[a] e is the elementary charge.

With the help of the ANTECHAMBER [107] module of AMBER14, we have determined all other General AMBER force field (GAFF) [108] parameters of these molecules. Partial charges of all of the atomic sites of both the host molecules are listed in Table 2-1 and 2-2. The configuration of all the host and guest molecules used for MD simulations in an aqueous medium is the gas phase Hartree-Fock optimized configuration. Both the host molecules have four units of negative charge, and these water-soluble hosts are neutralized with the addition of ammonium ions [105]. Four ammonium ions are added in each system. TIP3P model of water is used for this work [72]. To evaluate the complexation properties of these chiral epoxides in water with these two host molecules (as host-1a and host-1b), 22 different systems for normal MD simulations are considered, and the details of these systems are summarized in Table 2-3. Initial configurations of all the systems are prepared by PACKMOL [74] package. Sander module of AMBER14 is used for all MD

simulations. We have used a cubic box as a simulation box for every system. Periodic boundary conditions (PBC) are employed in all three directions for every simulation.

Table 2-3. Overview of systems[a]

System	N_{host}	$N_{NH_4^+}$	N_{guest}	N_{wat}	Box volume (nm^3)	M_{host} (M)
1a	1	4	0	2280	70.58	0.0235
1b	1	4	0	2320	71.43	0.0232
1a-g1r	1	4	1	2280	70.50	0.0235
1a-g1s	1	4	1	2280	70.27	0.0236
1b-g1r	1	4	1	2320	71.60	0.0232
1b-g1s	1	4	1	2320	71.34	0.0233
1a-g2r	1	4	1	2280	70.41	0.0236
1a-g2s	1	4	1	2280	70.35	0.0236
1b-g2r	1	4	1	2320	71.53	0.0232
1b-g2s	1	4	1	2320	71.72	0.0231
1a-g3	1	4	1	2280	70.33	0.0236
1b-g3	1	4	1	2320	71.74	0.0231
1a-g4	1	4	1	2280	70.52	0.0235
1b-g4	1	4	1	2320	71.64	0.0232
1a-g5r	1	4	1	2280	70.61	0.0235
1a-g5s	1	4	1	2280	70.22	0.0236
1b-g5r	1	4	1	2320	71.70	0.0231
1b-g5s	1	4	1	2320	71.43	0.0232
1a-g6r	1	4	1	2280	70.56	0.0235
1a-g6s	1	4	1	2280	70.50	0.0235
1b-g6r	1	4	1	2320	71.84	0.0231
1b-g6s	1	4	1	2320	71.79	0.0231

[a] N_{host}, $N_{NH_4^+}$, N_{guest}, and N_{wat} are the numbers of the host, ammonium ion, guest, and water molecules, respectively. M_{host} is the molar concentration of the host. 1a and 1b represent the host-1a and host-1b, respectively. 1a-g1r, 1b-g1s, etc. represent systems with guest-1r, guest-1s in host-1a and host-1b respectively, etc. 1a and 1b system does not contain any guest molecules.

All the covalent bonds involving hydrogen atom are constrained by using SHAKE algorithm [71]. For estimating all the short-range nonbonded interactions, a 10 Å cut-off distance is defined, and the Particle Mesh Ewald (PME) [73] is employed to treat all the long-range electrostatic interactions. Every simulation is performed by taking a 2 fs time step. Every system is introduced to 10000 steps of energy minimization, of which the first 4000 steps are the steepest descent minimization, and the rest 6000 steps are in the conjugate gradient method. All the systems are slowly heated from 0 to 298 K for 320 ps in the canonical (NVT) ensemble. We have performed 5 ns equilibration run (at 298 K temperature and 1 atm pressure) in isothermal-isobaric (NPT) ensemble. We have used Berendsen barostat [75] with 2 ps pressure relaxation time to maintain the intended 1 atm pressure. To maintain

298 K temperature during the simulation, Langevin dynamics [76] method with 1 ps^{-1} collision frequency is employed. Every system (as in Table 2-3) is introduced to 200 ns production run in NPT ensemble. A total of 17.4 μs of production run is performed. Our main goal in this research is to find out the stabilizing factors and mechanisms of these host-guest complexation processes.

Resulting MD simulation trajectories are analyzed with the help of CPPTRAJ module [77] of AMBER14. We have used the Visual Molecular Dynamics (VMD) [78] package for visualization and analysis purposes of the MD trajectories.

Binding free energy (ΔG^0_{bind}) of the host-guest complexes are calculated by using the Molecular Mechanics-Poisson Boltzmann Surface Area (MM-PBSA) [79, 80] method. Details of this method are discussed in the 'METHODOLOGY' section of Chapter 1 (Eq. 1.18). The potential of mean force (PMF) of these host-guest complexes are also analyzed, and details of this method are discussed in the 'METHODOLOGY' section of Chapter 1 (Eq. 1.24).

■ RESULTS AND DISCUSSIONS

Our result aims to the possibility of separation of epoxide enantiomers by endo-functionalized molecular tubes from aqueous medium. Representative snapshots of all 1:1 host-guest complexes, obtained from the last frame of the representative trajectories are depicted in Figure 2-2. Representative snapshots of all host-guest complexes give a preliminary idea of fully inserted host-guest complexes. Both the host molecules can place every guest molecules in their deep cavities. Every host molecule has two inwardly directed N-H protons and a large hydrophobic cavity (as it is made up of four naphthalene units). From snapshots, it is found that the oxygen atom of epoxide guests is placed itself in a head to head position with any one of the N-H protons of the host molecule. It is the preferred position for forming N-H$\cdots$O hydrogen bond. The hydrophobic part of these enantiomeric epoxide guest molecules can reside in the hydrophobic cavity of the host molecule. From these snapshots, we find that hydrogen bonding and hydrophobic effect work synergistically for the encapsulation of these epoxide guests with the host molecules. But, here we would like to mention that one representative snapshot does not provide much information about the different factors responsible for these host-guest complexes.

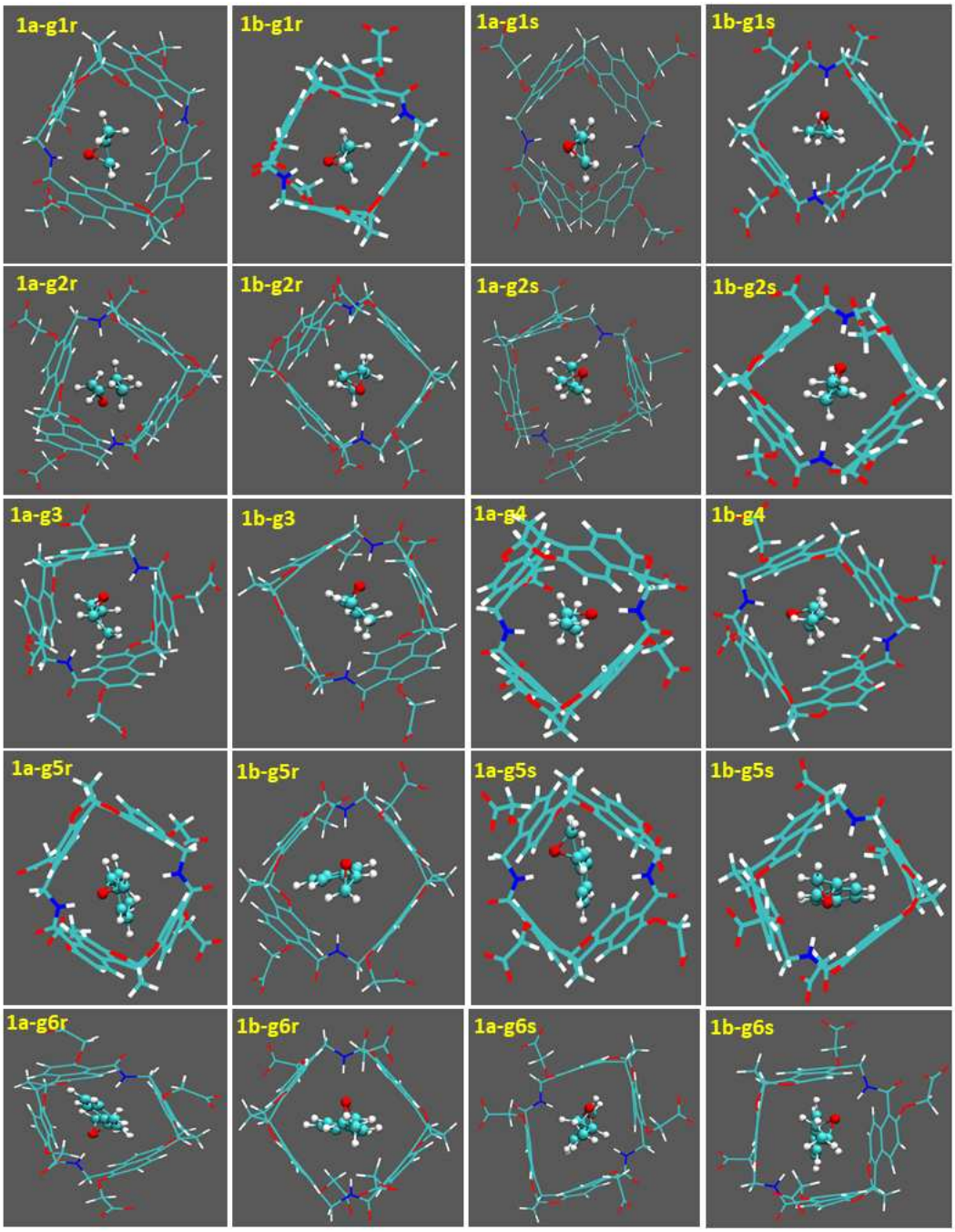

Figure 2-2. *Indicative snapshots of all host-guest complexes formed between a host and a guest molecule. Waters are excluded to enhance visual clarity.*

Internal Diameters

We first examine how these two host molecules are changed structurally after the

insertion of guest molecules into their cavities. For this, we have considered two perpendicular internal diameters by connecting two opposite atoms of the host molecules and examined its change as the simulation progresses. Schematic representation of these two internal diameters (for both host-1a and host-1b) are presented in Figure 2-3. In host-1a, diameter-I and diameter-II are imagined by connecting atom pairs C10-C64 and C47-C71, and for the same representation of host-1b, C15-C74 and C53-C96 atom pairs are taken, respectively. Due to the non-spherical nature of the host molecules, these two diameters are not equal to each other. Diameter-I is slightly larger than diameter-II. Average values of diameter-I and diameter-II, the absolute difference (Ad) between them, and the standard error values of Ad of all the systems are presented in Table 2-4. The change in these two diameter values behaves differently after the insertion of guest molecules into their respective cavities. After guest insertion, the diameter-I value is increased, but the diameter-II length is decreased for host molecules compared to the individual guest free host's diameter values. Hydrogen bonding (discussed later) between the host's 'N-H' protons and epoxide's 'O' atom is formed along the diameter-II. For this effect, diameter-II value is decreased, and to offset this effect, the diameter-I length is increased. The size and shape of the guest molecules are also responsible for the different range of diameter changes for various systems.

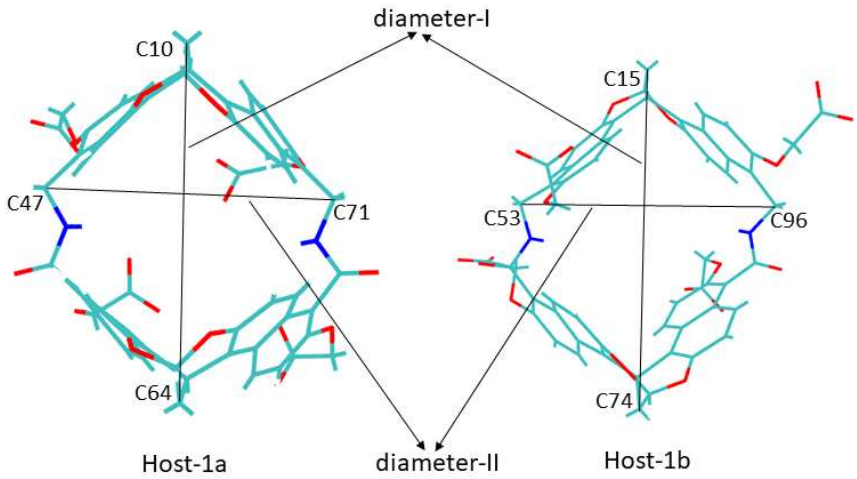

Figure 2-3. *Schematic representation of the two internal diameters of host-1a and host-1b are portrayed as diameter-I and diameter-II.*

Table 2-4. Average internal diameter[a]

System	Aid-I (Å)	Aid-II (Å)	Ad (Å)	Se (Å)
1a	10.98	9.40	1.58	± 0.0064
1a-g1r	11.16	9.32	1.84	± 0.0218
1a-g1s	11.15	9.32	1.83	± 0.0119
1a-g2r	11.49	9.35	2.14	± 0.0092
1a-g2s	11.51	9.35	2.16	± 0.0096
1a-g3	11.02	9.34	1.68	± 0.0304
1a-g4	11.22	9.34	1.88	± 0.0064
1a-g5r	12.01	9.12	2.89	± 0.0114
1a-g5s	11.17	8.94	2.23	± 0.0074
1a-g6r	11.95	9.21	2.75	± 0.0066
1a-g6s	11.31	8.94	2.36	± 0.0269
1b	13.13	9.66	3.51	± 0.0012
1b-g1r	13.19	9.60	3.59	± 0.0041
1b-g1s	13.20	9.60	3.60	± 0.0081
1b-g2r	13.15	9.62	3.53	± 0.0023
1b-g2s	13.15	9.62	3.53	± 0.1146
1b-g3	13.26	9.57	3.69	± 0.0548
1b-g4	13.15	9.63	3.52	± 0.0028
1b-g5r	13.36	9.39	3.97	± 0.0085
1b-g5s	13.35	9.40	3.95	± 0.0059
1b-g6r	13.21	9.57	3.64	± 0.0098
1b-g6s	13.20	9.59	3.61	± 0.0029

[a] Average values of internal diameter-I (Aid-I), internal diameter-II (Aid-II), the absolute difference (Ad) between them, and the standard errors (Se) of Ad of host-1a and host-1b of every system. Standard errors are estimated by block averaging method.

To get a clear picture of the structural change of the host molecules, we have determined the probability distribution functions of Ad for all the systems, and the same is presented in Figure 2-4 and Figure 2-5 for host-1a and the host-1b containing systems, respectively. For each system, Ad value vs. simulation time plot is shown in the insets of these plots. The maximum probability of Ad appears at 1.50 Å and 3.50 Å, respectively, for host-1a and host-1b, in which the systems devoid of any guest molecule and the same for guest containing systems appear at somewhat larger distances. This observation indicates more sampling of a less symmetric structure after the insertion of guest molecules into their respective cavities than free host-1a and host-1b. These findings suggest that host-1a and host-1b change structurally upon the inclusion of these epoxide guest molecules into their cavities. From the two internal diameter values and the absolute difference between them, it is clear that every host molecule gets more structural stability after the insertion of a

guest molecule into their cavities.

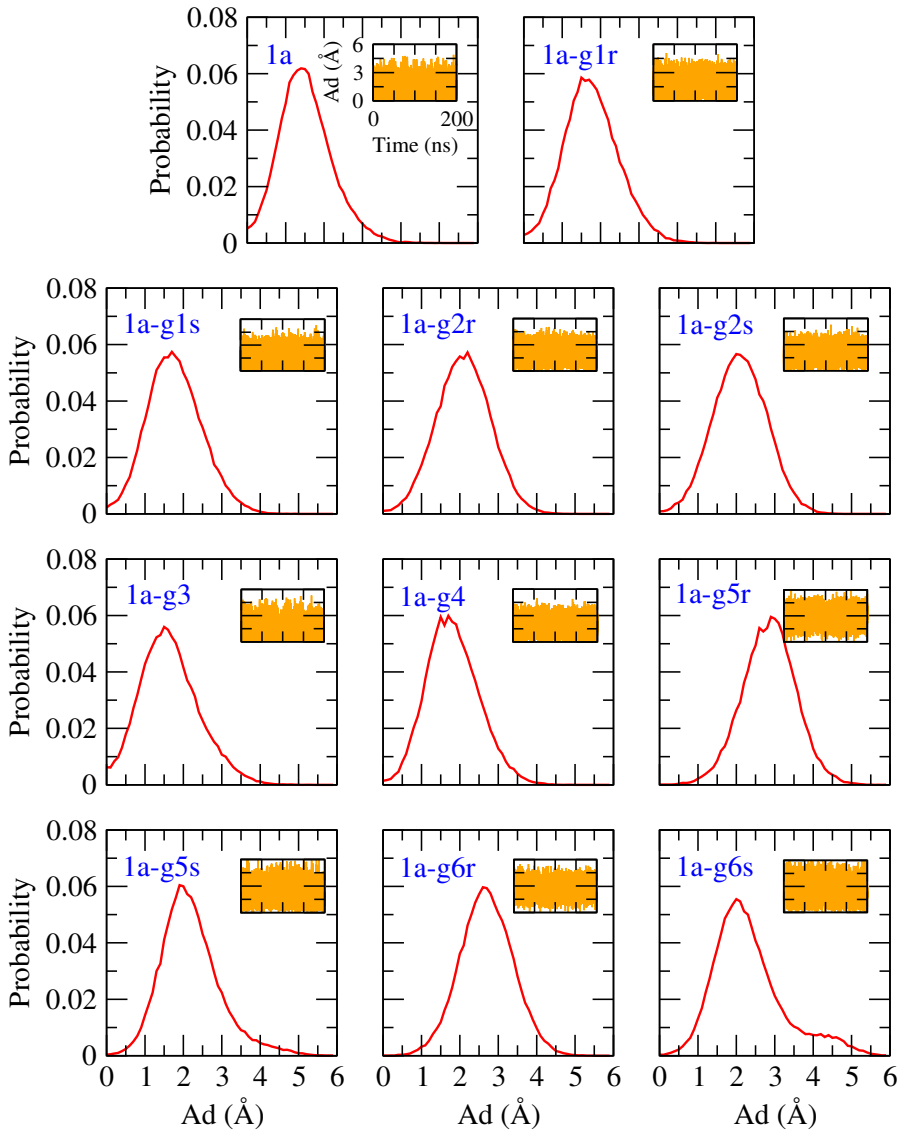

Figure 2-4. *The probability distribution functions of absolute difference (Ad) of host-1a. Ad values as a function of simulation time for every system are presented in insets.*

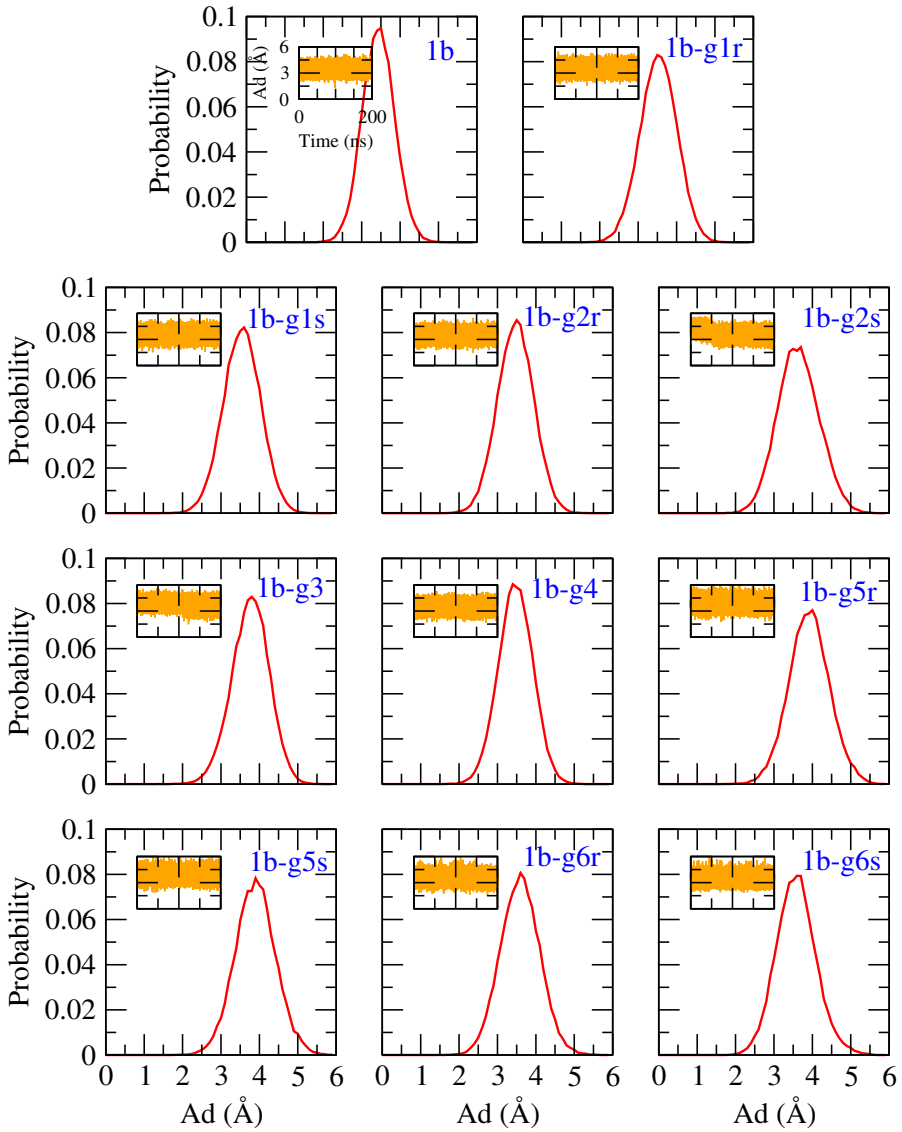

Figure 2-5. *The probability distribution functions of absolute difference (Ad) of host-1b. Ad values as a function of simulation time for every system are presented in insets.*

Hydrogen Bond Analysis

In this section, we are interested to see how this host-guest complexation depends

on the different types of hydrogen bonds. We have calculated the average number of hydrogen bonds between host and water, and host and guest molecules. We consider the geometric definition of hydrogen bond as used extensively by several researchers. We have considered [109–115] donor-acceptor cut-off distance $\leq$ 3.4 Å, and simultaneously, donor-acceptor-hydrogen cut-off angle $\leq 45^{o}$. These imposed restrictions are schematically represented in Figure 2-6.

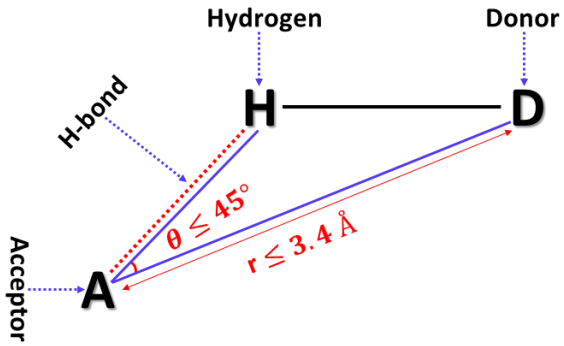

Figure 2-6. *The schematic representation of the imposed restrictions for hydrogen bond analysis.*

In host-1a, two nitrogen atoms that involve in hydrogen bonding are N6 and N8, and the same in host-1b are N1 and N3 atoms. The different types of average number of hydrogen bonds for all the systems are shown in Table 2-5. At first, we focus on the average number of hydrogen bonds between host-water and host's nitrogen atom-water. The host-water hydrogen bonds refer to the total number of hydrogen bonds formed by the different atomic sites of host molecules with water. The systems devoid of any guest molecule possess the highest number of host-water hydrogen bonds in the case of both host-1a and host-1b. In guest containing systems, the average number of this type of hydrogen bond decreases. System, which does not contain any guest molecule, all the hydrogen bonding donor sites of host form hydrogen bonds with water molecules but when we introduce guest molecule into the system, some of the host donor sites are now involved in hydrogen bonding with guest molecule, and these sites are now no longer available for hydrogen bonding with water.

Table 2-5. Hydrogen bond values

System	host-wat	N6/N1-wat	N8/N3-wat	host-gus	N6/N1-gus	N8/N3-gus
1a	23.70	0.49	0.48	–	–	–
1a-g1r	22.56	0.05	0.05	0.82	0.35	0.47
1a-g1s	23.22	0.05	0.04	0.82	0.39	0.43
1a-g2r	22.49	0.02	0.01	0.74	0.37	0.37
1a-g2s	22.08	0.02	0.01	0.73	0.34	0.39
1a-g3	22.35	0.01	0.01	0.86	0.44	0.42
1a-g4	22.89	0.01	0.01	0.89	0.44	0.45
1a-g5r	21.68	0.01	0.01	0.71	0.34	0.37
1a-g5s	22.55	0.01	0.01	0.77	0.42	0.35
1a-g6r	22.91	0.01	0.01	0.71	0.31	0.40
1a-g6s	21.14	0.01	0.01	0.89	0.47	0.42
1b	23.99	0.76	0.84	–	–	–
1b-g1r	22.41	0.12	0.12	0.89	0.39	0.50
1b-g1s	23.55	0.15	0.14	0.85	0.43	0.42
1b-g2r	22.75	0.02	0.02	0.89	0.40	0.49
1b-g2s	22.31	0.02	0.02	0.89	0.48	0.41
1b-g3	22.46	0.06	0.06	0.92	0.52	0.40
1b-g4	20.70	0.02	0.02	0.95	0.49	0.46
1b-g5r	20.41	0.01	0.02	0.76	0.44	0.32
1b-g5s	22.64	0.02	0.01	0.78	0.35	0.43
1b-g6r	22.96	0.03	0.02	0.94	0.53	0.41
1b-g6s	21.95	0.02	0.02	0.92	0.49	0.43

[a] Average number of hydrogen bonds between host and solvent water (host-wat), host-1a N6/host-1b N1 atomic sites-water (N6/N1-wat), host-1a N8/host-1b N3 atomic sites-water (N8/N3-wat), host and guest (host-gus), host-1a N6/host-1b N1 atomic sites-guest 'O' atom (N6/N1-gus), and host-1a N8/host-1b N3 atomic sites-guest 'O' atom (N8/N3-gus) for different systems.

As a result, there is a drop in the average number of host-water hydrogen bonds. Host's donor 'N-H' protons are involved in hydrogen bonding with the guest's acceptor 'O' atom. We have computed the number of hydrogen bonds between these 'N-H' protons and water molecules, which gives us precise information about how these 'N-H' protons are involved in hydrogen bonding with guests rather than water molecules. From Table 2-5, we can see that when the systems are devoid of any guest molecule, these two nitrogen atoms show a maximum number of hydrogen bonds with water, but when a guest molecule is introduced, the number of these hydrogen bonds fall drastically. These values indirectly prove the presence of hydrogen bonding between host and guest molecules. We are now interested in the number of hydrogen bonds between host and guest molecules and, more specifically, between the host's donor 'N-H' protons and guest's acceptor 'O' atoms. These types of hydrogen bonds for every system are also presented in Table 2-5. Every guest containing system has a significant amount of host-guest hydrogen bond number. The average number

of the host-guest hydrogen bond is the summation of the hydrogen bond numbers between two hydrogen atoms of the 'N-H' group (in host-1a, N6/N8-H, and host-1b, N1/N3-H) and guest acceptor oxygen atoms. In host molecules, besides these two nitrogen atom donor sites, no other sites are involved in hydrogen bonding with a guest molecule that goes inside the cavity. Also, every 'N-H' protons contribute almost equally to the total host-guest hydrogen bonding. This implies that a guest molecule does not remain fixed inside the host cavity and instead continuously flips its position inside the host's cavity. From here we can say that different types of hydrogen bonds (host-water, host's nitrogen atom-water, host-guest, and host's nitrogen atom-guest) analyses give the proof of every stable host-guest complexes.

MM-PBSA Analysis

The stability regarding each of these encapsulated guest molecules into the host cavity is quantitatively determined by determining the binding free energy (ΔG^0_{bind}) values. We have computed ΔG^0_{bind} by employing MM-PBSA/GBSA method. The last 4 ns MD simulation trajectories are used for the estimation of ΔG^0_{bind}. The ΔG^0_{bind} value (along with all of its constituents) and standard errors of these binding free energy values for each system are presented in Table 2-6. The magnitude of standard errors of these ΔG^0_{bind} values are minimal.

As can be noticed that van der Waals energy component (ΔE_{vdw}) [116–119] of every system is the main benefactor to the ΔG^0_{bind}. A high negative value of ΔE_{vdw} signifies strong hydrophobic and hydrogen bonding interactions between a host and guest molecule. In every host-guest complex, nearly one hydrogen bond is formed between the host donor 'N-H' and guest acceptor 'O' atom. So, van der Waals interaction due to hydrogen bond formation is almost the same for every system. With the increased hydrophobic portion of guest molecules (as the host remains same), the change in the value of ΔE_{vdw} becomes more apparent. Thus, in the host-guest complexes, for a given host, when guest molecule changes from g1 to g6, the value of ΔE_{vdw} becomes gradually more favorable. Electrostatic energy (ΔE_{ele}) component also has a negative value, but the change of its value is not as much prominent as ΔE_{vdw}. The reason behind different host-guest interactions is that host-1b has a more open tubular cavity than the bowl-shaped cavity of host-1a, and different amount of hydrophobic surface area of these guest molecules. ΔE_{vac} (ΔE_{vdw} + ΔE_{ele}) has a negative value of energy for each system. Thus, ΔE_{vac} is a welcome contributor to ΔG^0_{bind}. Electrostatic solvation free energy (ΔG_{PB}) is a hostile contributor (i.e., it has

positive energy value) to ΔG^0_{bind} for every system.

Table 2-6. Binding free energy values[a]

System	ΔE_{vdw}	ΔE_{ele}	ΔG_{PB}	ΔG_{NP}	$T\Delta S$	ΔG^0_{bind}	Se
1a-g1r	-13.60	-1.87	4.52	-1.16	-10.30	-1.81	± 0.071
1a-g1s	-13.86	-1.56	4.24	-1.15	-10.32	-2.01	± 0.069
1b-g1r	-13.38	-4.61	6.44	-1.15	-10.14	-2.56	± 0.073
1b-g1s	-12.73	-4.23	6.19	-1.18	-9.92	-2.03	± 0.082
1a-g2r	-16.83	-1.33	4.30	-1.35	-11.38	-3.83	± 0.094
1a-g2s	-16.71	-1.41	4.17	-1.34	-11.46	-3.83	± 0.087
1b-g2r	-16.91	-4.37	6.96	-1.33	-11.10	-4.55	± 0.086
1b-g2s	-16.84	-4.46	7.00	-1.33	-11.12	-4.51	± 0.095
1a-g3	-16.04	-2.45	4.71	-1.27	-11.83	-3.22	± 0.074
1b-g3	-16.64	-5.87	7.04	-1.15	-11.82	-4.80	± 0.083
1a-g4	-16.70	-2.66	5.64	-1.25	-10.89	-4.08	± 0.076
1b-g4	-17.00	-5.44	7.30	-1.19	-11.36	-4.97	± 0.089
1a-g5r	-23.01	-2.62	7.88	-1.40	-13.42	-5.73	± 0.098
1a-g5s	-21.32	-3.63	8.45	-1.61	-13.68	-4.43	± 0.097
1b-g5r	-21.42	-3.74	8.75	-1.39	-13.99	-3.81	± 0.107
1b-g5s	-20.34	-3.82	8.97	-1.36	-13.91	-2.64	± 0.100
1a-g6r	-25.50	-2.85	7.85	-1.48	-14.76	-7.22	± 0.103
1a-g6s	-23.54	-4.17	8.45	-1.48	-14.38	-6.36	± 0.102
1b-g6r	-23.39	-4.37	8.74	-1.45	-14.17	-6.30	± 0.109
1b-g6s	-21.76	-4.30	9.80	-1.69	-14.58	-3.37	± 0.097

[a] The total value and it's components of binding free energy (in kcal/mol) of all systems. Standard errors (Se) (in kcal/mol) of these binding free energies are also in the Table.

This result signifies the decrease of contact area between the solvent with both host and guest molecule upon insertion and, thus, a reduced amount of electrostatic interaction of the complexed host-guest system with water than the free host and guest molecule. The computed value of ΔG_{PB} is expected when the contact area between host and guest are significant; the value of ΔG_{PB} is also high (immense positive value, i.e., more unfavorable). ΔG_{NP} has a negative energy value (i.e., a favorable contributor to ΔG^0_{bind}) for each system. It implies non polar surface term accord favorably to these host-guest complex stability. However, ΔG_{NP} contribution is much lower compared to ΔE_{vdw}, and each system has the nearly same amount of ΔG_{NP} value. Also, ΔG_{solv} ($\Delta G_{PB} + \Delta G_{NP}$) is an unfavorable contributor (i.e., has positive value) to ΔG^0_{bind} for every system. From normal mode (NMODE) analysis, we get a negative value of $T\Delta S$ for all analyzed host-guest complexes, which is expected. This symbolizes an alleviation of the degree of freedom upon host-guest binding. A small guest molecule has more space into the host cavity compared to that of a large

guest molecule. Hence, a small guest molecule has more mobility inside the host cavity than the large guest molecule. Therefore, the loss of a degree of freedom is less in case of a small guest molecule into the host cavity, and as the size of the guest increases, this loss is also increased. All of these TΔS values are assigned with the approximate nature of NMODE analysis.

ΔG^0_{bind} (ΔE_{vac} + ΔG_{solv} - TΔS) has a negative value for every system. So, all of these host-guest complexes are energetically stable. Experimental values [105] of 1a-g5, 1b-g5, 1a-g6, and 1b-g6 complexes are -6.29, -5.57, -7.07, and -6.82 kcal/mol, respectively. From MM-PBSA analysis these values are -5.73 (or -4.43), -3.81 (or -2.64), -7.22 (or -6.36), and -6.30 (or -3.37) kcal/mol depending on 'R' or 'S' configuration of the guest molecules, respectively. Therefore, the experimental binding free energy value of these complexes are in well accordance with the estimated MM-PBSA energy values.

Overall, these host-guest bindings are driven by hydrophobic interaction between host and guest molecules with a supplementary contribution from hydrogen bonding. The two molecular tubes have similar binding affinities to all the guest molecules, but for host-1b is somewhat more promising to guest g1 to g4 and host-1a has a moderately more favorable interaction with guests g5 and g6 than host-1b. Large guest molecules (g5 and g6) show a significant energy difference between a pair of enantiomer with a particular host molecule, but for small guest molecules (g1 to g4), this energy difference is insignificant. We find that for guests g5 and g6, 'R' isomer shows a more binding affinity than 'S' isomer with a particular host molecule. Ruiz-Lòpez *et al.* [120] suggested that the energy differences concerned are small and close (or even smaller) to computational errors, as is frequently observed in enantio- or diastereoselectivity problems. Therefore, the chiral recognition capability is difficult to conclude definitively. However according to analysis, the isomers with more negative binding free energy can selectively binds with the receptor over the other isomers. Now, from Table 2-6, it is clear that 'R' and 'S' isomers of guests g5 and g6 form stable complex with a specific host with energy difference greater than 1 kcal/mole. Thus, we can say that 'R' isomer of guest g5 and g6 binds selectively over the 'S' isomers with both the receptors.

Umbrella Sampling (PMF Calculations)

We have estimated the potential of mean forces (PMFs) as a function of the COM-COM distance between the host and guest molecules in the Z-direction. We have analyzed the PMF of all the guest containing systems. The last frame configuration of normal MD

simulation is used as the initial configuration in umbrella sampling (US) simulation. In this method, an initial geometry produced after normal MD simulation is implemented to keep at a place in which molecules of interest at a growing COM distance are harmonically restrained. Restrained force helps host and its reference guest molecules to be fixed in a defined position of the reaction coordinate. Two neighboring windows must overlap with each other to obtain a smooth PMF curve. Due to the symmetric nature of both the host molecules, guest molecule can either enter or leave the cavity along the same path. A schematic representation for this US simulation is presented in Figure 2-7.

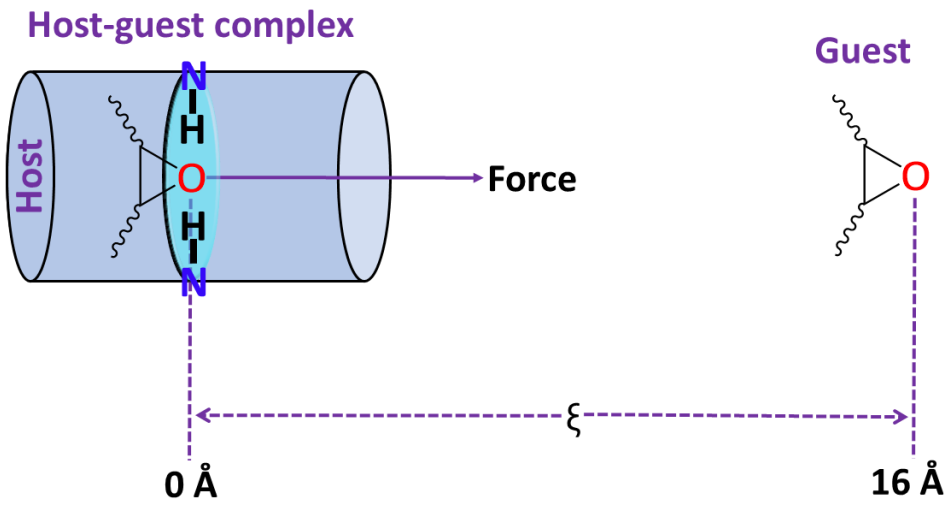

Figure 2-7. *Schematic representation of the umbrella sampling simulation by taking the host-guest center of mass (COM) - center of mass (COM) distance as the reaction coordinate.*

The PMF as a function of host-guest COM-COM distance for every system is shown in Figure 2-8. The main outcomes from these figures are: (i) PMF plots for systems 1b-g5r, 1b-g5s, 1b-g6r, and 1b-g6s contain two sharp minima, but all other systems contain only one sharp minimum. (ii) The first sharp minimum (appears at 1.12 Å for systems 1b-g1r and 1b-g1s, at 1.58 Å for systems 1b-g5r and 1b-g5s, at 2.27 Å for systems 1a-g5r, 1a-g5s, 1a-g6r, and 1a-g6s, at 1.35 Å for every other system) for every host-guest systems is for the fully inserted complexes, and it is referred to as contact minima (CM). In CM, the stability of a host-guest complex is maximum with the highest (negative) free energy value. Free energy values at CM for each systems are: -1.84 (1a-g1r), -1.98 (1a-g1s), -3.08 (1b-g1r),

-2.70 (1b-g1s), -2.00 (1a-g2r), -2.00 (1a-g2s), -3.90 (1b-g2r), -3.81 (1b-g2s), -2.51 (1a-g3), -3.07 (1b-g3), -2.71 (1a-g4), -3.32 (1b-g4), -2.79 (1a-g5r), -1.82 (1a-g5s), -1.74 (1b-g5r), -1.29 (1b-g5s), -4.54 (1a-g6r), -3.20 (1a-g6s) -3.05 (1b-g6r), and -1.64 (1b-g6s) kcal/mol.

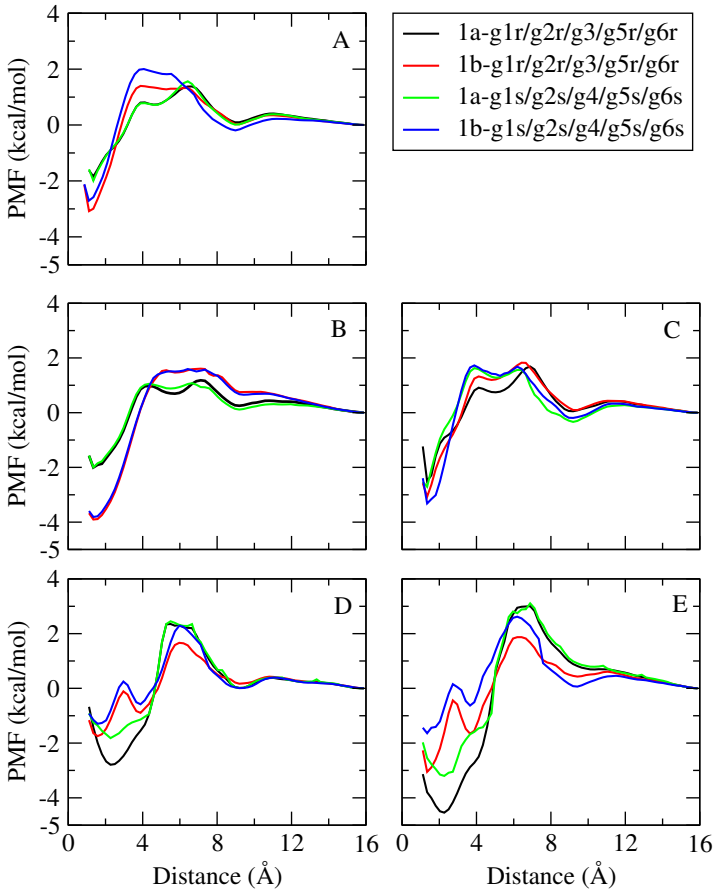

Figure 2-8. *PMF values as a function of the center of mass (COM) - center of mass (COM) distance between host and guest molecule of each system. 'A' contains systems 1a-g1r, 1b-g1r, 1a-g1s, and 1b-g1s, 'B' is for systems 1a-g2r, 1b-g2r, 1a-g2s, and 1b-g2s, 'C' has systems 1a-g3, 1b-g3, 1a-g4, and 1b-g4, 'D' is for systems 1a-g5r, 1b-g5r, 1a-g5s, and 1b-g5s, and 'E' contains systems 1a-g6r, 1b-g6r, 1a-g6s, and 1b-g6s. Standard errors of all data points (calculated using the block average method) fall within ± 0.04 kcal/mol.*

(iii) Those systems, which have only one sharp minimum, PMF curve above 9 Å COM-

COM distance, remains almost parallel with the COM-COM distance axis. This almost parallel line corresponds to the free host free guest state. So, for these systems, only two states are possible such as complexed host-guest and free host free guest state. Also, there is an energy barrier that separates these two states. This barrier of energy is different for every system, and every system has to overcome this amount of energy for changing its state from the complexed to the free host-guest state. (iv) The shallow second minima arise for the systems 1b-g5r, 1b-g5s, 1b-g6r, and 1b-g6s, and this minimum appears at 3.88 Å for the first two systems and 3.66 Å for the remaining two systems. This shallow second minimum for these systems arises due to somewhat more interaction between host and guest, but this interaction is very much weaker than CM state interaction. There is an energy barrier between CM state and second minima for these systems. Every system has to surpass this amount of energy for the transformation from CM state to second minima. After the second minima, the almost parallel line of PMF curve along the COM-COM distance axis (after around 9 Å) is for the free host free guest state. A barrier of energy also separates the second minimum and free host free guest state. So, the transformation from the second minima to free host free guest state is also energetically unfavorable.

From the above, we can say that every host-guest complex is mostly stabilized at fully inserted CM state, and free energy values (at CM) for every system are in well accordance with the binding free energy values estimated from MM-PBSA analysis. PMF plots (in Figure 2-8) for every host-guest complex shows a well deep contact minimum. The energy value in the contact well is the indicator of stable host-guest complexes. In contact minimum, for every 'R' and 'S' enantiomeric pair of the small guest molecules, with a specific host molecule, the energy difference is very less, but when we move from small guest molecules to large guest molecules, this energy difference between a particular enantiomeric pair of epoxide molecule becomes significant. This indicates that the possibility of enantiomeric separation of epoxide guest molecules with the help of these endo-functionalized molecular tube host molecules may not be accurate when the surface area of the epoxide guest is less, but when this surface area becomes large, precise separation of 'R' and 'S' epoxide enantiomers may possible.

Quantum Chemical Calculation

We now want to examine the types of nonbonded interactions that are responsible for making these host-guest complexes stable. For this, we employ a quantum-based noncovalent interaction reduced density gradient (NCI-RDG) technique [121]. Reduced density

gradient (RDG) and the sign of the second largest eigenvalue of electron density Hessian matrix at position 'r' (sign(λ_2)ρ) are a pair of very important functions for revealing weak interaction regions, they are collectively employed in NCI method. Weak interaction has a significant influence on the conformation of macromolecules, binding mode of proteins, and ligands; however, reproduction of electron density by *ab initio* and grid data calculation of RDG for such huge systems are always too time-consuming. Fortunately, it is found that weak interaction analysis under promolecular density is still reasonable.

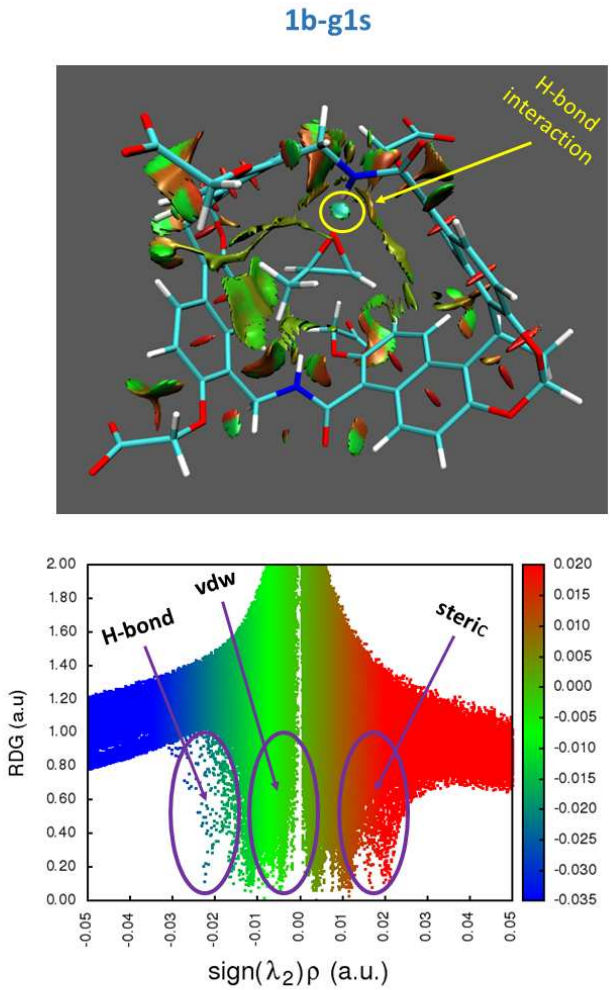

Figure 2-9. *Color-filled RDG isosurface delimitate noncovalent interaction (NCI) regions in 1b-g1s system. The vertical axis of this plot is reduced density gradient (RDG) and the horizontal axis is the sign of the second largest eigenvalue of electron density Hessian matrix at position 'r' (sign(λ_2)ρ).*

The host-guest gas-phase optimized structure from M06-2X/6-31G(d,p) level of theory is used. The default isosurface value of this scatter map (color-filled isosurface chart) is 0.5, and the default color is between -0.035 and 0.020. It is a meaningful way of classifying and visualizing weak interactions. The strong repulsive nonbonded steric interaction appears in red, attractive hydrogen bonding and van der Waals interactions are in blue and green colors, respectively. The analysis is done with the help of Multiwfn software [122, 123]. Weak nonbonded interaction isosurface and the 2D plot for the 1b-g1s system are shown in Figure 2-9, and the same for every other system are similar as of this, thus, these are not shown here. Repulsive (red) interactions for each system are for individual intramolecular steric repulsion in the host and guest molecule not due to intermolecular host-guest steric interaction. From Figure 2-9, it is clear that van der Waals and hydrogen bonding interactions are the main stabilizing factors in these host-guest complexes. van der Waals interaction is the prominent contributor to the stability of these complexes. Hydrogen bonding is also a stabilizing factor, but not as much prominent as van der Waals interaction.

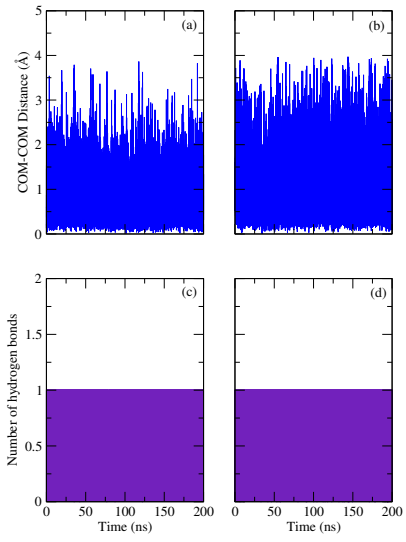

Figure 2-10. *Host-guest center of mass (COM) - center of mass (COM) distance and host-guest hydrogen bonds as a function of simulation time. (a) and (b) are for COM-COM distance for system 1a-g1r and 1b-g1r, respectively. (c) and (d) are the host-guest hydrogen bond values for system 1a-g1r and 1b-g1r, respectively.*

Now before summarizing the results of this study, we are interested to see the production phase of the MD simulations (200 ns) long enough to provide a good sampling of the conformational space of these systems or not? For the same, we have analyzed the host-guest center of mass (COM)-center of mass (COM) distance and host-guest hydrogen bonds (for systems 1a-g1r and 1b-g1r) with simulation time, and these are plotted in the Figure 2-10. From the COM-COM distances between host and guest (Figure 2-10(a) and (b)), it is clear that this distance remains essentially unchanged until the end of the simulation. Also, the host-guest hydrogen bonds (Figure 2-10(c) and (d)) remains constant throughout the trajectories. Thus, from here, we can say that the 200 ns production phase for these systems is long enough to provide a good sampling of the conformational space.

■ SUMMARY AND CONCLUSIONS

We have shown a fundamental mechanism of the possibility of how can the epoxide enantiomers be separated by synthetic macrocyclic receptors (endo-functionalized molecular tube (host-1a and host-1b)) in water by classical molecular dynamics simulation. The present study showcases with atomistic details of the main stabilizing factors in these recognition processes, structural stability of molecular tubes in water, and how we can use these molecular tubes as a CSP in chiral chromatography. Moreover, representative snapshots of all host-guest complexes give us the preliminary indication of the recognition of a particular epoxide enantiomer by the endo-functionalized molecular tubes. Our results show that every guest-induced receptor gets a more symmetrical structure compared to the host molecule devoid of any guest molecule. Thus, the inclusion of guests into the host cavity provides more structural stability to endo-functionalized molecular tube molecules and facilitates the recognition of epoxide enantiomers into its cavity. Different types of hydrogen bond analyses provide direct proof of the stability of these host-guest complexes. The host-water hydrogen bond provides indirect evidence of inclusion of guest molecules into the host cavity. The estimation of the number of hydrogen bonds between host and guest molecule gives a direct proof of inclusion of guest molecule into the host cavity and nearly one hydrogen bond is formed for every host-guest complex in which the acceptor 'N-H' protons of host molecules and donor 'O' atom of the epoxides are involved. The two 'N-H' protons of a host molecule form an almost equal number of hydrogen bonds with the guest 'O' atom, this indicates every guest molecule is movable into the host cavity and changes the position of its donor site into the host cavity. Binding free energy of host-guest complexes is determined by using the MM-PBSA method, as this method gives the bind-

ing free energy value that resembles the experimental binding free energy values. A strong and stable host-guest complexation between host endo-functionalized molecular tube and enantiomeric epoxide guest molecules are formed. This result also suggests that host-guest hydrophobic interaction is the main contributing factor along with hydrogen bonding interaction for the complexation process. Also, all of these complexation processes are enthalpy driven. Quantum chemical calculations also establish the fact that host-guest hydrophobic interaction is the main stabilizing factor along with a small contribution of hydrogen bonding interaction for these host-guest complexes. A biased sampling technique, such as umbrella sampling simulation, also provides information in support of stable host-guest complexes.

In this work, we have also analyzed the structure and energetics of chiral separation of some epoxide enantiomers by endo-functionalized molecular tubes. Our results imply that for small epoxide enantiomers (i.e., guest molecules which have less amount of hydrophobic surface area) is not possible to precisely separate by the host molecular tubes, but for the guests with a high amount of surface area (i.e., guests g5 and g6), these epoxide enantiomers may be separable by using these endo-functionalized molecular tubes in aqueous medium. Thus, in the chiral chromatography technique, these water-soluble endo-functionalized molecular tubes may be used as CSP in the separation of epoxide enantiomers having relatively sizeable hydrophobic surface area.

With the help of this study using these endo-functionalized molecular tubes, we may hope to open a vast range of application in enantiomeric separation field along with these epoxide enantiomers, taking advantage of their cavities having both the hydrophobic and hydrophilic part, recognize the guest molecule having both hydrophobic and hydrophilic portion, therefore, may be an excellent pole star for several enantiomeric separations.

Chapter 3

Stereoselective binding of peptides from aqueous medium with endo-functionalized molecular tubes

"I don't believe you have to be better than everybody else. I believe you have to be better than you ever thought you could be."

– Ken Venturi

Overview: The need to obtain enantiomerically pure isomers of amino acids and peptides is often realized in the field of biology and in the pharmaceutical industries. Research is underway to devise simple methods for the chiral resolution of amino acids from their racemic mixtures. Inspired from this objective, in our present work, we have computationally shown the possibility of chiral separation for the enantiomeric pairs of the two model peptides, namely, (d, l)-asparagine and (d, l)-phenylalanine in presence of water. For this purpose, we have used two synthetic supramolecular receptors named as host-1a and host-1b, respectively. Molecular dynamics simulation and quantum chemical methods are employed to analyze the structural features and the energy aspects involved in the separation process. The information obtained at the molecular level helps us gain better insights into the key interactions that operate to produce such enantioselectivity. We have also investigated the dynamics and changes in the water structure in vicinity of the host molecules, both in presence and absence of the model peptides. d- and l- isomers of the same peptide undergoes complexation with a particular host molecule registering a difference of more than 1 kcal/mole (obtained from PMF and MM-PBSA analyses) in their respective energies. This indicates that the chiral separation of the peptides with the help of these endo-functionalized molecular tube receptors may be energetically feasible. The connection between peptide stereochemistry and its interaction with the endo-functionalized hosts would be instrumental in designing novel segregation techniques that can be further extended to conformationally separate larger model peptides or proteins.

■ INTRODUCTION

Inspired from the chiral separation properties of organic epoxides (Chapter 2), we are now interested to see the stereoselective binding of peptides using these receptors (host-1a and host-1b, Figure 1-4 of Chapter 1) is possible or not. Thus, in Chapter 3, we have examined the stereoselective binding of peptides from the aqueous medium with these receptors.

Enantiomeric pairs are differentiable by their optical properties. An enantiomeric duo associate with a chiral framework with various propensities [94]. Many major chiral frameworks, including amino acids, peptides, proteins, sugars, carbohydrates, and nucleic acids are present in the human body. Drug molecules having these macromolecules as potential targets in their therapeutic pathway often show the expected biological activity in one of its enantiomers while its counterpart may demonstrate zero biological activity and can even be potentially harmful (unintentional adverse effects to the human body) [95]. The significance of a particular enantiomer in a pair is often recognized in numerous fields, including analytical chemistry, synthetic chemistry, medicinal science, forensic toxicology, food processing, agrochemicals, etc [95, 98]. Chiral molecules obtained with high optical purity are preferentially administered to patients to improve diagnostic efficiency. The synthesis as well as the separation of a single enantiomer of a compound is, therefore, the central concern for synthetic chemists [97]. The foundation of the pharmaceutical and biomedical industry lies in the synthesis and purification of chiral molecules [99]. Because of enantiomer‘s similar physical and chemical properties in an achiral environment, conventional separation techniques namely, chromatography, isolation and liquid-liquid extraction (these practices are mostly rely on the boiling point discrepancies or solubilities) are usually less effective [100, 101]. Various chiral filtering techniques such as gas chromatography (GC), high-performance liquid chromatography (HPLC), and capillary electrophoresis (CE) have been employed in recent times [100, 101]. Separation is essentially regulated by analyte contact with both the mobile and stationary phases of the system in these chromatographic procedures [102]. Cost effective and enhanced separation techniques involve the usage of a chiral component constituting the chiral stationary phase (CSP). The formulation of novel CSPs with significant separation abilities is the central problem posed in such separation techniques. Numerous supramolecular receptor-based CSPs have been explored recently for enantiomeric differentiation, including proteins, macrocyclic antibiotics, polysaccharides, crown ether, cyclodextrin, calixarene, and synthetic polymers [97].

Molecular recognition forms the fundamental basis for such methods of separation [101]. Izatt et al. [124] proposed some guidelines for effective enantiomeric separations with the help of chiral macrocyclic receptors. The rules are delineated as follows: (i) The macrocycles must form stable complexes with the guest enantiomers wherein repulsive interaction of one enantiomer with the host as compared to the other will dictate the desired stability; (ii) Structural complementarity of macrocycles and enantiomers determine the height of the chiral barrier; (iii) Higher the chiral barrier more efficient will be the chiral separation; and (iv) In case of strong enantiomeric recognition, lower conformational mobility of the complexes plays an important role. Two considerations viz., rigid macrocycles and interactions of multiple points guarantee a fixed dynamic structure. Keeping these rules in mind, one can identify the credibility of a synthetic macrocyclic receptor in the chiral recognition process. Enantiomeric recognition forms the basis of operation for innumerable classes of biomolecules. For example, their ability to differentiate between enantiomers in reaction catalysis is a feature of many enzyme systems. In living systems, recognition of chiral amine and protonated amine compounds are important as these act as precursors in numerous processes. Amino acids are major components of proteins, and their dynamic ability to influence complexes with several molecules provides different modes of interaction. Asymmetric sites in enzymes interact with the members of a substrates' enantiomeric pair at varying rates and different free energy values. In designing new asymmetric synthesis methods and chromatographic separation of enantiomers, a deeper understanding of the interactions in chiral recognition is useful. Chromatographic processes, capillary zone electrophoresis, and other techniques have shown the high performance of chiral macrocyclic compounds in enantiomeric separations. The resolved enantiomers include amino acids, different peptides, tocainides, racemic drugs, different amino derivatives, and other substances [124]. The study of chiral recognition of amino acids by bisnaphthalene containing macrocycles was carried out by Cram and his coworkers [15, 125, 126]. There exist reported instances of synthetic macrocycles that can selectively recognize chiral amines or peptides [127–132]. CSPs interact with different isomers with varying degrees of interaction. Owing to their exceptional selectivity for target molecules, this chiral separation procedure based on molecular recognition has gained considerable interest [102]. Receptors that are soluble and stable in water can be effectively used as a CSP. Enantioselectivity of chromatographic separation is determined by the difference in the Gibbs free energy change of the complexation of the two enantiomers. Thus, molecular insight into enantiomeric recognition would facilitate the quantification of chiral resolution in solutions as

well as provide novel ideas for designing new and more efficient macrocyclic systems.

In this chapter we have focused on the stereoselective binding of model peptides from the aqueous medium using two synthetic receptor molecules. These two receptors are designated as host-1a (syn) and host-1b (anti), known as endo-functionalized molecular tube (Figure 1-4 of Chapter 1). We have restricted our chiral resolution studies to aqueous solutions, in particular, as common practical problems often involve water as the solvent medium. d- and l- isomers of two peptides are used for this work. These peptides are d-asparagine (dasn), l-asparagine (lasn), d-phenylalanine (dphe) and l-phenylalanine (lphe). All the peptides are shown in Figure 3-1. We have employed an all-atom molecular dynamics (MD) simulation and quantum chemical analyses to explore the structural and energetic aspects of this chiral separation of model peptide molecules. In our present work we have reported this separation process of model chiral peptides by the said receptors following the work of Ruiz-Lòpez *et al.* [120]. It would be interesting to see how the host-guest encapsulation phenomenon perturbs the structural as well as dynamical aspects of water molecules in the domain of the first solvation shell of the host molecule. Microscopic details about the selectivity in the chiral recognition process can be inferred from such studies. The dynamics of water molecules in the vicinity of a macromolecule have been studied extensively in numerous micellar and cyclodextrin systems [133–138] but to the best of our knowledge no such insight is available for our systems of interest.

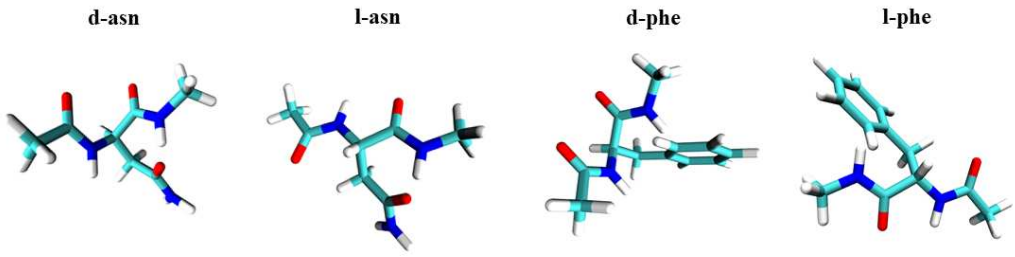

Figure 3-1. *Licorice representation of every chiral peptide used in this work.*

The remaining chapter is subdivided into three parts. 'COMPUTATIONAL DETAILS' section comprises of detailed description of the parameters and conditions used for the molecular dynamics simulation run. The results of the analyses carried out have been delineated and discussed in 'RESULTS AND DISCUSSIONS' section and the conclusions drawn from the work are summed up in 'SUMMARY AND CONCLUSIONS' section.

■ COMPUTATIONAL DETAILS

We outline the computational methodology that we adopted to evaluate the structure and energetics of different host-peptide complexes as well as to probe the local dynamics of water molecules in the vicinity of the host molecule. Here, we are interested to see the feasibility of chiral separation of model peptides by supramolecular receptors, host-1a and host-1b, in explicit water. We have employed atomistic molecular dynamics (MD) simulation and quantum mechanical calculations for the purpose. d- and l- isomers of two representative peptides from two different categories of amino acids (aa) are used for this work. These peptides are d-asparagine (dasn) and l-asparagine (lasn), from the the neutral but polar aa category and the aromatic aa represented by d-phenylalanine (dphe) and l-phenylalanine (lphe). The N-terminal and C-terminal of these aa were capped with acetyl (CH_3CO) and N-methyl ($NHCH_3$) group respectively, with the help of the LEaP module of AMBER14 [63] MD simulation package. AMBER ff14SB [139] force field was used for all the peptides. Optimization of the host molecules (host-1a and host-1b) and the ammonium ion are done with an HF/6-31+G** basis set of Gaussian09 [106] package. The RESP (restrained electrostatic potential) [67] module of AMBER14 computes the partial charges present at the atomic sites for the two host molecules and the ammonium ion. These partial charges for both the receptor molecules are detailed in Chapter 2 (Tables 2-1 and 2-2). The general AMBER force field (GAFF) [108] was used for modelling these two molecules and the ANTECHAMBER [107] program of AMBER14 was used to extract the force field parameters. The host molecules host-1a and host-1b carry four units of negative charge each and are neutralized by the same number of ammonium ions [105]. The three-point transferable interaction potential (TIP3P) water [72] model was used as an explicit solvent medium. 14 systems were prepared for this work, and specifics of these systems are listed in Table 3-1. Systems suffixed with 'ran' were created by randomly packing the model peptide molecule inside the simulation box and the ones without the 'ran' term were created with the model peptide molecule placed inside the cavity of the host. The PACKMOL [74] program was used for initial packing of the systems with a tolerance value of 2.0 Å . The parameters and the starting coordinates of these packed systems were prepared with the LEaP module of AMBER14, and the generated configurations were simulated with the sander implementation of AMBER14. A cubic simulation box with periodic boundary conditions (PBC) in all three directions were applied for each of the simulations. Constraint on every hydrogen containing covalent bond was ensured by applying the SHAKE

algorithm [71] with a tolerance value of 0.00001. A 10 Å cut-off distance was chosen for reckoning the short-range nonbonded interactions. For the long-range electrostatic interactions, the Particle Mesh Ewald (PME) [73] method was utilized. A time interval of 2 fs was allowed for the evaluation of equations of motion for the systems. An initial 10000 steps of energy minimization (among which initial 4000 steps are in steepest descent method and conjugate gradient method for the last 6000 steps) were performed for every simulation to eliminate erroneous contacts among the atoms in the systems. All the systems were then subjected to heating in a canonical (NVT) ensemble from 0 to 298 K for 320 ps.

Table 3-1. Overview of systems[a]

System	N_{host}	$N_{NH_4^+}$	N_{pep}	N_{wat}	Box volume (nm^3)	M_{host} (M)
1a	1	4	0	2280	70.58	0.0235
1a-dasn	1	4	1	2278	70.47	0.0236
1a-lasn	1	4	1	2279	70.48	0.0236
1a-dphe	1	4	1	2279	70.65	0.0235
1a-lphe	1	4	1	2279	70.77	0.0235
1b	1	4	0	2321	71.43	0.0232
1b-dasn	1	4	1	2320	71.69	0.0231
1b-lasn	1	4	1	2318	72.00	0.0230
1b-dphe	1	4	1	2319	71.72	0.0231
1b-lphe	1	4	1	2319	71.98	0.0230
1a-dasn-ran	1	4	1	5535	169.13	0.0098
1a-lphe-ran	1	4	1	5832	178.34	0.0093
1b-lasn-ran	1	4	1	5543	169.77	0.0098
1b-dphe-ran	1	4	1	5833	178.15	0.0093

[a] Specifics of all the systems for normal MD simulation. N_{host}, $N_{NH_4^+}$, N_{pep}, and N_{wat} represent the numbers of the host molecules, ammonium ions, peptide, and water molecules, respectively. M_{host} designates the concentration of the host molecules expressed in molarity. 1a and 1b are the host-1a and host-1b, respectively. 1a-dasn, 1b-lphe, etc., are the systems having dasn, lphe, etc., as the model peptides and the receptors are host-1a and host-1b respectively. Systems 1a and 1b are pure host-water systems without any peptide molecule. Systems with 'ran' term are created by randomly packing the peptide molecule inside the simulation box and systems without 'ran' term has the peptide initially packed inside the host molecules' cavity.

Following the heating step, equilibration of every simulation for 5 ns (at 298 K and 1 atm temperature and pressure, respectively) was attained in the isothermal-isobaric (NPT) ensemble. The temperature and pressure were retained by using the Berendsen barostat [75] with 2 ps pressure relaxation time and the Langevin thermostat [76] with 1 ps^{-1} collision frequency, respectively. 200 ns NPT production run was accomplished for every system mentioned in Table 3-1.

To gain insight into the dynamics and structural aspects of water molecules at the host surface, we have arbitrarily chosen the host-1b and four of its representative host-peptide systems, namely, 1b-dphe, 1b-lphe, 1b-dasn, and 1b-lasn for further analysis. The final configuration for all of these systems at the end of the previous (NPT) run were equilibrated for 10 ns under NVT to fix the volume of the individual boxes as mentioned in Table 3-1. The equilibrated systems were then subjected to a production in a micro-canonical ensemble (NVE) for an additional 50 ns with integration time step of 1 fs. Coordinate resetting while using SHAKE algorithm was made stringent with a reduced tolerance value of 5×10^{-7} to minimize the temperature drift of the systems during the constant energy run. The temperature attained by the systems 1b, 1b-dphe, 1b-lphe, 1b-dasn and 1b-lasn during the NVE production phase were 297.0 (± 0.1), 296.2 (± 0.4), 296.7 (± 0.2), 295.9 (± 0.5), and 297.0 (± 0.3), respectively. The coordinates of the system during production run were recorded with a time interval of 400 fs. Sections of the trajectory were obtained with an increased time resolution of 16 fs for evaluating the ultrafast dynamics of the system.

Around 12 μs of total production run was performed for this work. CPPTRAJ program [77] of AMBER14, codes written in FORTRAN 95 standard and Visual Molecular Dynamics (VMD) [78] package were used for analysis and visualization of the obtained simulation trajectories.

Binding free energy (ΔG^0_{bind}) of the host-guest complexes are calculated by using the Molecular Mechanics-Poisson Boltzmann Surface Area (MM-PBSA) [79, 80] method. Details of this method are discussed in the 'METHODOLOGY' section of Chapter 1 (Eq. 1.18). The potential of mean force (PMF) of these host-guest complexes are also analyzed, and details of this method are discussed in the 'METHODOLOGY' section of Chapter 1 (Eq. 1.24).

■ RESULTS AND DISCUSSIONS

In this present work, our main target is to find the probability of stable complex formation and the feasibility of chiral separation of model d- and l-peptides with endo-functionalized molecular tube receptors in aqueous medium. Systems without the 'ran' term are the principle systems and the ones suffixed 'ran' are considered for supporting evidences. We will try to establish our target by using the main systems. Supporting systems are merely used to check whether a randomly packed peptide is automatically inserted into the host cavity or not. For every reference made to the supporting systems, we have specified the word 'ran'; otherwise, 'system' indicates the main systems only.

Snapshots (taken from the last frame of the MD simulation trajectories) of peptide-host complexes for each system are presented in Figure 3-2.

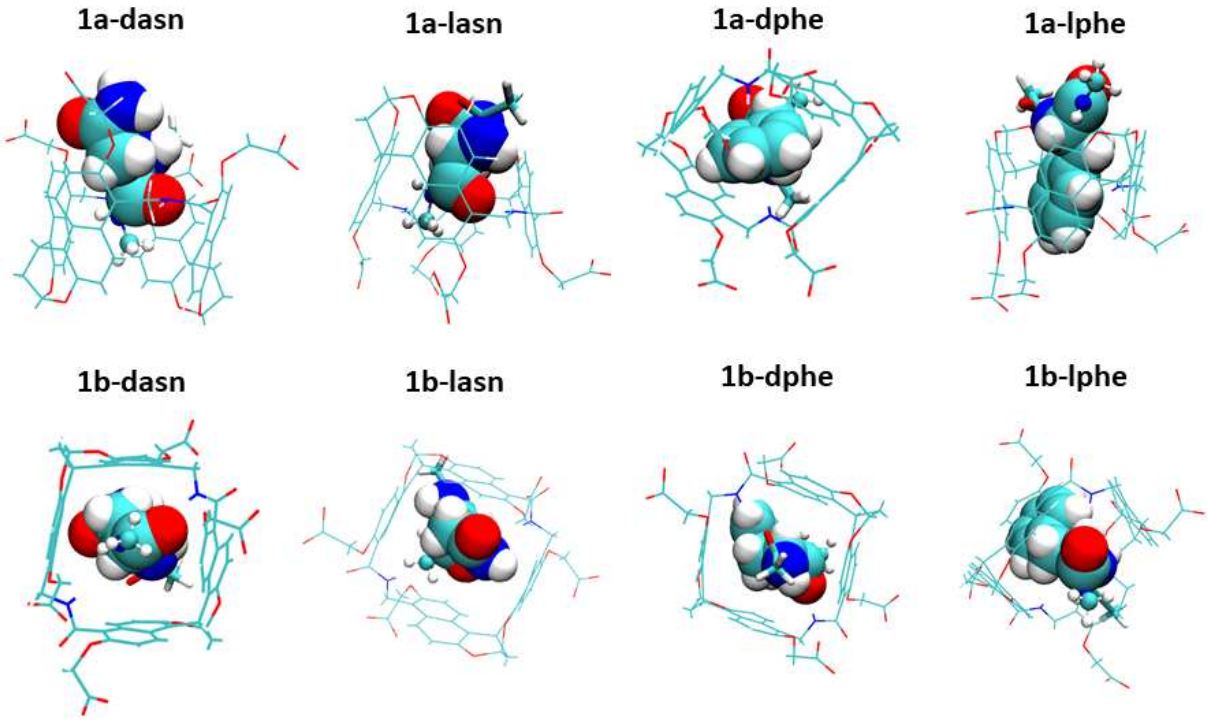

Figure 3-2. *Representative host-peptide complex snapshots of all the fixed systems. Only host and peptide molecules are presented in every snapshot to amplify the clarity of the image.*

From these snapshots, we get a preliminary idea of how these complexes are formed. Every peptide is fully inserted into the host cavity. Every hydrogen bond donor and acceptor are positioned for favorable hydrogen bond interaction with the peptides. Hydrophobic parts of these peptides achieve stability through interaction with the hydrophobic core of these host molecules. From here on, we discuss in detail every structural and energetic aspect of these peptide-host complexes.

Structural Analysis

At first, we will analyze the structural features of host-1a and host-1b with and without the guest molecule in its cavity. We have envisaged two internal diameters for the purpose. These diameters are formed by imaginarily linking two opposite atoms of the host and are marked as diameter-I and diameter-II. The internal diameters of host-1a and host-1b are schematically represented in Chapter 2 (Figure 2-3). In host-1a, diameter-I is considered as the distance between C10 and C64 and diameter-II is the distance between C47 with C71. C15-C74 and C53-C96 atom couples are defined as diameter-I and diameter-II in case of host-1b. The value for diameter-I is higher than diameter-II owing to the non-spherical structure of the host molecules under consideration. Table 3-2 consists of the average values of both the diameters, the absolute difference (Ad) between them and the standard error values of Ad (calculated by block averaging method) for all the systems.

Table 3-2. Average internal diameters[a]

System	Aid-I (Å)	Aid-II (Å)	Ad (Å)	Se (Å)
1a	10.98	9.40	1.58	± 0.0064
1a-dasn	11.34	9.52	1.82	± 0.0500
1a-lasn	11.48	9.44	2.04	± 0.2112
1a-dphe	11.47	9.49	1.98	± 0.1021
1a-lphe	11.49	9.51	1.98	± 0.2306
1b	13.13	9.66	3.51	± 0.0012
1b-dasn	13.05	9.78	3.27	± 0.0277
1b-lasn	13.08	9.77	3.31	± 0.0408
1b-dphe	13.03	9.84	3.19	± 0.0014
1b-lphe	13.08	9.85	3.23	± 0.0430

[a] The internal diameter-I (Aid-I), internal diameter-II (Aid-II), the absolute difference (Ad) of these two diameters, and the standard errors (Se) (estimated by block averaging method) of Ad for the host-1a and host-1b of every system are presented here.

For host-1a, the values of both the diameters increase with respect to the corresponding diameter value of the system without any guest molecule. But for host-1b, a minimal decrease of diameter-I value and increase of diameter-II value are observed compared to the 1b system. Thus, the Ad values of every guest containing host-1a are increased, and host-1b is decreased compared to the corresponding guest devoid systems. Size, shape and different complexation properties of the different host and guest molecules are mainly responsible for the distinct trends in diameter value change. To delve deeper into the non-identical trends in diameter change as exhibited by the two hosts, we have computed the

probability distribution functions of Ad for the systems under study. These are presented in Figures 3-3 and 3-4 for host-1a and host-1b containing systems, respectively. Ad value as a function of simulation time is also plotted at the insets of these plots. For systems 1a and 1b, the maximum probability of Ad appears at 1.50 Å and 3.50 Å , respectively.

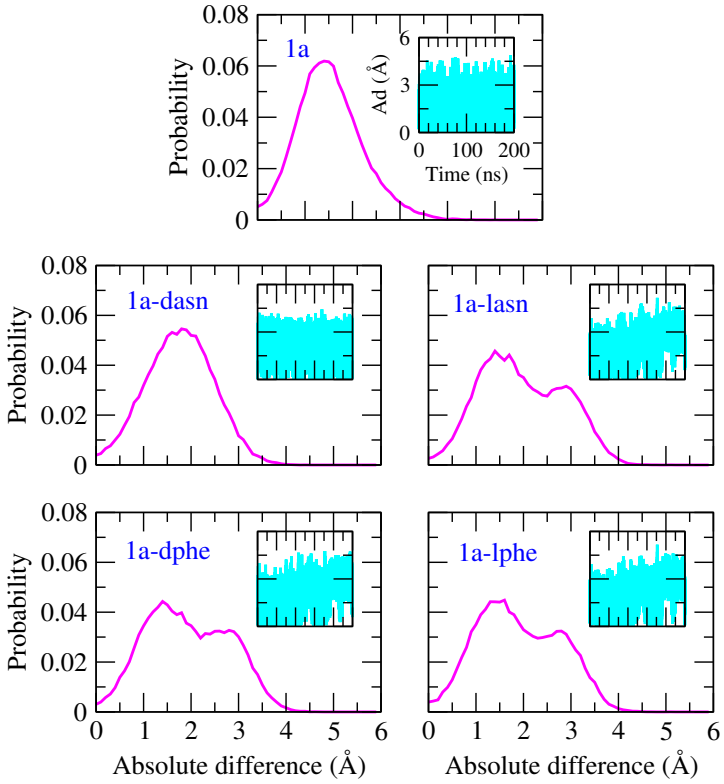

Figure 3-3. *The probability distributions of the absolute difference (Ad) between two internal host-1a diameters for different systems. Ad values are also represented in insets as a function of the simulation time.*

The distance at which maximum probability occurs is higher for host-1a and lower for host-1b compared to the systems in absence of the guest peptides. This inspection implies increased sampling of a less symmetric structure than free host-1a upon inclusion of guest molecules into the host cavity and increased sampling of a more symmetric structure than the free host-1b upon inclusion of guest molecules into the host cavity. From this analysis,

it is somewhat obvious that each host molecule becomes structurally more stable following the inclusion of peptides into their cavities.

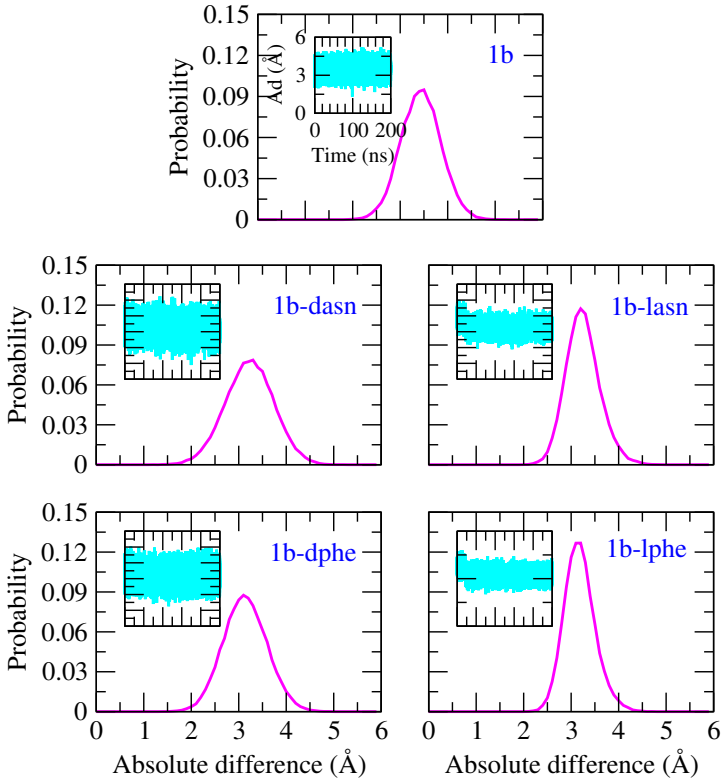

Figure 3-4. *The probability distribution of absolute difference (Ad) between two internal host-1b diameters for different systems. Ad values are also presented in insets as a function of the simulation time.*

In order to ensure good enantiomeric recognition, the low conformational flexibility of receptors plays an important function. Two factors, rigid macrocycles and multipoint interactions, ensure a fixed conformation of the complex [124]. To check the conformational flexibility of the receptor, we have calculated the root mean square deviation (RMSD) of the host molecule with respect to the initial structure for all the systems. These RMSD values for every system as a function of simulation time are plotted in Figure 3-5. Every RMSD value is within 1.5 Å. From these RMSD values, it is clear that for every host-peptide complex, each host molecule is conformationally stable and less flexible, and the

complex stability remains intact during simulation. So, according to Izatt et al. [124], we can say that these two receptors may be explored further for stereoselective binding of peptides from the aqueous medium.

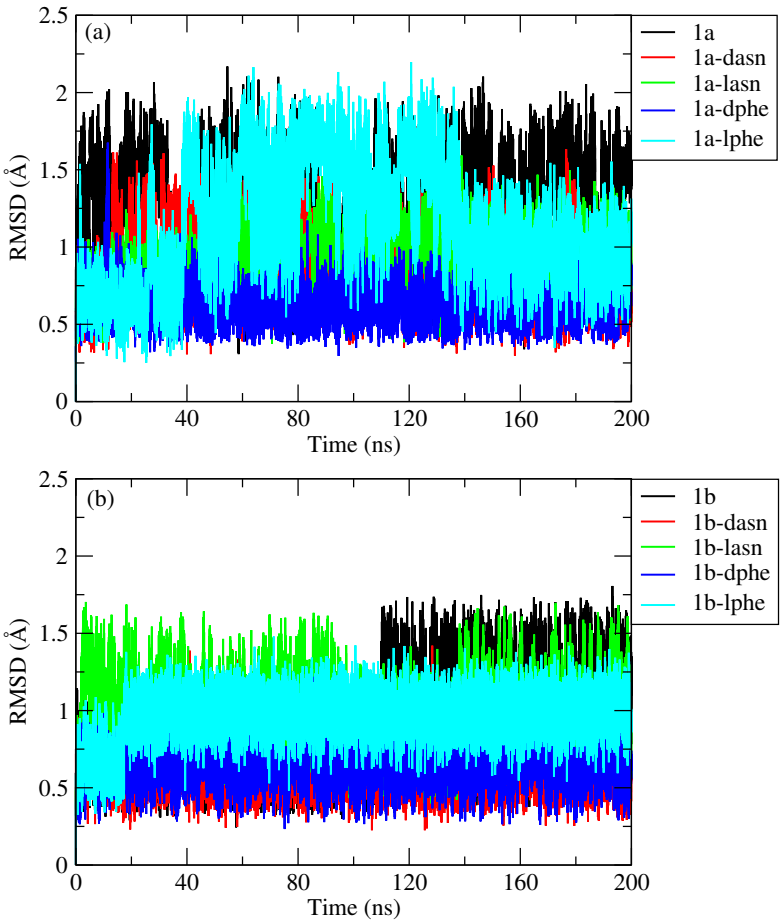

Figure 3-5. *The root means square deviation (RMSD) values of the receptor for every system as a function of simulation time is plotted here.*

Determination of Hydrogen Bonds

Hydrogen Bond Properties

From the snapshots, we are aware of the formation of encapsulation complexes

between endo-functionalized molecular tubes and model peptides. In this section, we will focus on how different types of hydrogen bonds helps to stabilize these complexes. We have categorized and calculated the hydrogen bonds as those between (i) host-water (HW), (ii) different atomic sites of host and water, (iii) host-peptide (HP), and (iv) different atomic sites of host and peptide for this purpose. To compute the number of hydrogen bonds, we have adhered to the geometric conditions accepted widely in previous works [109–115]. The cut-off distance (r_c) for donor-acceptor pair was chosen as, $r_c \leq 3.4$ Å , and the angle (θ_c) for donor-acceptor-hydrogen was allowed for $\theta_c \leq 45^o$. These geometric criteria are schematically presented in Figure 2-6 of Chapter 2. Both the host molecules have two 'N-H' hydrogen bond donor sites. N6 and N8 for host-1a and N1 and N3 for host-1b are the corresponding donor nitrogen sites in these two hosts. The computed hydrogen bond numbers for the systems under consideration are presented in Table 3-3. Here, we shift our focus to the average number of HW and hosts' nitrogen atom-water hydrogen bonds. Systems without any guest molecules have the highest number of HW hydrogen bonds. But, with the introduction of guest molecules into the host cavity this value is decreased. This observation indicates that some hydrogen bonding sites intrinsic to the host are now involved in the formation of hydrogen bonds with the guest peptides. These sites may be the 'N-H' donor sites of host molecules. To examine this, we have calculated the number of hydrogen bonds between the hosts' donor 'N-H' and the water molecules. This value is highest for the systems without any peptide molecule and becomes almost zero for the guest containing systems. This observation indirectly proves that these sites now preferentially partake in the formation of hydrogen bonds with the peptide molecule over water molecules. Next, we discuss in detail on the total number of HP hydrogen bonds. From Table 3-3 it is evident that every guest containing system has a cabalistic amount of HP hydrogen bonds. This explains partly the formation of stable host-guest complexes. The d- and l- 'asn' peptide form the highest and the corresponding 'phe' peptide (-d and -l) form the lowest number of hydrogen bonds with the hosts-1a and 1b. We explore further the atomistic details of these host-peptide hydrogen bonds. For this purpose, we have computed the hydrogen bond values between the hosts' donor 'N-H' group (in host-1a, N6/N8-H, and host-1b, N1/N3-H) and the peptides' acceptor atoms. The overall HP hydrogen bond number is the summation of the host's 'N-H'-peptide hydrogen bonds except for the 'asn' chiral isomers where other groups also participate. 'phe' form hydrogen bonds with almost exclusively with the host's 'N-H' donor sites. Some donor sites of 'asn' form hydrogen bonds with the hosts' side chain acceptor 'O' atoms. That is why these 'asn'

complexes show the highest number of hydrogen bonds with the host molecules. All the 'asn' complexes form an almost similar number of hydrogen bonds with both the nitrogen donor sites. But, 'phe' complexes form entirely all the hydrogen bonds with one nitrogen donor and zero with the other. This observation indicates that 'asn' can move inside the host cavity forming hydrogen bond with one site while simultaneously leaving the other site. The 'phe' molecule is somewhat restricted inside both the host molecules. Thus, it is now evident that hydrogen bonds between the guest-host duo play a key role in the encapsulation and stabilization of guest model peptides inside the cavity of the host.

Table 3-3. Hydrogen bond numbers[a]

System	host-wat	N6/N1-wat	N8/N3-wat	host-pep	N6/N1-pep	N8/N3-pep
1a	23.70	0.49	0.48	–	–	–
1a-dasn	22.37	0.01	0.02	1.23	0.43	0.42
1a-lasn	22.00	0.02	0.02	1.02	0.39	0.41
1a-dphe	20.34	0.01	0.01	0.69	0.69	0.00
1a-lphe	22.57	0.02	0.02	0.65	0.61	0.04
1b	23.99	0.76	0.84	–	–	–
1b-dasn	20.15	0.09	0.04	1.32	0.25	0.65
1b-lasn	21.17	0.04	0.05	1.11	0.45	0.40
1b-dphe	20.63	0.03	0.01	0.84	0.84	0.00
1b-lphe	22.25	0.01	0.01	0.84	0.78	0.06

[a] The values for the number of hydrogen bonds formed between the host molecules and water (host-wat), N6 atom of host-1a/N1 atom of host-1b with water (N6/N1-wat), N8 atom of host-1a/N3 atom of host-1b with water (N8/N3-water), host and peptide (host-pep), N6 atom of host-1a/N1 atom of host-1b with the peptides (N6/N1-pep), N8 atom of host-1a/N3 atom of host-1b with peptides(N8/N3-pep) for all the studied systems are depicted in this table.

Distribution of Water-Water Hydrogen Bonds

To understand the stabilizing role of hydrogen bonds in the event of host-guest complexation, it is important to investigate the distribution of water-water (WW) hydrogen bonds in the vicinity of the host and the host-guest complexes. The extensive hydrogen bond network, characteristic of pure water, is perturbed in presence of electrolytes [140–142], and macromolecules like micelles [143, 144], proteins [145], etc, having hydrogen bond donors and acceptors on their surface. The changes in the tetrahedral environment around each water molecule, induced by the macromolecule, reveal microscopic details about structural phenomenon occurring in the system. Here we study in detail the probability of a water molecule hydrogen bonded to 'n' neighboring water molecules (where

n = 1, 2, $\cdots$, 6) in pure TIP3P water system and for the systems 1b, 1b-dphe, 1b-lphe, 1b-dasn and 1b-lasn. The selectivity in the complexation process influenced by the dissimilar hydrogen bonding tendencies between the host and the different guests would reflect on HW hydrogen bond interactions. This, in turn, would change the WW hydrogen bonding pattern in the vicinity of the complexes.

For consideration of WW hydrogen bond, we adopt a geometric criteria reported for standard TIP3P model of water [146]. According to this criteria, two water molecules are considered hydrogen-bonded if the oxygen-oxygen distance, $r_{O\text{-}O}$, is less than 3.55 Å , the oxygen-hydrogen, $r_{O\text{-}H}$, bond distance is less than 2.45 Å and the oxygen-oxygen-hydrogen angle, $\theta_{O\text{-}O\text{-}H}$, is less than 30°. We have considered water molecules within 5 Å from the host surface in our calculations and compared the results with an independent simulation involving pure TIP3P water system under similar conditions. We ascribe this pure water system to represent the properties of the bulk as used in previous works [133]. The average number of WW hydrogen bonds $\langle n_{HB} \rangle$, per water molecule, for the different systems are calculated as:

$$\langle n_{HB} \rangle = \sum f_n \times n \tag{3.1}$$

where f_n denotes the fraction of water molecules involved in hydrogen bonding with 'n' number of water molecules. The results of the calculation are summmarised in Table 3-4.

Table 3-4. Water-water hydrogen bond distribution[a]

System	f_0	f_1	f_2	f_3	f_4	f_5	f_6	$\langle n_{HB} \rangle$
bulk	0.002	0.033	0.175	0.394	0.353	0.042	0.001	3.19
1b	0.006	0.069	0.253	0.391	0.253	0.027	0.000	2.89
1b-dasn	0.006	0.067	0.247	0.395	0.256	0.028	0.000	2.91
1b-lasn	0.006	0.070	0.254	0.391	0.252	0.027	0.000	2.90
1b-dphe	0.005	0.065	0.246	0.396	0.260	0.028	0.000	2.93
1b-lphe	0.005	0.067	0.250	0.393	0.257	0.027	0.000	2.91

[a] The water-water hydrogen bond distribution and the average number of hydrogen bonds per water molecule, $\langle n_{HB} \rangle$, within 5.0 Å from the surface for all the systems are presented here. The data for bulk is included for comparison.

From Figure 3-6 it is evident, that the presence of the host molecule modifies the WW hydrogen bonding pattern in its proximity. The probability distribution is skewed towards higher coordination numbers (n = 3, 4) for bulk water with $\langle n_{HB} \rangle$ per water molecule close to 3.2. The average value in the bulk agrees well with the value reported for standard TIP3P water in the literature [146]. In presence of the host-guest systems,

a spread in the distribution occurs with increasing weightage for the lower coordination numbers and subsequent decrease for the higher 'n' values.

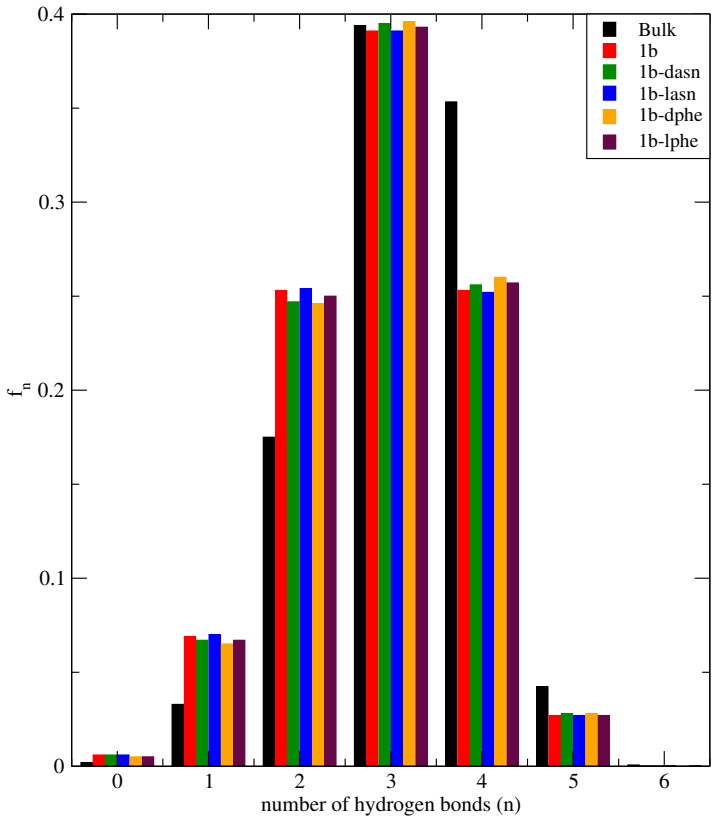

Figure 3-6. *The probability (f_n) of water molecules involved in hydrogen bonding with n number of water molecules for the systems 1b, 1b-dphe, 1b-lphe, 1b-dasn and 1b-lasn is presented in the form of a histogram here. The data for bulk is included for comparison.*

This results in an overall decline in $\langle n_{HB} \rangle$ within 5 Å from the surface for the systems under consideration, compared to that of bulk water. The presence of hydrogen bond donors and acceptors on the surface of the receptor 1b (forming HW bonds) that provide alternative sites of hydrogen bonding to the water molecules in their vicinity that explains this gross trend in the WW hydrogen bond data. The HW hydrogen bond data has been previously mentioned in Table 3-3. In absence of any guest peptide the hydrogen bonding sites for the host-1b are fully available to the nearby water molecules and shows a drop of 8.9% in the WW hydrogen bond value. With the introduction of the guest peptides into

the host cavity, there is no significant change in the WW hydrogen bond pattern near the host-peptide surface for all the systems.

Dynamical Analysis of Hydration Water

Translational Diffusion of Hydration Water Molecules

The dynamics of water in the hydration shell of cyclodextrin systems have been explored by Bandhopadhyay et al. [137]. Prior to this work, Nandi and Bagchi proposed the molecular hydrodynamics theory (MHT) and the multishell continuum model (MSCM) to explain the changes associated with coumarin entrapment inside cyclodextrin cavity [147]. In this part, we have investigated the translational diffusion of water molecules in the first hydration shell of host-1b for the systems 1b, 1b-dasn, 1b-lasn, 1b-dphe and 1b-lphe. Our aim is to study the effect of peptide encapsulation on the local dynamics of water for all the systems mentioned. We limited the hydration shell to a distance of 3.5 Å from the receptor surface based on the minima (at around 3 Å) obtained from the RDF plot between water and the host (Figure 3-7).

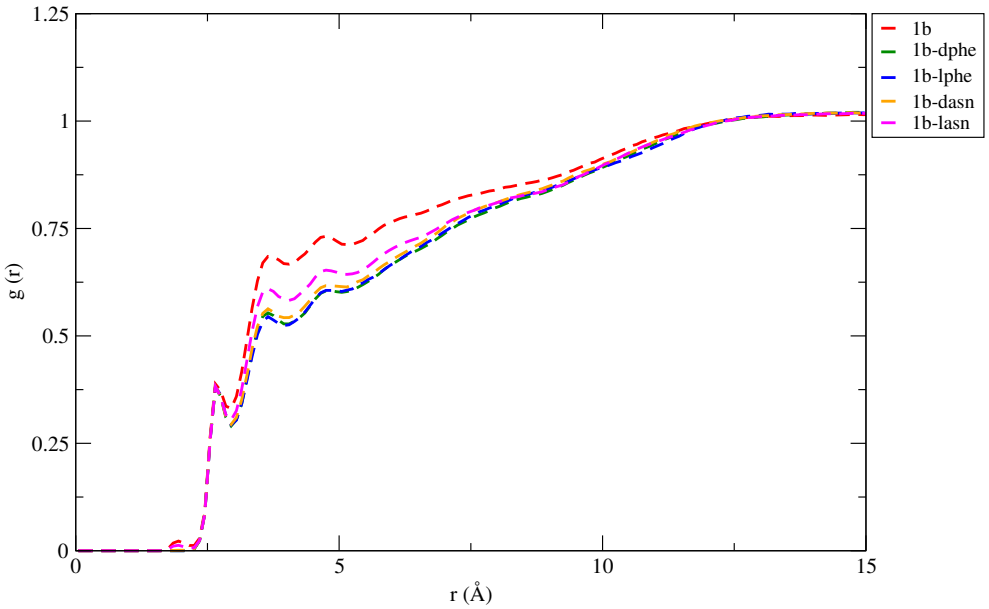

Figure 3-7. *Radial distribution function of water molecules with the surface of the host-1b for the systems 1b, 1b-dasn, 1b-lasn, 1b-dphe and 1b-lphe are represented here.*

The translational property of the water molecules is manifested in the mean squared displacement (MSD) of the water oxygen atom formulated as:

$$MSD = \left\langle |r_i(t) - r_i(0)|^2 \right\rangle \tag{3.2}$$

where $r_i(t)$ and $r_i(0)$ are the position vectors of the ith oxygen at time t = t and t = 0, respectively.

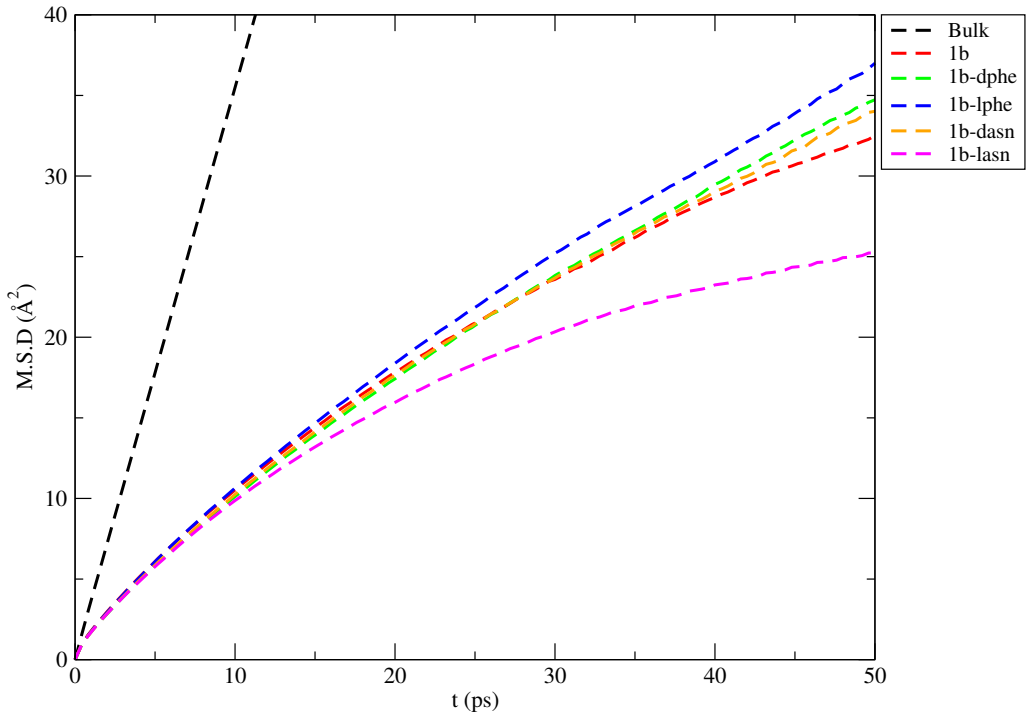

Figure 3-8. *Mean Square Displacement (MSD) of the hydration layer water for the systems 1b, 1b-dasn, 1b-lasn, 1b-dphe, and 1b-lphe is presented here. The plot for bulk water is incorporated for comparison.*

Water molecules that are present in the solvation shell at t = 0 are tagged and their trajectory is monitored with respect to time. The MSD analysis was carried out for the last 8 ns of the NVE trajectory recorded at a time interval of 400 fs and divided into multiple time origins 1.6 ps apart. At any instant of time, if a particular water molecule escapes the hydration layer then the correlation with the corresponding time origin is switched off for all the subsequent MD steps. This ensures that the contribution to MSD arises solely from the time duration during which the water molecule continuously resides inside the

solvation shell [148]. The algorithm also takes into account the re-entry of water molecules into the solvation shell to be correlated with other time origins. The trajectory of the water oxygen was unwrapped to eliminate the effects of periodic boundary condition before the MSD calculation was carried out. The diffusion coefficient (D_E) was calculated from the slope of the MSD *vs*. time plot based on Einsteins' formula

$$D_E = \lim_{\Delta t \to \infty} \frac{\langle \Delta r^2 \rangle}{2d\Delta t}, \tag{3.3}$$

where d is the dimensionality of the system. The slope of the MSD plots were calculated after linear fitting in the time range of 10 ps to 30 ps. The data for D_E is tabulated in Table 3-5 along with the corresponding correlation coefficients of the linear fit. The MSD profile for the hydration layer water are depicted in Figure 3-8.

Table 3-5. The diffusion coefficient (D_E)[a]

System	$D_E(10^{-9}m^2s^{-1})$	R^2
bulk	5.88	0.999
1b	1.08	0.998
1b-dasn	1.11	0.998
1b-lasn	0.86	0.996
1b-dphe	1.14	0.999
1b-lphe	1.20	0.999

[a] The diffusion coefficient (D_E) of hydration water for the five systems namely 1b, 1b-dphe, 1b-lphe, 1b-dasn and 1b-lasn are represented here along with the data for bulk water. The correlation coefficient (R^2) is provided to demonstrate the quality of the linear fit for the MSD plots.

The MSD for bulk water was obtained from an independent simulation of pure TIP3P water system carried out under similar conditions as that of the representative systems. The D_E value for bulk water ($5.88 \times 10^{-9}m^2s^{-1}$) is in accordance with the data cited in literature [146]. For all the systems, an initial steep increase in the MSD profile is observed for the first few picoseconds, characteristic of the ballistic motion of the water molecules in this timescale. With time, molecular collisions come into play due to which the mean squared displacement is slowed down. From Figure 3-8. it is clearly evident that the translational motion of the hydration shell water molecules is impeded in presence of the host and the host-guest systems. The restriction in mobility of the water molecules arises from their interaction with the receptor surface. The magnitude of deceleration is dependent on the nature of the system under consideration. In general, the 'phe' peptides being hydrophobic increase the diffusional motion of the water molecules in vicinity of the

host-1b. For the 'asn' peptides, the intrinsic polarity and the presence of hydrogen bonding sites on the peptide slows down the dynamics of the water molecules localized on the host surface. The host-1b in absence of the guest molecules records a diffusion coefficient value intermediate to the values of the other systems. All the systems except 1b-lasn, have greater translational freedom in the hydration water compared to 1b explained by the reduced host-water hydrogen bonding on insertion of the host. For the 'asn' peptide, the difference in the D_E values for the -d/-l pair is more prominent compared to 'phe' systems. The increased surface restriction of water for 1b-lasn can be explained by the hydrogen bonding of the nearby water with the host and the guest peptide as well as the electrostatic interaction of the peptide with water. The polar interaction being pronounced in lasn, may be indicative of the fact that it is more exposed to the solvent than its d-isomer.

Hydrogen Bond Dynamics

The changes in the WW hydrogen bonding pattern in presence of the receptor should also reflect on the dynamics and lifetime of WW hydrogen bonds in the hydration layer. Such modifications have been well explored for macromolecular systems like proteins [109, 149], electrolytes [112, 113, 141], DNA [150, 151], micelles [111, 133, 134], etc. The dynamical properties of the hydration layer WW hydrogen bonds are characterized with the help of the time correlation functions (TCFs), $C(t)$, known as intermittent hydrogen bond TCF and $S(t)$, i.e. continuous hydrogen bond correlation function $S(t)$. These functions were introduced by Stillinger [152,153] and later explored by Luzar and Chandler [154–157] and are formulated as:
Continuous hydrogen bond TCF S(t):

$$S(t) = \frac{\langle h(0)H(t)\rangle}{\langle h(0)h(0)\rangle} \tag{3.4}$$

and the intermittent hydrogen bond TCF C(t):

$$C(t) = \frac{\langle h(0)h(t)\rangle}{\langle h(0)h(0)\rangle} \tag{3.5}$$

where $h(t)$ assumes a value 1 when a particular WW pair is hydrogen bonded at time t and 0 if no hydrogen bond exists between them. The $H(t)$ function on the other hand takes a value of 1, if and only if, the WW pair remains hydrogen bonded from time $t = 0$ to $t = t$ and 0 otherwise. The definition of $S(t)$ does not allow for bond breaking in the steps between $t = 0$ to $t = t$ and is considered as a measure of the true lifetime of a hydrogen bond, that is, the time duration for which a hydrogen bond stays intact after its formation

at $t = 0$. $C(t)$ on the other hand accounts for bond breaking phenomena due to re-crossing of the energy barrier between the hydrogen bonded state and the free state as well as the diffusive nature of the water molecules and is thus a measure of the relaxation time of a hydrogen bond [112, 141]. In general, the relaxation time of a hydrogen bond is an order of magnitude higher than its lifetime [158].

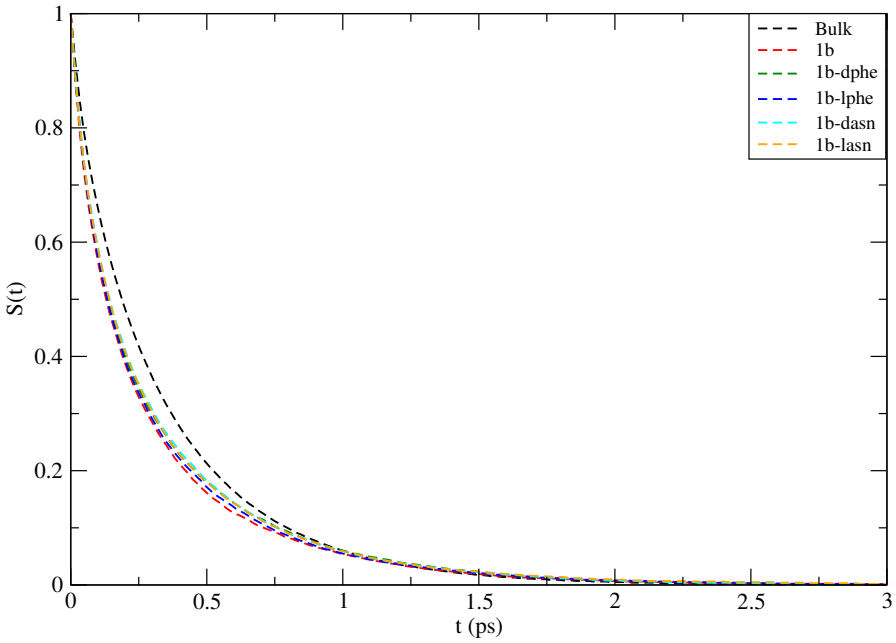

Figure 3-9. *Continuous hydrogen bond time correlation function (TCF) curves for water-water hydrogen bonding in the hydration shell of the systems 1b, 1b-dasn, 1b-lasn, 1b-dphe and 1b-lphe are represented here. The decay curve for bulk water is provided for comparison.*

In this section, we have calculated the WW hydrogen bond mean relaxation time $\langle\tau_R\rangle$ and the mean lifetime $\langle\tau_S\rangle$ for the hydration water molecules in the systems 1b, 1b-dphe, 1b-lphe, 1b-dasn, 1b-lasn and compared the values with bulk water. The results of the bulk were calculated from an independent simulation as already mentioned in the previous section. The $S(t)$ *vs.* t curves for all the systems are depicted in Figure 3-9. The lifetime values ($\langle\tau_S\rangle$) were obtained via integration of the $S(t)$ curves [141]. The mean relaxation lifetimes were obtained after tri-exponential fitting of the $C(t)$ *vs.* t decay curves shown in Figure 3-10 [159]. The data obtained from calculations are summarized in Table

3-6. The amplitude (a_i) and the decay time constants (τ_i) for the bond relaxation are given in detail in Table 3-7.

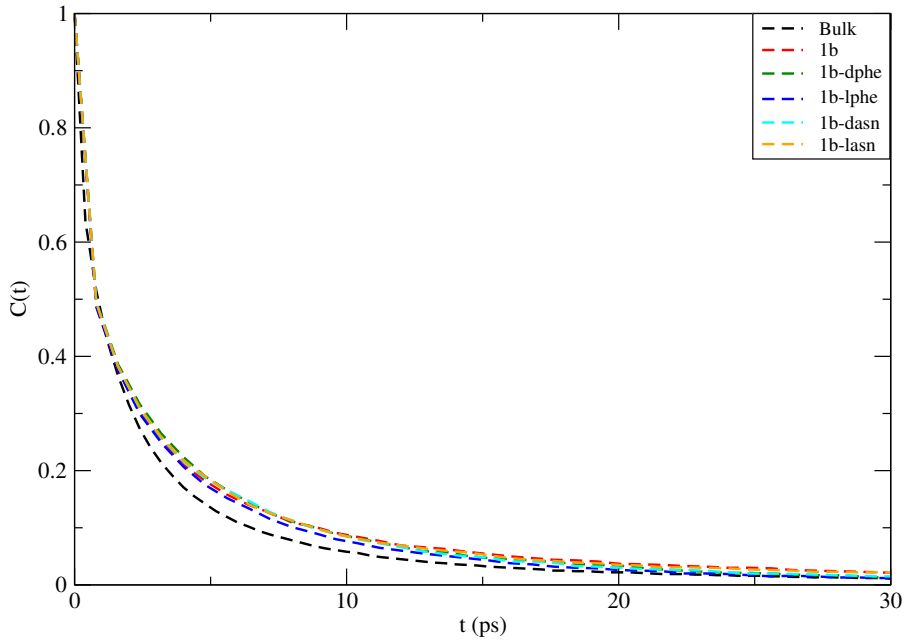

Figure 3-10. *Intermittent hydrogen bond time correlation function (TCF) curves for water-water hydrogen bonding in the hydration shell of the systems 1b, 1b-dasn, 1b-lasn, 1b-dphe and 1b-lphe are represented here. The relaxation profile for bulk water is provided for comparison.*

Table 3-6. Hydrogen bond lifetime[a]

System	$< \tau_S >$	$< \tau_R >$
bulk	0.32	2.80
1b	0.27	3.86
1b-dasn	0.29	3.42
1b-lasn	0.29	3.96
1b-dphe	0.29	3.34
1b-lphe	0.28	3.08

[a] The mean lifetime $< \tau_S >$ and the relaxation lifetime $< \tau_R >$ of the WW hydrogen bond in the hydration layer of the systems 1b, 1b-dphe, 1b-lphe, 1b-dasn and 1b-lasn are represented here. The data for bulk is given for comparison. All the units are in ps.

Table 3-7. The amplitudes a_i's and the time constants τ_i's for the tri-exponential fit of the water-water intermittent hydrogen bond time correlation functions are represented here.

System	a_1	τ_1 (ps)	a_2	τ_2 (ps)	a_3	τ_3 (ps)
bulk	0.09	15.36	0.55	2.40	0.36	0.28
1b	0.09	23.42	0.43	3.64	0.48	0.38
1b-dasn	0.10	16.54	0.42	3.75	0.48	0.39
1b-lasn	0.04	42.30	0.42	4.55	0.51	0.43
1b-dphe	0.13	13.83	0.43	3.26	0.44	0.32
1b-lphe	0.12	13.24	0.43	3.08	0.44	0.32

The lifetime for WW hydrogen bond in the bulk is 0.32 which is close to the value reported in literature for TIP3P water [160]. An initial fast decay is observed in $S(t)$ due to the librational motion of the water oxygen atoms. This followed by a slow decay that diminishes to 0 around 3 ps. An overall a slight decline in WW hydrogen bond lifetime is observed in the solvation shell compared to bulk water for all the systems. A reduction of 15.65% in the mean lifetime is noted for the system 1b where the availability of hydrogen bonding sites on the host surface leads to interruption of the WW hydrogen bonds in its vicinity. This observation is in agreement with the host-water hydrogen bond value of 23.99 in 1b, the highest among all the systems under consideration. The insertion of peptides into the host cavity leads to marginal increase in the lifetime values compared to the host only system. This is explained by the formation of hydrogen bonds between the host and the guest peptides that leads to decrease in the possible number of binding sites on the host surface and as a result the WW hydrogen bonding in the region is preserved for longer time durations.

The relaxation lifetime of the hydrogen bonds is dependent on the surface confinement of the hydration layer water molecules. More the interaction of the solvation water molecules with the surface, slower will be the relaxation phenomena. The lifetime values as evident from Table 3-6 is slower for all the systems compared to bulk water. This emphasizes the fact that the mobility of the surface water molecules is restricted by hydrogen bonding with the host surface. The maximum relaxation time for 1b-lasn is also reflected in the slow diffusion of hydration water as evident from the MSD plots. The translational motion of water is relatively free for 1b-dasn compared to 1b-lasn and as a result the relaxation occurs at comparatively faster timescales. For the 1b-phe systems the time required for hydrogen bond relaxation is less compared to the 1b-asn systems, consistent with the

higher diffusibility of water molecules in the hydration shell of these systems explained by the hydrophobicity of the phe peptides. The role of diffusional motion in hydrogen bond relaxation time is also seen for the phe systems where the higher mobility in case of host-lphe is manifested in the lower $< \tau_R >$ value of lphe compared to dphe. The higher mobility in lphe may be due to the higher solvent exposure of the peptide as compared to dphe.

Quantum Chemical Calculation

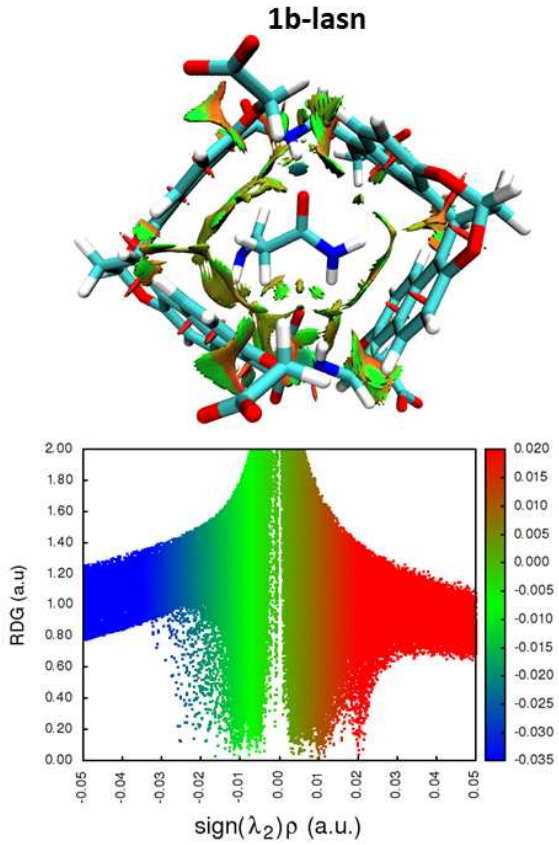

Figure 3-11. *Representation of noncovalent interaction (NCI) obtained from the quantum-based Color-filled RDG isosurface method of 1b-lasn host-peptide systems. The vertical axis of this plot is reduced density gradient (RDG) and the horizontal axis is the sign of the second largest eigenvalue of electron density Hessian matrix at position 'r' (sign(λ_2)ρ).*

After gaining insight about the dynamics of solvation water, in this section we are interested in seeing the influence of the host-peptide hydrophobic (nonbonded) in-

teraction on the stabilization of these complexes. For this purpose, we have applied a quantum mechanics based noncovalent interaction reduced density gradient (NCI-RDG) protocol [121, 161]. Some details of this method are provided in Chapter 2. Host-peptide systems are quantum-mechanically optimized in the gas-phase by using M06-2X/6-31G(d,p) level of theory. This optimized structure is then used for further analysis. A scatter map (color-filled isosurface chart) is constructed from this analysis by applying a default isosurface value of 0.5 and a default color range of -0.035 and 0.020. The scatter maps convey information about the different types of nonbonded interactions and hydrogen bonding interactions present in a system. Nonbonded steric repulsion, attractive van der Waals, and hydrogen bonding interaction are presented in red, green, and bluish green, respectively. Multiwfn algorithm [122, 123] is employed for the analysis purpose. Figure 3-11 contains the nonbonded interaction isosurface and the 2D plot of different interaction regions of 1b-lasn systems. This plot is almost same for every other systems, thus, is not shown here. From this representation, it is clear that every system has steric repulsion and nonbonded hydrophobic and hydrogen bonding interaction. The steric repulsion arises from the intramolecular steric hindrance provided by a particular host molecule, but not in the host-peptide complexes. So, from this analysis, we may say that hydrogen bonding and nonbonded hydrophobic interactions are mainly responsible for stabilizing these complexes.

MM-PBSA Analysis

From the results discussed above, it is clear that every system forms stable host-guest complex. Here, we will concentrate on the energetics of these stable host-peptide complexes. For the same, we have computed the binding free energy (ΔG^0_{bind}) values of all of the host-peptide complexes by using MM-PBSA/GBSA method. We have used the last 4 ns of the trajectories to compute these ΔG^0_{bind} values. Table 3-8 contains the ΔG^0_{bind} values as well as all of its components for all the host-peptide systems. The standard errors for all of these ΔG^0_{bind} values are also mentioned in Table 3-8.

Among all the contributors to ΔG^0_{bind}, van der Waals energy parameter (ΔE_{vdw}) [116, 117, 119] is of prime importance. A high negative value of ΔE_{vdw} for each and every host-peptide complex implies the strong hydrophobic interaction between the host and the peptide molecule. Different amount of ΔE_{vdw} values for different systems are attributed to the different hydrophobic sites of different host and peptide molecules. Each ΔE_{vdw} term contributes favorably to the ΔG^0_{bind}. Electrostatic interaction energy (ΔE_{ele}) also contributes favorably to the ΔG^0_{bind} energy values, i.e., ΔE_{ele} also has negative energy

values. These favorable ΔE_{ele} terms are due to the attractive interaction between the partial charges of host and peptide molecules.

Table 3-8. Binding free energy values[a]

System	ΔE_{vdw}	ΔE_{ele}	ΔG_{PB}	ΔG_{NP}	$T\Delta S$	ΔG^0_{bind}	Se
1a-dasn	-24.22	-8.28	15.28	-2.11	-18.22	-1.11	± 0.199
1a-lasn	-25.02	-9.54	15.72	-1.78	-17.41	-3.21	± 0.219
1a-dphe	-28.13	-9.82	17.82	-1.94	-18.17	-3.90	± 0.091
1a-lphe	-29.58	-9.73	18.42	-1.82	-17.59	-5.12	± 0.088
1b-dasn	-24.16	-13.87	14.74	-1.93	-18.82	-6.40	± 0.212
1b-lasn	-22.61	-11.58	13.97	-2.02	-18.26	-3.98	± 0.101
1b-dphe	-28.51	-12.92	15.90	-1.97	-19.36	-8.14	± 0.106
1b-lphe	-26.55	-10.77	15.26	-1.95	-18.70	-5.31	± 0.184

[a] Binding free energy (in kcal/mol) value along with all of its constituents of all the studied systems and the standard errors (Se) (in kcal/mol) in the computation of binding free energies are presented here.

But, ΔE_{ele} value is much less than the ΔE_{vdw} energy values. Every host-1b containing systems have higher negative ΔE_{ele} energy values than the corresponding host-1a containing systems. This is due to the fact that the tubular cavity of host-1b is more open and places a particular peptide more comfortably than the bowl shaped cavity of host-1a. Thus, ΔE_{vac} (ΔE_{vdw} + ΔE_{ele}) energy values are highly negative, i.e., contributing favorably to the ΔG^0_{bind} for each and every system. Electrostatic solvation free energy (ΔG_{PB}) has a positive value of energy, i.e., an unfavorable contributor to the ΔG^0_{bind} for every system. Individual host and peptide molecule have a high contact area with the solvent molecules, but when the host and peptide forms complex, contacts with the solvent molecule gets reduced. This reduced contact area with the solvent is responsible for the unfavorable ΔG_{PB} energy values. Contrary to ΔG_{PB} energy values, ΔG_{NP} energy terms contribute favorably to the ΔG^0_{bind} energy values for each system. Every system contributes almost the same negative energy value to the ΔG^0_{bind}. This less amount of favorable ΔG_{NP} value cannot counter balance the adverse ΔG_{PB} energy contributions. Thus, ΔG_{solv} (ΔG_{PB} + ΔG_{NP}) becomes an unfavorable contributor to the ΔG^0_{bind} for each and every system. Entropy contribution ($T\Delta S$) values (obtained from the NMODE analysis) have high negative values for every host-peptide system. This indicates the decrease in the degree of freedom due to the host-peptide binding. This is obvious, as inserted peptide into the host cavity is less mobile than the free peptide molecule in water solvent. Thus, entropy terms contribute unfavorably to the ΔG^0_{bind}. Remember here that all of these $T\Delta S$ energy contributors are attributed to the approximate nature of NMODE analysis. Every host-peptide system has

negative ΔG^0_{bind} (ΔE_{vac} + ΔG_{solv} - TΔS) energy values. Thus, each of these host-peptide systems is energetically favorable, i.e., stable.

Thus, we can infer that these host-peptide complexes are mainly stabilized by hydrogen bonding and hydrophobic interactions. For host-1a containing systems, the l-peptides are capable of forming more energetically favorable complexes. But, for host-1b containing systems, a reverse trend is observed, i.e., d-peptides are involved in more stable complexes with the host. Ruiz-Lòpez *et al.* [120] proposed that the differences in complexation energies are minute and can be accounted as (or even closer) computational errors, often seen in enantio- or diastereoselectivity studies. The chiral recognition capacity thus is difficult to conclude confidently. The chiral isomers that exhibit higher negative binding free energy will, therefore, selectively bind to the receptor over the other isomers. d- and l-isomers of the same peptide with a particular host molecule form complexes with an energy difference between 1.5 to 3 kcal/mole. Thus, it suggests that l-peptides with host-1a and d-peptides with host-1b binds selectively over d- and l-peptides, respectively.

Umbrella Sampling (PMF Calculations)

Here, our aim is to explore the energy variation of these complexation processes along a reaction coordinate. Force constant value used for this biased simulation technique helps the host and guest molecule to be fixed at a particular point on the reaction coordinate. Every two nearby windows must overlap to produce a smooth PMF curve. Both the host molecules employed for this work are symmetric. Thus, the guest molecule can either enter or leave the cavity along the same path. The PMF profile as a function of host-peptide COM-COM distance for all the peptide containing systems is presented in Figure 3-12. The primary features of these PMF profiles are as follows: (i) A minimum is present for every PMF profile. These sharp minima are known as contact minima (CM). The CM for every system does not appear at a fixed distance. Different systems exhibit different distance values given as, 1.11 (1a-lasn, 1b-dasn), 2.09 (1a-dasn), 1.35 (1a-dphe), 1.60 (1a-lphe, 1b-dphe), 1.85 (1b-lasn, 1b-lphe) Å. (ii) This CM region corresponds to the fully inserted host-peptide systems. The stability of every complex is maximum at the CM region. Free energy values at the CM region of these complexes are: -1.15 (1a-dasn), -2.89 (1a-lasn), -2.01 (1a-dphe), -3.62 (1a-lphe), -3.64 (1b-dasn), -1.19 (1b-lasn), -5.12 (1b-dphe), and -2.05 (1b-lphe) kcal/mol. (iii) After the CM region, the free energy value of these complexes increases and reaches a maximum value. This region signifies the energy barrier. After this barrier, the energy value decreases and around 6-8 Å, the energy value becomes

parallel to COM-COM coordinate axis. This parallel region characterizes the free host-free guest state.

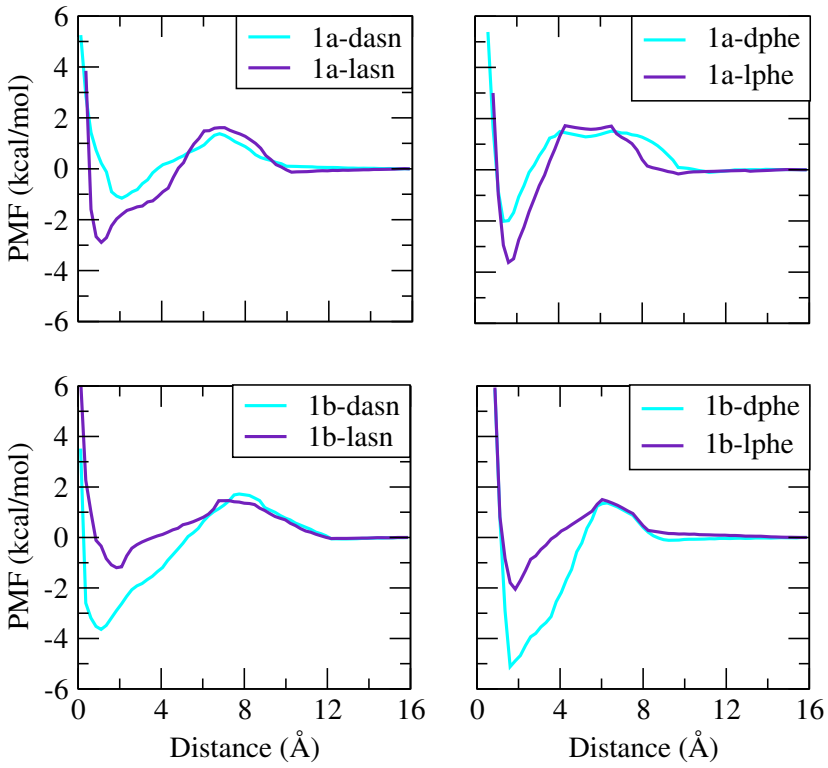

Figure 3-12. *The potential of mean force (PMF) of all the systems is represented here. These PMF values are obtained with the center of mass (COM) - center of mass (COM) distance between host and peptide molecule. We have also evaluated the standard error of these data set by using the block average method, and all of these error values are within the ± 0.16 kcal/mol.*

(iv) The complexed host-guest and free host-guest states are differentiated with an energy barrier. This barrier height again, is different for different systems. The barrier energy values for the systems are: 2.53 (1a-dasn), 4.51 (1a-lasn), 3.52 (1a-dphe), 5.34 (1a-lphe), 5.36 (1b-dasn), 2.65 (1b-lasn), 6.49 (1b-dphe), 3.55 (1b-lphe) kcal/mol. These are the respective amount of energies required to overcome the change of state of the systems from

complexed to free host-guest. Thus, change of the complexation status from one state to another is energetically not favorable. The fact that dasn is more well placed in the cavity of the host-1b compared to lasn can be seen from their corresponding COM-COM distances of 1.11 and 1.85 Å , respectively. This explains the higher solvent exposure of 1b-lasn relative to 1b-dasn system that corollary explains the reduced mobility of water molecules for the 1b-lasn system. One more interesting features from these PMF profiles are energy value increases when the reaction coordinate goes to zero. This may be due to the steric repulsion between the hosts' inwardly directed 'N-H' protons and the corresponding guest moiety. This orientation and interaction between host and guest molecules also affect the energy barriers to change the state of these complexed systems.

From the PMF analysis, we may conclude that every host-peptide system becomes most stable at the CM regions. The free energy value in the CM region resembles the computed binding free energy values from MM-PBSA protocol. The sharp CM region indicates highly stable host-peptide complexes. A particular chiral guest pair (i.e., d- and l- isomer of a peptide) in presence of a particular receptor molecule displayed a meaningful amount of free energy difference (1.5-3 kcal/mol). Thus, we can say that the chiral separation of these peptides with the help of endo-functionalized molecular tube receptors may be feasible.

Convergence of Simulation

The convergence of MD simulation trajectories is one of the problems in the nano second time scale of MD study. Convergence is a prime condition to check the reliability of a study. For this, we are interested to see if 200 ns of simulation is enough to attain convergence. For this purpose, we have considered the whole 200 ns trajectories of 1a-lasn and 1b-lasn systems. We have monitored the host-peptide center of mass (COM) - center of mass (COM) distance and host-peptide hydrogen bonds as a function of simulation time. These are plotted in Figure 3-13. As the peptide is initially packed into the host's cavity, COM - COM distance remains essentially constant from the beginning to the end of the simulation for both the systems. Host - peptide hydrogen bond values also remain constant throughout the simulation trajectories for both the chosen systems. The analyzed parameters are very important to understand the host-guest complexation process. As these two parameters remain constant throughout the entire trajectory, we may predict that our 200 ns trajectories are enough to achieve convergence in each of the simulations.

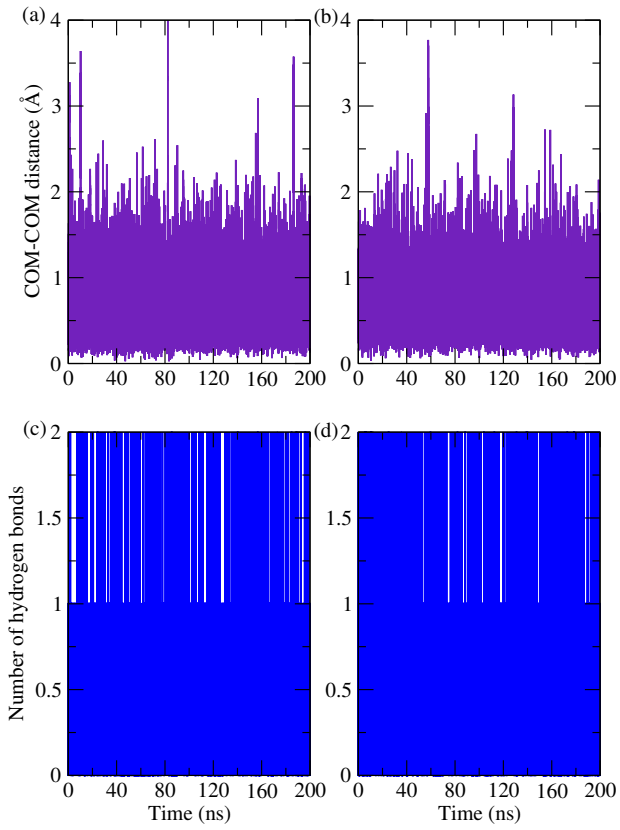

Figure 3-13. *The variation in the distance between the host-peptide center of masses (COM) and the total number of host-peptide hydrogen bonds plotted as function of MD duration. (a) and (b) are for COM-COM distance for system 1a-lasn and 1b-lasn, respectively. (c) and (d) are the host-peptide hydrogen bond values for system 1a-lasn and 1b-lasn, respectively.*

Dependence on Initial Configuration

At last, we are interested to see if a randomly packed peptide inside the simulation box automatically inserts itself into the host cavity or not. For the same, we have prepared some host-peptide systems by randomly packing host and peptide molecules inside the simulation box. These systems are designated by the 'ran' term as stated above, and details of these systems are in Table 3-1. Every randomly packed system is subjected to a 200 ns simulation run. To check the insertion property of these randomly packed

systems, we have calculated the COM - COM distance between host and peptide molecule throughout the trajectory for every randomly packed system, and these are presented in Figure 3-14.

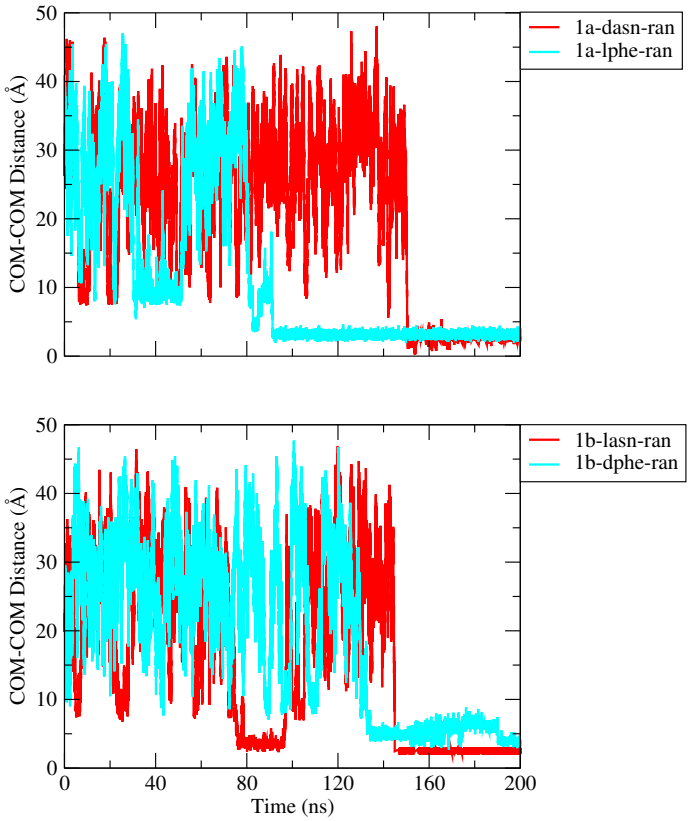

Figure 3-14. *Host-peptide center of mass (COM) - center of mass (COM) distance as a function of 200 ns simulation time of all the randomly packed systems.*

Every system has higher COM - COM value initially. But, once the guest peptide molecule inserted into the host cavity, the COM - COM distance of every host-peptide complexes falls in the range of stable host-guest complexes. After some time from the onset of the simulation, every peptide molecule entered the host cavity. This insertion time is different for different host-peptide systems because it depends on the initial packing geometry and orientation of the molecules in a particular system. But, once a peptide molecule is inserted into the host cavity, it remains in the cavity throughout the simulation, as seen from the

Figure 3-14. Thus, automatic encapsulation of these chiral peptides is certainly possible from the aqueous medium with the help of these endo-functionalized molecular tubes, as seen from the results irrespective of the manner in which the systems are packed initially.

■ SUMMARY AND CONCLUSIONS

In the present work, we have shown the structural aspects and the energetics involved in the chiral separation of two model dipeptides, namely, (d, l)-asparagine and (d, l)-phenylalanine with the help of two synthetic supramolecular receptors (host-1a and host-1b) in solvent water. We have studied the interactions operating in the host-peptide complexes and the associated structural changes to gain better understanding of the chiral segregation process. We have also investigated the dynamics and the changes in the water structure for selected host-guest complexes close to the receptor surface. From the snapshots provided for every host-guest pair, it is clear that the peptide molecule resides inside the cavity of the host for the entire simulation run. Analysis shows that both the host molecules are conformationally stable and less flexible and the stability of every host-peptide system remains intact during the simulation. Thus, we can say that these two receptors may further be explored for the stereoselective binding of peptides from the aqueous medium. Various types of hydrogen bond determination also satisfies our proposition for stable host-guest complex formation. Presence of the host and the host-peptide complexes affect the translational diffusion and the hydrogen bond lifetime values of water molecules near the surface compared to that of bulk water. From quantum-chemical reduced density gradient analysis, it is established that the host-guest hydrophobic interactions along with the hydrogen bonding interactions are the main stabilizing factors operating in these host-peptide complexes. The binding free energy values obtained clearly indicate that the formation of stable host-peptide complexes is an enthalpically favorable process. Variation of potential of mean force along the COM-COM distance obtained from umbrella sampling technique further suggests the formation of stable host-peptide complexes. The PMF profiles register a minimum corresponding to a particular COM-COM distance for all the host-guest systems. This distance, also known as the contact minimum is dependent on the stereochemistry of the guest peptides and the identity of the host molecule under consideration. From MM-PBSA and PMF analyses, it is clear that l-peptides form more stable complexes with host-1a and d-peptides with host-1b as compared to their respective isomeric counterparts. On comparing the efficiency of the host molecules in complex formation, it is observed that the host-1b forms more stable complexes as compared to host-

1a. d- and l- isomers of the same peptide form complexes with a particular host molecule with an energy difference of 1 kcal/mole (confirmed via MM-PBSA and PMF calculations). Thus, we can say that the chiral separation of these model peptides with the help of these endo-functionalized molecular tubes may be attainable from the energy point of view.

The connection so derived from our studies between the peptide stereochemistry and the influence it has while interacting with the host would be beneficial in designing improved molecular receptors with better complexation ability. The ideas obtained may be further implemented to resolve larger peptides and proteins as model systems that are conformationally more complex.

Chapter 4

Exploration on the drug solubility enhancement in aqueous medium with the help of endo-functionalized molecular tubes

"Great achievement is usually born of great sacrifice, and is never the result of selfishness."

— Napoleon Hill

Overview: One major problem in the pharmaceutical industry is the aqueous solubility of newly developed orally administered drug candidates. More than 50 % of the newly developed drug molecules suffer from low aqueous solubility. The therapeutic effects of drug molecules are majorly dependent on the bioavailability and, in essence, on the solubility of the used drug molecules. Thus, enhancement of drug solubility of sparingly soluble drug molecules is the need of modern times. Considering the high importance of drug solubility, we have computationally shown the enhancement of drug solubility for the seven class II (poorly water-soluble) drug molecules in water medium. The uses of supramolecular macrocycles have immense importance in the same field. Thus, we have used two synthetic supramolecular receptors named host-1a and host-1b to enhance the water solubility of fluorouracil, albendazole, camptothecin, clopidogrel, indomethacin, melphalan, and tolfenamic acid drug molecules. Biomedical engagements of a supramolecular receptor commence with the formation of stable host-drug complexes. These complexations enhance the water solubility of drug molecules and sustain the release rate and bioavailability of drug molecules. Thus, in this work, we focus on the formation of stable host-drug complexes in water medium. Molecular dynamics simulation and quantum chemical methods are applied to analyze the structural features and the energetics involved in the host-drug complexation process. The information obtained at the atomistic level helps us gain better insights into the key interactions that operate to produce such highly stable complexes. Thus, we can propose that these two supramolecular receptors may be used as drug solubilizing agents, and patients will well-being from this theranostic application shortly.

■ INTRODUCTION

After elucidating the stereoselective or enantioselective properties of host-1a and host-1b (Figure 1-4 of Chapter 1) in Chapters 2 and 3, we are now interested in using these receptors as a drug solubility enhancement agent for poorly water-soluble drug molecules. Therefore, here (in Chapter 4), we have explored the drug solubility enhancement in aqueous medium with the help of these receptor molecules.

The solubility of newly formulated drugs in water is one of the most important criteria to be established. The most recent and common ways to drug delivery are tablets. Thus, the drug must be soluble in water, in particular for orally administered drugs. Moreover, it poses a big challenge in the formulation of drugs, as the solubility of many newly developed drugs in water is exceedingly limited. Low water-soluble drug molecules can be categorized as class II (low solubility/high permeability) and class IV (low solubility/low permeability) according to Biopharmaceutics Classification System (BCS) [162–165]. Todays' main problem in the pharmaceutical industry is, therefore, aqueous solubility strategies, with about 50 % of newly developed drug candidates suffering from poor aqueous solubility. Weak aqueous solubility has many adverse effects, such as decreased irregular or poor absorption of drugs, which can cause undesirable side effects or lack of therapeutic potential [166]. Methods used to increase the water solubility of drug candidates are therefore urgently needed. Accordingly, methods were created for trapping and improving the rate of dissolution of high-energy forms of active pharmaceutical ingredients (APIs), including the formation of nanocrystalline solid forms or solid API dispersions [167, 168]. Salt forming, and the use of drug-dendrimer fabricates, pharmaceutical co-crystals, pro-drugs, carbon nanotubes, and complexation within a supramolecular receptor are other known strategies to enhance drug solubility [169–176].

Uses of supramolecular receptors or containers to solubilize water-insoluble or barely soluble drug molecules by forming host-drug encapsulated complexes are popular in recent times [44, 176–205]. A host molecule offers a cavity to encapsulate a guest molecule in a typical host-guest inclusion complex through noncovalent interactions. In contrast with covalent interactions, there are many benefits of noncovalent interactions. Moreover, the noncovalent interactions offer simple and fast approaches to creating supramolecular structures, which may prevent several synthesis steps and a complicated purification process during fabrications [202]. These supramolecular encapsulation processes are often environmentally safe and cost-effective. Supramolecular materials can be produced

through intrinsic self-assembly by combining the building blocks in the solution under atmospheric conditions. There is a broad description of supramolecular materials, including any substance composed of components related by noncovalent interactions and undergoing naturalistic disassembly or assembly processes. Due to comparatively mild and complex interactions of the noncovalent linkage, supramolecular materials then have reversibility, enabling the supramolecular structures to be easily dissociated and reconstructed at a minimum energy rate. There is, therefore, the capacity of the supramolecular materials to be recycled and remediated from any outside mechanical stress. In addition, it has an adaptive potential in response to external stimuli that can allow supramolecular materials to alter their shapes. With external stimulus, the supramolecular materials will reconfigure their configurations or morphologies to the most stable states driven by reducing Gibbs free energy [202]. This evolutionary ability can also be used to develop and build stimulus-efficient supramolecular functional materials implemented in various fields, including polymer gels and fluorescent sensing. The construction of supramolecular structures will include several unprecedented therapeutic and diagnostic tools for the nanomedicine field. Under the concept of supramolecular chemistry, host-guest interaction based on macrocyclic receptors is a very significant phenomenon among different noncovalent interactions that have been extensively investigated [202]. With such host-guest incorporation, two or more chemical moieties may be integrated, providing immense possibilities to construct new supramolecular frameworks. In the last few decades, there has been the development of several macrocyclic entities and their derivatives such as pillar[n]arenes, cucurbit[n]urils (CBs), cyclophanes, cyclodextrins (CDs), crown ethers, and calixarenes (CAs), etc [202]. Such macrocyclic receptors are known to be the hosts, contain a cavity to trap the guest molecules. Traditionally, the external structure of the host molecules promotes interaction with the adjacent solvent, while the internal characteristics of their cavities facilitate the inclusion of guests by hydrophobic, hydrogen bonding, electrostatic interaction, and special molecular shape or size alignment, etc. Encapsulation in the aqueous solution of hydrophobic guest molecules into hydrophobic cavities of macrocyclic molecules is the most common case [202]. This host-guest connection is relatively stable and provides a stable and enduring link for the development of supramolecular devices. CBs, CAs, and CDs have gained growing importance among these macrocyclic receptors, particularly for their applications in the biomedical field [44, 176–188, 190–194, 196–200, 202–204]. One of the key reasons for this is that these receptors are biologically conciliatory and have good biocompatibility. The host-guest complex formation based on these macrocyclic molecules justifies a basic and

reversible process, allowing supramolecular stimuli-responsive systems to construct [202]. To improve the water solubility of drugs, the regulatory method employs the complexation between water-soluble macrocyclic molecules and drugs in the supramolecular chemical environment. It can also defend drug molecules against chemical reactions and photochemical and thermal degradation in biological contexts by creating such host-guest complexes. The chemical behavior of delivered drugs could also be modified by the drug encapsulated into the host cavity. Host-guest inclusion complexes offer a sustained therapeutic benefit by the sustainable release of drug molecules from the host cavity. The drug can be distributed in a controlled manner with external forces, including pH changes, thermal change, and competitive binding, to disassociate host-guest complexes [206]. This research field is ongoing, particularly on the toxicity of the hosts' functional groups to enhance of water solubility. However, more research on the same topics showed that these macrocyclic molecules have tremendous application potential for biomedical applications [202]. Lastly, supramolecular receptors used to enhance the drug solubilization should possess some criteria. These criteria are: (i) host structure should be flexible to place a large number of insoluble APIs; (ii) the host-drug complexes should not exhibit improper kinetics of dissociation; (iii) preparations of these host molecules should have a minimum number of steps to diminish the production cost; (iv) should be stable and soluble in water; and lastly, (v) structure of these hosts should not contain undesirable transition-metal ions [202].

Here, we have focused on enhancing drug solubilization in an aqueous medium by using these two synthetic macrocyclic host molecules (host-1a and host-1b) (Figure 1-4 of Chapter 1). They satisfy most of the criteria mentioned above to be used as supramolecular receptors for drug solubilization in an aqueous medium [38, 105]. We have restricted our drug solubilization studies in aqueous solution, particularly as common practical problems often involve water as the solvent medium. We have used seven drug molecules to enhance their solubilities using these macrocyclic receptors. These drug molecules are fluorouracil (flu), melphalan (mel), and camptothecin (cam) belonging to the anticancer, albendazole (alb) belonging to anthelmintics, clopidogrel (clo) from the antiplatelet, indomethacin (ind), and tolfenamic acid (tol) from the nonsteroidal anti-inflammatory drugs. All these drug molecules are shown in Figure 4-1. We have employed a series of all-atom molecular dynamics (MD) simulations and quantum chemical analyses to explore this drug solubilization processes' structural and energetic aspects. Microscopic details about the drug solubilization using macrocyclic receptors can be inferred from such studies.

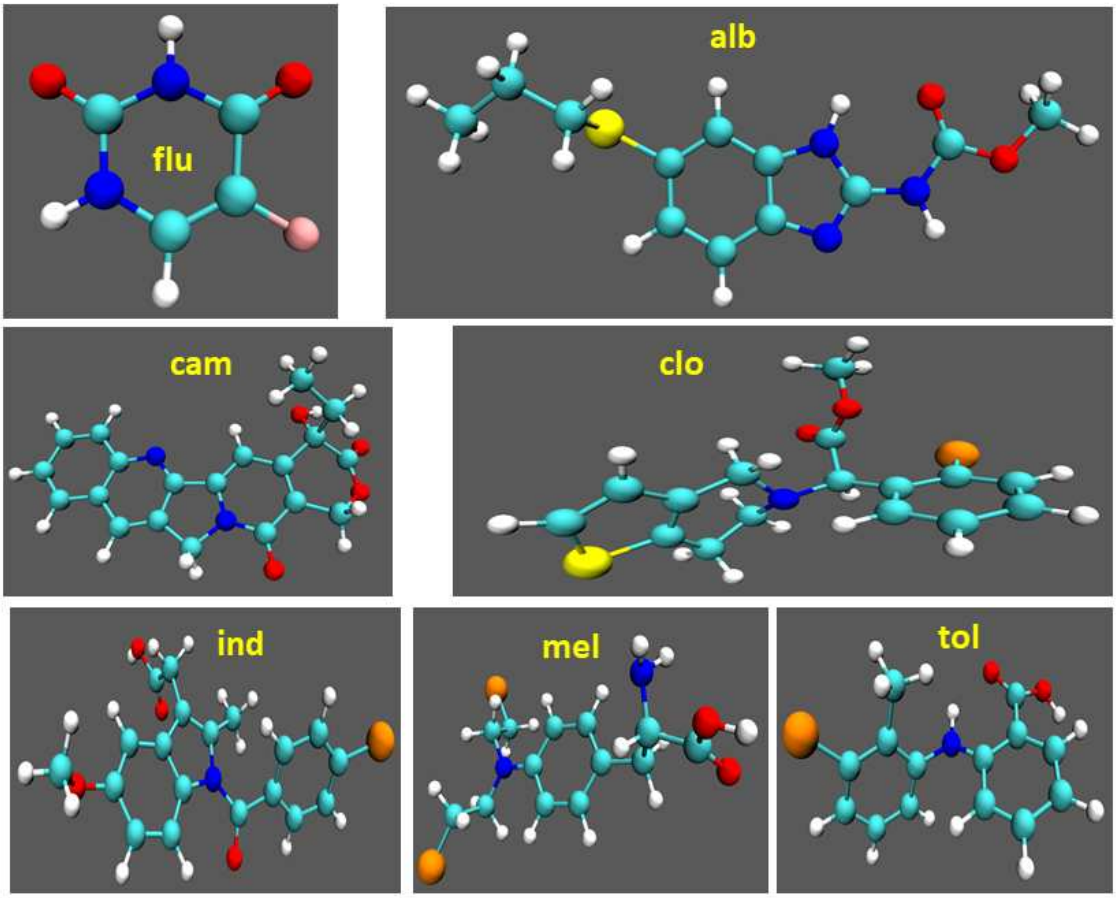

Figure 4-1. *CPK representation of every drug molecule used in this work. 'flu','alb', 'cam', 'clo', 'ind', 'mel', 'tol' represents fluorouracil, albendazole, camptothecin, clopidogrel, indomethacin, melphalan, and tolfenamic acid drug molecules, respectively.*

The remaining chapter is subdivided into three parts. Section 'COMPUTATIONAL DETAILS' comprises a detailed description of the parameters and conditions used for the molecular dynamics simulation run. The results of the analyses carried out have been delineated and discussed in section 'RESULTS AND DISCUSSIONS', and the conclusions drawn from the work are summed up in section 'SUMMARY AND CONCLUSIONS'.

■ COMPUTATIONAL DETAILS

We outline the computational methodology that we adopted to evaluate the struc-

ture and energetics of different host-drug complexes. Here, we are interested to see the feasibility of the solubility enhancement of some important drug molecules by supramolecular receptors, host-1a and host-1b, in explicit water. We have employed classical molecular dynamics (MD) simulation and quantum mechanical calculations for this purpose. Seven representative drug molecules from different categories are used for this work (Figure 4-1). Optimization of the host molecules (host-1a and host-1b), all the drug molecules, and the ammonium ion are done with an HF/6-31+G** basis set of Gaussian09 [106] package. The RESP (restrained electrostatic potential) [67] module of AMBER14 [63] computes the partial charges present at the atomic sites for the two host molecules, all the drug molecules, and the ammonium ion. These charges for both the host molecules are detailed in Tables 2-1 and 2-2 of Chapter 2. The general AMBER force field (GAFF) [108] was used to model these host, drug molecules, ammonium ion, and the ANTECHAMBER [107] program of AMBER14 to extract the force field parameters. The host molecules, host-1a and host-1b carry four units of negative charge each and are neutralized by the same number of ammonium ions [38]. The three-point transferable interaction potential (TIP3P) water [72] model is used as an explicit solvent medium. 30 systems are prepared for this work, and they are listed in Tables 4-1 and 4-2. Systems suffixed with 'ran' were created by randomly packing the drug molecule inside the simulation box (but outside the host's cavity). The ones without the 'ran' term were created with the drug molecule placed inside the hosts' cavity. The PACKMOL [74] program is used to pack the systems with a tolerance value of 2.0 Å. The parameters and the starting coordinates of these packed systems are prepared with the LEaP module of AMBER14, and the generated configurations are simulated with the SANDER implementation of AMBER14. A cubic simulation box with periodic boundary conditions (PBC) in all three directions is applied for each of the simulations. Constraint on every hydrogen-containing covalent bond is ensured by applying the SHAKE algorithm [71] with a tolerance value of 1×10^{-5}. A 10 Å cut-off distance was chosen for reckoning the short-ranged nonbonded interactions. For the long-range electrostatic interactions, the Particle Mesh Ewald (PME) [73] method is utilized. A time interval of 2 fs was allowed for the evaluation of equations of motion. An initial 10000 steps of energy minimization (among which the initial 4000 steps are in the steepest descent method and conjugate gradient method for the last 6000 steps) are performed for every simulation to eliminate erroneous contacts among the atoms in the systems. All the systems are then subjected to heating in a canonical (NVT) ensemble from 0 to 298 K for 320 ps. Following the heating step, equilibration of every simulation for 5 ns (at 298 K and 1 atm temper-

ature and pressure, respectively) is attained in the isothermal-isobaric (NPT) ensemble. The temperature and pressure are retained using the Berendsen barostat [75] with 2 ps pressure relaxation time and the Langevin thermostat [76] with 1 ps^{-1} collision frequency, respectively. 200 ns NPT production run is accomplished for every system mentioned in Tables 4-1 and 4-2. Approximately 15 μs of total production run is performed for this work. CPPTRAJ program [77] of AMBER14 and Visual Molecular Dynamics (VMD) [78] package is used to analyze and visualize of the obtained simulation trajectories. The whole 200 ns trajectories are taken for analysis purposes.

Table 4-1. Overview of systems[a]

System	N_{host}	$N_{NH_4^+}$	N_{drug}	N_{wat}	Box volume (nm^3)	M_{host} (M)
1a	1	4	0	2280	70.58	0.0235
1a-flu	1	4	1	2280	70.60	0.0235
1a-alb	1	4	1	2272	70.39	0.0236
1a-cam	1	4	1	2276	70.51	0.0235
1a-clo	1	4	1	2276	70.66	0.0235
1a-ind	1	4	1	2270	70.63	0.0235
1a-mel	1	4	1	2277	70.79	0.0234
1a-tol	1	4	1	2279	70.26	0.0236
1b	1	4	0	2321	71.43	0.0232
1b-flu	1	4	1	2320	71.72	0.0231
1b-alb	1	4	1	2313	71.45	0.0232
1b-cam	1	4	1	2315	71.98	0.0231
1b-clo	1	4	1	2317	71.51	0.0232
1b-ind	1	4	1	2315	71.86	0.0231
1b-mel	1	4	1	2317	72.10	0.0230
1b-tol	1	4	1	2319	71.87	0.0231

[a] Descriptions of all the systems used for this work. N_{host} is the numbers of the host, $N_{NH_4^+}$ is the numbers of the ammonium ion, N_{drug} is the numbers of the drug molecules, and N_{wat} is the number of water molecules. The molar concentration of the host molecule is represented by the M_{host}. Host-1a and host-1b are represented by 1a and 1b, respectively. 1a-flu, 1b-alb, etc., is the systems of host-1a and host-1b with the drug flu, alb respectively, etc. Pure host-water systems without any drug molecules are represented by 1a and 1b. These systems are prepared by initially packed the drug molecule inside the host cavity.

Table 4-2. Overview of systems[a]

System	N_{host}	$N_{NH_4^+}$	N_{drug}	N_{wat}	Box volume (nm^3)	M_{host} (M)
1a-flu-ran	1	4	1	5079	156.63	0.0106
1a-alb-ran	1	4	1	5617	175.03	0.0095
1a-cam-ran	1	4	1	5343	163.60	0.0107
1a-clo-ran	1	4	1	5411	169.23	0.0098
1a-ind-ran	1	4	1	5979	186.98	0.0089
1a-mel-ran	1	4	1	5616	174.98	0.0095
1a-tol-ran	1	4	1	5558	171.54	0.0098
1b-flu-ran	1	4	1	5596	172.26	0.0096
1b-alb-ran	1	4	1	5643	175.43	0.0095
1b-cam-ran	1	4	1	5338	163.61	0.0101
1b-clo-ran	1	4	1	5498	171.72	0.0097
1b-ind-ran	1	4	1	5431	170.72	0.0097
1b-mel-ran	1	4	1	5416	169.22	0.0098
1b-tol-ran	1	4	1	5264	164.53	0.0101

[a] Descriptions of all the randomly packed systems used for this work. N_{host} is the numbers of the host, $N_{NH_4^+}$ is the numbers of the ammonium ion, N_{drug} is the numbers of the drug molecules, and N_{wat} is the number of water molecules. The molar concentration of the host molecule is represented by M_{host}. Host-1a and host-1b are represented by 1a and 1b, respectively. 1a-cam-ran, 1b-clo-ran, etc., is the systems of host-1a and host-1b with the drug cam, clo respectively, etc. These systems with the 'ran' terms created by randomly packed the drug molecule inside the simulation box.

Binding free energy (ΔG^0_{bind}) of the host-guest complexes are calculated by using the Molecular Mechanics-Poisson Boltzmann Surface Area (MM-PBSA) [79, 80] method. Details of this method are discussed in the 'METHODOLOGY' section of Chapter 1 (Eq. 1.18). The potential of mean force (PMF) of these host-guest complexes are also analyzed, and details of this method are discussed in the 'METHODOLOGY' section of Chapter 1 (Eq. 1.24).

■ RESULTS AND DISCUSSIONS

In the present chapter, our main aim is to find the probability of stable host-guest complex formation and the feasibility of drug solubility enhancement of some important class of drug molecules with endo-functionalized molecular tube receptors in an aqueous medium. Systems without the 'ran' term are the principle systems, and the ones suffixed 'ran' are considered for supporting evidence. We will try to establish our goal by using the main systems. Supporting systems are merely used to check whether a randomly packed drug molecule is automatically inserted into the host cavity or not. We have specified the word 'ran' for every reference made to the supporting systems; otherwise, 'system' indicates

the main systems only.

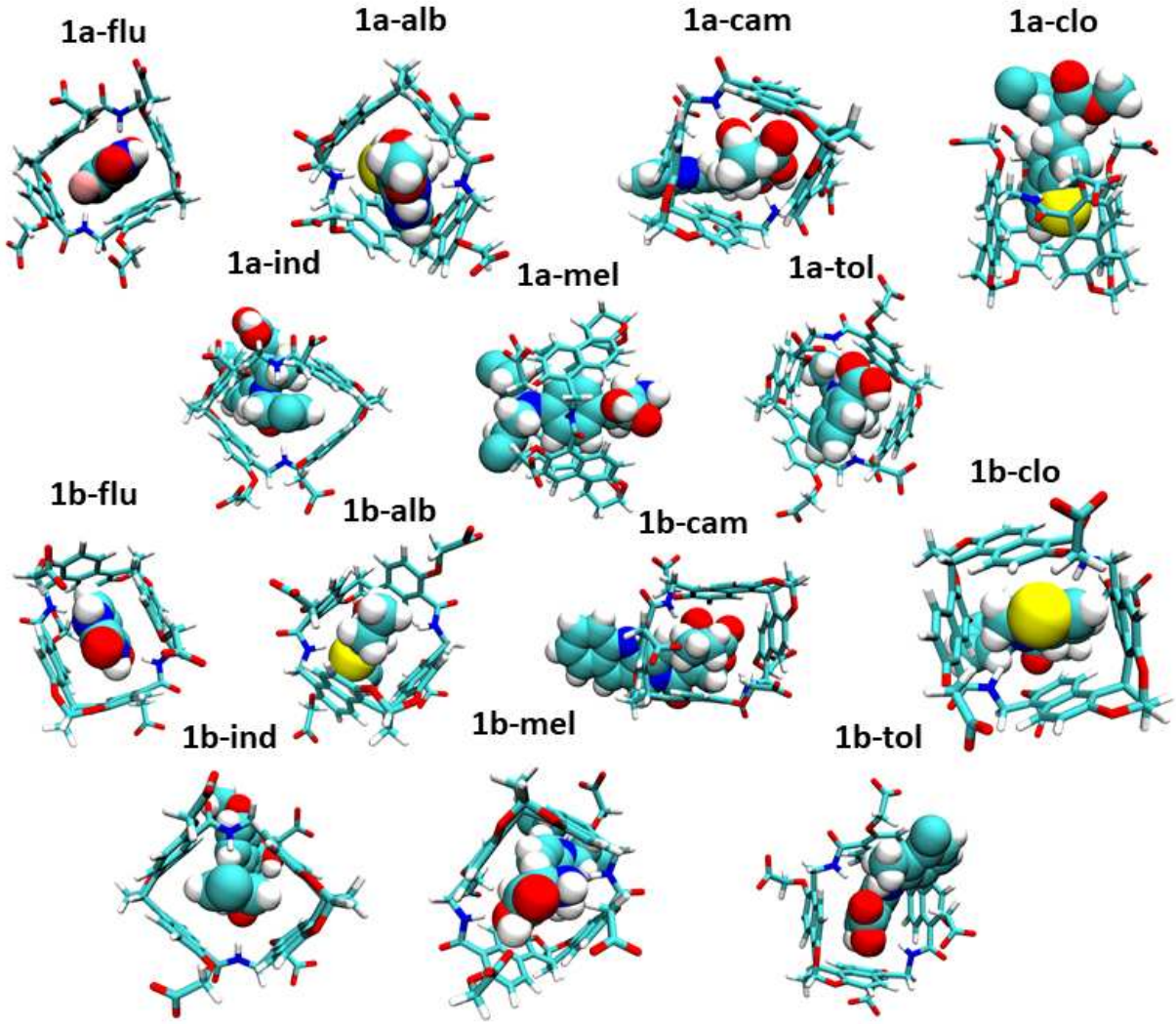

Figure 4-2. *Representative host-drug complex snapshots of all the fixed systems. Only host and drug molecules are presented in every snapshot to amplify the clarity of the image.*

Snapshots (taken from the last frame of the MD simulation trajectories) of drug-host complexes for each system are presented in Figure 4-2. From these snapshots, we get a preliminary idea of how these complexes are formed. Every smaller-sized drug molecule is fully inserted into the host cavity, and the bigger drug molecule is inserted as well, but some of its portions also remain outside the host cavity. Hydrogen bond donor and acceptor atoms of the host molecule are positioned for favorable hydrogen bond interaction with

the drug molecule. Hydrophobic parts of these drug molecules achieve stability through interaction with the hydrophobic core of these host molecules. From here on, we discuss in detail every structural and energetic aspect of these drug-host complexes.

Internal Diameters

Table 4-3. Average internal diameter[a]

System	Aid-I (Å)	Aid-II (Å)	Ad (Å)	Se (Å)
1a	10.98	9.40	1.58	± 0.0064
1a-flu	11.22	9.25	1.97	± 0.0730
1a-alb	12.80	9.26	3.54	± 0.0084
1a-cam	13.86	8.60	5.27	± 0.0021
1a-clo	12.96	9.14	3.82	± 0.0045
1a-ind	13.62	8.87	4.75	± 0.0057
1a-mel	13.25	8.95	4.30	± 0.0115
1a-tol	12.48	9.06	3.41	± 0.0047
1b	13.13	9.66	3.51	± 0.0012
1b-flu	13.15	9.62	3.53	± 0.0377
1b-alb	13.25	9.60	3.65	± 0.0110
1b-cam	13.55	9.12	4.43	± 0.0218
1b-clo	13.19	9.55	3.64	± 0.0433
1b-ind	13.47	9.56	3.91	± 0.0199
1b-mel	13.28	9.56	3.72	± 0.1118
1b-tol	13.16	9.62	3.54	± 0.0311

[a] Average values of internal diameter-I (Aid-I), internal diameter-II (Aid-II), the absolute difference (Ad) between them, and the standard errors (Se) of Ad of host-1a and host-1b of every system are presented in this table. Standard errors are estimated by the block averaging method.

At first, we analyze the structural features of host-1a and host-1b with and without the guest drug molecule in its cavity. We have envisaged two internal diameters for this purpose. Schematic representation and details of these diameters are presented in Figure 2-3 of Chapter 2. Table 4-3 consists of the average values of both the diameters, the absolute difference (Ad) between them, and the standard error values of Ad (calculated by block averaging method) for all systems. For both the host molecules, the diameters' values increase concerning the corresponding diameter value of the system without any guest molecule. Thus, the Ad values of every guest containing system are increased compared to the corresponding guest devoid systems for a particular host molecule. To delve deeper into the non-identical trends in diameter change as exhibited by the two hosts, we have

computed the probability distribution functions of Ad for the systems under study. Figures 4-3 and 4-4 display these values for the systems with host-1a and host-1b, respectively. Ad values as a function of simulation time are also plotted at the insets of these plots. Maximum probabilities for systems 1a and 1b appear at 1.50 Å and 3.50 Å , respectively. The distance at which maximum probability appears is higher for both the host molecules than the systems in the absence of the guest drug. This effect is maximum for the drug-containing host-1a systems compared to the host-1b systems. From this analysis, it is somewhat obvious that each host molecule becomes structurally more stable following drug molecules' inclusion into their cavities.

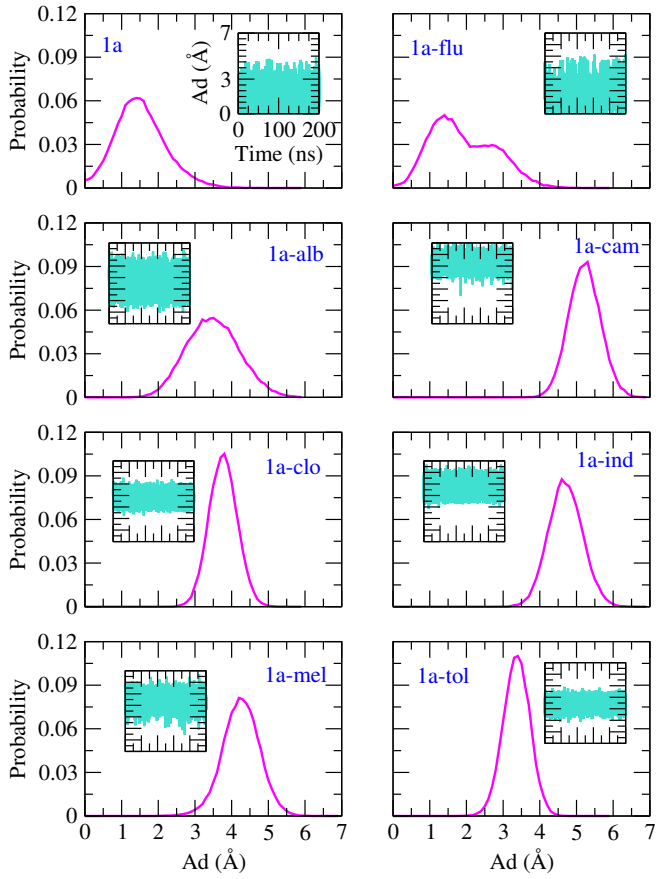

Figure 4-3. *The probability distributions of the absolute difference (Ad) between two internal host-1a diameters for different systems. Insets contain the Ad values with simulation time.*

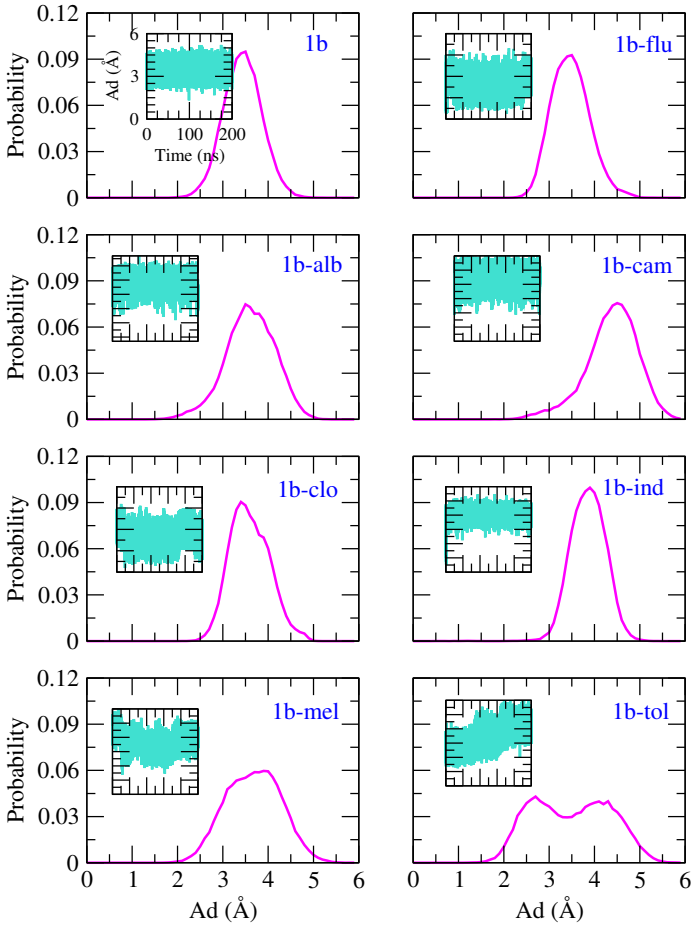

Figure 4-4. *The probability distribution of absolute difference (Ad) between two internal host-1b diameters for different systems. Insets contain the Ad values with simulation time.*

To examine these host-drug complexes' conformational flexibility and stability during MD simulation, we have calculated the root mean square deviation (RMSD) of the host structures compared to the the initial host structure. These RMSD values for every system as a function of simulation time are plotted in Figure 4-5. Every RMSD value is within 1.5 Å. From these RMSD values, it is clear that each host molecule is conformationally stable and less flexible for every host-drug complex, and the stability of the complex remains intact during simulation. Thus, all of the above observations signify the formation of stable host-drug complexes.

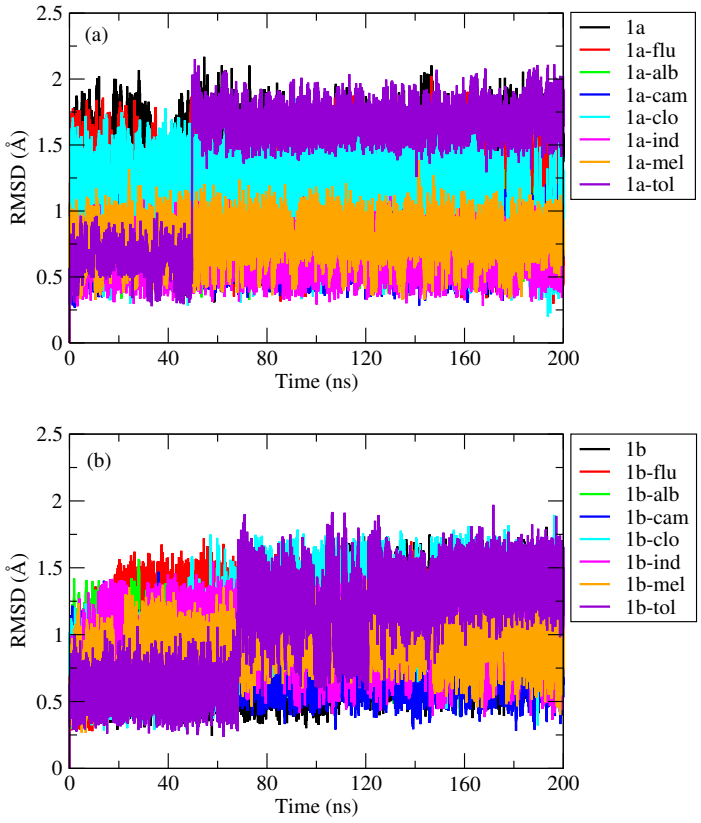

Figure 4-5. *The root means square deviation (RMSD) values of the receptor concerning the first frame for every system as a function of simulation time are plotted here.*

As Ad values increase when compared to the guest free host molecule and RMSD value remains in a stable range, it can say that these two host molecules are flexible enough to place insoluble APIs.

Hydrogen Bond Analysis

From the snapshots, we see the formation of encapsulation complexes between endo-functionalized molecular tubes and drug molecules. In this section, we focus on how different types of hydrogen bonds help to stabilize these complexes. We have categorized and calculated the average number of hydrogen bonds between (i) host-water (HW), (ii) different atomic sites of host and water, (iii) host-drug (HD), and (iv) different atomic

sites of host and drug molecule. The cut-off distance (r_c) for the donor-acceptor pair was chosen as $r_c \leq 3.4$ Å , and the angle (θ_c) for donor-acceptor-hydrogen was allowed for $\theta_c \leq 45^o$ [109–115]. These geometric criteria are schematically presented in Figure 2-6 of Chapter 2. Both the host molecules have two 'N-H' hydrogen bond donor sites, *i.e.,* N6 and N8 for host-1a, and N1 and N3 for host-1b are the corresponding donor nitrogen sites in these two hosts. The computed hydrogen bond numbers for the systems under consideration are presented in Table 4-4. Here, we shift our focus to the average number of HW and host's nitrogen atom-water hydrogen bonds. Systems without any guest molecules have the highest number of HW hydrogen bonds. But, with the introduction of guest molecules into the host cavity, this value is decreased modestly. In free host-water systems, water molecules reside inside the host cavity and form hydrogen bonds. But, when we introduce drug molecules into the system, these cavity water leaves the cavity, and large-sized drug molecules also affect the surface host-water interaction. This finding indicates that some hydrogen bonding sites intrinsic to the host are now involved in forming hydrogen bonds with the guest drug molecules. These sites may be the 'N-H' donor sites of host molecules. To examine this, we have calculated the number of hydrogen bonds between the hosts' donor 'N-H' and the water molecules. This value is the highest for the systems without any drug molecule and becomes almost zero for the guest-containing systems. This observation indirectly suggests that these host sites now preferentially partake in the formation of hydrogen bonds with the drug molecule over water molecules. Next, we discuss in detail the total number of HD hydrogen bonds. From Table 4-4, it is evident that every drug-containing system has a significant amount of HD hydrogen bonds. This partly explains the formation of stable host-drug complexes. We explore further the atomistic details of these host-drug hydrogen bonds. For this purpose, we have computed the hydrogen bond values between the hosts' donor 'N-H' group (in host-1a, N6/N8-H, and host-1b, N1/N3-H) and the drugs' acceptor atoms. The overall HD hydrogen bond number is the summation of the hosts' 'N-H'-drug hydrogen bonds only for the small 'flu' drug molecule, but for the large size drug molecules, HD hydrogen bond number exceeds the summation of the hosts' 'N-H'-drug hydrogen bonds. Small size 'flu' is fully inserted into these host's cavities and some portion of these larger size drug molecules resides outside the host cavity and forms hydrogen bonds with the hosts' side-chain atoms. For larger-sized drug molecules, drug molecules whose polar atoms reside only inside the host cavity show less HD hydrogen bonds than those larger-size drug molecules whose polar atoms reside inside as well as outside of the host cavity. Host-1a forms maximum number of HD hydrogen bonds with

'tol' drug molecules, whereas host-1b forms the maximum number of HD hydrogen bonds with the 'mel' drug.

Table 4-4. Hydrogen bond values

System	host-wat	N6/N1-wat	N8/N3-wat	host-drug	N6/N1-drug	N8/N3-drug
1a	23.70	0.49	0.48	–	–	–
1a-flu	21.82	0.03	0.03	0.85	0.42	0.43
1a-alb	20.10	0.01	0.00	0.87	0.47	0.12
1a-cam	20.97	0.00	0.00	0.98	0.30	0.22
1a-clo	21.53	0.01	0.01	0.73	0.15	0.38
1a-ind	21.62	0.00	0.00	0.63	0.21	0.22
1a-mel	21.86	0.00	0.00	1.04	0.30	0.38
1a-tol	20.41	0.00	0.01	1.15	0.28	0.42
1b	23.99	0.76	0.84	–	–	–
1b-flu	21.61	0.05	0.02	0.94	0.12	0.82
1b-alb	19.72	0.01	0.03	1.25	0.09	0.85
1b-cam	21.33	0.03	0.05	1.18	0.40	0.20
1b-clo	20.53	0.01	0.01	0.88	0.23	0.35
1b-ind	22.00	0.00	0.00	0.77	0.24	0.29
1b-mel	19.37	0.02	0.01	1.84	0.72	0.71
1b-tol	20.96	0.01	0.01	1.35	0.24	0.42

[a] The first column of this table represents the system; the second column is for the hydrogen bond values between host and water (host-wat), the third column represents the hydrogen bond values between host-1a N6/host-1b N1 atomic sites-water (N6/N1-wat), the fourth column is for the hydrogen bond values of host-1a N8/host-1b N3 atomic sites-water (N8/N3-wat), the fifth column contains the number of host and drug (host-drug) hydrogen bonds, sixth and seventh columns are for the host-1a N6/host-1b N1 atomic sites-drug (N6/N1-drug) and host-1a N8/host-1b N3 atomic sites-drug (N8/N3-drug) hydrogen bond numbers.

MM-PBSA Analysis

From the results discussed above, it is clear that every system forms a stable host-guest complex. Here, we concentrate on the energetics of these stable host-drug complexes. For the same, we have computed the binding free energy (ΔG^0_{bind}) values of all the host-drug complexes using the MM-PBSA method. We have used the last 4 ns of the MD simulation trajectories to compute these ΔG^0_{bind} values. Table 4-5 contains the ΔG^0_{bind} values and all of its components for all the host-drug systems. The standard errors for all of these ΔG^0_{bind} values are also incorporated in Table 4-5.

Among all the contributors to ΔG^0_{bind}, the van der Waals energy parameter (ΔE_{vdw}) [116, 117, 119] is of prime importance. A high negative value of ΔE_{vdw} for every host-drug complex implies the strong hydrophobic interaction between the host and the drug

molecule. Different amounts of ΔE_{vdw} values for different systems are attributed to the different hydrophobic sites of different host and drug molecules.

Table 4-5. Binding free energy values[a]

System	ΔE_{vdw}	ΔE_{ele}	ΔG_{PB}	ΔG_{NP}	$T\Delta S$	ΔG^0_{bind}	Se
1a-flu	-22.00	-2.75	11.85	-1.16	-10.38	-3.68	± 0.098
1a-alb	-27.57	-7.32	13.23	-1.90	-15.93	-7.63	± 0.140
1a-cam	-20.00	-14.97	14.34	-1.39	-17.02	-5.00	± 0.082
1a-clo	-26.16	-4.52	12.19	-1.96	-13.87	-6.58	± 0.088
1a-ind	-27.24	-6.24	12.50	-1.76	-16.03	-6.71	± 0.079
1a-mel	-33.67	-8.67	16.56	-2.31	-20.63	-7.46	± 0.098
1a-tol	-22.71	-6.56	12.38	-1.80	-11.50	-7.19	± 0.154
1b-flu	-23.56	-4.03	12.03	-1.03	-10.93	-5.66	± 0.049
1b-alb	-33.27	-8.19	15.21	-1.43	-18.64	-9.04	± 0.129
1b-cam	-24.34	-15.03	17.39	-1.73	-17.50	-6.21	± 0.145
1b-clo	-26.91	-5.86	14.35	-2.19	-13.62	-6.99	± 0.093
1b-ind	-30.32	-9.06	15.03	-1.56	-17.01	-8.90	± 0.231
1b-mel	-35.77	-10.78	19.39	-2.20	-21.05	-8.31	± 0.166
1b-tol	-24.89	-9.36	15.19	-1.70	-12.38	-8.38	± 0.098

[a] This table contains the values of binding free energy (ΔG^0_{bind}) (in kcal/mol) along with all of its constituents and the value of standard errors (Se) (in kcal/mol) – calculated from block average method – of ΔG^0_{bind} of all the systems used for this work.

Electrostatic interaction energy (ΔE_{ele}) also contributes favorably to the ΔG^0_{bind} energy value, i.e., ΔE_{ele} also has a negative energy value. These favorable ΔE_{ele} terms are due to the attractive interaction between the partial charges of the host and drug molecules. But, the ΔE_{ele} value is much less favorable than the ΔE_{vdw} energy values except for the 'cam' drug-containing systems. For 1a-cam and 1b-cam systems, the ΔE_{ele} energy value is highly favorable, and they contribute significantly to the total host-drug interaction energies. Thus, ΔE_{vac} ($\Delta E_{vdw} + \Delta E_{ele}$) energy values are highly negative, i.e., contributing favorably to the ΔG^0_{bind} for every system. Electrostatic solvation free energy (ΔG_{PB}) has a positive value of energy, i.e., an unfavorable contributor to the ΔG^0_{bind} for every system. Individual host and drug molecule have a high contact area with the solvent molecules, but when the host and drug form complex, contacts with the solvent molecule get reduced. This reduced contact area with the solvent is responsible for the unfavorable ΔG_{PB} energy values. Contrary to ΔG_{PB} energy values, ΔG_{NP} energy terms contribute favorably to each systems' ΔG^0_{bind} energy values. This less favorable ΔG_{NP} value cannot counterbalance the adverse ΔG_{PB} energy contributions. Thus, ΔG_{solv} ($\Delta G_{PB} + \Delta G_{NP}$) becomes an unfavorable contributor to the ΔG^0_{bind} for each system. Entropy contribution ($T\Delta S$) values

(obtained from the NMODE analysis) have high negative values for every host-drug system. This indicates the decrease in the degree of freedom of the 'drug molecule' due to the host-drug binding. This is obvious, as inserted drug into the host cavity is less mobile than the free drug molecule in water solvent. Thus, entropy terms contribute unfavorably to the ΔG^0_{bind}. Note that all of these TΔS energy contributors are attributed to the approximate nature of NMODE analysis. Every host-drug system has negative ΔG^0_{bind} (ΔE_{vac} + ΔG_{solv} - TΔS) energy values. Thus, each host-drug complex is energetically favorable, i.e., stable, and for a particular drug molecule, host-1b forms more stable complexes than the host-1a as indicated from the binding free energy values.

Umbrella Sampling (PMF Calculations)

Next, we have computed the potential of mean forces (PMFs) by taking the host-drug COM-COM distance along the z-axis as the reaction coordinate. The configuration of the last frame of every normal MD simulation is considered as the initial configuration for the biased umbrella sampling (US) method. Force constant value used for this biased simulation technique helps the host and guest molecule be fixed at a particular point on the reaction coordinate. The PMF profiles as a function of host-drug COM-COM distance for all the drug-containing systems are presented in Figure 4-6. The primary features of these PMF profiles are as follows: (i) A minimum is present for every PMF profile. These sharp minima are known as contact minima (CM). (ii) This CM region corresponds to the fully inserted host-drug systems. The stability of every complex is maximum at the CM region. Free energy values at the CM region of these complexes are: -2.29 (1a-flu), -3.12 (1b-flu), -3.83 (1a-alb), -6.62 (1b-alb), -3.48 (1a-cam), -4.50 (1b-cam), -3.70 (1a-clo), -4.98 (1b-clo), -5.91 (1a-ind), -7.23 (1b-ind), -6.57 (1a-mel), -8.19 (1b-mel), -5.90 (1a-tol) and -7.04 (1b-tol) kcal/mol. (iii) After the CM region, the free energy value of these complexes increases and reaches a maximum value. This region signifies the energy barrier. After this barrier, the energy value decreases, and around 6-10 Å, the energy value becomes parallel to COM-COM coordinate axis. This parallel region characterizes the free host-free guest state. (iv) The complexed host-guest and free host-guest states are separated with an energy barrier. This barrier height, again, is different for different systems. This respective amount of energies required to change the state of the systems from complex to free host-guest. Thus, change of the complexation status from one state to another is energetically not favorable.

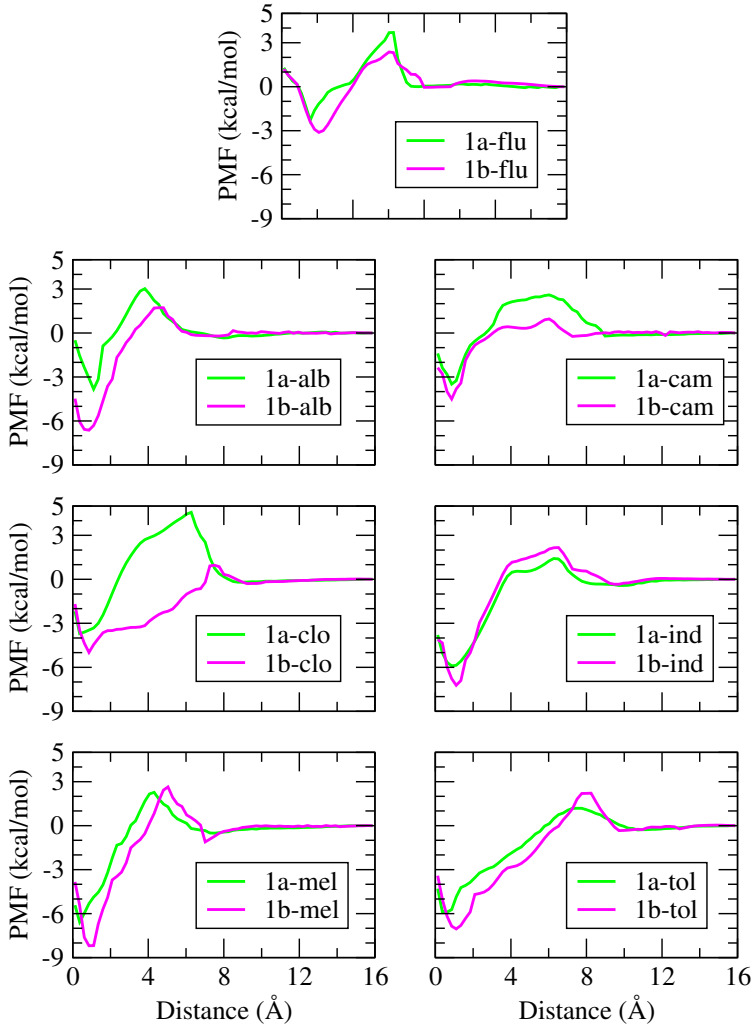

Figure 4-6. *The potential of mean force (PMF) of all the systems is represented here. These PMF values are obtained with the host-drug center of mass (COM) - center of mass (COM) distance. We have also evaluated the standard error of these data sets using the block average method, and all of these error values are within the ± 0.23 kcal/mol.*

From the PMF analysis, we can propose that every host-drug complex becomes stable at the CM regions. The free energy value in the CM region resembles the computed binding free energy values from the MM-PBSA protocol. It is proved that a particular drug molecule forms a more stable complex with host-1b compared to host-1a.

Convergence of Simulation

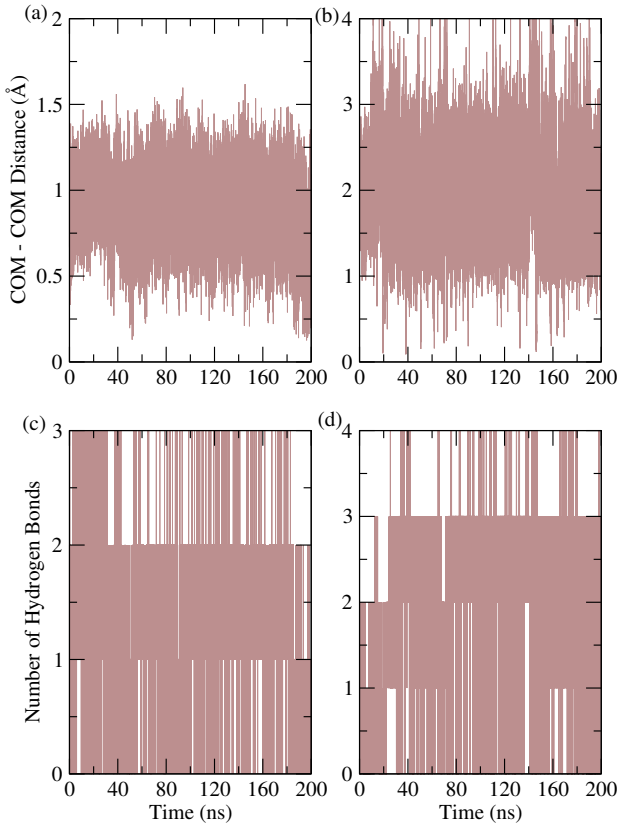

Figure 4-7. *The variation in the distance between the host-drug center of mass (COM) and the total number of host-drug hydrogen bonds plotted as a function of MD duration. (a) and (b) are for COM-COM distance for system 1a-flu and 1b-alb, respectively. (c) and (d) are the host-drug hydrogen bond values for system 1a-tol and 1b-mel, respectively.*

The convergence of MD simulation trajectories is one of the problems in the nanosecond time scale of the MD study. For this, we are interested to see if 200 ns of simulation is enough to attain convergence. For this purpose, we have considered the whole 200 ns trajectories of 1a-flu, 1a-tol, 1b-alb, and 1b-mel systems. We have monitored the host-drug center of mass (COM)-center of mass (COM) distance for systems 1a-flu and 1b-alb, and host-drug hydrogen bonds for systems 1a-tol and 1b-mel systems as a function of simulation time. These are plotted in Figure 4-7. As the drug is initially packed into the host's cavity, COM-COM distance remains essentially constant from the beginning to

the end of the simulation for both systems. Host-drug hydrogen bond values also remain constant throughout the simulation trajectories for both the chosen systems. The analyzed parameters are very important to understand the host-drug complexation process. As these two parameters remain constant throughout the entire trajectory, we may predict that our 200 ns trajectories are enough to achieve convergence in each of the simulations.

Dependence on Initial Configuration

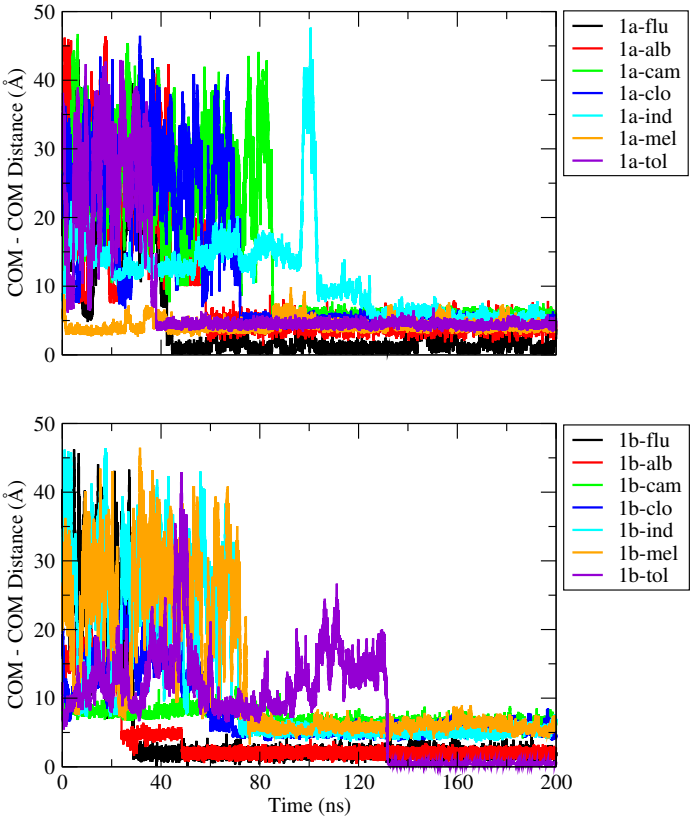

Figure 4-8. *Host-drug center of mass (COM) - center of mass (COM) distance as a function of 200 ns simulation time of all the randomly packed systems.*

We are interested to see if a randomly packed drug molecule inside the simulation box automatically inserts itself into the host cavity or not. For the same, we have prepared some host-drug systems by randomly packing host and drug molecules inside the simulation box. These systems are designated by the 'ran' term as stated above, and details of these

systems are shown in Table 4-2. Every randomly packed system is subjected to a 200 ns simulation run. To check the insertion property of these randomly packed drug molecules, we have calculated the COM-COM distance between host and drug molecules throughout the trajectory for every randomly packed system. These are presented in Figure 4-8. Every system has a higher COM-COM value initially. But, once the guest drug molecule is inserted into the host cavity, the COM-COM distance of every host-drug complexes falls in the range of stable host-guest complexes. After some time from the onset of the simulation, every drug molecule enters the host cavity. This insertion time is different for different host-drug systems because it depends on the initial packing geometry, the nature of the guest molecule, and the orientation of the guest molecules in a particular system. But, once a drug molecule is inserted into the host cavity, it remains in the cavity throughout the simulation, as seen from Figure 4-8. Thus, automatic encapsulation of these drug molecules is certainly possible from the aqueous medium with the help of these endo-functionalized molecular tubes, as seen from the results irrespective of how the systems are packed initially.

Quantum Chemical Calculation

Quantum mechanical calculation is explicitly used in this section only. Every other analysis discussed in this chapter is MD simulation-based analysis.

In this section, we are interested in exploring the influence of the host-drug hydrophobic (nonbonded) interaction on stabilizing these complexes. For this purpose, we have applied a quantum mechanical-based noncovalent interaction reduced density gradient (NCI-RDG) protocol [121, 161]. Every host-drug complex is quantum-mechanically optimized in the gas phase using the M06-2X/6-31G(d,p) level of theory. This optimized structure is then used for further analysis. Dispersion correction is not used in this analysis. Nonbonded steric repulsion, attractive van der Waals, and hydrogen bonding interaction are presented in red, green, and bluish-green colors. Weak hydrogen bonds are in bluish-green, and strong hydrogen bonds are in blue. The multiwfn algorithm [122, 123] is employed for the analysis purpose. Figure 4-9 contains the nonbonded interaction isosurface and the 2D plot of different interaction region for 1b-flu system. All other systems have the same representation, thus, not shown here. From this representation, it is clear that every system has steric repulsion, nonbonded hydrophobic, and hydrogen bonding interaction. The steric repulsion arises from the intramolecular steric hindrance provided by a particular host molecule but not in the host-drug complexes. A larger amount of hydrophobic host cavity provides every drug molecules a comfortable reside inside their cavities. Thus, a

larger amount of host-drug hydrophobic interactions is taken place. So, from this analysis, we can infer that hydrogen bonding and nonbonded hydrophobic interactions are mainly responsible for stabilizing these host-drug complexes.

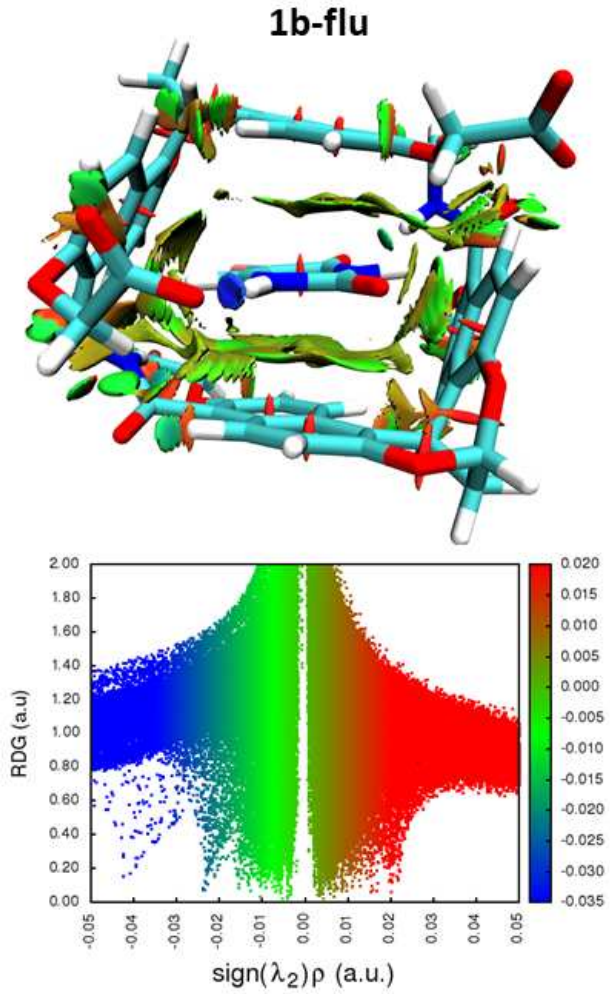

Figure 4-9. *Representation of noncovalent interaction (NCI) obtained from the quantum-based Color-filled RDG isosurface method of 1b-flu host-drug systems. The vertical axis of this plot is reduced density gradient (RDG) and the horizontal axis is the sign of the second largest eigenvalue of electron density Hessian matrix at position 'r' (sign(λ_2)ρ).*

■ SUMMARY AND CONCLUSIONS

Supramolecular chemistry has been employed in various applications every year

since its invention. Scientists have made huge exertion in the last two decades to the biomedical engagement of supramolecular receptors. These engagements are based on noncovalent interaction. These noncovalent interactions are host-guest hydrogen bonding interaction, hydrophobic or hydrophilic interaction, electrostatic interaction, van der Waals interaction, and so on. Due to the comparatively mild and complex interactions of the noncovalent linkage, supramolecular materials then have reversibility, enabling the supramolecular structures to be easily dissociated and reconstructed at a minimum energy rate, which meets the generic criteria in biomedical engagement. Photosensitizers and bioimaging agents also get stability and prospering their photodynamic or fluorescence activity in biophysical systems by forming host-guest complexes with supramolecular receptors [202].

Considering these high vogues of macrocyclic receptors in biomedical fields, here we have used two synthetic macrocyclic host molecules to enhance the solubility of sparingly soluble drug molecules, as enhancement of drug solubilization is the need of modern time. We have used seven class II drug molecules and two receptors (host-1a and host-1b) for this purpose. Biomedical engagements of a supramolecular receptor commence with the formation of stable host-guest complexes with the drug molecules. These complexations enhance the water solubility of drug molecules and sustained the release rate and bioavailability of drug molecules [202]. Thus, in this work, we focus on the formation of stable host-drug complexes in water medium. From the snapshots provided for every host-guest pair, it is clear that the drug molecule resides inside the cavity of the host for the entire simulation run. Structural analysis shows that both the host molecules are conformationally stable and flexible, and the stability of every host-drug system remains intact during the simulation. Various types of hydrogen bond determination also satisfy our proposition for stable host-drug complex formation. The binding free energy values obtained indicate that the formation of stable host-drug complexes is an enthalpically favorable process. Variation of the potential of mean force along the COM-COM distance obtained from the umbrella sampling technique further suggests the formation of stable host-drug complexes.

From every structural and energetic aspect, it is clear that both the host molecules form stable host-drug complexes with all the seven drug molecules. Thus, we propose that these two supramolecular receptors may be used as drug solubilizing agents, and patients will benefit from this theranostic application shortly.

Chapter 5

Prediction of local thermodynamics of water in and around endo-functionalized molecular tube receptors: an approach using grid inhomogeneous solvation theory

"It is surmounting difficulties that makes heroes."

– Louis Pasteur

Overview: Water molecules in and around a receptor play a significant role in the guest/ligand binding process. Here, we discuss the waters' role in the guest binding process of small miniature receptor endo-functionalized molecular tubes (host-1a and host-1b). We have portrayed this using classical molecular dynamics (MD) simulation and grid inhomogeneous solvation theory (GIST). Trajectories from MD simulation have been utilized in GIST methodology to estimate different localized thermodynamic parameters at different regions of these receptors. These small receptors reveal a surprisingly detailed solvation structure, thermodynamic pattern, and offer comprehensive insights. The torus site with high water density is especially relevant within the receptor binding sites in the solvation structure. Water molecules are energetically unstable inside (i.e., torus and cavity regions) of these host molecules. This water instability offers some guest molecules extremely high binding affinities inside these host cavities. Also, we are curious to see the effect of electrostatic on these thermodynamic parameters. For this, we have used a nonpolar version of these host molecules in which all partial charges of the atomic sites of both these receptors are artificially set to zero. Every energetic and entropic solvation parameters are less perturbed for nonpolar host molecules than the corresponding regular host molecules. The water molecules inside the nonpolar host cavity are less strongly bound than the corresponding regular host molecules. Thus, the value of free energy for removing water molecules from a particular region of a purely nonpolar host molecule is more favorable than the corresponding regular host molecule.

■ INTRODUCTION

All the major applications shown in Chapters 2, 3, and 4 are mainly based on host-guest complexation in the aqueous medium. But the role of water molecules in the complexation of these receptors (host-1a and host-1b, Figure 1-4 in Chapter 1) is not elucidated yet. Thus, in Chapter 5, we investigate the role of water molecules in these host-guest complexation procedures.

Molecular recognition, which is the encapsulation of a molecule by another one in a solvent like water, is not possible to completely understand simply in terms of molecular interactions between two molecules that recognize each other. Water molecules in every recognition process play an important role. Water molecule effectively reduces the receptor-ligand (or host-guest) interactions by engaging in hydrogen bonding interaction (with solutes), as well as by having hydrophobic interactions [116, 117, 161, 207] between solutes' nonpolar components. Almost all of the mechanisms through which water has binding impact are well established [208–213], and water influences can be identified to a great extent for both implicit [214–219] and explicit [72, 220–224] water models. Yet, our understanding of the role of water in molecular recognition still has puzzles and gaps. Even though the hydrophobic effect can be interpreted reasonably well in simple nonpolar surfaces, many solutes such as proteins, DNA, and supramolecular receptors contain complex polarity profiles and surfaces, in which water can have unique features than water on more unadorned surfaces. Therefore, a small cleft of the surface causes water clusters to grow with decreased hydrogen bond values. This facilitates the transformation of these water molecules into bulk, where they recover several more possibilities for lost hydrogen bonding interactions [225–228]. Such distinctive cases do not necessarily have classical instances of hydrophobic impact [229, 230]. If a macromolecule associate with other molecules or drug-like small molecules, the work of decimating surface water into bulk will significantly affect the binding free energy value [210, 213, 231–237]. Consequently, both molecular recognition and nonspecific aggregation of molecules in an aqueous solution are of central concern for water properties on molecular surfaces. Simultaneously, water can make favorable van der Waals interactions between the polar and the apolar portions, and it can accept and donate hydrogen bonds with polar parts. This interactivity makes it difficult for a drug molecule to remove water molecules from binding sites to the bulk. However, the hydrophobic effect tends to make the hydration of apolar surfaces adverse, presumably due to a mixture of entropic and enthalpic effects, thus making it much easier to displace water molecules. It

is also suggested that an interacting map of receptor-water in a binding site produces a three-dimensional prototype replicating strongly binding drugs [235]. Therefore, the hydration of binding sites contains valuable insights about the core features that even a drug molecule could recreate when the drug is binding with its target.

Despite the complicated interactions of water-receptor in conventional binding sites, many advanced computational techniques used in the structural design of small molecules have generalized water treatments, such as continuum models of solvent, without considering the topological limits of the small size and hydrogen binding configuration of water molecules. New computer-based methods have been developed to calculate and envision water structures and thermodynamics at surfaces through the application of the inhomogeneous solvation theory (IST) [238–242] to simulate solute molecules in explicit water. Many of these methods, including WaterMap [225, 235], solvation thermodynamics of ordered water (STOW) [243], and others [244–246], are simple to use by computing the density distribution of water from distinct locations. This restriction has been tackled with the execution of grid-based inhomogeneous solvation theory, known as GIST [228, 247–250]. GIST discretizes the layering propagation of water density and other properties over a fine three-dimensional grid rather than converging local orientational water entropy is solved by the use of an extremely useful nearest-neighbor (NN) approach in comparison to histogram methods that need more sampling to achieve sufficient convergence [251, 252]. GIST may further benefit from the fact that regions with lower densities contribute significantly less to the displaced waters' total orientational entropy than those regions with higher density regions. Such density-weighting implies that the total integral of the orientational entropy may be converged with an appropriate tolerance over a volume comprising both high and low density regions, such that the high density regions get converged well. The grid methodology also makes it easy to focus on regions where a high water density occurs, just like in other techniques, despite modifying its forms.

In this chapter, we have applied the GIST methodology on two previously synthesized [38] supramolecular receptors, known as host-1a and host-1b (Figure 1-4 of Chapter 1). These receptors are very small and are known as the endo-functionalized molecular tubes [59, 60]. The reason behind choosing these two receptors is that these two small synthetic receptors can bind many environmentally and industrially relevant small molecules from an aqueous medium with a profound affinity [38, 105, 253–256]. Thus, we are very curious to know the thermodynamics behind these strong host-guest complexes and water molecules' role during the complexation processes. Previously no such work has been done

to deduce the function and thermodynamics of water molecules behind the above-mentioned strong affinity of these types of supramolecular receptors. Molecular dynamics (MD) simulation trajectories in the explicit solvent are utilized to compute the water molecules' local thermodynamics in and around (at different regions) of these two receptor molecules. From this study, one can able to understand the different thermodynamic properties of water molecules in and around these endo-functionalized receptor molecules.

The rest of the chapter is organized as follows. The materials used in this study and the theories, and computational details of MD simulation and GIST analysis are provided in section 'MATERIALS AND METHODS'. Our results are provided in 'RESULTS' section, and these findings are discussed in 'DISCUSSIONS' section. All of these findings are summarized in 'SUMMARY AND CONCLUSIONS' section.

■ MATERIALS AND METHODS

Grid Inhomogeneous Solvation Theory (GIST)

GIST has been developed by Gilson et al. [248]. Within GIST, the spatial integrals used in the theory of inhomogeneous solvation [241,242] are replaced by discrete sums over the voxels of a three-dimensional grid, where the quantities on the grid are determined from the stored molecular dynamics (MD) simulation frames. GIST describes the relative density of water in voxel k to that of bulk water, $g(r_{\mathrm{k}})$, as follows:

$$g(r_{\mathrm{k}}) = \frac{\rho(r_{\mathrm{k}})}{\rho^0} = \frac{n(r_{\mathrm{k}})}{\rho^0 V_{\mathrm{k}}} \tag{5.1}$$

Here, the voxel index is k, and the center position of voxel k is r_{k}. The number density of bulk waters is ρ^0, and the number density of water molecules in voxel k is $\rho(r_{\mathrm{k}})$. V_{k} is the voxel k volume, and $n(r_{\mathrm{k}})$ is the average number of voxel k waters over all frames used for GIST analysis. In this analysis, if its oxygen atom is in the voxel, then a water molecule will be in voxel k (assumed), and $g(r_{\mathrm{k}})$ is supposed to be uniform within each voxel. For any water molecules in the voxel k, the translational ($S_{\mathrm{tr}}(r_{\mathrm{k}})$) and orientational ($S_{\mathrm{or}}(r_{\mathrm{k}})$) entropies, and the interaction energies (which include electrostatic and van der Waals interactions) with a solute or other water molecules in the voxel k, $E_{\mathrm{sw}}(r_{\mathrm{k}})$ or $E_{\mathrm{ww}}(r_{\mathrm{k}})$, are measured for each voxel by employing $g(r_{\mathrm{k}})$ and force field parameters employed for the MD simulation. If the solvation entropies and solvation interaction energies in the voxel k are determined by dividing these values by the number of water molecules in that voxels, these quantities are known as the normalized thermodynamic quantities and defined

as $\Delta S^{w}_{\mathrm{tr}}(r_{\mathrm{k}})$, $\Delta S^{w}_{\mathrm{or}}(r_{\mathrm{k}})$, $\Delta E^{w}_{\mathrm{sw}}(r_{\mathrm{k}})$, and $\Delta E^{w}_{\mathrm{ww}}(r_{\mathrm{k}})$ [248]. But when these quantities are not divided with water numbers (i.e., these values are for all the water molecules), are known as the non-normalized quantity and defined as $\Delta S_{\mathrm{tr}}(r_{\mathrm{k}})$, $\Delta S_{\mathrm{or}}(r_{\mathrm{k}})$, $\Delta E_{\mathrm{sw}}(r_{\mathrm{k}})$, and $\Delta E_{\mathrm{ww}}(r_{\mathrm{k}})$ in the voxel k.

Normalized thermodynamic parameters are defined as follows to compare these thermodynamic parameters among different systems or different regions [257]:

$$T\Delta S^{w}_{tr}(R) = \frac{1}{n(R)} T\Delta S_{tr}(R) = \frac{1}{n(R)} \sum_{k\in R} T\Delta S_{tr}(r_{\mathrm{k}}), \tag{5.2}$$

$$T\Delta S^{w}_{or}(R) = \frac{1}{n(R)} T\Delta S_{or}(R) = \frac{1}{n(R)} \sum_{k\in R} T\Delta S_{or}(r_{\mathrm{k}}), \tag{5.3}$$

$$\Delta E^{w}_{sw}(R) = \frac{1}{n(R)} \Delta E_{sw}(R) = \frac{1}{n(R)} \sum_{k\in R} \Delta E_{sw}(r_{\mathrm{k}}), \tag{5.4}$$

$$\Delta E^{w}_{ww}(R) = \frac{1}{n(R)} \Delta E_{ww}(R) = \frac{1}{n(R)} \left(E_{ww}(R) - E^{0}_{ww}(R)\right) = \frac{1}{n(R)} \left(\sum_{k\in R} E_{ww}(r_{\mathrm{k}}) - \rho^{0} V(R) \epsilon^{0}_{ww} \right), \tag{5.5}$$

$$\Delta E^{w}_{ww}(R) = \frac{1}{n(R)} \left(\sum_{k\in R} E_{ww}(r_{\mathrm{k}}) - \frac{\rho^{0}}{\rho(R)} n(R) \epsilon^{0}_{ww} \right), \tag{5.6}$$

$$V(R) = \sum_{k\in R} V_{\mathrm{k}}, \tag{5.7}$$

$$n(R) = \sum_{k\in R} n(r_{\mathrm{k}}), \tag{5.8}$$

$$\rho(R) = \frac{n(R)}{V(R)}, \tag{5.9}$$

where ϵ^{0}_{ww} and T represents the mean water-water interaction energy for bulk water and absolute temperature, respectively. R is the region within the simulation framework defined for GIST analysis. V(R) is the sum of the volume of voxels included in region R, n(R) is the average number of water molecules in region R across all frames, and ρ(R) is the number density of water molecules in region R. The water-water interaction energy for bulk water in region R is E^{0}_{ww}(R) is described in the original article [248] as n(R)ϵ^{0}_{ww}. With this definition, the water density in region R, ρ(R) = n(R) / V(R), may vary from the true bulk water density, ρ^{0}. Using the description of the original article [248], ΔE_{ww}(R) is underestimated

in the case of $\rho(\mathrm{R}) > \rho^0$, while $\Delta E_{\mathrm{ww}}(\mathrm{R})$ is overestimated in the case of $\rho(\mathrm{R}) < \rho^0$. Thus, in the current study, as shown in equations 5.5 and 5.6, $\mathrm{E}^0_{ww}(\mathrm{R})$ is redefined as $\rho^0 \mathrm{V}(\mathrm{R})\epsilon^0_{ww}$ $= \frac{\rho^0}{\rho(R)} n(R)\epsilon^0_{ww}$ [257]. In this analysis, we set the number density, ρ^0, to 0.0329 Å^{-3}, and the mean water-water interaction energy ϵ^0_{ww}, to -9.533 kcal/mol per water molecule as reference values for bulk TIP3P water [72,258]. Total entropy change in region R is defined as:

$$T\Delta S^w_{total}(R) = T\Delta S^w_{tr}(R) + T\Delta S^w_{or}(R), \tag{5.10}$$

and, similarly, total interaction energy change in region R is defined as:

$$\Delta E^w_{total}(R) = \Delta E^w_{sw}(R) + \Delta E^w_{ww}(R), \tag{5.11}$$

Lastly, the difference of normalized average free energy relative to bulk water in region R can also be written as:

$$\Delta G^w(R) = -T\Delta S^w_{tr}(R) - T\Delta S^w_{or}(R) + \Delta E^w_{sw}(R) + \Delta E^w_{ww}(R). \tag{5.12}$$

As shown in Eq. 5.12, the difference in enthalpy between a water molecule in region R and that in bulk water corresponds to $\Delta E^w_{sw}(\mathrm{R}) + \Delta E^w_{ww}(\mathrm{R})$. The corresponding non-normalized average free energy is represented as ΔG.

Materials

We have selected two receptors host-1a and host-1b to investigate these endo-functionalized molecular tube receptors' hydration properties. We have conducted one simulation, which consists of the host molecule with normal partial charges and a different simulation, where partial charges of all host atoms are set to zero to investigate electrostatics' role in solvation. Host molecules with normal partial charges and zero partial charges are termed as regular and nonpolar hosts. The optimization of two host molecules (host-1a and host-1b) and ammonium ion is performed using an HF/6-31+G** basis set of Gaussian 09 [106]. The RESP (restrained electrostatic potential) [67] module of AMBER14 [63] measures the partial charges of every atomic site of all these molecules. All other General AMBER Force Field (GAFF) [108] parameters for these molecules are calculated using the ANTECHAMBER [107] module of AMBER14. Partial charges for all the atomic positions of both the host molecules are presented in Chapter 2 (Tables 2-1 and 2-2). The Hartree-Fock (HF) gas phase optimized configurations for both host molecules are used for MD simulations in an aqueous medium. The addition of four regular ammonium ions neutralizes both the regular host molecules [38, 105] and four nonpolar ammonium ions

(ammonium ion with zero partial charges at every atomic site) with every nonpolar host molecules to maintain a similar environment. This work is carried out using the three-point transferable interaction potential (TIP3P) model of water [72]. Regular host-1a (as well as nonpolar host-1a) and regular host-1b (as well as nonpolar host-1b) are immersed in a rectangular box of 1684 and 1692 TIP3P water molecules, respectively (Table 5-1). The PACKMOL [74] package prepares the initial configurations for all systems.

Table 5-1. Overview of Systems[a]

System	N_{host}	$N_{NH_4^+}$	N_{wat}
Regular host-1a	1	4	1684
Regular host-1b	1	4	1692
Nonpolar host-1a	1	4	1684
Nonpolar host-1b	1	4	1692

[a] For nonpolar host molecules, ammonium ions are also nonpolar. N_{host}, $N_{NH_4^+}$, and N_{wat} are the numbers of the host, ammonium ion, and water molecules, respectively.

Molecular Dynamics Simulation

The sander module of AMBER14 is used for every MD simulation of this work. For each simulation, periodic boundary conditions (PBC) are employed in all three directions. Using the SHAKE algorithm [71], all covalent bonds involving hydrogen atoms are constrained. A 10 Å cut-off distance is defined to estimate the short-ranged nonbonded interactions, and the Particle Mesh Ewald (PME) [73] is used to treat all long-ranged electrostatic interactions. Each simulation is carried out by taking a time step of 2 fs. Every system is introduced to 20000 steps (the first 4000 steps are in steepest descent, and the rest 16000 steps are in conjugate gradient method) of energy minimization. We have restrained the whole host molecule in the first minimization and only the hosts' heavy atom in the second minimization. Every system is slowly heated from 0 to 300 K in steps of 50 K for 120 ps (in the canonical (NVT) ensemble). Then, 10 ns equilibration is performed in the isothermal-isobaric (NPT) ensemble at 300 K temperature and 1 atm pressure. We have used Berendsen barostat [75] with a pressure relaxation time of 2 ps to maintain the expected pressure of 1 atm. Langevin dynamics [76] method with 1 ps^{-1} collision frequency is employed to maintain 300 K temperature during the simulation. Then each system is introduced to 5 ns equilibration and followed by a 1 μs production run in the NVT ensemble. Host's heavy atoms are restrained during every equilibration and production run. 10 kcal/$Å^2$ force constant is used for every harmonic restraint.

Analysis of Molecular Dynamics Simulation Data

We have used the GIST module [258] in the CPPTRAJ module [77] in AMBER14 to explore the thermodynamic parameters of the solvent molecules surrounding these endo-functionalized receptors. We have calculated these thermodynamic properties in and around these receptor molecules.

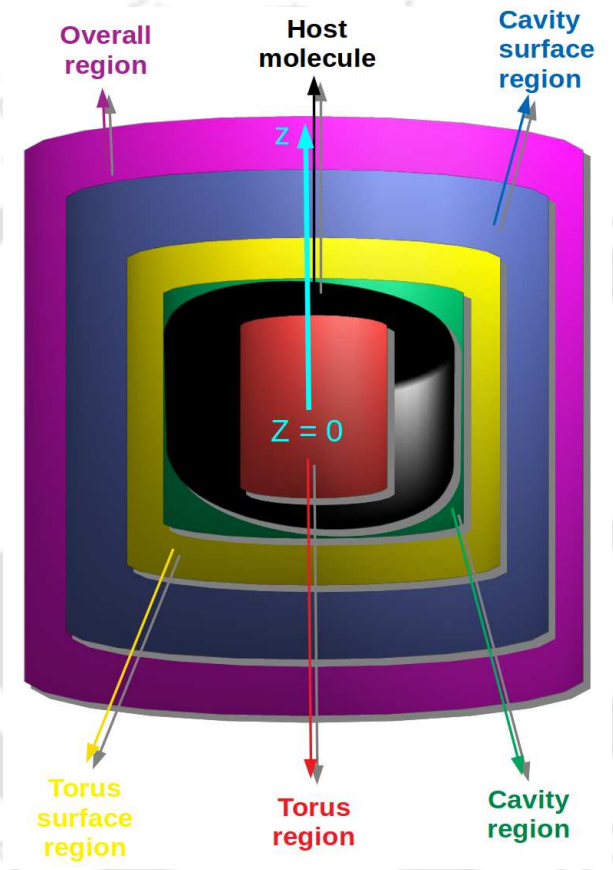

Figure 5-1. *The size and position of different grid boxes for these host molecules used for the analysis of different thermodynamic properties are schematically presented here. Central position of the host molecules is selected as z=0.*

Overall GIST box size is 20 Å × 20 Å × 21 Å. We have also chosen four different regions (four rectangular 3D grid boxes of different dimensions) to get a comparative picture of water thermodynamics in and around these receptor molecules. These regions are defined as torus (6 Å × 6 Å × 7 Å), cavity (10 Å × 10 Å × 11 Å), torus surface (13 Å × 13 Å × 14 Å), and cavity surface (15 Å × 15 Å × 16 Å) regions (all these regions are schematically represented in Figure 5-1). Torus and cavity regions are inside the host cavity,

and other two regions are around the host cavity. All these regions are rectangular. We have selected these regions as of the work of Nguyen et al. [248]. Z-axis passes through the host cavity and central position of the host molecules is selected as z=0 (Figure 5-1). The grid spacing is 0.5 Å along each axis, as this provides a precise representation of the local water density. These thermodynamic properties are visualized using the Visual Molecular Dynamics (VMD) [78] software package. We have used the last 100 ns production run trajectories for GIST analysis. Before applying GIST analysis, we have removed all the ammonium ions from the simulation boxes because GIST assumes that the solute of interest includes all molecules in the simulation box except water molecules [257].

■ RESULTS

We begin with the GIST analysis of waters' local thermodynamic properties for both the regular host molecules (host-1a and host-1b) and their nonpolar modified forms. For both regular and nonpolar receptors, we introduce a statistical analysis of the same information. From this analysis, one can fully understand the solvation properties and the ligand-binding capabilities of these host molecules and the functions of water molecules during the ligand-binding process. These properties are very important during a complexation process (in between host and preferred guest molecule) and will help to understand the actual mechanism behind these complexation processes, provided a suitable host is present in the respective system.

Structural and Thermodynamic Visualization of Water

Regular Host

Host-1a and host-1b are an essential class of macrocyclic receptors and can encapsulate different environmentally and chemically important guest molecules from an aqueous medium [38, 105, 253–256]. Thus, to know the role of water molecules during these encapsulations, detailed thermodynamic analysis is necessary. Different thermodynamic parameters in different regions of regular host-1a are presented in Table 5-2 (top), and the same for regular host-1b is presented in Table 5-3 (top). Every quantity in this table is the normalized thermodynamic quantity.

Table 5-2. Normalized thermodynamic quantities[a]

Region	n(R)	$-T\Delta S^w_{tr}$	$-T\Delta S^w_{or}$	ΔE^w_{total}	ΔE^w_{sw}	ΔE^w_{ww}	ΔG^w
		Regular host-1a					
Torus	2.8	0.38	0.98	2.12	-5.74	7.86	3.48
Cavity	5.1	0.33	0.76	1.96	-4.76	6.72	3.05
Torus Surface	10.3	0.15	0.39	-0.33	-1.92	1.59	0.21
Cavity Surface	24.4	0.13	0.34	-0.29	-1.85	1.56	0.18
		Nonpolar host-1a					
Torus	2.2	0.25	0.48	3.86	-2.35	6.21	4.59
Cavity	3.9	0.20	0.36	3.51	-1.31	4.82	4.07
Torus Surface	9.9	0.14	0.26	-0.06	-0.71	0.65	0.34
Cavity Surface	24.2	0.11	0.23	-0.03	-0.69	0.66	0.30

[a] Normalized thermodynamic quantities in various regions of regular (top) and nonpolar (bottom) host-1a. All normalized energy values are expressed in kcal/mol. The average number of water molecules in any region is represented by n(R), and all other parameters are described in the method section.

Table 5-3. Normalized thermodynamic quantities[a]

Region	n(R)	$-T\Delta S^w_{tr}$	$-T\Delta S^w_{or}$	ΔE^w_{total}	ΔE^w_{sw}	ΔE^w_{ww}	ΔG^w
		Regular host-1b					
Torus	2.9	0.42	1.12	0.14	-8.92	9.06	1.68
Cavity	5.4	0.38	0.94	0.09	-7.84	7.93	1.41
Torus Surface	10.6	0.16	0.55	-1.90	-4.62	2.72	-1.19
Cavity Surface	24.9	0.14	0.43	-1.55	-4.06	2.51	-0.98
		Nonpolar host-1b					
Torus	2.4	0.30	0.58	2.55	-4.82	7.37	3.43
Cavity	4.1	0.26	0.49	2.25	-3.98	6.23	3.00
Torus Surface	10.1	0.14	0.36	-0.67	-1.65	0.98	-0.17
Cavity Surface	24.5	0.13	0.28	-0.65	-1.58	0.93	-0.24

[a] Normalized thermodynamic quantities in various regions of regular (top) and nonpolar (bottom) host-1b. Every energy value is expressed in kcal/mol. The average number of water molecules in any region is represented by n(R), and all other parameters are described in the method section.

Translational Entropy and Water Density:

The contour of local translational entropy ($-T\Delta S^w_{tr}$) contribution to the free energy of solvation (ΔG^w) in and around regular host-1a and regular host-1b is displayed in Figure 5-2 (Figure 5-2(a) and Figure 5-2(b) are for regular host-1a, and Figure 5-2(c) and Figure 5-2(d) are for regular host-1b). The numerical values of these entropy contributions are listed in Tables 5-2 and 5-3. According to GIST theory [248], this value is linked to the local water density. Thus, translational entropy contours are directly related to the contours of local water density.

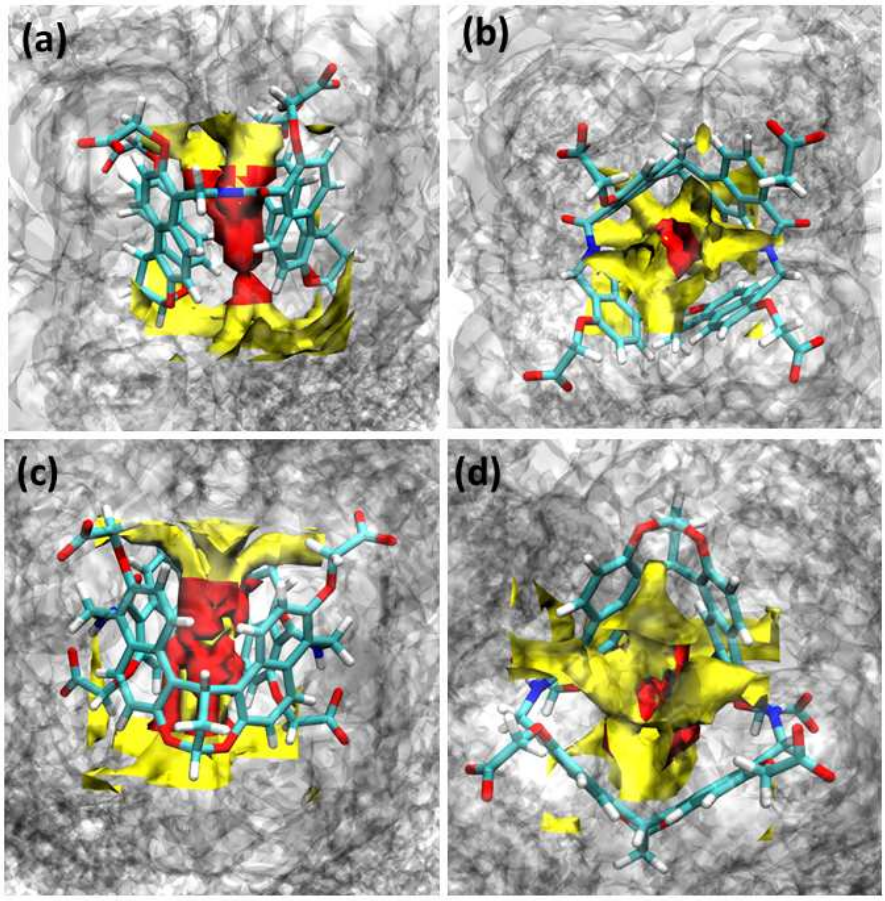

Figure 5-2. *Normalized translational entropy contours for both the regular host molecules. (a) and (b) are for the regular host-1a, and (c) and (d) are for regular host-1b. The left panel and right panel of this figure are the side view and top view, respectively. Translational entropy contours at different regions are represented in different colors, like red (torus), yellow (cavity), and white in ghost representation (overall). 0.5, 1.0 and 0.75 isovalue is used for torus, cavity and overall region contour lines, respectively.*

The most noticeable part of this density plot for both the receptor is the red torus and yellow cavity region of slightly unfavorable translational entropy values (unfavorable in terms of the contribution to the ΔG^w. As, -TΔS^w_{tr} is more positive, ΔG^w becomes more positive, i.e., water molecules become more unfavorable) (see Table 5-2 and Table 5-3), and prosperous water density in the whole cavity of both these host molecules (Figure 5-2). As one move from the center of both the regular host molecule, water molecules become translationally less ordered. Thus, we can say that water molecules are translationally

less favored (concerning the contribution to ΔG^w) in the torus region and getting more translational stability as they move from torus to cavity to torus surface to cavity surface region. The translational entropy gain due to a water molecules' displacing from the torus and cavity region is very less but higher than the displacement of water from other regions of both the regular host-1a (Table 5-2) and regular host-1b (Table 5-3). Thus, for a guest molecule that will displace these water molecules from the torus and cavity regions, these corresponding translational entropy will gain in the form of complexation binding free energy, and ligand gets stabilized inside the cavity of both the regular host molecules.

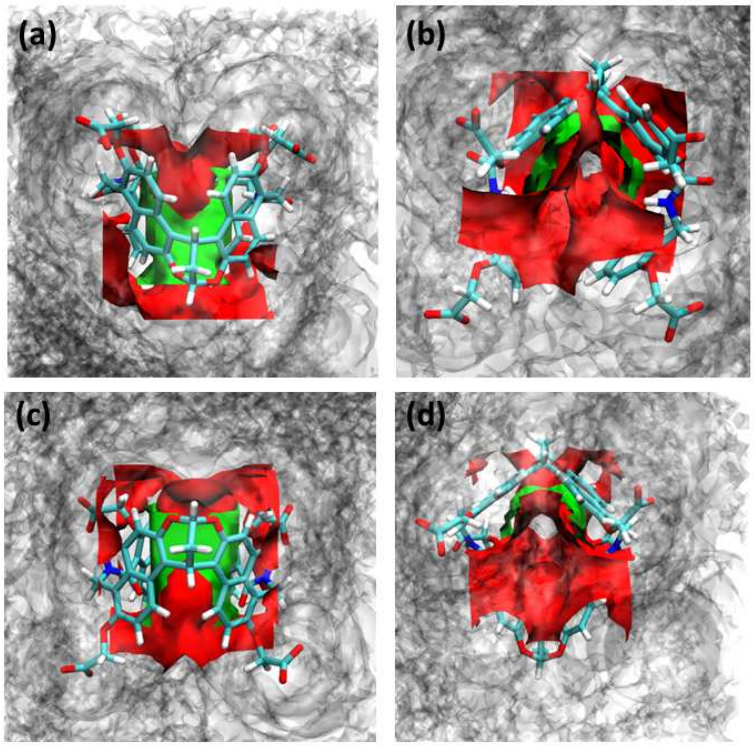

Figure 5-3. *Normalized water hydrogen density contours for regular host-1a ((a) and (b)) and regular host-1b ((c) and (d)). The left panel and right panel of this figure represent the side and top view, respectively. Hydrogen density contours at torus is in green, at cavity is in red, and the overall region is in white (ghost). 0.5, 1.0 and 0.75 isovalue is used for torus, cavity and overall region contour lines, respectively.*

Figure 5-3 shows the contours of the density of water hydrogen atom at different regions of regular host-1a, and regular host-1b (Figure 5-3(a) and Figure 5-3(b) are for regular host-1a, and Figure 5-3(c) and Figure 5-3(d) are for regular host-1b). These figures

also support high-density water molecules in the torus (green) and cavity (red) regions of both the regular host molecules. This localization of hydrogen density inside the regular host molecule's cavity region is because of the hydrogen bonding interaction of the water oxygen atom and the host's N-H protons. A significant amount of water is present inside the cavity of both the regular host molecule. Therefore, those guest molecules which can displace all or some of the water molecules and form a more strong interaction with the receptor molecule than the receptor with water can place themselves into the cavity of regular host-1a and regular host-1b. This is one of the criteria to form stable host-guest complexes with both these receptors.

Orientational Entropy:

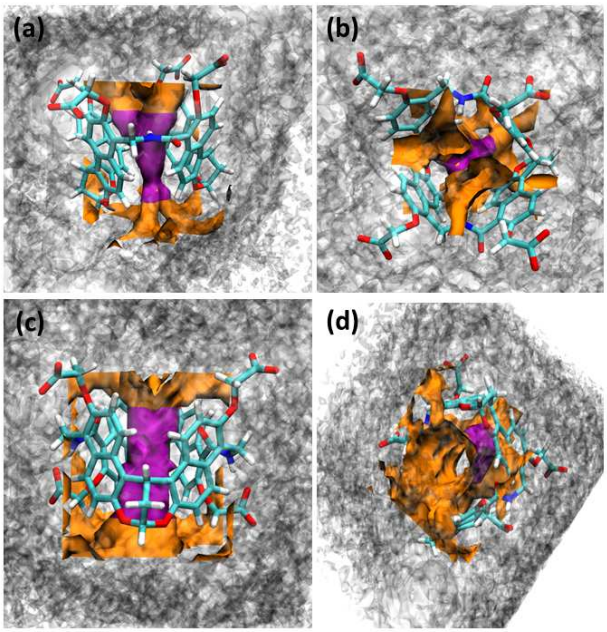

Figure 5-4. *Normalized orientational entropy contours for both the regular host molecules. The left and right panels are for side and top view, respectively. (a) and (b) are for the regular host-1a, and (c) and (d) are for the regular host-1b. Torus, cavity, and overall regions are represented in purple, orange, and white (ghost), respectively. 0.5, 1.0 and 0.75 isovalue is used for torus, cavity and overall region contour lines, respectively.*

Orientational entropy (-TΔS^{w}_{or}) contours in different regions of both regular host-1a and regular host-1b are plotted in Figure 5-4 (Figure 5-4(a) and Figure 5-4(b) are for regular host-1a, and Figure 5-4(c) and Figure 5-4(d) are for regular host-1b). Water

molecules are orientationally ordered in and around both the regular host molecules but are most orientationally ordered in the torus and cavity regions (see Table 5-2 and Table 5-3). Thus, orientational entropy unfavorably contributes to the free energy of solvation, and this is maximum for the torus and cavity water molecules. The most orientationally ordered water density for both the regular host molecules are shown in purple (torus) and orange (cavity) (see Figure 5-4). These ordered water molecules have resulted from the hydrogen bonding between water and host molecules. Surface water molecules (white, ghost in Figure 5-4) are less orientationally ordered. Thus, it can be said that water molecules are orientationally less favored (for the contribution to ΔG^w) at the torus region and become more and more favorable as they move from torus to cavity surface region. This orientational entropy gain due to the displacing of water molecules is very significant for torus and cavity region and less significant for torus surface and cavity surface for both the regular host molecules and also, these values for regular host-1b are more significant than regular host-1a at every discussed region (see Table 5-2 and Table 5-3). Therefore, when any guest molecule can displace the water molecules from the torus and cavity regions, these corresponding orientational entropies will gain in the form of complexation binding free energy, and ligand gets stabilized inside the cavity.

Total Entropy:

Total entropy (-TΔS^w_{total}) is the summation of translational and orientational entropy. Water molecules at every region of both the regular host molecules are translationally (very less) and orientationally (highly) ordered. Thus, water molecules become entropically ordered in every region of both the regular host molecules. Most entropically ordered water molecules are found at the torus region, followed by the cavity region, and water molecules are entropically more ordered at every region of regular host-1b than the corresponding region of regular host-1a. Therefore, entropy has an unfavorable contribution to the free energy of solvation in every region of both the regular host molecules. Thus, water molecules are more entropically unfavored (concerning the contribution to ΔG^w) at torus, and it tends to become somewhat less unfavorable as one moves from the torus to the cavity surface region. Therefore, when any guest molecule replaces the water molecules from both these host molecules' whole cavity the corresponding entropic contribution will be gained to the complexation binding free energy values.

Total Solvation Energy:

Total solvation energy is the sum of solute-water and water-water interaction energy. Normalized solvation energy values at different regions of regular host-1a and regular host-1b are presented in Table 5-2 and Table 5-3, respectively. Total solvation energy is unfavorable inside the host and is favorable around the host for both the regular host molecules. This energy term is much more unfavorable for regular host-1a compared to the slightly unfavorable for regular host-1b (inside the host) and much more favorable for regular host-1b compared to the slightly favorable regular host-1a (around the host molecule). In the torus and cavity regions, water molecules interact adversely with their context, and water molecules in these regions are also entropically adverse. From our simulation data, maximum water density is found in the torus and cavity regions for both the host molecules. Thus, torus and cavity waters are energetically less stable. These water molecules are removable by suitable guest molecules, involving strong interactions with the host molecules, and can place themselves within these host molecules' cavities.

Host-Water and Water-Water Interaction Energies:

In each voxel, the total energy is decomposed into the interactions between the solute-water and water-water interactions. Absolute value of solute-water and water-water interactions are higher than the total energy value (see the top portion of Table 5-2 and Table 5-3), but these two energy values compensate each other in every region for both the regular host molecules. Contour plots of solute-water interaction are plotted in Figure 5-5 (Figure 5-5(a) and Figure 5-5(b) are for regular host-1a, and Figure 5-5(c) and Figure 5-5(d) are for regular host-1b) and water-water interaction contours are plotted in Figure 5-6 (Figure 5-6(a) and Figure 5-6(b) represent regular host-1a, and Figure 5-6(c) and Figure 5-6(d) are for regular host-1b). For solute-water contours, the torus and cavity regions are represented in red and yellow colors, respectively, and in water-water contours, cyan and yellow colors represent the torus and cavity regions, respectively. Solute-water interaction is the most favorable inside the host, and this interaction becomes less favorable around the host surface for both the regular host molecules. Torus region has the most favorable attractive solute-water interaction energy followed by the cavity, torus surface, and cavity surface regions (this is true for both the regular host molecules). Also, solute-water interaction energy is significantly more favorable for regular host-1b than regular host-1a in every region, as mentioned above. The presence of strong hydrogen bonding interaction between host and water in the torus and cavity regions is also supported by

this highly attractive host-water interaction energy in these regions.

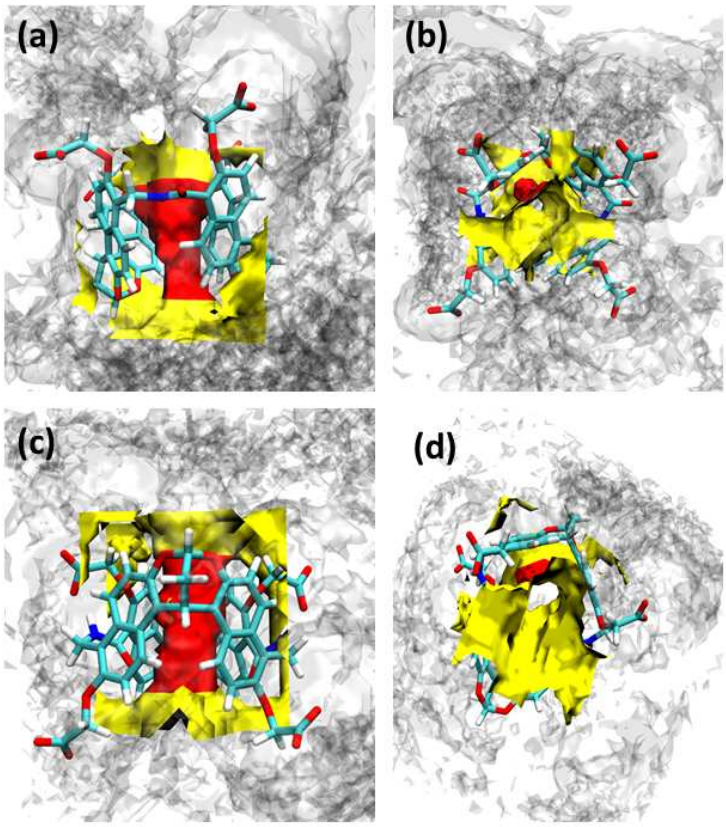

Figure 5-5. *Normalized solute-water interaction energy contours for both the regular host molecules. The side view and top view of these representations are in the left and right panel, respectively. (a) and (b) are for regular host-1a, and (c) and (d) are for regular host-1b. Red, yellow, and white (ghost) represent the torus, cavity, and overall regions. 0.5, 0.5 and 0.75 isovalue is used for torus, cavity and overall region contour lines, respectively.*

On the other hand, water-water interaction energy (see Table 5-2 and Table 5-3 and Figure 5-6) is unfavorable concerning the contribution to ΔG^{w} for both the regular host molecules. This is because host molecules' presence weakens the interaction between the water molecules concerning bulk water, and this weakening will be more prominent with the increase of host-water interaction. This comes primarily from the hosts' simple excluded volume, which decreases the number of neighbors around the water molecule. It is more clearly reflected within the hosts' torus and cavity regions. Additionally, the host forms strong hydrogen bonds at the torus and cavity regions with water molecules, thereby

preventing them from making hydrogen bonds with other water molecules.

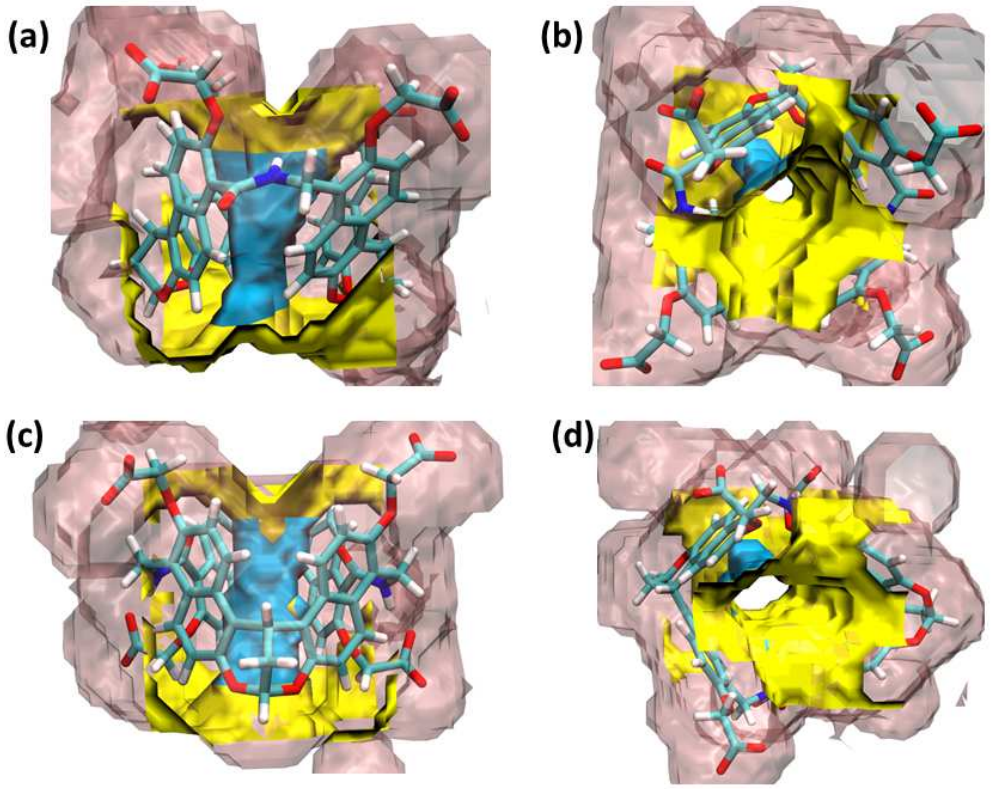

Figure 5-6. *Normalized water-water interaction energy contours for regular host-1a ((a) and (b)), and regular host-1b ((c) and (d)). The left and right panel represents the side and top view, respectively. The torus, cavity, and overall region of both these host molecules are represented by cyan, yellow, and pink (transparent), respectively. 0.5, 1.0 and 1.0 isovalue is used for torus, cavity and overall region contour lines, respectively.*

Now, as host-water interaction is more favorable for regular host-1b than regular host-1a, that is why water-water interaction becomes more unfavorable for regular host-1b than regular host-1a. However, these hostileness are not as prominent as that of the stability gain due to solute-water interaction. This indicates the total solvation energy for regular host-1b becomes more favorable than regular host-1a in every region, as mentioned earlier.

Nonpolar Host

We have searched the extent of the ordering of water molecules in and around both host-1a and host-1b molecules by simulating the artificial versions of these host molecules,

in which all of the partial charges of both the host molecules are set to zero while all other parameters are left unaltered. These two modified versions of the host, i.e., regular host-1a and regular host-1b are defined as nonpolar host-1a and nonpolar host-1b, respectively. Different normalized thermodynamic parameters estimated in different regions of nonpolar host-1a and nonpolar host-1b are presented in Table 5-2 (bottom) and Table 5-3 (bottom), respectively. The translational entropy contours of both the nonpolar host molecule are depicted in Figure 5-7 (Figure 5-7(a) and Figure 5-7(b) are for nonpolar host-1a, and Figure 5-7(c) and Figure 5-7(d) are for nonpolar host-1b) and orientational entropy contours are presented in Figure 5-8 (Figure 5-8(a) and Figure 5-8(b) are for nonpolar host-1a, and Figure 5-8(c) and Figure 5-8(d) are for nonpolar host-1b).

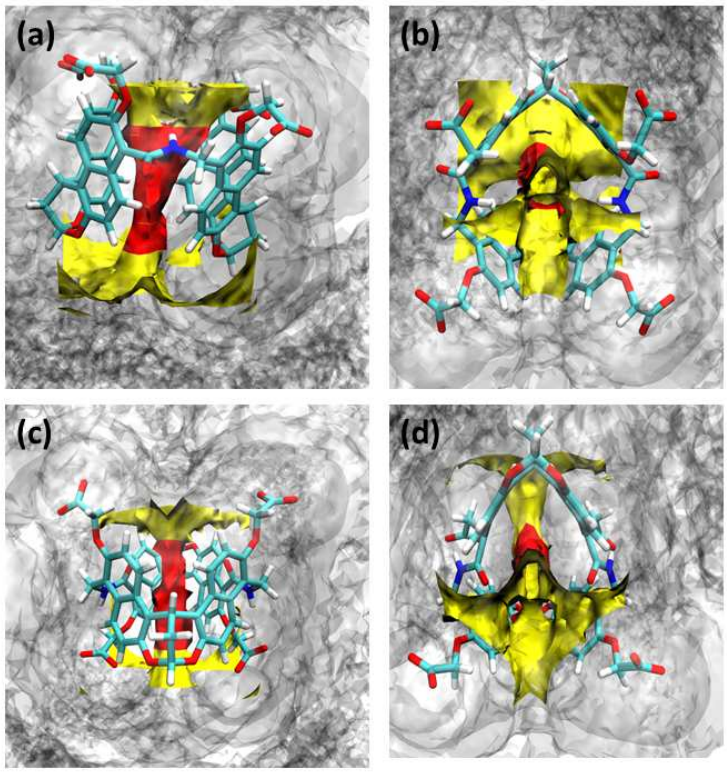

Figure 5-7. *Translational entropy contours are presented here for both the nonpolar host molecules. (a) and (b) are for nonpolar host-1a, and (c) and (d) are for nonpolar host-1b. The left and right panels are the side and top view, respectively. Translational entropy contours at different regions are represented in different colors, like red (torus), yellow (cavity), and white (overall). 0.5, 1.0 and 0.75 isovalue is used for torus, cavity and overall region contour lines, respectively.*

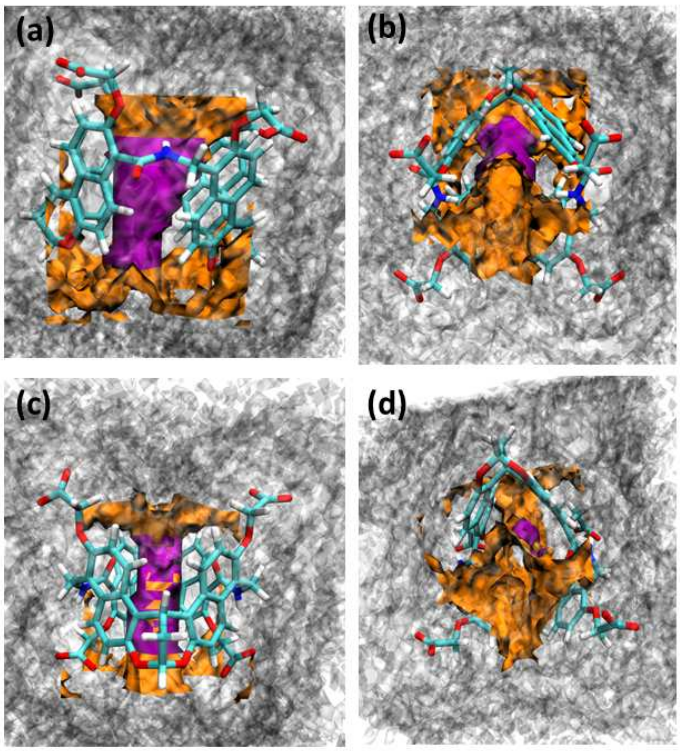

Figure 5-8. *Orientational entropy contours for nonpolar host-1a ((a) and (b)), and nonpolar host-1b ((c) and (d)). Side and top views are in the left and right panel, respectively. Torus, cavity, and overall regions are represented in purple, orange, and white, respectively. 0.5, 1.0 and 0.75 isovalue is used for torus, cavity and overall region contour lines, respectively.*

The nonpolar hosts' translational entropy contours are closely similar to those of the regular host molecules (Figure 5-2). As regular host molecules, the water molecules in nonpolar host-1b systems are translationally somewhat more ordered than nonpolar host-1a. The densely populated torus is still present in particular for both the nonpolar host molecules. The water molecules' translational ordering is less than that of each regions' corresponding regular host molecules. Therefore, it can be inferred that packaging contributes more to create the dense torus region than polar interactions. This decrease in the density value corresponds to the decreased mean number of water molecules in the nonpolar cavity, as shown in Table 5-2 and Table 5-3 by the value of n(R). The decreased water consumption is in line with the expectations for these artificially hydrophobic host molecules. This disorder in local density is a more general effect of the perturbation theory to dense homogeneous

liquids [259]. This homogeneous liquid result does not apply to the exterior of the host molecules, but to the interior, for which turning on or off the electrostatic attractions affects on local densities. These results indicate that the hydrogen bonding with the host is not responsible for these translational orders but rather for the shape and packaging, as mentioned above. On the other hand, the orientational ordering of water molecules in and around the host molecules is affected more due to the turning off the partial charges of the hosts' atomic sites. In the torus and cavity region, the reduction in the water molecules' orientation is important relative to the torus surface and cavity surface regions of both the nonpolar host molecules. Also, water molecules in systems of nonpolar host-1b are orientationally more ordered than nonpolar host-1a. Hydrogen bonding (between host and water) is affected more in the torus and cavity regions due to turning off the electrostatic host-guest interactions. For this, the reduction of orientational ordering is more at the torus and cavity regions. Therefore, we can conclude that the translational ordering of the packaging effect is somewhat significant, but electrostatic interaction is mainly responsible for the orientational ordering for both host-1a and host-1b molecules.

Next, we discuss the effect of electrostatic host-guest interactions on the solvation energy. As we turn off the electrostatic host-guest attraction, solute-water interaction becomes less favorable in every region concerning the corresponding regular host molecule (see Table 5-2 and Table 5-3). This is due to the reduction in the hydrogen bonding interactions between host and water molecules. Remarkable decrease in interaction between nonpolar host molecule and water in the torus and cavity regions compared to the torus surface and cavity surface regions. Thus, we can also say that the maximum decrease in the hydrogen bonding interaction occurs in the torus and cavity regions. Like regular host molecules, solute-water interaction is more favorable for nonpolar host-1b than nonpolar host-1a. Water-water interaction energy becomes somewhat more favorable in each of these regions of both the nonpolar host molecules than the regular host molecule (see Table 5-2 and Table 5-3). Here also, water-water interaction energy is more unfavorable for nonpolar host-1b than nonpolar host-1a. However, the gain of water-water interaction energy does not compensate for the loss of solute-water (favorable) interaction energy for both the nonpolar host molecules. Therefore, total solvation energy becomes more unfavorable at every mentioned region of nonpolar host molecules than regular host molecules. Again, nonpolar host-1b has more favorable solvation energy compared to nonpolar host-1a. Also, the difference of one water molecules' normalized average free energy relative to bulk water (ΔG^w) becomes more unfavorable than the regular host molecules at the regions (see Table

5-2 and Table 5-3).

Quantitative Analysis of the Contributions to Local Solvation

In this section, we discuss the thermodynamics for hydration of local water molecules, taking advantage of the ability of GIST to explore the regions of various dimensions and types. We are mainly interested in regions in and around the receptor molecules, the high water density toroidal area (torus region), the receptor's binding cavity (cavity region), and two sequential regions termed as torus surface and cavity surface.

Regular Host

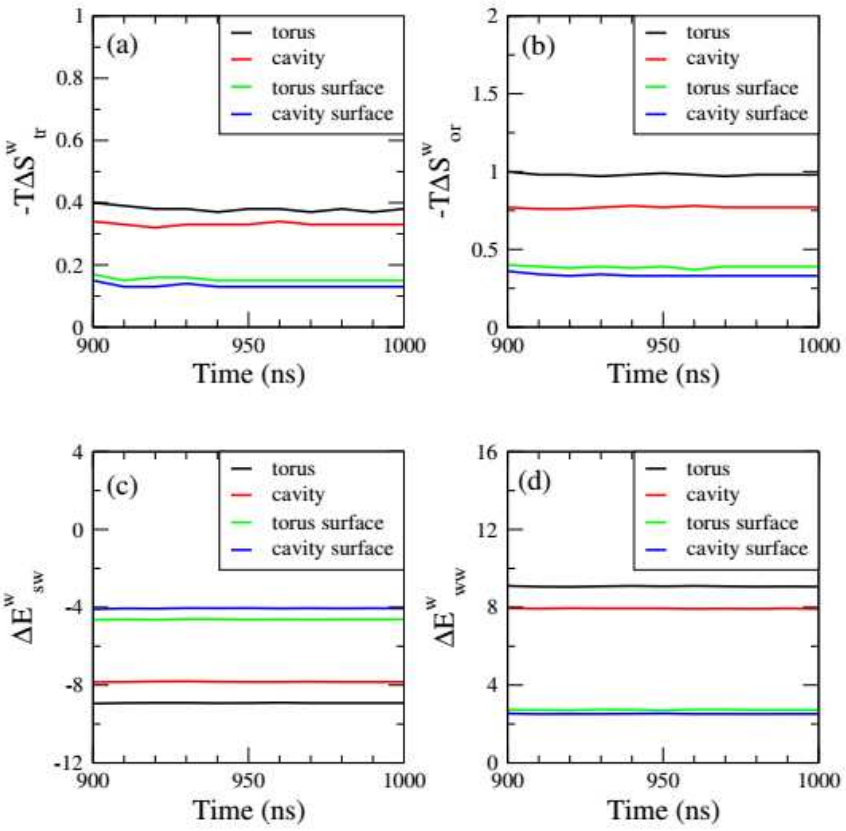

Figure 5-9. *The convergence of water thermodynamic properties with simulation time (ns) at four regions, such as the torus, cavity, torus surface, and cavity surface. (a) and (b) are for the translational and orientational entropies for regular host-1a, and (c) and (d) are the solute-water and water-water interaction energies of regular host-1b, respectively. 900 ns, 950 ns, 1000 ns data on the horizontal axis calculated from the trajectory between 891 ns and 900 ns, 941 ns and 950 ns, 991 ns and 1000 ns, respectively, and so on.*

The normalized thermodynamic properties of water concerning their corresponding bulk values at each region of both the regular host molecules (Table 5-2 and Table 5-3) are discussed here. Every thermodynamic quantity is well converged. For showing the convergence of these thermodynamic properties, some of these properties for both the regular host molecules in every region are plotted with simulation time (last 100 ns) and they are presented in Figure 5-9. The data in Table 5-2 and Table 5-3 for all four regions indicate the same qualitative trend for unfavorable translational and orientational entropies, which means more ordering of water molecules in those regions than bulk water. The water molecules' interactions are less favorable in these regions than the bulk water because the host occupies spaces that else be occupied by water molecules.

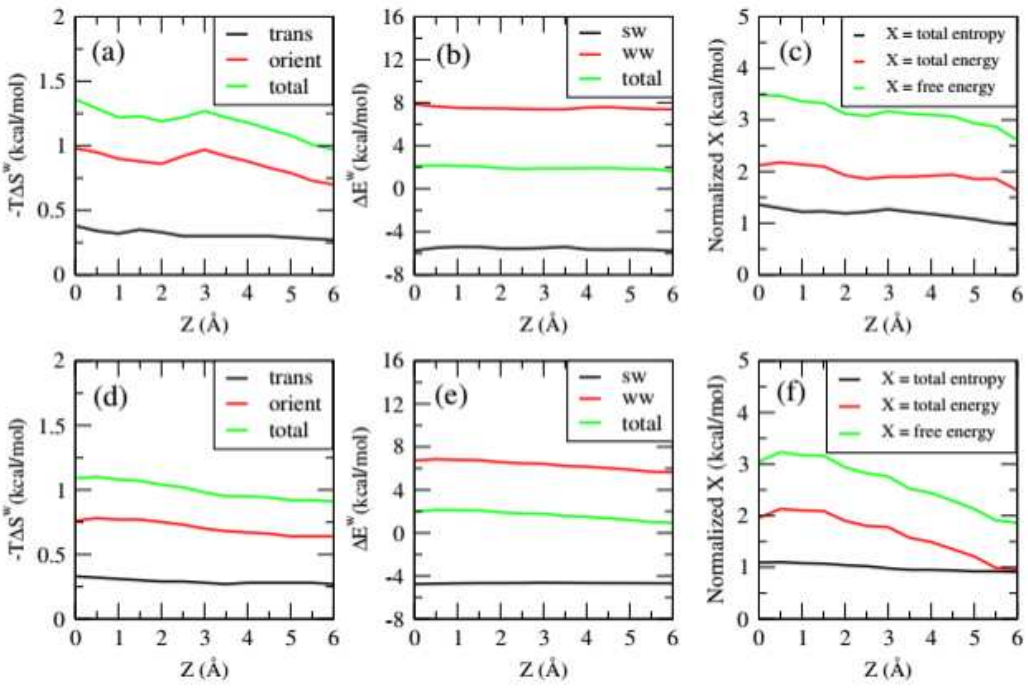

Figure 5-10. *Thermodynamic properties as a function of z-distance for regular host-1a. Upper panel ((a), (b), and (c)) is for the interior and bottom panel ((d), (e), and (f)) is for the exterior thermodynamic properties.*

The beneficial interactions between solute and waters partly sustain the adverse water-water

interactions and entropic contributions. These effects make the normalized free energy (ΔG^{w}) an unfavorable quantity. It makes water molecules thermodynamically unfavorable in these regions rather than bulk water. Next, we are interested to see how these normalized thermodynamic quantities change when we shift the center of the grid box along the z-direction. We have done this analysis both in and around both the regular host molecules. Each time, we have shifted the z-distance by 0.5 Å. The first distance is assumed as 0 Å for both the interior and exterior of these host molecules. These thermodynamic properties as a function of z-distance are plotted in Figure 5-10 (for regular host-1a) and Figure 5-11 (for regular host-1b). The interior and exterior thermodynamic properties of the receptors are in the top and bottom row, respectively, for both the figures (Figure 5-10 and Figure 5-11).

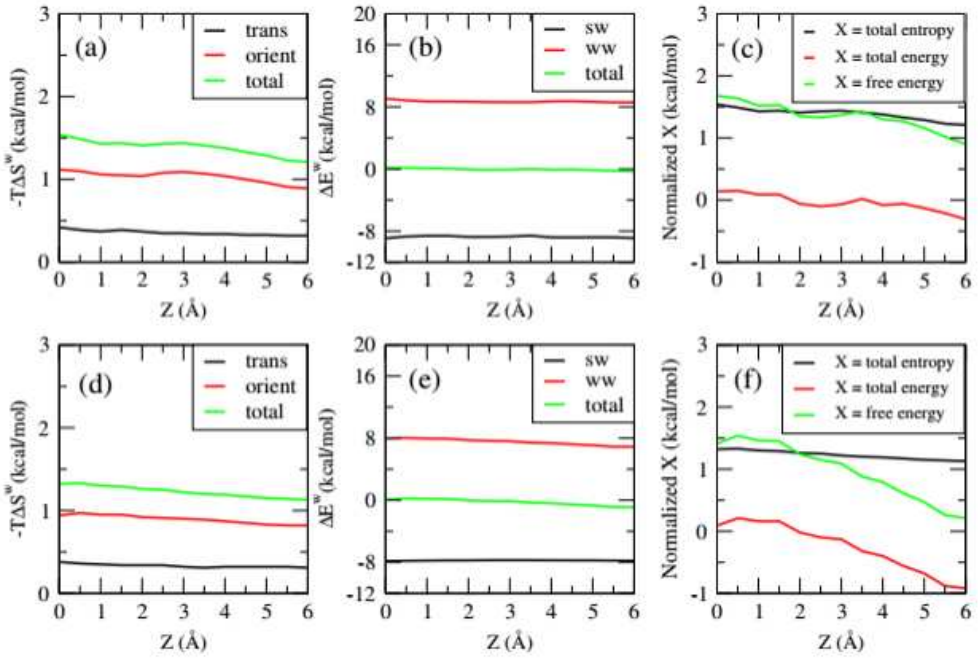

Figure 5-11. *Thermodynamic properties as a function of z-distance for regular host-1b. Top row ((a), (b), and (c)) is for the interior and bottom row ((d), (e), and (f)) is for the exterior thermodynamic properties.*

From Figure 5-10(a) and Figure 5-11(a), the penalty for orientational entropy is higher than the translational entropic penalties inside the host for both the regular host molecules.

Moreover, translational, orientational, and total entropic penalty is higher for regular host-1b than for regular host-1a within the receptor. Solute-water interaction energy (Figure 5-10(b) and Figure 5-11(b)) is favorable everywhere within the receptors, and this favorable host-water interaction energy partly or wholly balances the unfavorable water-water interaction energy. Regular host-1b gives almost zero total interaction and regular host-1a gives some unfavorable total interaction everywhere within the receptors. Again, solute-water interaction energy is more favorable, and water-water interaction energy is more unfavorable for host-1b than host-1a entirely within the receptors. Analogous plots of net entropy, energy, and free energy for regular host-1a and regular host-1b are plotted in Figure 5-10(c) and Figure 5-11(c). For regular host-1a, the free energy penalty contains both entropic and energy contribution, and energy has slightly more contributions than entropy everywhere within the receptors. On the other hand, for regular host-1b (Figure 5-11(c)), the total free energy penalty is mainly entropic due to the abolition of solute-water and water-water interaction energy. The bottom row of Figure 5-10 and Figure 5-11 contains the analogous plot for the receptors' outer surface. Figure 5-10(e), Figure 5-10(f), Figure 5-11(e), and Figure 5-11(f) are analogous to that of the corresponding top row plots but show less thermodynamic perturbation than the corresponding interior thermodynamic parameters. Now, for the exterior of regular host-1a (Figure 5-10(f)), energy contribution is slightly higher than the entropic contribution to the free energy. The decrease of entropic contribution is not prominent with z-distance, but the decrease of energy contribution with z-distance is prominent. On the other hand, for regular host-1b (Figure 5-11(f)), the entropic contribution is higher than the energy contribution to the free energy, and here also, a decrease of entropic contribution is not prominent with z-distance, but the decrease of energy contribution with z-distance is prominent.

Table 5-4. Non-normalized thermodynamic quantities[a]

Region	$T\Delta S_{tr}$	$T\Delta S_{or}$	$-\Delta E_{total}$	$-\Delta E_{sw}$	$-\Delta E_{ww}$	$-\Delta G$
		Regular host-1a				
Torus	-1.06	-2.74	13.13	16.07	-2.94	9.33
Cavity	-1.68	-3.88	9.07	24.28	-15.21	3.51
		Nonpolar host-1a				
Torus	-0.55	-1.06	10.57	5.17	5.40	8.96
Cavity	-0.98	-1.40	5.38	5.11	0.27	3.00

[a] The torus and cavity regions of regular (top) and nonpolar (bottom) host-1a non-normalized thermodynamic properties for water. Every energy value is expressed in kcal/mol. Every thermodynamic parameter is described in the method section.

Table 5-4 and Table 5-5 explain the findings for host-1a and host-1b of extracting and transferring all water molecules from the cavity and torus regions into the bulk. In both, the tables top portions are for regular host, and bottom portions are for nonpolar host molecules.

Table 5-5. Non-normalized thermodynamic quantities[a]

Region	$T\Delta S_{tr}$	$T\Delta S_{or}$	$-\Delta E_{total}$	$-\Delta E_{sw}$	$-\Delta E_{ww}$	$-\Delta G$
		Regular host-1b				
Torus	-1.22	-3.25	18.66	25.87	-7.21	14.19
Cavity	-2.05	-5.08	18.58	42.34	-23.76	11.45
		Nonpolar host-1b				
Torus	-0.72	-1.39	12.95	11.57	1.38	10.84
Cavity	-1.07	-2.01	9.84	16.32	-6.48	6.76

[a] The torus and cavity regions of regular (top) and nonpolar (bottom) host-1b non-normalized thermodynamic properties for water. Every energy value is expressed in kcal/mol. Each of the mentioned thermodynamic quantities is described in the method section.

These values are non-normalized thermodynamic quantity (which is already discussed above in the materials and method sections). They do not consider the thermodynamics of reorganizing the rest of the water as other IST approaches [248]. Remember that such thermodynamic contributions are just the average water numbers in a specific area (n(R)), multiplies the consequent normalized values except water-water interaction energy and, therefore, the free energy values. The reason behind this is the interaction of water pairs within every region would be doubly-counted simply by multiplying the ΔE^{w}_{ww} by the average waters in a region (such as the torus). There is no double-count for the non-normalized thermodynamic quantity stated here, and the value of bulk water average water-water interaction energy is also mentioned, which is approximately -9.533 kcal/mol for the TIP3P water model [258]. Such developments in accounting have resulted in a change in the sign for ΔG compared to ΔG^{w}. From Tables 5-4 and 5-5, it can be seen that the total entropic driving forces for the displacement of water molecules from the cavity region is -5.56 and -7.13 kcal/mol for regular host-1a and regular host-1b, respectively, and the same from the torus region of regular host-1a and regular host-1b is about -3.80 and -4.47 kcal/mol, respectively. About two-thirds of these values are orientational, and one-third of translational contributions comply with the normalized water thermodynamic properties (Tables 5-2 and 5-3). The transmission of water to bulk also results in significantly better interactions between water molecules but the loss of effective interactions between solute-water. The significant energy

loss and the slightly compensative rises in entropy contribute to free energy penalties in both regular hosts for moving water from the cavity and torus regions for both the regular host molecules. For regular host-1a, these free energy penalties are 9.33 and 3.51 kcal/mol, respectively, and the same for regular host-1b are 14.19 and 11.45 kcal/mol, respectively. When all the torus waters are stripped completely, then other water molecule's stripping to completely vacate the cavity has very little thermodynamic influence. Therefore, the water molecules on the torus would control the total removal of water from the cavity. Tables 5-4 and 5-5 will demonstrate a thermodynamically disadvantageous binding of a guest molecule due to the positive free energy value for removing water molecules. Therefore, the guest must create its energetic interactions with the host molecule and be very similar to the displaced water. This energetic gain leads to favorable binding free energy values for stable host-guest complexes.

Nonpolar Host

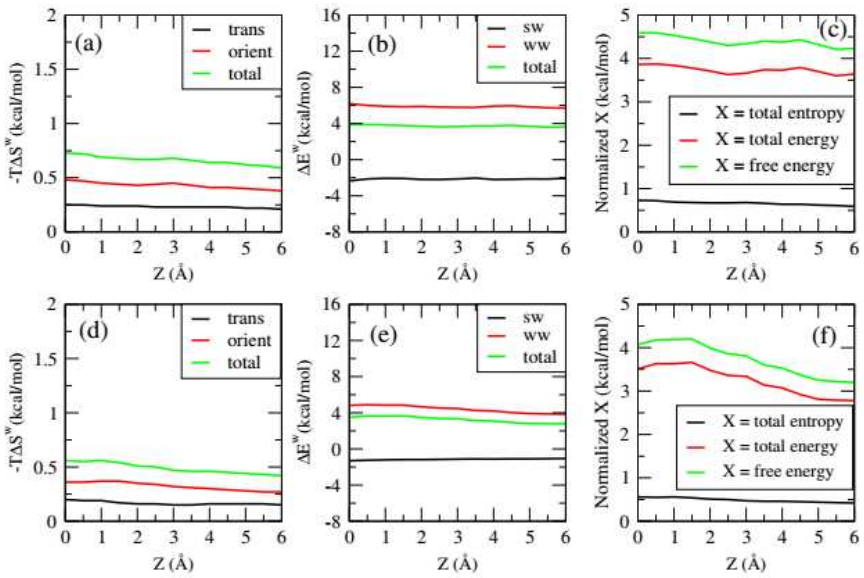

Figure 5-12. *Thermodynamic properties as a function of z-distance for nonpolar host-1a. Upper row ((a), (b), and (c)) is for the interior and bottom row ((d), (e), and (f)) is for the exterior thermodynamic properties.*

Analogous findings are shown in Tables 5-2 to 5-5 for both nonpolar host molecules for a model of the same host molecules in which all the partial charges are artificially set at zero. Every thermodynamic parameter for these nonpolar host molecules shows the same statistical convergence as the regular host molecules (not shown).

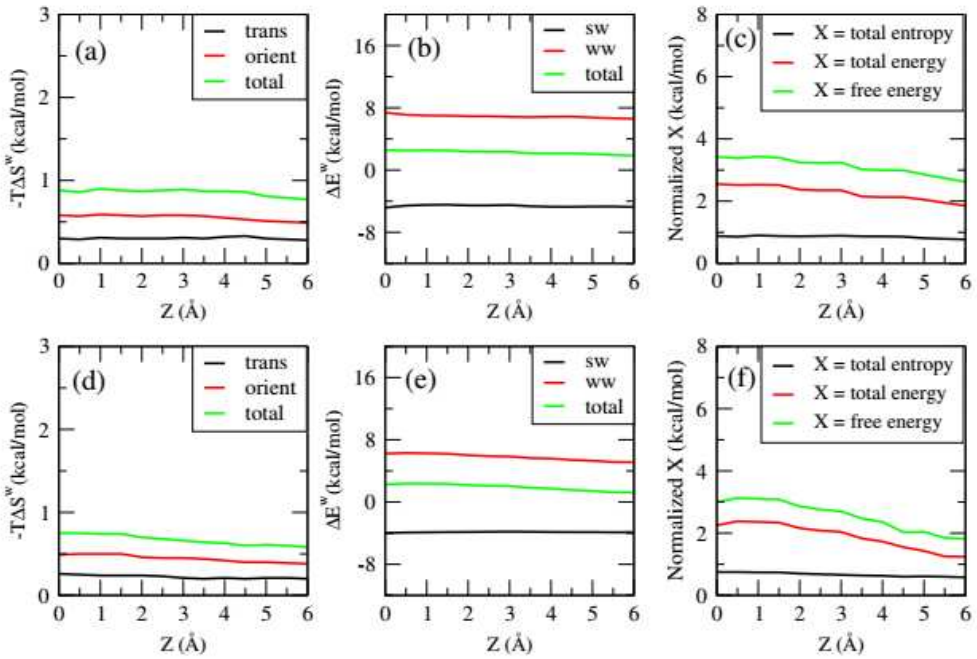

Figure 5-13. *Thermodynamic properties as a function of z-distance for nonpolar host-1b. Top row ((a), (b), and (c)) is for the interior and bottom row ((d), (e), and (f)) is for the exterior thermodynamic properties of nonpolar host-1b.*

Tables 5-2 and 5-3 show a similar overall trend in four different regions of unfavorable entropy, favorable solute-water interaction energy and adverse water-water interactive energy for the nonpolar host molecules. While the specific thermodynamic quantitys' value is smaller than for the regular host molecule, the net effect is that the normalized free energies are more adverse here. This is attributed to the lower host-water interactions, as the nonpolar host does not have favorable electrostatic interactions with the water molecules. The interactions between water-water are less advantageous in the nonpolar host molecule, possibly due to the lack of electrostatic interactions with the host molecule. The entropic

penalties in these nonpolar models are, in the same way, relatively smaller. Figures 5-12 and 5-13 show detailed analysis of the water characteristics in layers along the z-distance of the nonpolar host-1a and nonpolar host-1b, respectively. The entropic contributions along z-distance (Figure 5-12(a) and Figure 5-13(a)) everywhere inside the receptor is identical to the corresponding regular host. The only difference is that less amount of entropic penalty for nonpolar hosts than the corresponding regular host molecule. From the energy profiles of the nonpolar host molecules (Figure 5-12(b) and Figure 5-13(b)), favorable solute-water interaction energy loss is much more prominent than the loss of unfavorable water-water interaction energy. This results in a more unfavorable total energy penalty than the corresponding regular host molecule everywhere inside the nonpolar receptors. Total entropy, energy, and free energy plots (Figure 5-12(c) and Figure 5-13(c)) for both the nonpolar host molecules show the importance of energy as an adverse definitive to the free energy in these modified versions of host-1a and host-1b. The bottom row of Figure 5-12 and Figure 5-13 refer to the analogous plot at the outer surface of the receptors. The thermodynamic profiles are very much like the interior thermodynamic properties but show less thermodynamic perturbation than the corresponding interior thermodynamic parameters.

Now, from the water displacement study (Tables 5-4 and 5-5), it can say that an almost equal free energy penalty (for the displacement of water molecules from a particular region) for the nonpolar host-1a and nonpolar host-1b is much less in comparison with the corresponding regular host molecules. It satisfies the hydrophobic molecule standards (when every other aspect is equal), causing a greater propensity to bind guest molecules to the nonpolar receptor molecule.

■ DISCUSSIONS

Structure and thermodynamic parameters of hydrated biomolecules and other important solute molecules are some of the major concerns. Computer simulations have provided useful insights into these from 1978 onwards [260]. The Inhomogeneous Solvation Theory (IST) [241, 242] design has recently produced a basis for groundbreaking computational methods [225,235,243] that use explicit water simulations to provide useful hydrating water thermodynamics, including its entropy effect and effect on the ligand-binding process [212, 235, 236, 261–264]. The focus of these methods has been on discreet, densely populated water sites. Still, water distribution in a binding pocket cannot always be easily segregated into discrete regions. In a binding pocket, low-occupancy areas also may have their ligand-binding consequences. The grid implementation of IST (GIST), describes in

the three-dimensional framework, which might include a broad range of interest, addresses this and several other issues as shown in this current study of host-1a and host-1b receptors. This method makes it possible to view and analyze solvation thermodynamics in any part of the region of interest. GIST is not locally based, and therefore, explicitly refers to the high-, medium-, and low-water density regions, which provides a smooth illustration of the solvation structure and thermodynamic properties. Also, all the thermodynamic properties during our study converge well (Figure 5-9). Using GIST methodology, the solvation structure and thermodynamical function can be illustrated in guest recognition (by a suitable receptor). Compared to previous implementations of IST, GIST will aid in determining areas where water is displaced by a ligand and is similarly able to detect regions with a moderate to low water density, which would be well occupied by ligand atoms. As the GIST does not involve the partitioning of water density into distinct locations, can also analyze broader solvation structures like the high torus density regions identified in this study. More information is possible with the capability of GIST to differentiate and visualize the regional host-water and water-water energy contributions. To achieve high affinity during the ligand binding with a suitable receptor molecule, visualization of the host-water interactions will point to the regions where strongly interacted water with a receptor need to be substituted for ligand associations.

These small receptors reveal a surprisingly detailed solvation structure and thermodynamic pattern, and offer a comprehensive insight. In the solvation structure, the torus site with high water density is especially relevant within the receptor binding site. For both the receptors, regular host-1a and host-1b, water molecules are arranged translationally and orientationally in the torus region. The torus regions' water molecules in host-1a are energetically unfavorable (by a value of 2 kcal / mol) compared to the bulk of water (because torus waters loose approximately 8 kcal / mol water-water interaction energy, but host-water interaction energy favored in about 6 kcal / mol). On the other hand, these water molecules are energetically unfavorable by approximately 0 kcal / mol compared to bulk water for regular host-1b (as loss of water-water interaction and gain due to solute-water interaction energy are roughly equal). The value of free energy for removing the water molecules from both the regions (torus and cavity) of both the receptors is unfavorable (because they have unfavorable positive free energy values) (see Tables 5-4 and 5-5). Nevertheless, in these regions, the water molecules are usually disordered. This finding is physically rational since the cavity is filled continuously during the simulation by water molecules. It is also essential to recognize that the remaining water molecules are

not relaxed following the displacement of other water molecules, and therefore may overestimate the costs of displacement [248]. While the unfavorable normalized water properties of torus and cavity (relative to bulk) are not high enough to spontaneously dewetting, can still improve the guest binding affinity. This is comprehensible by considering different thermodynamic properties of Tables 5-4 and 5-5 for regular host-1a and regular hot-1b. From these tables, the main problem for extracting these waters into the bulk is the interaction energy between solute and water, which can be adjusted for by interactions between the relevant guest molecule and the receptor. Besides, it would be possible to achieve an extremely high association of the host with a guest, which mirrored the cavity regions' maximum interaction energy between solute and water (-24 and -42 kcal/mol for host-1a and host-1b, respectively). The water instability within these tiny receptor molecules can thus be part of the reason why some guest molecules can achieve extremely high binding affinities inside the cavity of these host molecules [265]. Note that additional factors such as guest desolvation, realignment of water molecules, configurational entropy changes during the guest binding procedure shall be included in a full account [266].

To study the function of polar interactions in the solvation of host-1a and host-1b, we have used the GIST technique on these host molecules with arbitrarily set zero partial charges for all the atoms and used the same water model. Energetic and entropic solvation parameters for water molecules are less perturbed in every aspect at the binding sites of nonpolar receptors than those in the regular host molecules (Tables 5-2 and 5-3). Still, their final effect is, those water molecules that reside at the binding sites of nonpolar receptors are less strongly bound than the corresponding regular host molecules. Consequently, the value of free energy for removing the water molecules from a particular region of nonpolar host molecule is more favorable than the corresponding regular host molecules (Tables 5-4 and 5-5). The approximate number of water molecules in nonpolar host molecules' binding site is reduced relative to the corresponding regular host molecules (Tables 5-2 and 5-3). Such observations correlate the solvation standards between the hydrophobic molecule and a polar molecule. Analysis of the different solvation properties shows an image of balancing solute-water interaction energy against the interactions between water-water and the entropic terms. Physically this is logical. The stronger interactions between water molecules and the polar host over the nonpolar host reduce entropy and avoid the maximization of their contact with other water molecules. The nonpolar host also has a torus site with a high water density, such as the corresponding regular host molecules is somewhat surprising. This trait in the nonpolar receptors, although somewhat lower in

density (Figures 5-7 and 5-8) than the corresponding regular host molecules (Figures 5-2 and 5-4), indicates that this occurs primarily from the packaging of the structure rather than from any attractive forces between the receptor and waters. These results stress the importance of confinement on the water structure and thermodynamics properties.

Such statistics show clearly that the water inside the receptor, translationally and orientationally, is more organized than the water around the receptor for every host molecule. Moreover, the waters' energy inside the receptor is much less preferred than that of the waters outside the receptors. When the host molecules' charges are turned off to form corresponding nonpolar hosts, which render it incompatible with forming hydrogen bonds with the hosts' N-H protons. Therefore, while eliminating the system charges reduces entropic orders inside the receptors, it is interesting that the interior of both nonpolar receptors contains the most translationally ordered (torus) region. Likewise, while the water molecules outside the receptors can compensate for the loss of favorable interaction with the receptors by forming stronger interactions with nearby water molecules, the inner water molecules cannot adapt to the loss of favorable interactions (solute-water) and become energetically unfavorable. Such results demonstrate that the confinements are largely responsible for the unfavorable energy and entropic effects of water in the interior torus area, specifically the enthalpy-entropy balance for these receptor molecules has been broken down. So, it is possible to infer that the host molecules have lost beneficial interactions with other waters within the cavity, and their contact with the receptor is not as strong as the energy penalties due to water-water interactions while being more organized than bulk water, which makes these water molecules less entropic.

From Tables 5-4 and 5-5, we can also say that the removal of water molecules from a particular location of host-1a is easier than host-1b. Due to this, when a guest molecule will be able to replaced these water molecules (partially or fully) from the receptors' cavity and formed a host-guest complex, then the host-guest complex will be energetically more stable for host-1b than for host-1a.

Lastly, we are interested to see how close the optimized structure is to the solution structure for both the host molecules. For the same, we have analyzed the root means square deviation (RMSD) values of these host molecules with reference with their optimized (initial) structure. We have prepared two more systems consisting of these host molecules solvated in pure TIP3P water and carried out a production run of additional 60 ns. The RMSD of the host molecules with simulation time are in Figure 5-14. RMSD value for host-1a and host-1b is around 1.5 and 1.0 Å, respectively and these values remain almost

constant throughout the simulation. From the RMSD values, it is clear that each host molecule is conformationally stable and less flexible in the solution phase compared to their corresponding optimized (initial) structure. Thus, use of these optimized host structure is adequate for those above analyses.

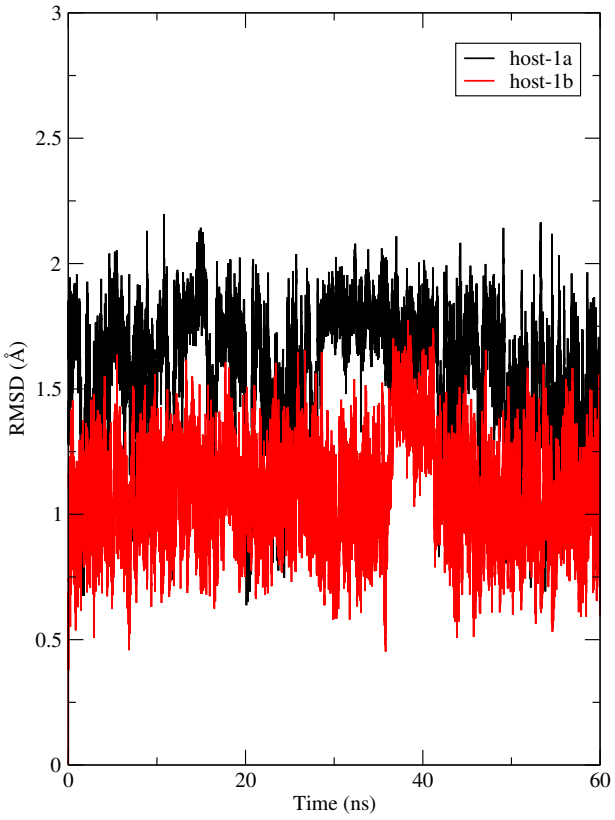

Figure 5-14. *The root means square deviation (RMSD) values of the host-1a and host-1b with compared to the optimized (initial) structure of the corresponding host molecules as a function of simulation time is plotted here.*

■ SUMMARY AND CONCLUSIONS

We have used classical MD simulation and GIST methodology to study the water molecules' role inside and outside the receptors cavity during the guest encapsulation process. The grid methodology also makes it easy to focus on regions where a high water density is present. Two receptor molecules (host-1a and host-1b) – known as endo-functionalized

molecular tubes – are used for this study. These two receptors can encapsulate many environmentally and industrially important molecules from water. Also, to investigate the effect of electrostatic, we have used the nonpolar version of these receptors in which all the partial charges of the atomic sites of both these receptors are artificially set to zero. The water molecules are translationally less favored in the torus region and getting more stability as they move from the torus to the cavity surface region for both the regular host molecules. The presence of hydrogen (of water) density inside the host molecules is due to the hydrogen bonding between the water oxygen atom and hosts' N–H protons. A high density of water molecules is present inside both the regular host molecules. Orientational entropy also contributes unfavorably to the solvation free energy and is maximum inside the receptor molecules. Thus, when any guest molecule replaces these water molecules from inside the hosts' whole cavity, corresponding entropic contribution will be gained to the binding free energy for both these receptors. For both these regular host molecules, total solvation energy is unfavorable inside the host and favorable around the receptor. Solute-water interaction is favorable inside the host molecule. So, those guest molecules form stronger interactions with the host than the host-water interactions, replace the water molecules and form a strong host-guest complex. On the other hand, unfavorable water-water interaction is partly or fully balanced by favorable solute-water interactions. Every energetic and entropic solvation parameters are less perturbed for nonpolar host molecules than the corresponding regular host molecules. Thus, the value of the free energy for removing water molecules from a particular region of purely nonpolar host molecules is more favorable than the corresponding regular host molecules. The dense torus region in both the nonpolar host molecules demonstrates that packaging contributes more to create the dense torus region. These results indicate the importance of confinement on the water structure. These small host molecules uncover the detailed solvation structure, thermodynamic pattern and offer a comprehensive insight into the formation of strong host-guest complexes.

Chapter 6

Insights into the complexation between endo-functionalized molecular tube and strongly hydrophilic guest molecules in aqueous solution, and its' stability dependency on the guest concentration

"There is no law except the law that there is no law."

— John Archibald Wheeler

Chapter 5 proves that host-1b is a better complexing agent than host-1a. Thus, in Chapter 6, we use host-1b (Figure 1-4 of Chapter 1) to encapsulate four different environmentally important molecules from the water medium. We hope this process may keep water free from industrial pollution by encapsulating industrial pollutant from water medium.

The possibility of complexation of a host, endo-functionalized naphthotube having bisnaphthalene cleft architecture (host-1b), with four different strongly neutral hydrophilic guest molecules namely, 1,4-dioxane (14D), acetone, DMSO, and DMF in water and the effect of the guest concentration on these complexes' stability is examined by using classical molecular dynamics simulation. These type of molecular tubes have recently received significant attention due to its usefulness as supramolecular catalysis and its ability for selective recognition of biologically and environmentally important neutral molecules in the aqueous solution. The PMF and MM-PBSA calculations reveal host-1b/14D complexation is energetically most stable, and the synergistic host-guest hydrophobic, and hydrogen bonding interactions play profound roles in the stability of these host-guest complexes. Specifically, as the host cavity contains a small hydrophilic part and a large hydrophobic part, so guest molecules having both these parts form hydrogen bonds with the hosts' hydrophilic part and make favorable hydrophobic interaction with the hydrophobic part of the host at the time of complexation. We also examine the effect of the concentration of different guest molecules on the host-guest complexation ability by determining different types of hydrogen bond properties, preferential interaction parameters, water-inserted guest interaction energy parameters, host-guest binding free energy, and potential of mean force. From the calculated free energy values obtained from MM-PBSA and PMF calculation, it is revealed that as the concentration of guest decreases, the free energy becomes less favorable.

The chapter is divided into two parts. Part A focuses on the complexation between host-1b and four different strongly neutral hydrophilic guest molecules. On the other hand, Part B concentrates on the effect of guest concentration on these complexes' stability.

Part A:

Synergistic host-guest hydrophobic and hydrogen bonding interactions in the complexation between endo-functionalized molecular tube and strongly hydrophilic guest molecules in aqueous solution

Overview: The propensity of complex formation of a host, endo-functionalized naphthotube having bisnaphthalene cleft architecture (host-1b), with four different strongly neutral hydrophilic guest molecules namely 1,4-dioxane (14D), acetone, DMSO, and DMF in water is examined by using classical molecular dynamics simulation. This type of molecular tubes have received significant attention recently due to their usefulness as supramolecular catalysis and for their ability of the selective recognition of biologically and environmentally important neutral molecules in aqueous solution. We sequentially address the role of different guest molecules on the structural change of host-1b, the role of host-inserted guest and water-inserted guest hydrogen bond properties and host-guest binding free energies in the complexation. The derivatives of our findings are: (a) the host changes its shape upon insertion of guest molecule and the magnitude of its changed shape depends on the type and nature of guest molecule; (b) a complete insertion of guest into the cavity of host-1b is observed only for guest 14D; and (c) a complete removal of water molecules from the hosts' cavity for guest 14D and the presence of a single water molecule is found to present for all other guest molecules. The PMF and MM-PBSA calculations reveal host-1b/14D complexation is energetically most stable and the synergistic host-guest hydrophobic and hydrogen bonding interactions play profound roles in the stability of these host-guest complexes. In specific, as the host cavity contains a small hydrophilic part and a large hydrophobic part, so guest molecules having both these parts form hydrogen bonds with the hydrophilic part of the host as well as make favorable hydrophobic interaction with the hydrophobic part of the host at the time of complexation.

■ INTRODUCTION

In supramolecular chemistry, the synthesized receptors, in special, the converging connecting groups are formed by taking the factors of their complementarity of sizes, shapes and charge distributions with the substrate, mimicking biological functionalities in enzyme-substrate binding [267]. Selective recognition of neutral hydrophilic molecules in an aqueous solvent is a challenging task for artificial molecular receptors [268–271], and very few systems are able to do this work [272–282]. Hydrophilic biomolecules, such as sugars, can be recognized by neutral receptors with a high level of selectivity [283]. Neutral hydrophilic molecules contain polar groups as well as nonpolar (hydrophobic) parts. Thus, for selective recognition of these guest molecules by the host molecules would require favorable host-guest interactions with both polar and nonpolar groups of them simultaneously. To gain a high level of binding interactions, hydrophilic effects and noncovalent interactions, such as hydrogen bonds, should work simultaneously. Artificial receptors having a hydrophobic cavity, are able to selectively recognize neutral hydrophilic molecules in aqueous solution [272–282]. For being more effective, other two factors are: (a) the cavity of the receptor should be deep adequate to remain separated from the bulk water, which approves the hydrophobic effect to handle the recognition of the hydrophobic parts, and (b) the sites of the receptors, which form hydrogen bonds i.e., the complementary functional groups, should remain in a perfect position in the deep cavity away from the entry, thereby allowing the noncovalent interactions to conduct in a comparatively hydrophobic environment in the cavity by releasing water molecules. Hydrophobic effects and noncovalent interactions can thus play synergistically in this way. Other water-soluble macrocycles, such as β-cyclodextrin and cucurbit[6]uril, are not able to effectively bind this neutral hydrophilic molecules [284]. Glass and coworkers [53–55] reported a pair of molecular tubes (the acid form of molecular tubes 1a and 1b) with bisnaphthalene cleft [56–58] architecture. When both the bisnaphthalene clefts are in parallel orientations (syn) it is labelled as host-1a and when they are in antiparallel orientations (anti) it is referred as host-1b (Figure 1-4 of Chapter 1). For the recognition of lipid molecules in water through hydrophobic effects, these molecular tubes were used [53, 54]. A deep look into the host-1a and host-1b revealed that the amide N-H bonds are directed towards the cavity. For this reason, they are referred to as endo-functionalized molecular tubes and they fulfill all the criteria mentioned above for the recognition of neutral hydrophilic molecules present in aqueous solution. The binding pockets of 1a and 1b are neutral since the charged carboxylate groups only provide

water solubility.

As discussed above, albeit quite briefly, that a few number of experimental research works have been devoted to deduce the mechanism by which endo-functionalized receptors work in regard to recognize the neutral hydrophilic guest molecules from their aqueous solutions but without much success. As a result, this type of molecular tube still attracts much needed attention. Since, the molecular dynamics (MD) simulations can provide a detailed molecular level understanding of host-guest interactions, which, sometimes, can not be obtained from the conventional experiments, in this part, the complexation properties of host-1b (Figure 1-4 of Chapter 1) with guests 1,4-dioxane, acetone, dimethyl sulfoxide and dimethyl formamide in water are investigated by using classical molecular dynamics (MD) simulation. Here it is worth to mention that, to the best of our knowledge no classical MD simulation study has been performed so far for this type of host-guest interactions in aqueous solutions. We analyze the obtained MD simulation trajectories for getting the outcome of host-1b internal diameters due to insertion phenomenon and to acquire brief knowledge of behaviors of these guest molecules inside the host-1b. The pliability and stirring of host-1b in the host-guest complexed and uncomplexed form are searched. By using the Molecular Mechanics-Poisson Boltzmann Surface Area (MM-PBSA) method, we also calculate the binding free energy of each of the host-guest complexes. We have also taken into account all the components of binding free energies and pursued further for searching the main factors liable for complexation process. The Potential of Mean Forces (PMFs) for different systems are also calculated as a function of host-guest distance for gaining more knowledge about the energy barriers, which may subsist at the time of insertion phenomenon.

■ COMPUTATIONAL DETAILS

Optimizations of ground state geometry of host-1b and ammonium ion were performed by using ab initio HF/6-31+G** method of Gaussian 09 [106]. The RESP (restrained electrostatic potential) [67] module of AMBER14 [63] was used for calculating the partial charges of all the atomic sites of both molecules. The other parameters of all the atomic sites of host-1b and ammonium ion were taken from the General AMBER force field (GAFF) [108] using the ANTECHAMBER [107] module of AMBER14. The newly developed atomic partial charges of host-1b is shown in Table 2-2 of Chapter 2. To neutralize the four unit negative charges of each of the host-1b molecule, four NH_4^+ counterions were added at the time of initial system preparation. Note that, host-1b used for MD runs has the

same configuration as the Hartree-Fock optimized configuration in the gas phase. Four guest molecules e. g., 1,4-dioxane (14D), acetone, dimethyl sulfoxide (DMSO) and dimethyl formamide (DMF) were used for this work. OPLS/AA force field parameters and partial charges of all the atomic sites of these guest molecules were taken from the literatures [285–291]. The three point transferable intermolecular potential (TIP3P) [72] model of water was employed for this work. To study the inclusion properties of these guest molecules into host-1b cavity, 5 different systems were considered, and the details are abridged in Table 6A-1. Systems S0-S4 refer to the presence of guest molecules with a regime of concentrations. On the other hand systems P1-P4 are considered for umbrella sampling (discussed below). The PACKMOL [74] package was used for generating all the initial configurations of all the systems. Sander module of AMBER14 package was employed for running the molecular dynamics simulation. For each of the systems, one cubic box was used to place all the molecules. Periodic boundary conditions (PBC) were adopted in all three directions and for all simulations. The SHAKE algorithm [71] was used to constrain the covalent bonds entangling hydrogen atoms. The cut-off distance of 10 Å was set for all short-ranged nonbonded interactions and a 2 fs time step was used for all simulations. For the purpose of calculating the long-ranged electrostatic interactions, Particle Mesh Ewald (PME) [73] method was employed. The systems were first energy minimized with 4000 steps of steepest descent, followed by 6000 steps in conjugate gradient method. Every system was then heated for 320 ps in a canonical ensemble (NVT), by gradually increasing the temperature from 0 to 298 K. Another 5 ns simulation in isothermal-isobaric ensemble (NPT) was conducted for achieving equilibration at 298 K temperature and 1 atm pressure. For each of the systems, 60 ns production run was carried out in NPT ensemble. In the NPT ensemble, the system was coupled with a Berendsen barostat [75] with a pressure relaxation time of 2 ps to maintain 1 atm pressure throughout the simulation. For controlling the temperature at 298 K, Langevin dynamics [76] method with a collision frequency of 1 ps^{-1} was applied.

CPPTRAJ module of AMBER was used for conducting the analysis of the obtained MD trajectories. Visual Molecular Dynamics (VMD) [78] program was used for visualizing the obtained MD trajectories, as well as for analysis purposes whenever required.

Binding free energy (ΔG^0_{bind}) of the host-guest complexes are calculated by using the Molecular Mechanics-Poisson Boltzmann Surface Area (MM-PBSA) [79, 80] method. Details of this method are discussed in the 'METHODOLOGY' section of Chapter 1 (Eq. 1.18). Entropic contribution is not calculated here. The potential of mean force (PMF)

of these host-guest complexes are also analyzed, and details of this method are discussed in the 'METHODOLOGY' section of Chapter 1 (Eq. 1.24). Here, only difference is that reaction coordinate (r) changed from 0 to 19.5 Å .

Table 6A-1. Overview of systems[a]

System	N_{host}	$N_{NH_4^+}$	N_{guest}	N_{wat}	Box volume (nm^3)	$M_{host-1b}$ (M)
S0	1	4	0	5000	153.17	0.0108
S1	1	4	10	5000	154.48	0.0107
S2	1	4	10	5000	153.77	0.0108
S3	1	4	10	5000	153.94	0.0108
S4	1	4	10	5000	154.15	0.0108
P1	1	4	1	2000	62.03	0.0268
P2	1	4	1	2000	61.99	0.0268
P3	1	4	1	2000	62.05	0.0268
P4	1	4	1	2000	61.95	0.0268

[a] N_{host}, $N_{NH_4^+}$, N_{guest} and N_{wat}, respectively, are the number of host-1b, ammonium ion, guest, and water molecules. 'M' is the molar concentration of host-1b. S1/P1, S2/P2, S3/P3 and S4/P4 systems are for the guest molecule 14D, acetone, DMSO and DMF, respectively.

■ RESULTS AND DISCUSSIONS

60 nanosecond MD simulations for host-1b and its' complexes with different guest molecules with varying compositions were performed in the aqueous solvent to find out the main driving force for the host-guest complexations and the stability order of the complexes.

The snapshots of the analogous 1:1 host-guest complexes for different systems obtained from the last frame of the respective trajectories are shown in Figure 6A-1. The snapshot of host-1b/14D shows a total insertion of the guest 14D into hosts' cavity. As the cavity of molecular tube 1b is made of by four naphthalene units, the cavity is electron rich and at the same time hydrophobic in nature. For the presence of inwardly directed amide N-H protons, the appropriate size of the hydrophilic guest molecules having hydrogen bond acceptors and hydrophobic surfaces are required in order to enhance the encapsulation of the guest molecule properly in this cavity. Guest 14D is a superior guest molecule, as, its two oxygen atoms are placed in the right mensuration as hydrogen bond acceptors and the rest part of its molecular surface is hydrophobic. In this context, it is worth to mention that in the previous ^{1}H NMR spectroscopic experiments [38], an extensive amount (-1.90 ppm) of the upfield shift was noticed for the guest 14D with host-1b in water. This type of upfield shielding value could onliest be narrated by the complete insertion of the guest 14D in the host cavity.

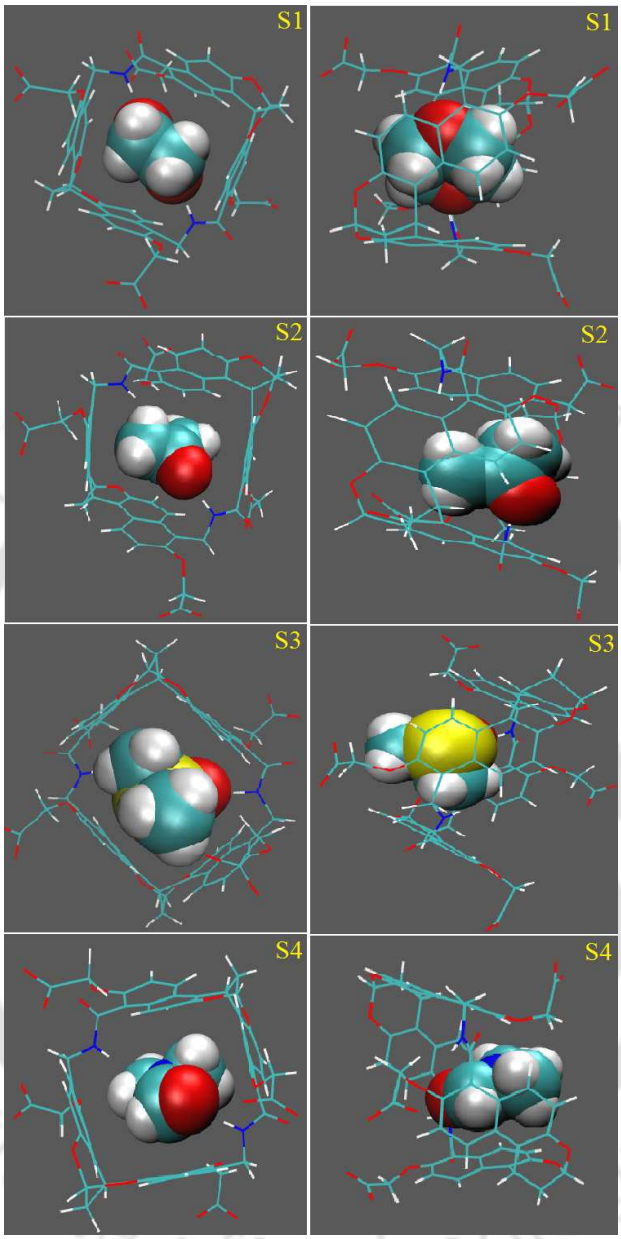

Figure 6A-1. *Snapshots of different host-guest complexes. Left panel and right panel refer to top and side view respectively. Water molecules and ammonium ions are left off to increase the visual clarity.*

Moreover, this type of complexation can be expressed as the energetically favorable hydrogen bonding interactions between the amide proton of host-1b and the oxygen atom of 14D, at the same time hydrophobic portion of 14D was placed in the hydrophobic cavity. On the other hand, the snapshots of host-1b/acetone, host-1b/DMSO, and host-1b/DMF expose the partial inclusions of guests acetone, DMSO, and DMF into the cavity of host-1b. Previously reported results of ^{1}H NMR spectroscopic experiments showed moderate amount

(-0.053, -0.064 and -0.033 ppm for host-1b/acetone, host-1b/DMSO and host-1b/DMF system, respectively) of upfield shielding for these systems indicating partial insertion of these guest molecules inside the host cavity. Differences in the inclusion properties of the different guest molecules in the similar host can be attributed to the different amount of hydrogen bonding interactions between hosts' donor atoms and guests' acceptor atom/atoms, and the different amount of hydrophobic surface area available for different guest molecules.

Internal Diameters

To examine the effect of different guest molecules insertion on the structural change of the host-1b molecule two internal diameters are considered (Figure 2-3 of Chapter 2). Since the host molecule is not spherical, these two diameters, namely diameter-1 and diameter-2, are by no means equal. These two diameters are drawn by considering two imaginary lines connecting two opposite atoms C15-C74 (for diameter-1) and C53-C96 (for diameter-2). In Table 6A-2, we present the average values of these diameters for different systems considered, the absolute difference (Ad) between them, and the standard deviations (Sd) of Ad of host-1b of every system. It is noticed that for the host-1b the average of diameter-1 is higher than that of diameter-2. Insertion of a guest molecule into the host-1b has two opposing effects in regard to change in the average values of these two diameters. In specific, the encapsulation of guest molecule causes a sharp decrease in the average value of diameter-1 whereas, the insertion of a guest leads to an enhancement in the value of diameter-2.

Table 6A-2. Average internal diameter[a]

System	Aid-I (Å)	Aid-II (Å)	Ad (Å)	Sd (Å)
S0	13.56	9.60	3.96	± 0.55
S1	13.04	9.80	3.24	± 0.45
S2	13.14	9.72	3.42	± 0.35
S3	13.22	9.74	3.48	± 0.40
S4	13.22	9.62	3.60	± 0.51

[a] Average values of internal diameter-I (Aid-I), internal diameter-II (Aid-II), the absolute difference (Ad) between them, and the standard deviations (Sd) of Ad of host-1b of every system.

Interestingly, the effect of guest insertion in the host-1b is most profound for 14D in which a maximum deviation in the average values of both the diameters (in comparison to the system devoid of any guest i.e., system S0) is observed and this is followed by the guest

acetone. For the guests DMSO and DMF, we observe a modest change in the average values of these two diameters. The encapsulation of these guest molecules into the cavity of host-1b generates the scruple of its cavity accordant to N-H$\cdots$O hydrogen bonding interactions (discussed below).

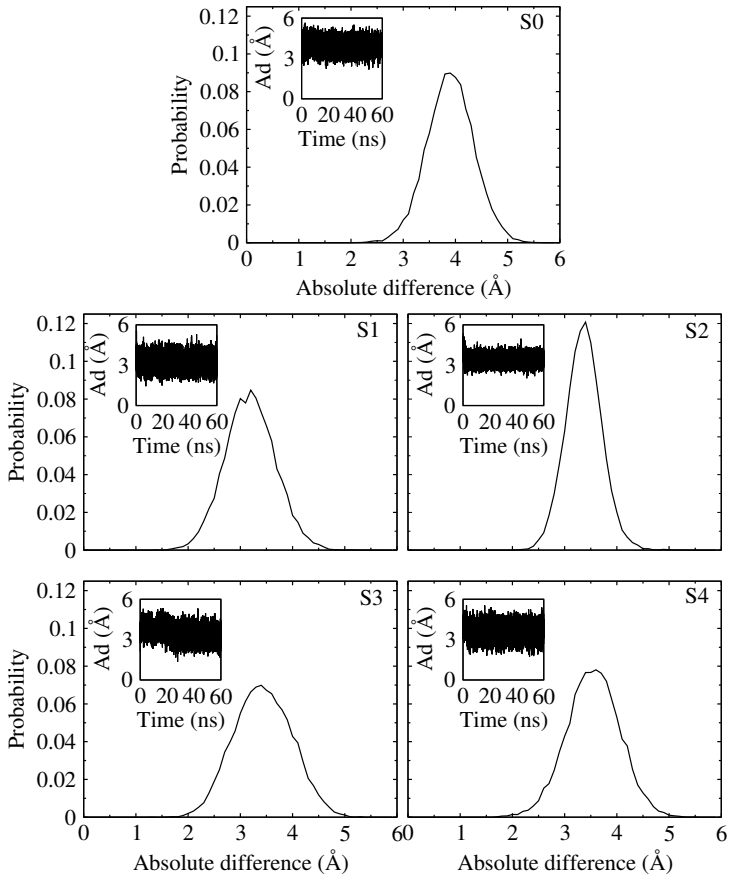

Figure 6A-2. *The probability distribution functions of absolute difference (Ad) between two perpendicular internal diameters of host-1b. For all the systems, the change in the Ad values as simulation progresses are also shown in the insets.*

For better perceptioning, the change in the conformation of the molecular-tube like host-1b molecule due to the insertion of the guest molecule, the probability distribution functions of the absolute difference between these two internal diameters (Ad) are estimated and they are shown in Figure 6A-2. The insets of Figure 6A-2 present the change in Ad

values versus simulation time for different systems. Besides this, the average Ad values for different systems and their standard deviations are given in Table 6A-2. Ad for the free host-1b shows a maximum probability at around 3.90 Å and the maximum probability for the host-guest complexes are found in somewhat shorter distance than that for the system devoid of any guest molecule. This implies sampling of a more symmetric structure than free host upon insertion of guest molecule. The resembling average value for the absolute difference between two internal diameters is also decreased upon complex formation. This observation evidently debunks that the conformational change of the host-1b structure is commenced by the guest insertion. Next, we calculate the average distortion value for the host molecule induced by guest molecules with respect to the free host molecule. We have found an average decrement in the Ad values by 18 % , 14 % , 12 % and 9 % for the complexes with guest 14D, acetone, DMSO, and DMF, respectively.

Hydrogen Bond Properties

Hydrogen bonding interactions play a crucial role in controlling the stability of highly hydrophilic neutral guest molecules inside the cavity of the endo-functionalized molecular tube. A brief introduction of the different types of hydrogen bond are given in Table 6A-3. A donor-acceptor cut-off distance $\leq$ 3.4 Å and donor-acceptor-hydrogen cut-off angle of $\leq 45^o$ is used for hydrogen bond analysis purposes (Figure 2-6 of Chapter 2) [109–115].

Table 6A-3. Hydrogen bond values

System	host-wat	N1-wat	N3-wat	host-gus
S0	25.40	0.85	0.67	–
S1	23.11	0.02	0.01	1.91
S2	23.98	0.42	0.31	0.57
S3	24.65	0.71	0.51	0.57
S4	23.90	0.32	0.23	0.58

[a] Average number of hydrogen bonds between host and solvent water (host-wat), host-1b N1 atomic sites-water (N1-wat), host-1b N3 atomic sites-water (N3-wat), host and guest (host-gus) for different systems.

In comparison to the free host-water average hydrogen bond number, a modest drop in its value is noticed for systems containing guest molecules. We have also estimated the number of hydrogen bonds between the hosts' nitrogen atoms (N1 and N3) and water molecules and also the same is shown in Table 6A-3. From this table, it is apparent that the N1

and N3 atoms of host-1b engage in hydrogen bonding interactions with the surrounding water molecules when there is no guest molecule present. Interestingly, for system S1, this type of host-water hydrogen bonding interactions is extremely small suggesting that there is essentially no hydrogen bond formation between N1 and N3 atoms of host-1b and water when the guest 14D is incorporated. This finding indicates, albeit indirectly, the complete insertion of guest 14D in the cavity of host-1b, which makes the N1 and N3 atoms unavailable for hydrogen bonding with water molecules. This observation further indicates that water molecules are rearranged close to both end of the host-1b during the insertion process. As reported previously, every hydrogen bond has an average energy value in the range of 5-7 kcal/mol (5 kcal/mol is for O-H$\cdots$O and 6.9 kcal/mol for O-H$\cdots$N) [292,293]. Now, when guest insertion process is taking place into the host cavity, the rupture of some of the hydrogen bonds between host-1b and the solvent water molecules are taking place. Because of the breaking of these hydrogen bonds, some amount of energy is released. This facile the enthalpy driven insertion process and provides the stability to the host-guest complexes.

The number of hydrogen bonds between host-1b and the inserted guest molecule is also presented in Table 6A-3. Here it is worth mentioning that the term "inserted guest molecule" refers to a specific guest molecule out of 10 guest molecules present in a given system. Remarkably, it can be seen that system S1 shows the maximum number of the host-guest hydrogen bonds and the other three systems show almost similar values.

We have also analyzed the average number of hydrogen bonds between the inserted guest and water molecules. The pattern of this type of hydrogen bonds versus simulation time is shown in Figure 6A-3. It is clear that the number of hydrogen bonds drops after the insertion of these guest molecules into the host cavity. From these observations, we can conclude that the full insertion is taking place only for the guest 14D and it remains in the deep cavity of the host for rest of the simulation time. On the other hand, the other three guest molecules show partial insertions, these gusts position themselves in somewhat exterior positions of the host cavity. These findings are in well accordance with the snapshots of different systems presented in Figure 6A-1 as well as the average number of hydrogen bonds between N1 and N3 atoms of host-1b with water (Table 6A-3).

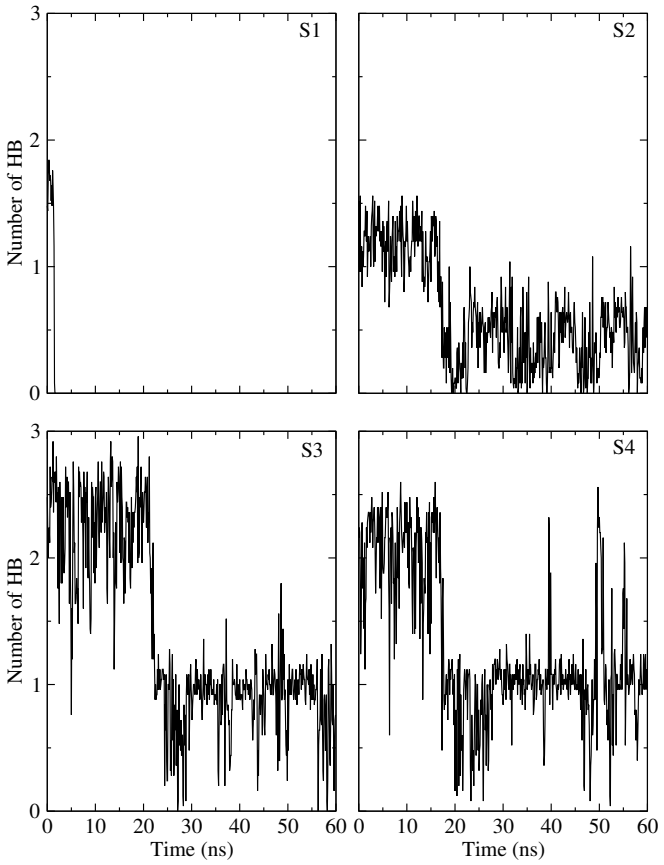

Figure 6A-3. *Water-inserted guest intermolecular hydrogen bonds (HB) as a function of simulation time for different systems.*

Contour Density Plot

The water mass density [294] around the reference inserted guest molecule (into the host cavity) is examined for different systems and the same are shown in Figure 6A-4. The mass density maps are built using VMD [78] program, with an isovalue of 0.3 Å. We have calculated the mass density maps by taking a water-inserted guest molecule cut-off distance of 3.40 Å. As can be seen that for system S1, a very low water density around the reference guest molecule appears. An enhancement in the water density around the reference guest molecule is observed for other three systems. This is because, for S1 system, 14D guest molecule forms a fully inserted host-guest complex and it remains in the

deep hydrophobic cavity of the host-1b. This accounts for the low water density around the inserted guest for S1 system. But, for other three systems, as these guest molecules form partially inserted complexes a prominent water density around each of these guest molecules is found. These observations suggest that the guest molecules occupy somewhat exterior positions of the host cavity. These results also resemble with the water-inserted guest intermolecular average number of hydrogen bonds (Figure 6A-3) and also act as corroborative evidence of what we observed from the snapshots of different systems (Figure 6A-1).

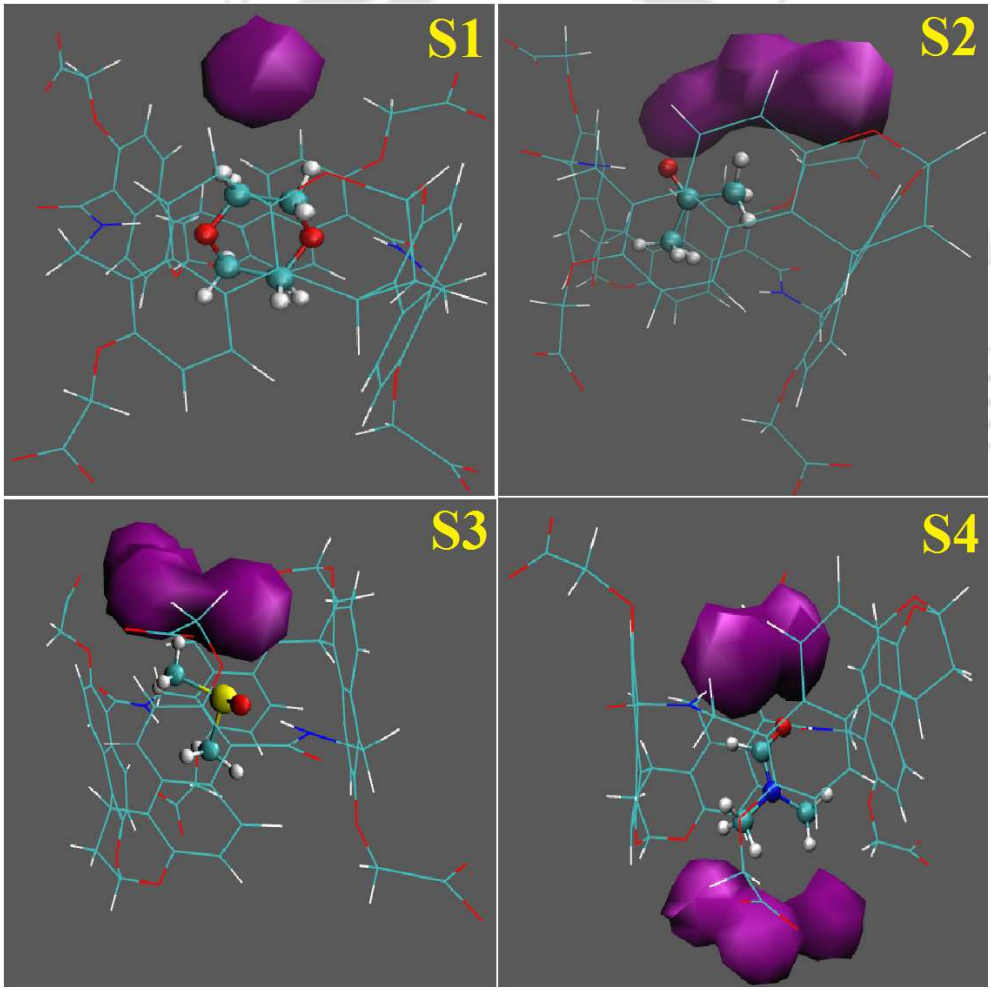

Figure 6A-4. *Contours of the water density within 3.40 Å around a reference inserted guest molecule for different systems.*

Host-Guest COM-COM Distance

For different systems, we present our host-guest COM-COM distance versus simulation time plot in Figure 6A-5. It is apparent that for each and every guest molecules once inserted into the host cavity, it remains inside the cavity until the end of the simulation (i.e., no exchange between guest molecules takes place). This finding also resembles the host-guest average number of hydrogen bonds presented above. The average values of host-guest COM-COM distances after the insertion of guest molecules are 0.44, 2.07, 1.96 and 2.27 Å respectively, for systems S1, S2, S3, and S4.

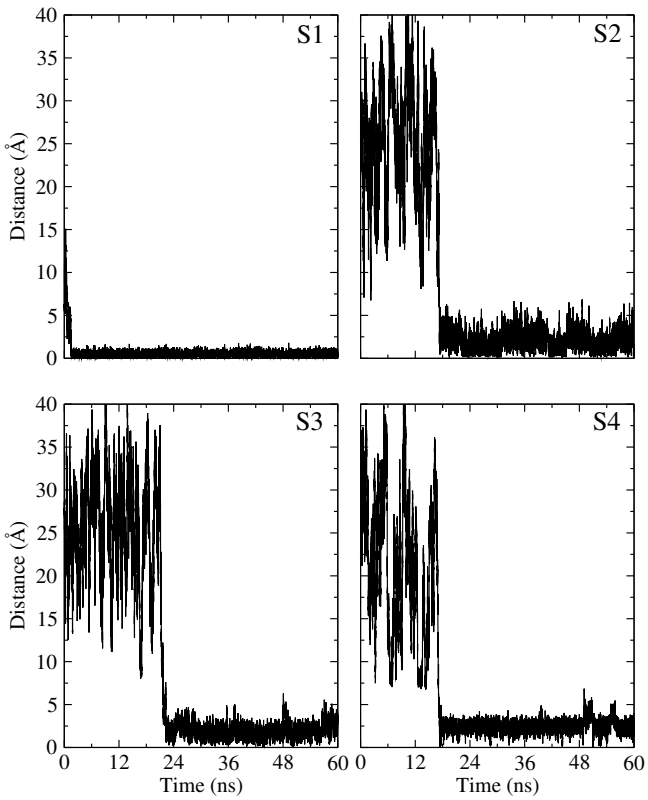

Figure 6A-5. *Host-inserted guest center of mass to center of mass (COM-COM) distance as a function of simulation time for different systems.*

So, this also supports the fact that host-1b/14D forms a fully inserted complex. Since

other three host/guest systems show the somewhat larger value of COM-COM distance than host-1b/14D, these values correspond to partially inserted complexes.

MM-PBSA Analysis

In recent years a promising method, Molecular Mechanics-Poisson Boltzmann surface area (MM-PBSA) [79], is being used to determine the binding free energies of macromolecules and their complexes. The MM-PBSA procedure is 10 times faster than the conventional free energy perturbation techniques suggesting that the former is computationally less expensive, as it emerges on continuum solvent model. In our study, every component of the binding free energies is calculated to determine the type of host-guest interactions that are accountable for complexation. This method, we believe, would give more insights into the driving force for the inclusion of guest molecules inside the cavity of host-1b.

For different systems, the value of the host-guest binding free energies (in kcal/mol) are obtained from the MM-PBSA analyses of the last 4 ns MD trajectories and they are listed in Table 6A-4.

Table 6A-4. Binding free energy values[a]

System	ΔE_{vdw}	ΔE_{ele}	ΔG_{PB}	ΔG_{NP}	ΔG^{0}_{bind}
S1	-27.98	-10.17	12.43	-19.15	-44.87
S2	-22.20	-8.10	12.68	-17.67	-35.29
S3	-22.85	-15.46	20.75	-17.39	-34.95
S4	-16.51	-9.34	15.29	-13.96	-24.52

[a] The binding free energy values of different systems. All energy values are expressed in kcal/mol unit.

An entire view on the results displays that the main contribution to the binding free energy is the favorable host-guest van der Waals interactions (ΔE_{vdw}). This indicates the pronounced role of the host-guest hydrophobic interactions. The system containing host-1b/14D shows the most favorable van der Waals contribution in stabilizing the host-guest complex. For host-1b/14D, this result is expected since the two oxygen atoms of 14D are positioned in the right geometry and act as hydrogen bond acceptors while the rest of its molecular surface is hydrophobic. But for the other guest molecules, the number of hydrogen bond acceptor is one and also the difference in van der Waals interaction energy for them is due to the different amount of hydrophobic surfaces they possess. Electrostatic interactions (ΔE_{ele}) are also attractive for all systems. Further, the value of ΔE_{ele} is the

most favorable for host-1b/DMSO system. This signifies that the electrostatic interaction also plays a role (but not as significant as that of ΔE_{vdw}) in the complexation process. $\Delta E_{vac}(\Delta E_{ele} + \Delta E_{vdw})$ of all the complexes has a favorable contribution to the complex stability i.e., it contributes a negative value of energy to the ΔG^0_{bind}. Concentrating on the electrostatic solvation energy (ΔG_{PB}), we find that it has an unfavorable positive value of energy for all the complexes. This is ascribed as the decrease in the contact area between the solvent and both host and guest molecules at the time of the insertion process. As a result, the host-guest complexes contribute less amount of electrostatic interactions with the solvent water molecules in comparison to the free host and guest molecules. The highest positive value of ΔG_{PB} is for host-1b/DMSO complex which is followed by host-1b/DMF complex. The host-1b/acetone and host-1b/14D complexes have much lower ΔG_{PB} values. The apolar solvation free energy (ΔG_{NP}) values are negative for all the complexes. The most favorable ΔG_{NP} value is obtained for the host-1b/14D complex which is closely followed by host-1b/acetone and host-1b/DMSO complexes and the host-1b/DMF complex is the least favorable. These negative ΔG_{NP} values reveal that the apolar surface terms contribute positively to the stability of the complexes. Now, ΔG_{solv} (i.e. $\Delta G_{PB} + \Delta G_{NP}$) term is negative for host-1b/14D and host-1b/acetone complexes but it is positive for host-1b/DMSO and host-1b/DMF complexes. The ΔG_{solv} value is acting as a major factor for the higher stability of 14D and acetone complexes in comparison to the DMSO and DMF complexes.

Thus, the different binding free energies (ΔG^0_{bind}) for the host-guest complexes suggest that the tendency of the host-1b molecule to form complex with these guest molecules is in the order of host-1b/14D > host-1b/acetone > host-1b/DMSO > host-1b/DMF.

Umbrella Sampling (PMF Calculations)

We calculate the potential of mean forces (PMFs) between host-1b and different guest molecules separately. For this, we consider four different systems P1-P4 (Table 6A-1). For all the systems, we have generated the initial configurations for umbrella sampling by using PACKMOL. Then we perform normal MD simulation run for all the systems. For each system, the configuration obtained in normal MD was used as the initial configuration for umbrella sampling. The PMF of a system with 'N' molecules can be defined as the potential, which gives the average force acting on the reference particle over all the configurations of all the n+1$\cdots$N number of particles at any fixed configuration keeping fixed a set of 1$\cdots$n particles. To be specific PMF can be used to know how the free energy changes

as a function of a coordinate of the system studied. In order to calculate the PMFs of different systems considered in this study, a series of umbrella sampling [89] simulations are performed. In this method, a set of initial configurations are generated, each of them corresponds to a location wherein the molecule of interest is harmonically restrained at increasing COM distance from a reference molecule using an umbrella biasing potential.

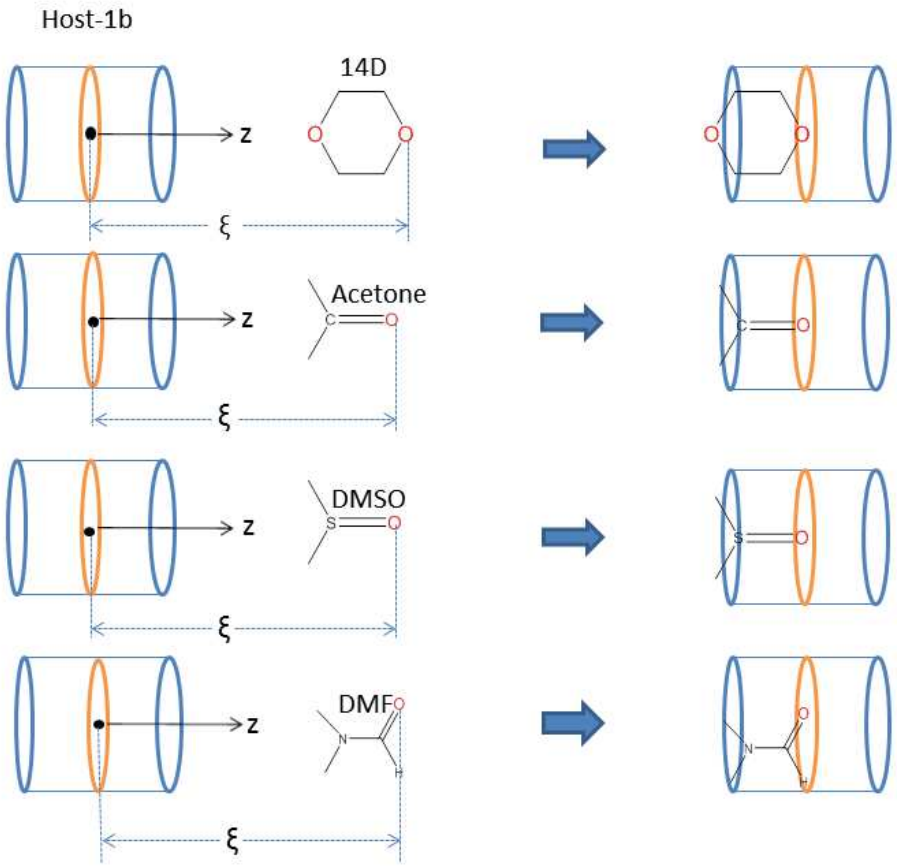

Figure 6A-6. *Schematic representations of the inclusion direction of different guest molecules threading through the cavity of host-1b. The origin is set at the center of mass of two nitrogen atoms of host-1b.*

The application of restraint allows the molecule to sample the configurational space in a defined region (along with a reaction co-ordinate) between it and its reference molecule. It should be noted here that the windows must allow for a slight overlap in order to generate PMF curve in a proper manner. Since both end of the host-1b is symmetric only one path is available for the guest molecule to leave the host. We have chosen the reaction coordinate along z-axis. For different systems, the schematic representation for the path of

the umbrella sampling is presented in Figure 6A-6.

In Figure 6A-7, the PMFs for above four host-guest systems are plotted as a function of COM-COM distances (r).

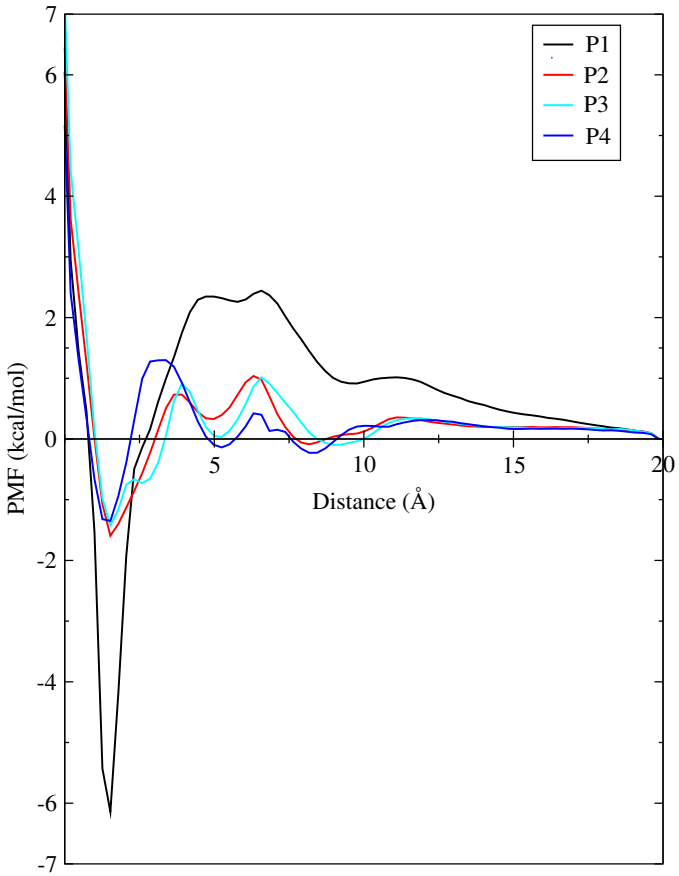

Figure 6A-7. *PMF profiles for insertion of different guest molecules into the host-1b cavity for different systems.*

The broad features that we can derive from this figure are: (i) appearance of a sharp minimum at around 1.5 Å host-guest distance, which corresponds to the insertion of guest molecules into the cavity of the host-1b, (ii) a second minimum which appears at around 5 Å (except for the guest 14D), is attributed to the solvent-separated-minimum (SSM), and (iii) these two minima are separated by an energy barrier appears between 3-5 Å distance. The second minimum (at 5 Å) for P2, P3 and P4 systems are identified as SSM through

visualization by VMD (Figure 6A-8).

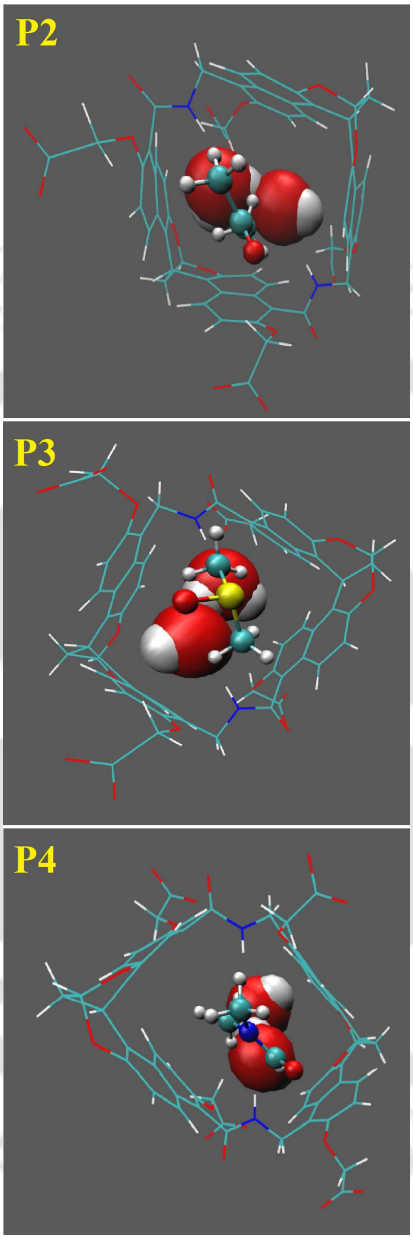

Figure 6A-8. *The visualization of solvent-separated-minimum (SSM) structures for P2, P3 and P4 systems. These snapshots are prepared when the distance between the center-of-mass of host and the center-of-mass of guest is 5 Å . Only the water molecules (represented as vdW) present between the host-1b (represented as lines) and the guest molecules (represented as CPK) are considered. Other water molecules are left-off to enhance the visual clarity.*

Thus, in order to achieve the state in which the guest is inserted into the host from the SSM-

state one barrier of energy ranging 1-2.25 kcal/mol (depending upon the guest molecule) has to overcome. Further, a close look at the different PMF values (at ≈1.5 Å distance) reveals that the insertion of 14D into the host-1b cavity is energetically most favorable. The PMFs of rest three guest molecules show a very similar PMF values. On the other hand, the SSM-state for the guest 14D is the least favorable one. Nevertheless, the different PMF values at ≈1.5 Å suggest that the host-1b/14D host-guest complexation is significantly more favorable (about -4.7 kcal/mol) than that for other three host-guest complexes.

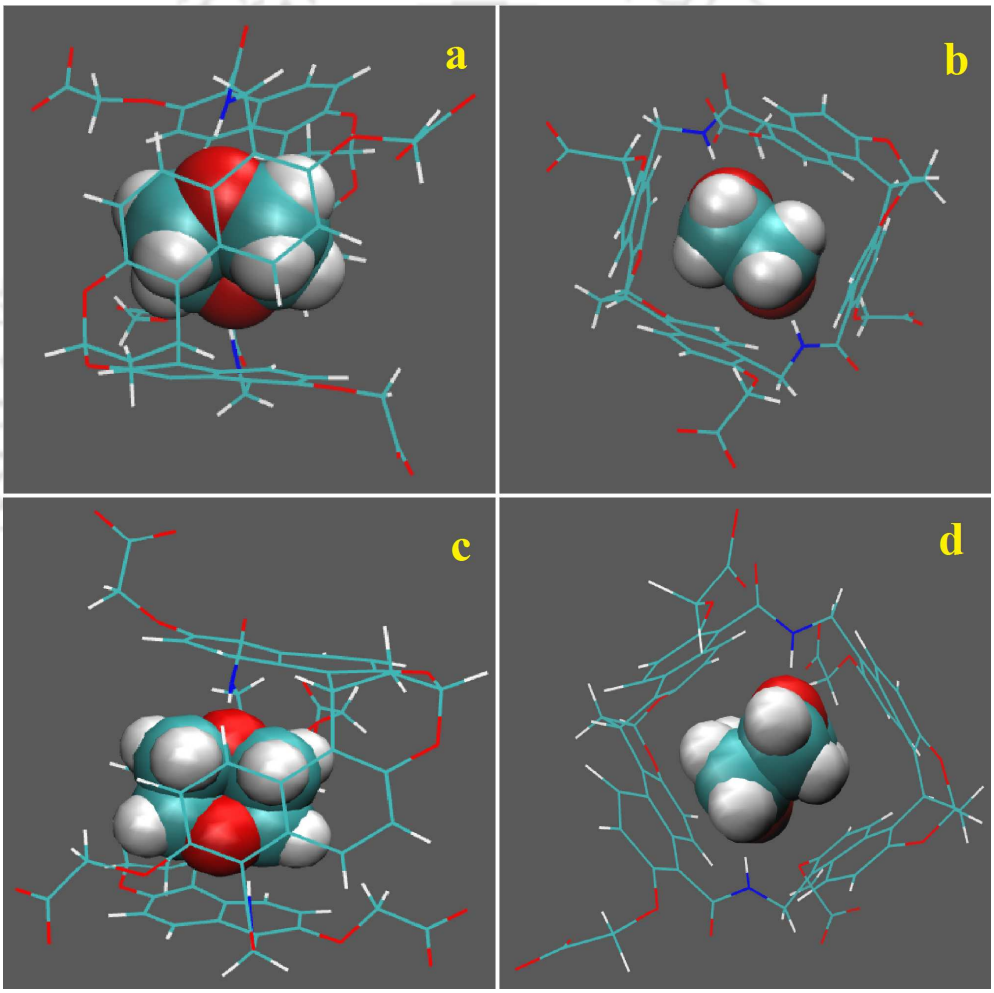

Figure 6A-9. *(a) and (b) are the snapshots for system S1 and (c) and (d) are the snapshots for system S1-test. Left and right panels represent side and top view, respectively.*

Before summarizing the results obtained in this study we would like to remark that we further examine if the initial configurations of our simulations cause any bias in the results. Towards this, we prepare a test system (S1-test) which contains identical

number of different molecules as that of system S1. Then for system S1-test, we prepare an initial configuration (by PACKMOL) which is very different from that of the initial configuration of system S1. The newly generated initial configuration of system S1-test is further subjected to a separate 60 ns MD simulation run. Then the results of system S1 and system S1-test are compared by considering the snapshots (Figure 6A-9), average diameter values (Table 6A-5) and the values of free energy of binding calculated by MM-PBSA method (Table 6A-6). The very similar results produced by both system S1 and system S1-test rules out the biasness of starting configuration of the simulation on the results.

Table 6A-5. Average internal diameter[a]

System	Average value of diameter-1 (Å)	Average value of diameter-2 (Å)
S1	13.04	9.80
S1-test	13.07	9.79

[a] Average internal diameter-1 and internal diameter-2 of host-1b for S1 and S1-test system.

Table 6A-6. Binding free energy values[a]

System	ΔE_{vdw}	ΔE_{ele}	ΔG_{PB}	ΔG_{NP}	ΔG^0_{bind}
S1	-27.98	-10.17	12.43	-19.15	-44.87
S1-test	-27.99	-10.12	12.46	-19.10	-44.75

[a] The binding free energy values of S1 and S1-test system. All energy values are expressed in kcal/mol unit.

■ SUMMARY AND CONCLUSIONS

We present a study of encapsulation of strongly hydrophilic molecules like 14D, acetone, DMSO, and DMF by endo-functionalized molecular tube host-1b from the aqueous solution. This type of naphthotube can be used as a supramolecular catalysis and for the recognition of biologically or environmentally important neutral molecules. These macrocyclic receptors, which are based on naphthol, avowedly mark up the scope of supramolecular chemistry. Receptor molecules, usually do not engage in any competition for hydrogen bonding with the bulk solvent water because their hydrogen bond donors are covered up in their grave cavities and lay aside from the bulk solvent. Host-guest hydrophobic interactions and hydrogen bonds work synergistically for high stability and high selectivity in the

complexation. The above-mentioned molecular receptors could gain selective recognition of the group 2B carcinogen and persistent environmental contaminant 14D. We also suspect that the idea displayed in this study can act as a guidance to difference synthetic receptors for the recognition of other environmentally or biologically important neutral hydrophilic molecules. The complexation procedures of these above-mentioned guest molecules with the endo-functionalized molecular tube are persuaded by classical molecular dynamics simulations, MM-PBSA, and umbrella sampling method. Moreover, the analyses of host-solvent water hydrogen bond numbers show the absence of any solvent water molecule inside the host for the guest 14D, whereas, for the other three guest molecules the presence of nearly one water molecule inside the host's cavity. The estimations of the host-guest center of mass distances for different systems suggest a complete insertion of the guest 14D and partial insertions of rest of the three guest molecules. The results of PMF calculations (done by using umbrella sampling techniques) further suggest that the host-1b/14D complexation is energetically most stable. This observation is in well accordance with the calculated binding free energy values (obtained from MM-PBSA calculations) of different host-guest complexes. The macrocycle host changes its shape due to the insertion of guest molecule. MM-PBSA calculations show that the host-guest van der Waals interactions play a major role for the stable complexes. The movability of these guest molecules inside the molecular tube cavity faces a very less amount of energetic barrier (except for the guest 14D). From the findings of our study, we hope, this type of endo-functionalized molecular tubes will have great applications in materials science and biomedical industries.

Part B:

How does the complexation ability between host endo-functionalized molecular tube and strongly hydrophilic guest molecules in water depend on guest concentration?

Overview: We have already shown in Chapter 6 (Part A) the main factors responsible in the complexation between an endo-functionalized molecular tube and different strongly hydrophilic guest molecules in water. These types of molecular tubes have gained a significant importance for encapsulating many environmentally and biologically important molecules. Here, we have examined how does this type of complexation ability depend on concentration of guest molecules? We use classical molecular dynamics together with MM-PBSA method for this purpose. We examine the effect of concentration of different guest molecules on the host-guest complexation ability by determining different types of hydrogen bond properties, preferential interaction parameter, water-inserted guest interaction energy parameter, host-guest binding free energy and potential of mean force. From the calculated free energy values obtained from MM-PBSA and PMF calculation, it is revealed that as the concentration of guest decreases the free energy becomes less favorable.

■ INTRODUCTION

Binding nature of two molecules is determined by molecular recognition - a very common mode in biological and chemical processes. For this, comprehending molecular recognition is of interest in elementary studies and it has real infliction in chemical industries and drug discovery. Molecular binding can be identified by thermodynamic study. Molecular binding aptitude is a candid characterizer of recognition and can be determined experimentally by calorimetry [295, 296].

Macrocyclic receptors are one of the important types of molecule, which are used in recognition - known as supramolecular chemistry, a very important part in chemistry [1, 297, 298]. An invention of every new macrocyclic receptor accelerates the advancement of supramolecular chemistry. Host-guest complexation of supramolecular chemistry is a tremendous important process in chemistry. Some important types of synthetic molecular receptor are crown ether [19], cyclodextrin [23], calixarenes [25], cucurbiturils [26], recorcinarenes [28], cyclotriveratrylene [29], pillarenes [30]. In recent times, some naphthalene based molecular receptors have been synthesized, such as cyclotetrachromotropylene (CTCT) [37], in which four naphthyl units are connected by methylene bridge. These types of receptors with short methylene bridge face steric hindrance and has a very small cavity. For this, it has very weak complexation ability. So, these types of receptors are of limited uses.

The complexation ability of these types of receptors can be increased by replacing the short methylene functional groups with larger functional groups into their structures. Connecting groups in synthesized molecular receptors are taken by considering the complementarity of size, shape and charge distributions with the substrate or guest, mimicking the biological productiveness in enzyme-substrate binding [267]. Very recently, Jiang et al. [38] synthesized a molecular receptor in which a couple of naphthol based molecular clefts are connected by amide functional group. In these molecular tubes when both the bis naphthalene clefts are connected in the same orientations (syn) it is known as host-1a and when these are in different orientations (anti) it is labelled as host-1b (Figure 1-4 of Chapter 1). Note that, molecular recognition takes place by weak noncovalent interaction between host and guest molecule. The above-mentioned, two hosts have both hydrophilic and hydrophobic parts. So, these host molecules can interact with polar and nonpolar parts of guest molecule simultaneously. Thus, the hydrophobic effect and noncovalent interactions can take place simultaneously.

In this part, we use classical molecular dynamics (MD) simulation techniques to investigate the effect of guest concentration on the complex formation ability of host-1b (Figure 1-4 of Chapter 1). We consider a range of different hydrophilic guest molecules in aqueous solvent medium. Guest molecules, which are used for this work are 1,4-dioxane, acetone, dimethyl sulfoxide, and dimethyl formamide. Our goal is to acquire a brief knowledge of stability dependency of these host-guest complexes with guest concentration. Moreover, we have estimated the binding free energy of each and every host-guest complexes of all the systems by employing the Molecular-Mechanics-Poisson-Boltzmann Surface Area (MM-PBSA) method. We have taken all the components of binding free energy and searched the stability dependency of these host-guest complexes with guest concentration for a particular type of guest molecule. We have also determined Potential of Mean Forces (PMFs) of each and every systems. This gives a clear vision about the energy barrier, which may present during the insertion of guest molecule in the hosts' cavity.

The remainder of this part is divided into three sections. Section 'COMPUTATIONAL DETAILS' describes the details of modelling and simulation. The results are discussed in section 'RESULTS AND DISCUSSIONS' and our results are briefly summarized in section 'SUMMARY AND CONCLUSIONS'.

■ COMPUTATIONAL DETAILS

At first the geometry of host-1b and ammonium ion were energy optimized by considering ab initio HF/6-31+G** method with the help of Gaussian 09 [106]. Then the RESP (restrained electrostatic potential) [67] suite of AMBER14 [63] was employed to obtain the partial charges of each and every atomic sites of both host-1b and ammonium ion. For these molecules, other force field parameters of all the atomic sites were obtained from the General AMBER force field (GAFF) [108] of ANTECHAMBER [107] suite of AMBER14. The derived partial charges of all the atomic sites of host-1b are reported in Table 2-2 of Chapter 2. As host-1b has four units of negative charge, four NH_4^+ counter ions were added for neutralizing each of the systems. Four solute molecules e. g., 1,4-dioxane (14D), acetone, dimethyl sulfoxide (DMSO), and dimethylformamide (DMF) were used as guest for this purpose. The OPLS/AA force field parameters were adopted for these guest molecules [285–291]. Three-point transferable intermolecular potential (TIP3P) [72] water model was employed for this work. In this study, 20 different systems are prepared by changing the number of water molecules and these are presented in Table 6B-1 (among these systems, system S0-a, S1-a, S2-a, S3-a and S4-a were used as system S0, S1, S2, S3

and S4 respectively, in Chapter 6 (Part A)).

Table 6B-1. Overview of systems[a]

System	N_{host}	$N_{NH_4^+}$	N_{guest}	N_{wat}	Box volume (nm^3)	M_{guest} (M)
S0-a	1	4	0	5000	153.17	0.000
S0-b	1	4	0	10000	305.49	0.000
S0-c	1	4	0	15000	456.98	0.000
S0-d	1	4	0	20000	608.89	0.000
S1-a	1	4	10	5000	154.48	0.107
S1-b	1	4	10	10000	306.48	0.054
S1-c	1	4	10	15000	457.69	0.036
S1-d	1	4	10	20000	610.10	0.027
S2-a	1	4	10	5000	153.77	0.108
S2-b	1	4	10	10000	306.45	0.054
S2-c	1	4	10	15000	457.96	0.036
S2-d	1	4	10	20000	609.78	0.027
S3-a	1	4	10	5000	153.94	0.108
S3-b	1	4	10	10000	306.17	0.054
S3-c	1	4	10	15000	458.22	0.036
S3-d	1	4	10	20000	609.95	0.027
S4-a	1	4	10	5000	154.15	0.108
S4-b	1	4	10	10000	306.00	0.054
S4-c	1	4	10	15000	457.96	0.036
S4-d	1	4	10	20000	609.91	0.027

[a] The number of host-1b, ammonium ion, different guest molecule, and water molecules are represented by N_{host}, $N_{NH_4^+}$, N_{guest}, and N_{wat}, respectively. The molar concentration of guest is represented by M_{guest}. System S0 is devoid of any guest molecule and others system S1-S4 contain guest molecules 14D, acetone, DMSO, and DMF, respectively. 'a', 'b', 'c', and 'd' are for 5000, 10000, 15000, and 20000 water molecules, respectively.

The initial configurations of all the systems were generated by using the PACKMOL [74] package. The molecular dynamics simulations were performed with the help of sander suite of AMBER14. A Cubic box was used for each and every systems. All the short ranged nonbonded interactions were treated by employing a 10 Å cut-off distance. For estimating long-ranged electrostatic interactions, the Particle Mesh Ewald (PME) algorithm [73] was applied. For all simulations periodic boundary conditions were employed in all the directions. All simulations were carried out with an integration time steps of 2 fs. All covalent bonds containing hydrogen atoms were constrained by the use of SHAKE algorithm [71].

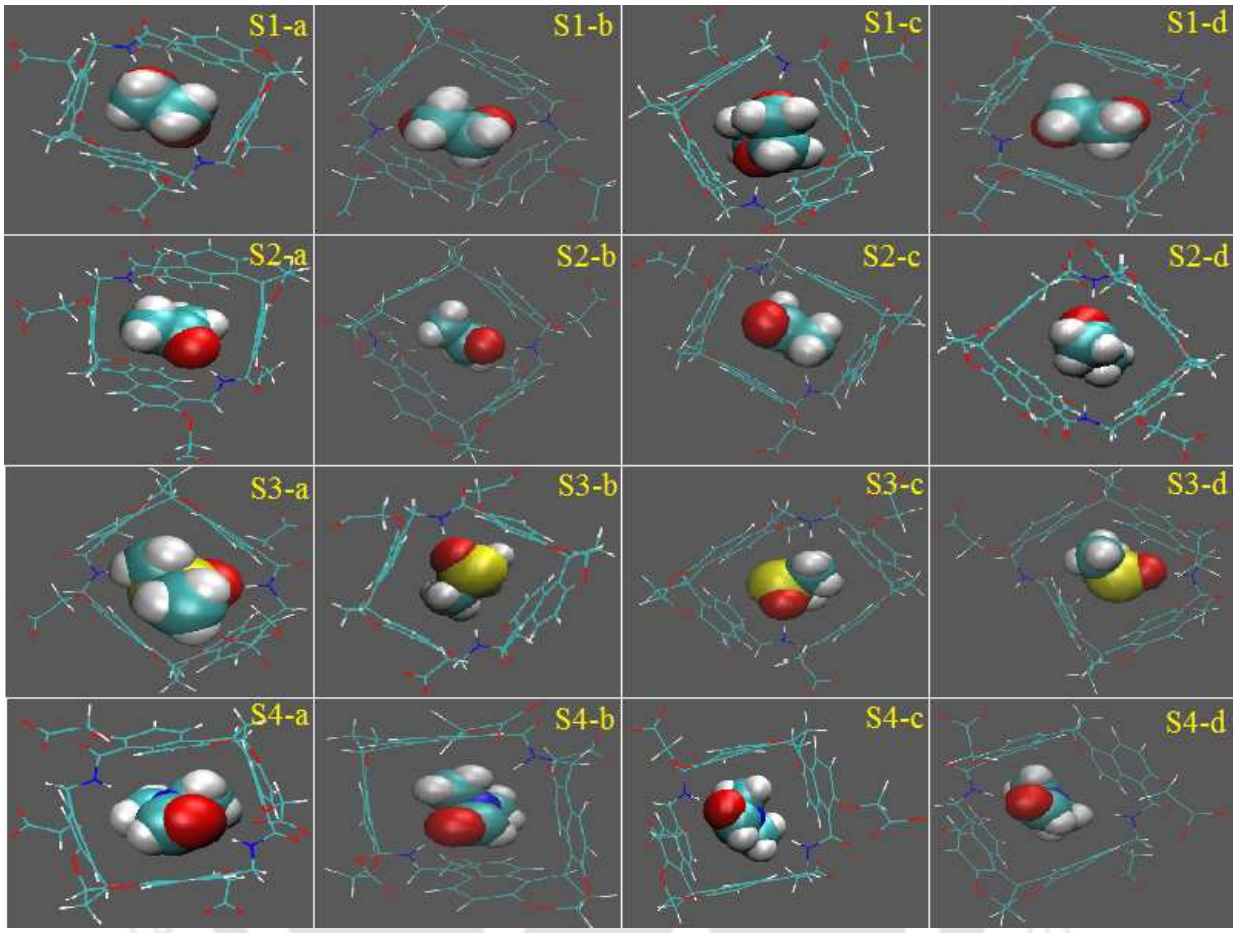

Figure 6B-1. *1:1 host-guest complexes of all guest containing systems are represented by these snapshots. For better clarity, water molecules and ammonium ions are excluded.*

Energy minimization was done by 4000 steps steepest descent (SD), followed by 6000 steps in conjugate gradient (CG) method. Every system was heated slowly from 0 to 298 K in a canonical ensemble (NVT) for 320 ps, followed by 5 ns equilibration in an isothermal-isobaric ensemble (NPT) at 1 atm pressure. Subsequently, simulations were then expanded to 60 ns in NPT ensemble for data analysis. The pressure of the system (in NPT ensemble) was maintained with a Berendsen barostat [75] by using a 2 ps pressure relaxation time. Temperature of the simulation box was maintained by using Langevin dynamics [76] method with 1 ps^{-1} collision frequency. The MD trajectories were analyzed with the help of CPPTRAJ module of AMBER14. Some of the analyses and visualizations of the MD trajectories were carried out using Visual Molecular Dynamics (VMD) [78] program.

Binding free energy (ΔG^0_{bind}) of the host-guest complexes are calculated by using

the Molecular Mechanics-Poisson Boltzmann Surface Area (MM-PBSA) [79, 80] method. Details of this method are discussed in the 'METHODOLOGY' section of Chapter 1 (Eq. 1.18).

■ RESULTS AND DISCUSSIONS

Different MD simulation are carried out of complexes of host-1b with different guest molecules and their various concentrations in aqueous solvent. Our aim is to find out the stability order of different host-guest complexes as the guest concentration is changed.

The snapshots of all systems (which contains 1:1 host-guest complex) are displayed in Figure 6B-1 (among these snapshots S1-a, S2-a, S3-a and S4-a snapshots were used in Chapter 6 (Part A), as snapshots for S1, S2, S3 and S4 systems, respectively). From this figure, it is seen that all the systems of host-1b/14D show fully inserted 1:1 host-guest complex but all other systems such as host-1b/acetone, host-1b/DMSO, and host-1b/DMF show partially inserted 1:1 host-guest complex. Here it is to be remembered that these snapshots are used as representative purposes only as they do not shed lights into the stability of different host-guest complexes.

Internal Diameters

The host molecule is not spherical in shape. So, it has two unequal diameters. We have shown these in Figure 2-3 of Chapter 2 by linking two converse atoms C15-C74 (for diameter-1) and C53-C96 (for diameter-2). Above-mentioned guests get inserted into the host cavity and for this insertion process, host molecule changes its shape, which we have shown from the changing value of these two diameters. The average value of these two diameters, the absolute difference (Ad) between them, and the standard error of Ad are shown in Table 6B-2. Diameter-1 has the higher value than diameter-2. Interestingly, a system with higher concentration (for all guest containing systems) shows a much less Ad value and it increases as concentration decreases for a particular type of guest molecule. Now, when Ad value is less the host molecule adopts a somewhat symmetric structure than the host having higher Ad value. We have also estimated the probability distribution functions of the Ad values of different systems and they are presented in Figure 6B-2. Insets of these figures refer to the Ad value vs simulation time plot. From Figure 6B-2 it is clear that systems with a particular guest show a maximum probability of Ad at minimum distance for the highest concentration and as the concentration decreases the position of the maximum probability shifts to higher distance. Lesser the value of Ad greater will be

the conformational stability of host-1b as less value of Ad implies the higher symmetric structure of host-1b [299]. So, these findings suggest that as concentration decreases, the stability of host-guest complex also decreases for a particular type of guest molecule.

Table 6B-2. Average internal diameter[a]

System	Aid-1 (Å)	Aid-2 (Å)	Ad (Å)	Se (Å)
S0-a	13.56	9.60	3.96	± 0.003
S0-b	13.57	9.61	3.96	± 0.107
S0-c	13.56	9.56	4.00	± 0.005
S0-d	13.57	9.57	4.00	± 0.074
S1-a	13.04	9.80	3.24	± 0.012
S1-b	13.11	9.76	3.35	± 0.019
S1-c	13.12	9.72	3.40	± 0.005
S1-d	13.19	9.78	3.41	± 0.004
S2-a	13.14	9.72	3.42	± 0.011
S2-b	13.22	9.73	3.49	± 0.025
S2-c	13.16	9.66	3.50	± 0.006
S2-d	13.19	9.63	3.55	± 0.010
S3-a	13.22	9.74	3.48	± 0.025
S3-b	13.19	9.63	3.55	± 0.009
S3-c	13.21	9.65	3.56	± 0.024
S3-d	13.22	9.62	3.60	± 0.018
S4-a	13.22	9.62	3.60	± 0.018
S4-b	13.31	9.65	3.66	± 0.005
S4-c	13.35	9.67	3.68	± 0.010
S4-d	13.42	9.67	3.75	± 0.013

[a] Average values of internal diameter-1 (Aid-1), internal diameter-2 (Aid-2), absolute difference (Ad) between them, and the standard errors (Se) of Ad of all systems for host-1b.

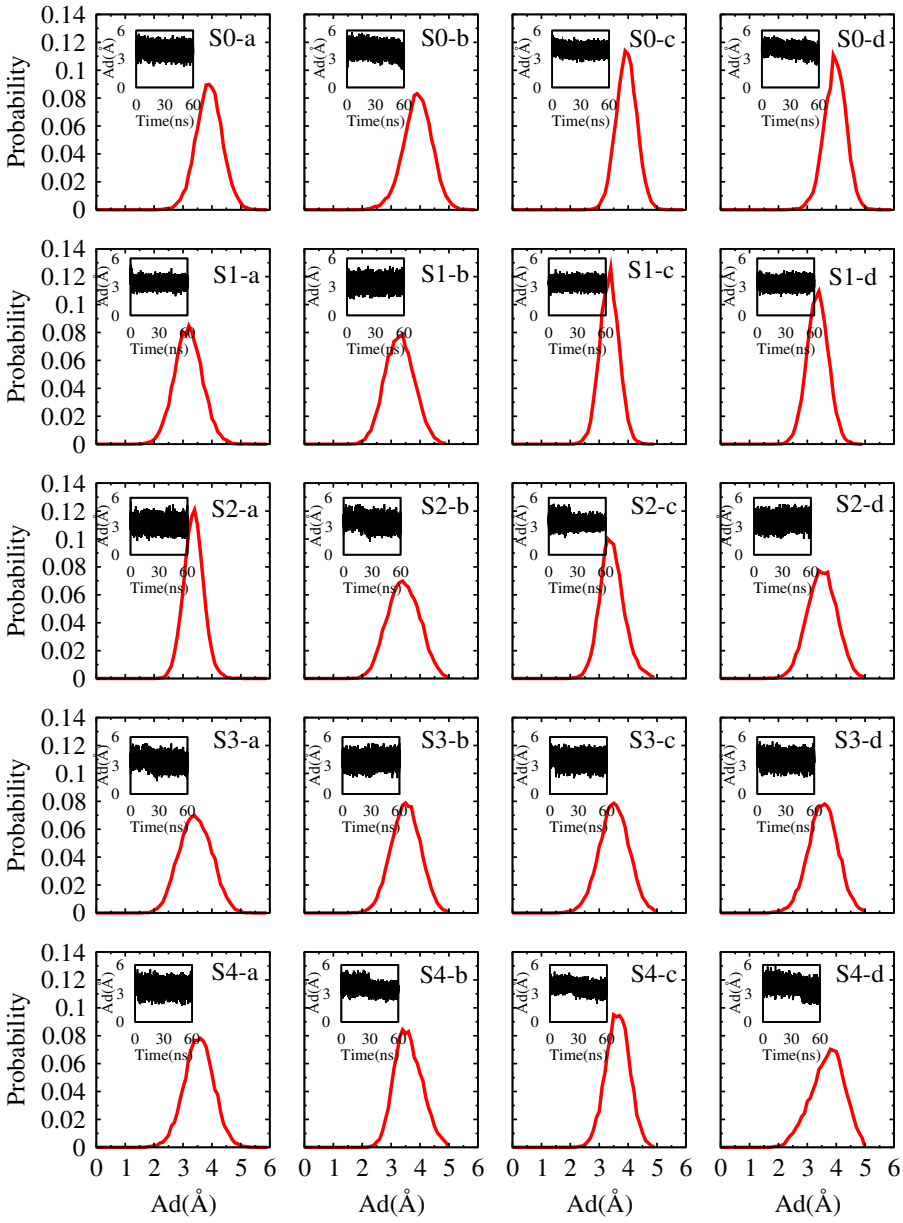

Figure 6B-2. *The probability distribution functions of absolute difference (Ad) of host-1b. Ad values as a function of simulation time for every system are also shown in the insets.*

Hydrogen Bond Properties

Table 6B-3. Hydrogen bond values[a]

System	host-wat	N1-wat	N3-wat	host-gus	gus-wat
S0-a	25.40	0.85	0.67	–	–
S0-b	27.30	0.87	0.68	–	–
S0-c	27.40	0.86	0.84	–	–
S0-d	29.80	0.89	0.88	–	–
S1-a	23.11	0.02	0.01	1.91	0.00006
S1-b	27.14	0.21	0.31	1.25	0.0001
S1-c	27.30	0.23	0.44	1.18	0.05
S1-d	29.46	0.32	0.45	1.03	0.38
S2-a	23.98	0.42	0.31	0.57	0.72
S2-b	25.23	0.44	0.32	0.55	0.88
S2-c	26.31	0.47	0.31	0.41	0.90
S2-d	27.40	0.51	0.45	0.25	0.97
S3-a	24.65	0.71	0.51	0.57	0.88
S3-b	24.90	0.84	0.49	0.40	0.90
S3-c	26.60	0.87	0.54	0.24	0.97
S3-d	26.74	0.89	0.67	0.10	1.01
S4-a	23.90	0.32	0.23	0.58	0.99
S4-b	25.53	0.43	0.46	0.30	1.05
S4-c	26.70	0.47	0.32	0.15	1.07
S4-d	27.12	0.53	0.54	0.09	1.12

[a] Average number of hydrogen bonds between host and solvent water (host-wat), host-1b N1 atomic sites-water (N1-wat), host-1b N3 atomic sites-water (N3-wat), host and inserted guest (host-gus), and inserted guest-water (gus-wat) for different systems.

The dependency of stability of these host-guest complexes as the guest concentration is changed can be explained with the help of hydrogen bonding interactions. For analyzing different types of hydrogen bonds, a donor-acceptor cut-off distance of ≤ 3.4 Å is used and simultaneously, donor-acceptor-hydrogen cut-off angle of $\leq 45^o$ is taken (see Figure 2-6 of Chapter 2). The number of hydrogen bonds between host and water molecules is provided in Table 6B-3. It shows a simple trend. As the number of water molecules increases (i.e., concentration decreases), this type of hydrogen bond value also increases for a particular type of guest molecule. This indicates that those host atoms, which are responsible for this type of hydrogen bond formation, is now more available to water molecules. Next, we calculate the hydrogen bonds in between host atomic sites in which N1 and N3 atomic sites act as hydrogen bond active sites and water molecules (Table

6B-3). It is apparent that as the concentration of the system decreases (for a particular type of guest molecule) the number of hydrogen bonds increases. As concentration decreases the availability of these nitrogens to water increases.

The average number of host-guest hydrogen bond values are also presented in Table 6B-3. Guests' donor atom/atoms form a hydrogen bond with hosts' acceptor atoms. As discussed above, it is clear that as the concentration of a system decreases (for a particular type of guest molecule) the availability of host acceptor atoms increases to water molecules and so, it is expected to decrease host-guest hydrogen bond numbers. As per the expectation as concentration decreases, number of hydrogen bonds between host and inserted guest molecule decreases.

Further, we estimate the average number of hydrogen bonds between guest (which get inserted into the host cavity) and water molecules (Table 6B-3). As concentration is decreased (for a particular type of guest molecules) the value of this type of hydrogen bond increases. From here, we can infer that with decreasing concentration the availability of this inserted guest increases to water and decreases to host molecule.

Preferential Interaction Parameters

From above, it is somewhat clear that complexation ability of different guest molecule with host endo-functionalized molecular tube is decreased as the concentration of guest decreases. Thus, it would be helpful to determine the preferential interaction parameter, τ, for predicting the effect of guest concentration on the complexation ability of different host-guest systems. For this, we use the Kirkwood-Buff theory [300–306], which gives a statistical thermodynamics approach for calculating the preferential interaction parameter, τ, of guest molecule with host molecule over water molecule (τ^g_{hw}). τ^g_{hw} can be written as:

$$\tau^g_{hw} = \rho_h(G_{gh} - G_{gw}) \tag{6.1}$$

where g, h, and w represent guest, host, and water molecules, respectively. ρ_h is the number density of the host molecule of different systems. G_{gh} and G_{gw} symbolizes Kirkwood-Buff integrals and the value of these integrals are obtained from the host center of mass-guest oxygen and guest oxygen-water oxygen distribution function, respectively. G_{ij} (for species i and j) in a grand canonical ensemble is defined as:

$$G_{ij} = 4\pi \int_0^\infty [g_{ij}(r) - 1] r^2 dr \tag{6.2}$$

Again, for closed system, this equation becomes:

$$G_{ij} \approx 4\pi \int_0^R [g_{ij}(r) - 1] r^2 dr \tag{6.3}$$

where R represents the distance where the value of the above integral approaches zero and $g_{ij}(r)$ is pair correlation function. A positive value of τ^g_{hw}, reveals the preference of host-guest interaction over guest-water interaction and its negative value implies the preferential hydration of the guest molecules over host-guest interaction.

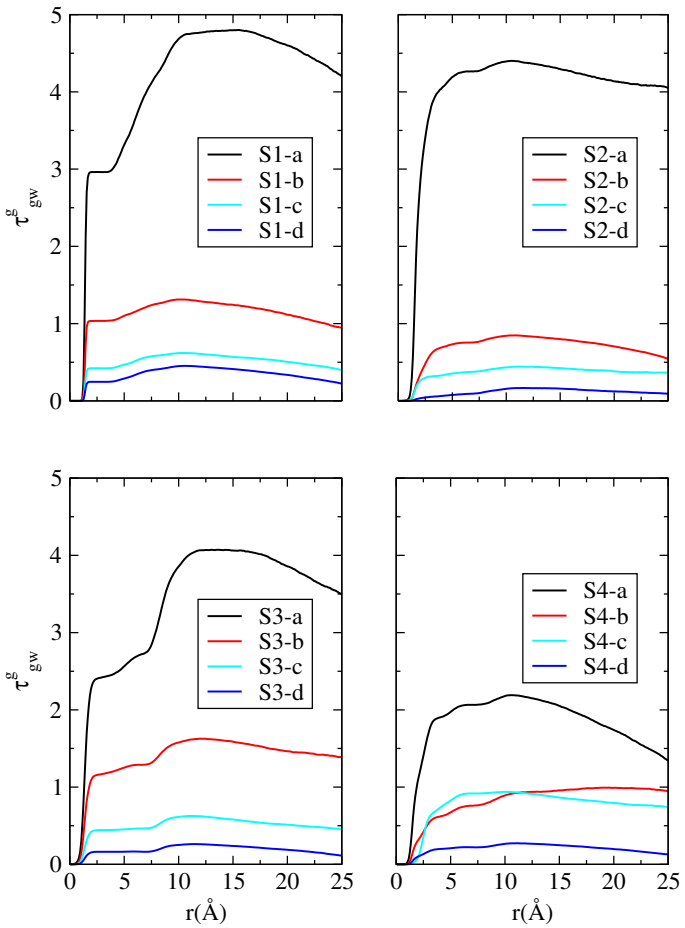

Figure 6B-3. *Preferential interaction parameters of guest molecule with host molecule over water for all the systems.*

The τ_{hw}^{g} values as function of distance (r) of all the systems is presented in Figure 6B-3. It is quite evident that the system which contains maximum guest concentration shows maximum positive value of τ_{hw}^{g} and as the guest concentration decreases preferential interaction parameter also decreases. So, the concluding remarks of this observation is that the host-guest complexation stability decreases as the concentration of the guest decreases.

Inserted Guest-Water Interaction Energy

Table 6B-4. Average interaction energies[a]

System	van der Waals (vdW)	Electrostatic	Total
S1-a	-2.25	-1.10	-3.35
S1-b	-2.35	-1.13	-3.48
S1-c	-2.40	-1.17	-3.57
S1-d	-2.53	-1.23	-3.76
S2-a	-1.86	-4.12	-5.98
S2-b	-1.93	-4.63	-6.56
S2-c	-2.03	-4.92	-6.95
S2-d	-2.23	-5.17	-7.40
S3-a	-1.56	-12.57	-14.13
S3-b	-1.60	-12.83	-14.43
S3-c	-1.67	-13.73	-15.40
S3-d	-1.72	-14.27	-15.99
S4-a	-1.80	-16.44	-18.24
S4-b	-1.86	-16.61	-18.47
S4-c	-1.90	-17.05	-18.95
S4-d	-1.92	-17.18	-19.10

[a] Average of van der Waals (vdW), electrostatic, and total interaction energies of inserted guest and water molecules (all values are in kcal/mol unit).

For all the systems, among the 10 guest molecules the one that gets inserted into the host cavity is considered as 'inserted guest' molecule. We calculate the interaction energy between inserted guest and water molecules by using the NAMD energy plugin of VMD [78]. Total value of this interaction energy is the combination of van der Waals (vdW) and electrostatic components. The average interaction energy values of all the systems are presented in Table 6B-4. It is seen that for S1 systems the main contributor of interaction energy is the vdW energy. But for S2-S4 systems the main contributor to the total interaction energy is the electrostatic energy. Moreover, for all the systems of S1 and S2, the difference between vdW and electrostatic energy is much less but for all S3 and

S4 systems, this difference is much greater in magnitude. Again, for all the systems of a particular guest molecule, the value of these total interaction energy become more favorable (i.e., has more negative value) as the concentration of the guest decreases. This indicates that for the highest guest concentration system, the inserted guest molecule interact less with water molecules. This indirectly implies more host-guest interactions (shown in MM-PBSA subsection) and this trend gets reversed with the decrease of guest concentration.

MM-PBSA Analysis

For quantitative estimate of stability of host-guest complexes as the guest concentration is changed the binding free energy of each and every system is determined. We use the MM-PBSA tool to compute the value of binding free energies of 14D, acetone, DMSO, and DMF by host-1b at different concentration levels of guests. The energy component of these different energetic terms (in kcal/mol) are listed in Table 6B-5. The MM-PBSA analysis was performed by taking the last 4 ns of MD trajectory.

A deep look into the table reveals that van der Waals (ΔE_{vdw}) interaction is the main contributor for giving stability to the complexes. Electrostatic interactions (ΔE_{ele}) are also favorable though they are less negative than that of ΔE_{vdw}. Every system shows a favorable negative value of ΔE_{vdw} and ΔE_{ele} and these values become less favorable as the guest concentration of the system decreases. Electrostatic solvation energy (ΔG_{PB}) shows an unfavorable contribution (i.e., positive value) to ΔG^0_{bind} for each and every system. Apolar solvation free energy (ΔG_{NP}) value has a favorable contribution to the value of ΔG^0_{bind} for every system. This energy value becomes less favorable with decrease of guest concentration for a particular type of guest molecules. Interestingly, the ΔG_{solv} (ΔG_{PB} + ΔG_{NP}) has negative values for all host-1b/14D and host-1b/acetone systems but has positive values for all host-1b/DMSO and host-1b/DMF systems.

Concentrating on ΔG^0_{bind} for all the systems it is noticed that the binding of host and guest is favorable. Moreover, we find that free energy of binding for the guest 14D is more negative compared to other systems. This infers that complexation ability of different guest molecules follows the order 14D > acetone > DMSO > DMF. Now, focusing on the effect of concentration of a particular guest molecule on the ΔG^0_{bind} value indicates that as the concentration decreases free energy change becomes more positive and this is valid for all the guest molecules.

Table 6B-5. Binding free energy values[a]

System	ΔE_{vdw}	ΔE_{ele}	ΔG_{PB}	ΔG_{NP}	ΔG^{0}_{bind}
S1-a	-27.98	-10.17	12.43	-19.15	-44.87
S1-b	-26.91	-10.52	12.46	-18.31	-43.28
S1-c	-19.74	-10.38	9.55	-12.81	-33.38
S1-d	-18.80	-10.18	8.74	-12.01	-32.25
S2-a	-22.20	-8.10	12.68	-17.67	-35.29
S2-b	-20.41	-7.95	11.10	-15.79	-33.05
S2-c	-17.91	-6.56	10.41	-14.32	-28.38
S2-d	-12.57	-4.83	7.14	-9.82	-20.08
S3-a	-22.85	-15.46	20.75	-17.39	-34.95
S3-b	-15.98	-10.06	13.80	-12.52	-24.76
S3-c	-12.77	-7.38	10.25	-9.92	-19.82
S3-d	-12.46	-8.48	11.74	-9.31	-18.51
S4-a	-16.51	-9.34	15.29	-13.96	-24.52
S4-b	-13.07	-7.39	12.09	-10.89	-19.26
S4-c	-12.13	-7.42	11.32	-10.23	-18.46
S4-d	-11.62	-7.48	11.13	-9.79	-17.76

[a] All the components and the total value of binding free energy (in kcal/mol) for all guest containing systems.

Potential of Mean Force

The PMF profiles of host-guest complexes in the aqueous solution of varying concentrations are displayed in Figure 6B-4. Each PMF curve of all S1 and S2 systems (i.e. for guest 14D and acetone, respectively) shows two minima separated by a maxima and every PMF curve for all S3 and S4 systems (i.e., for guest DMSO and DMF, respectively) display three minima separated by two maxima. The first sharp minima at about 1.2 to 1.5 Å for every system is for the fully inserted complex and can be termed as contact minima (CM). The second minima which appears at ∼5-6 Å are designated as solvent separated minimum (SSM). In between every two neighboring minima, there is a maxima i.e., every two neighboring minima is separated by a barrier of energy. In order to achieve SSM state from CM state a guest molecule has to cross a desolvation barrier having energies ranging from 2.5 kcal/mol to 6.5 kcal/mol depending on the system and type of guest molecule e.g., the barrier height for 14D containing system of highest guest concentration (S1-a) is approximately 6.5 kcal/mol, which decreases monotonously as the concentration of the guest molecule is decreased. A sharp decrease in the well depth of CM is also observed as the guest concentration decreases and this is true for all guest molecules consider in this study.

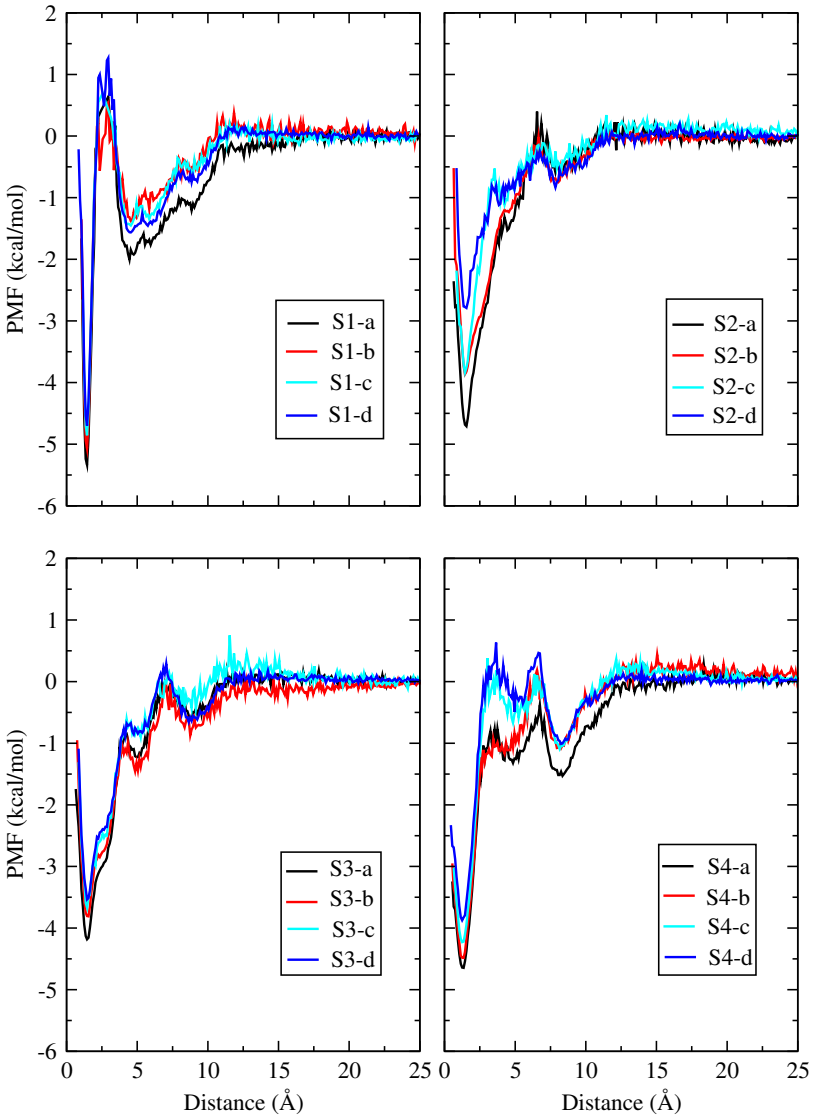

Figure 6B-4. *PMF values as a function of host-guest distance for all guest containing systems.*

For systems containing acetone molecules (S2 systems) a profound effect of guests' concentration on the well depth of the first minimum is observed. In specific, as the concentration of acetone decreases the CM state becomes unfavorable. Moreover, for this system we would not observe any sharp SSM state. For DMSO and DMF containing systems, the

appearance of second and third minima in the PMF curves suggest that these molecules are strongly correlated with the hosts' nitrogen atoms.

■ SUMMARY AND CONCLUSIONS

We introduce here the concentration dependency in the complexation between endo-functionalized molecular tube (host-1b) and strongly hydrophilic guest molecules like 14D, acetone, DMSO, and DMF in water. Host molecule of this form can be used as a catalyst and for encapsulation of neutral molecules that are important in the view of biology and environment. These naphthol based supramolecular receptors candidly uplift the territory of supramolecular chemistry. Here both hydrophobic and hydrogen bonding interaction are responsible for the high stability and high selectivity of these type of complexation process. Stability dependency of these complexes with guest concentration is examined by classical molecular dynamics simulation and MM-PBSA method. Analysis of internal diameter of host-1b molecule implies that the shape of macrocyclic host alters due to insertion phenomenon and the maximum change is found in the highest guest concentration system. Analysis of different types of hydrogen bond values provides information about the stability of host-guest complexes. In specific the complexation ability decreases as the guest concentration decreases for a particular type of guest molecule. This is also supported by the calculation of preferential interaction parameter of guest with host over water molecule and interaction energy between inserted guest and water molecules. These findings are in accordance with the energy values (calculated from the MM-PBSA method) of different systems. Every component of binding free energy is less favorable and the value of binding free energy also becomes less favorable as the guest concentration is decreased. The result of the PMF calculation further suggests that this host-guest complexation becomes energetically less favorable as the guest concentration decreases. All of these findings conclude a remarks that the stability of these type host-guest complexes decreases as the guest concentration of these system is decreased.

Chapter 7

Translocation of endo-functionalized molecular tubes across different lipid bilayers

"Scientific discovery and scientific knowledge have been achieved only by those who have gone in pursuit of it without any practical purpose whatsoever in view."

– Max Planck

Overview: Various artificial receptors, such as calixarenes, cyclodextrins, cucurbit[n]urils, and their acyclic compounds, pliiar[n]arenes, deep cavitands, and molecular tweezers can permeate the lipid membranes and they are used as drug carriers to improve the drug solubility, stability, and bioavailability. Inspired by these, we have employed atomistic molecular dynamics simulation to examine the effects of endo-functionalized molecular tubes or naphthotubes (host-1a and host-1b) on seven different types of model lipid bilayers and the permeation properties of these receptors through these model lipid bilayers. Lipid types include six model lipid bilayers (POPC, POPE, DOPC, POPG, DPPE, POPE/POPG) and one realistic membrane (yeast). We observe that these receptors spontaneously translocated toward these model lipid bilayers head regions and do not proceed further into these lipid bilayers tail regions (reside at the interface between lipid head and lipid tail region) except for the DPPE containing systems. In the DPPE model lipid bilayer-containing systems (1a-dppe and 1b-dppe), receptor molecules are only absorbed on the bilayer surface and reside at the interface between lipid head and water. This finding is also supported by the biased free energy and position-dependent diffusion coefficient (D(Z)) profiles of these translocation processes. Passive transport of these receptors may be possible through these model lipid bilayers (due to low barrier height) except for DPPE bilayer-containing systems (that have a very high energy barrier at the center). The results from these simulations provide insight into the biocompatibility of host-1a or host-1b in microscopic detail. Based on this work, more research is needed to fully comprehend the role of these synthesized receptors as a prospective drug carrier.

■ INTRODUCTION

As of now, in this thesis, host-1a and host-1b (Figure 1-4 of Chapter 1) are used for enantiomeric or chiral separation procedure, enhancement of poorly water-soluble drug solubilization, and encapsulation of environmentally important contaminants from the aqueous medium. Now, we are interested to see these two receptors can be used for drug delivery purposes or not. The first and foremost criterion for any molecules that show promising in drug delivery is to permeate lipid bilayers. Thus, in Chapter 7, we focus on the permeation properties of these two receptors through different lipid bilayers.

The lipid bilayer provides a natural obstacle, isolating the cells' interior from its exterior. Molecular movement through a lipid membrane is a central mechanism in the critical biological process. The capacity of cells to control the infusion and translocation of nutrients, neurotransmitters, pharmaceutical drugs, and xenobiotics via biological membranes is a fundamental physicochemical property [307, 308]. Molecular transportation mechanisms through bilayers can be categorized into two categories; active transportation and passive transportation. The former needs a regulatory appliance (with energy intake) that conveys target molecules in the opposite direction of the concentration gradient, while the latter is accomplished by an entropy-driven, nonspecific diffusion mechanism of the molecule across the membrane. The majority of small neutral molecules and drug molecules are passively transferred through the membrane. As a result, in basic biological science and medical and pharmaceutical applications, understanding the mechanism of passive permeation is important [309, 310]. The majority of large biomolecules and biologically significant ions are less permeable and pass the membrane through highly sophisticated mechanisms such as endocytosis, channels, pores, or carrier proteins [307, 311]. In recent times, supramolecular chemists have developed and found various artificial receptors, such as calixarenes, cyclodextrins, cucurbit[n]urils, and their acyclic compounds, pliiar[n]arenes, deep cavitands, and molecular tweezers and found the permeation and interaction properties with model membranes [41–50]. These receptors can act as a drug delivery system and deliver drugs or many other important components through lipid bilayers by encapsulating these molecules into their cavities [50, 51]. Nanocarriers can alter the physicochemical characteristics of the integrated molecules; they influence the cytotoxic effect of inserted drugs, and can resolve physiological barriers of the integrated molecules. Therefore, nanovesicles are now utilized to improve drug efficacy, reduce serious complications, and shield drugs from chemical modification, which can undermine the efficacy or result in producing harmful secondary

compounds [52].

For probing the molecular mechanism of membrane permeation systems, molecular dynamics (MD) simulation may be very useful [312, 313]. MD is an effective computer simulation method for studying biomolecular structures at the microscopic level that are difficult to analyze using traditional experimental approaches [314]. The use of atomistic-level MD simulations to investigate the diffusion of small molecules across a lipid membrane has grown in popularity as computing power and scientific force field parameterization has improved [315]. On the other hand, an implacable MD simulation is not specifically useful since the standard time scale of MD becomes too limited to track the entire permeability mechanism through the membrane explicitly. As a result, an alternate approach based on a permeability paradigm is necessary. The inhomogeneous solubility-diffusion model has been used in the majority of MD studies on membrane permeability. The free energy profile and diffusion coefficients are calculated using this model along the reaction coordinate, which is normally chosen as the direction of the permeant along the bilayer normal [51]. There have been some effective MD models of the interaction/transport of small therapeutic agents with/through model membranes [50, 316–320]. For a precise data analysis, these models benefit from taking specific inputs from various regions of the complicated, heterogeneous architecture of biomembranes, which include a wide range of lipid and membrane protein groups [321, 322]. Moreover, the effect of complex lipid bilayers that resemble realistic systems can be studied as a whole to explain how the structure functions in such diverse environments [323–325]. Current findings in MD simulation have reflected on a broad range of molecules that passively diffuse across lipid membranes, including water [326, 327], small molecules [328–333], model drug molecules [313, 334], analgesics [332, 335], drug delivery systems [50,336,337], dyes [338], other lipids [339,340], nanoparticles [341–348], toxins [349], small peptides [350, 351], and even transmembrane proteins [352, 353]. Concerning the potential of mean force (PMF), the results have repeatedly shown that small nonpolar molecules are preferred in the bilayer center, while polar molecules appear to interact favorably with lipid head groups and face an energy barrier in the bilayer center.

The present chapter is focused on the permeation properties of two synthetic supramolecular receptors through seven different types of model lipid bilayers. These two receptors are host-1a (syn) and host-1b (anti) (Figure 1-4 of Chapter 1). Model lipid bilayers are also different from one another. Among these model membranes, five are pure lipid bilayers (1-palmitoyl-2-oleoyl-sn-glycero-3-phosphoethanolamine (POPE), 1-palmitoyl-2-oleoyl-sn-glycero-3-phosphoglycerol (POPG), 1-palmitoyl-2-oleoyl-sn-glycero-3-

phosphocholine (POPC), 1,2-dipalmitoyl-sn-glycero-3-phosphoethanolamine (DPPE), 1,2-dioleoyl-sn-glycero-3-phosphocholine (DOPC)), one model membrane is the 3:1 mixture of POPE and POPG, and last one is the realistic Yeast model membrane (combination of DOPC, POPE, 1,2-dipalmitoyl-sn-glycero-3-phosphocholine (DPPC), 1-palmitoyl-2-oleoyl-sn-glycero-3-phosphate (POPA), 1-palmitoyl-2-oleoyl-sn-glycero-3-phospho-L-serine (POPS), and cholesterol (CHL)). We have employed all-atom MD simulation and biased umbrella sampling simulation to explore the microscopic details of the interactions and permeation aspects of these two receptors through these model lipid bilayers.

The remaining chapter is subdivided into three parts. Section 'MATERIALS AND METHODS' comprises the detailed description of the materials and methods used for the molecular dynamics simulation run. The analyses carried out are delineated and discussed in section 'RESULTS AND DISCUSSIONS', and the conclusions drawn from the chapter are summed up in section 'SUMMARY AND CONCLUSIONS'.

■ MATERIALS AND METHODS

System Preparation

We have performed the molecular dynamics (MD) simulation study of two synthetic supramolecular receptors (Figure 1-4 of Chapter 1) with seven different types of model lipid bilayers. An adequate detail of these model membranes is presented in Table 7-1. The upper and lower leaflet of these lipid bilayers contain an equal number of lipid molecules. The composition of the yeast model membrane system is taken from the work of Sunhwan et al. [355]. All these model membranes are prepared with the CHARMM-GUI membrane builder module [356,357]. AMBER format topology and coordinates are modeled from the LEaP module of the AMBER18 [358] MD simulation package. AMBER lipid17 [359] force field is used for all these lipid molecules. 50 number of TIP3P [72] water molecules per lipid is added to solvate these membrane systems. Every system contains 0.15 (M) KCl salt concentration. Monovalent ion parameters for K^+ and Cl^- ions compatible with the TIP3P water model are employed from Joung and Chethams' work [360]. Lipid molecules which contain negative charge are neutralized by the equal number of K^+ ions. The synthetic receptor molecules (host-1a and host-1b) are optimized with an HF/6-31+G** basis set of Gaussian09 [106] package. Partial charges of every atomic site of these host molecules are computed with the RESP (restrained electrostatic potential) [67] module of AMBER14. These partial charges are available in Tables 2-1 and 2-2 of Chapter 2.

Table 7-1. Description of model lipid bilayers[a]

Pure Model Membranes				
Lipid type	Charge	Transition temperature (K)	no. of lipids	
DPPE	0	336.15	128	
POPE	0	298.15	128	
DOPC	0	256.15	128	
POPG	-1	275.15	128	
POPC	0	275.15	128	
Mixed Model Membrane				
Lipid type	no. of lipids	Lipid type	no. of lipids	Total no. of lipids
POPE	96	POPG	32	128
Yeast Model Membranes				
Lipid type	Charge	Transition temperature (K)	no. of lipids	
DPPC	0	314.15	20	
POPA	-1	301.15	20	
DOPC	0	256.15	100	
POPS	-1	287.15	10	
POPE	0	298.15	60	
CHL	0	NA	60	

[a] A detailed description of all the model lipid bilayers. The total number of lipids divided equally into two leaflets. The transition temperature of these lipids is previously reported [354]. NA means not applicable.

Table 7-2. Overview of systems[a]

System	Host type	Lipid type	Number of Molecules (host:lipid:water)	Starting Distance (Å)	Box Size (Å × Å × Å)
1a-pope	host-1a	POPE	1:128:6400	30.0 / 0.0	60.24×60.02×94.68
1a-dopc	host-1a	DOPC	1:128:6400	30.0 / 0.0	70.53×64.83×77.50
1a-popg	host-1a	POPG	1:128:6400	30.0 / 0.0	65.97×62.96×83.53
1a-popc	host-1a	POPC	1:128:6400	30.0 / 0.0	87.61×49.42×80.53
1a-dppe	host-1a	DPPE	1:128:6400	30.0 / 0.0	50.02×54.22×120.10
1a-mixed	host-1a	POPE/POPG	1:128:6400	30.0 / 0.0	54.39×69.41×90.51
1a-yeast	host-1a	Yeast	1:270:13500	30.0 / 0.0	75.90×97.35×96.32
1b-pope	host-1b	POPE	1:128:6400	30.0 / 0.0	57.25×65.37×95.77
1b-dopc	host-1b	DOPC	1:128:6400	30.0 / 0.0	73.40×64.33×78.53
1b-popg	host-1b	POPG	1:128:6400	30.0 / 0.0	78.13×55.38×80.27
1b-popc	host-1b	POPC	1:128:6400	30.0 / 0.0	65.52×68.56×78.04
1b-dppe	host-1b	DPPE	1:128:6400	30.0 / 0.0	50.20×55.31×117.60
1b-mixed	host-1b	POPE/POPG	1:128:6400	30.0 / 0.0	59.97×64.61×91.75
1b-yeast	host-1b	Yeast	1:270:13500	30.0 / 0.0	74.08×95.78×98.26

[a] Specifics of all the systems presented here. Host type, lipid type, and the number of different molecules present in a particular system, and the box length of that particular system are also depicted here. Starting distance is the distance between host and lipid bilayer center (z=0 Å). Every system is prepared twice, one with 30 Å and another with 0 Å distance between host and lipid bilayer center. Systems with 30 Å distance are for normal MD simulation and with 0 Å distance are for umbrella sampling simulation (discussed later).

The general AMBER force field (GAFF) [108] is used for modeling these two host molecules, and the ANTECHAMBER [107] program of AMBER14 is used to extract the force field

parameters. Four units of negative charge of these host molecules are neutralized by an equal number of K^+ ions [105].

To check the adsorption property of the two receptor molecules into those lipid bilayers, as mentioned earlier, every receptor molecule is initially placed at 30 Å distance from the center (z=0 Å) of these membranes with the help of the PACKMOL [74] package. Details of these systems are in Table 7-2. We have also prepared another 14 systems with the same composition but the only difference is that the receptor molecule is initially residing at the center (z=0 Å) of the lipid bilayer (Table 7-2). The topology and initial coordinate of these packed systems are modeled with the LEaP module of AMBER18.

Molecular Dynamics Simulation

All the prepared systems are simulated with the sander implementations of AMBER18. The periodic boundary conditions (PBC) in all three directions are applied for all these simulations. Constraint on every hydrogen-containing covalent bond is ensured by applying the SHAKE algorithm [71] with a tolerance value of 0.00001. A 10 Å cut-off distance is chosen for reckoning the short-range nonbonded interactions. For the long-range electrostatic interactions, the Particle Mesh Ewald (PME) [73] method is implemented. A time interval of 2 fs is allowed for the evaluation of equations of motion for the systems. An initial 10000 steps of energy minimization (among which initial 5000 steps are in the steepest descent method and conjugate gradient method for the last 5000 steps) are performed for every simulation to eliminate erroneous contacts among the atoms in the systems. The temperature of each system is maintained at 303.15 K. This is below the gel-liquid transition temperature of 336.15 K for DPPE, and above 275.15 K for POPG and POPC, 256.15 K for DOPC, and 298.15 K for POPE [354, 361]. 5 ns equilibration of every system (at 1 atm pressure and 298 K temperature) is attained in the isothermal-isobaric (NPT) ensemble. The desired pressure and temperature are retained using the Berendsen barostat [75] with 2 ps pressure relaxation time and the Langevin thermostat [76] with 1 ps^{-1} collision frequency, respectively. Every system (Table 7-2) (in which receptors are 30.0 Å away from the center of the bilayer) is introduced to a 500 ns NPT production run. CPPTRAJ module [77] of AMBER18 and Visual Molecular Dynamics (VMD) [78] package are used to analyze and visualize of the obtained simulation trajectories whenever required.

Free Energy Profiles

Free energy profiles are created with the AMBER18 center-of-mass (COM) um-

brella restraint code [89]. These energy profiles calculate the free energy profile of the transfer for a receptor molecule through the membrane. Systems with receptor molecules at the center of the lipid bilayer (Table 7-2) are used for this analysis. Methodology used here is somewhat different from the discussed methodology in the 'METHODOLOGY' section of Chapter 1. Z-direction distance (r) of the COM of bilayer and COM of the receptor is considered as the reaction coordinate (ξ). These energy profiles are determined from +40.0 Å to –40.0 Å of the reaction coordinate with a 1.0 Å distance between two consecutive bins. Thus, 81 bins are present for every free energy profile. A restraint force constant of 2.5 kcal/mol/Å^2 is applied along the z-direction. The receptor molecule is pulled from the center of the membrane (z=0.0 Å) out into the water phase (z=+40.0 or –40.0 Å). The simulation procedure followed for umbrella sampling (US) simulation is identical to the previous NPT run. Each US simulation window was introduced to 10000 steps of minimization (of which 5000 steps follow the steepest descent method followed by 5000 steps of conjugate gradient minimization), followed by 10 ns of equilibration and 10 ns production run simulation. Thus, 810 ns of total production run simulation is performed for each system. The unbiased probability distribution P(ξ) of each window position is computed with the Weighted Histogram Analysis Method (WHAM) [92, 93] program. From here, we get the PMF values as discussed in the 'METHODOLOGY' section of Chapter 1 (Eq. 1.24).

■ RESULTS AND DISCUSSIONS

Permeation of Receptors into Model Lipid Bilayer

At first, we focus on the permeation properties of these receptors into the model lipid bilayer. Representative snapshots of the position of host-1a or host-1b into different model lipid bilayers after 500 ns of simulation run are presented in Figure 7-1. Time evolution of the snapshots (i.e., snapshots at 0, 250, and 500 ns simulation time) of all the systems are presented in Figures 7-2 to 7-8. Details of these figures are in respective caption. Initially, these receptors are placed at 30.0 Å away from the bilayer center. From the last frame of the simulation trajectories, it is clear that receptor molecules are absorbed into the lipid bilayer head group for all the model lipid bilayers, but their positions from the bilayer center vary for different model bilayers. Thus, we get a preliminary idea about the insertion of these receptors into the model lipid bilayers from these snapshots.

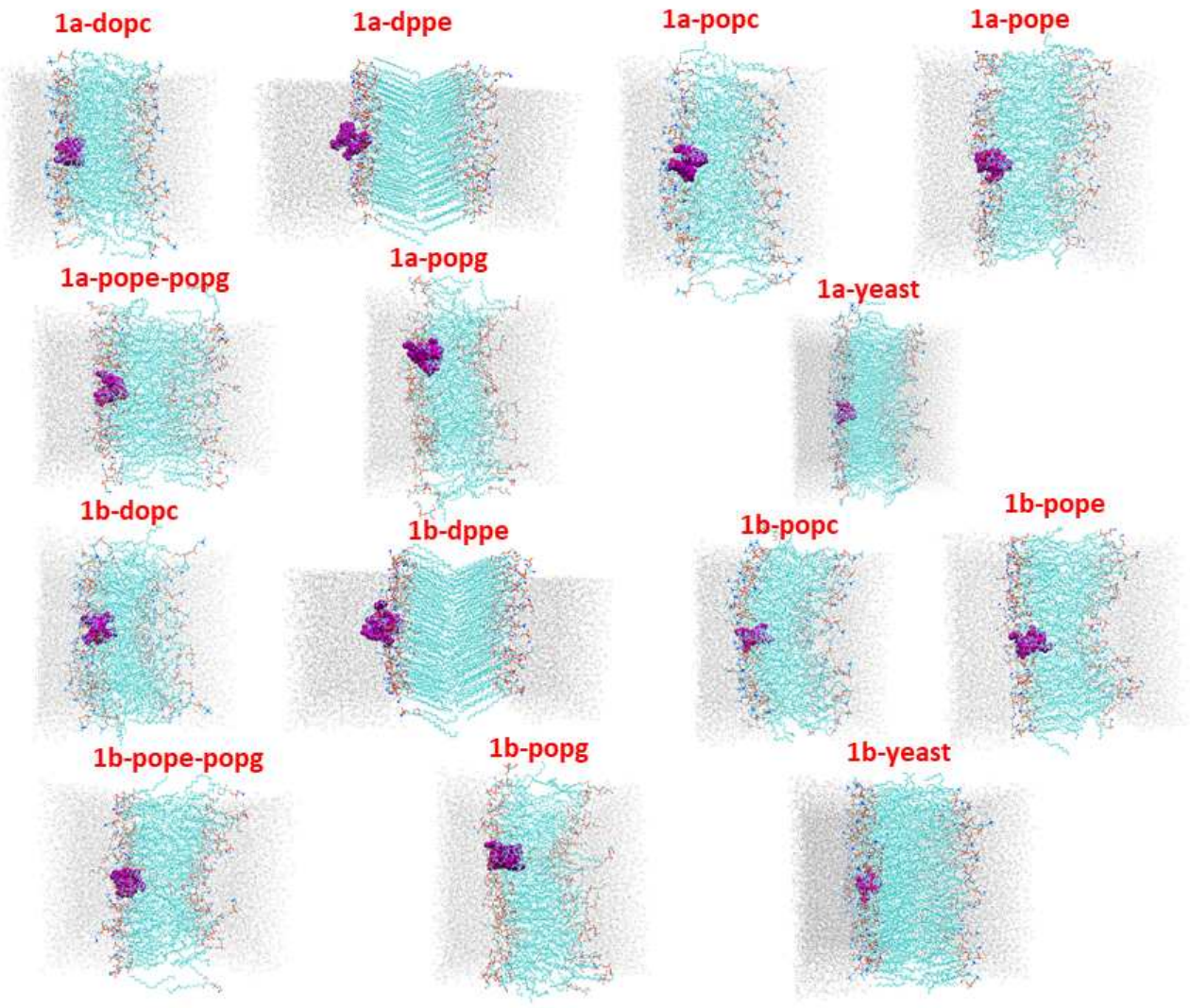

Figure 7-1. *Representative snapshots of host-1a or host-1b into different model lipid bilayers after 500 ns of simulation time. Receptor molecules are presented in vdW representation (purple), lipid heads and tails are represented in lines, and water molecules are presented in point (silver). Ions are excluded to enhance visual clarity.*

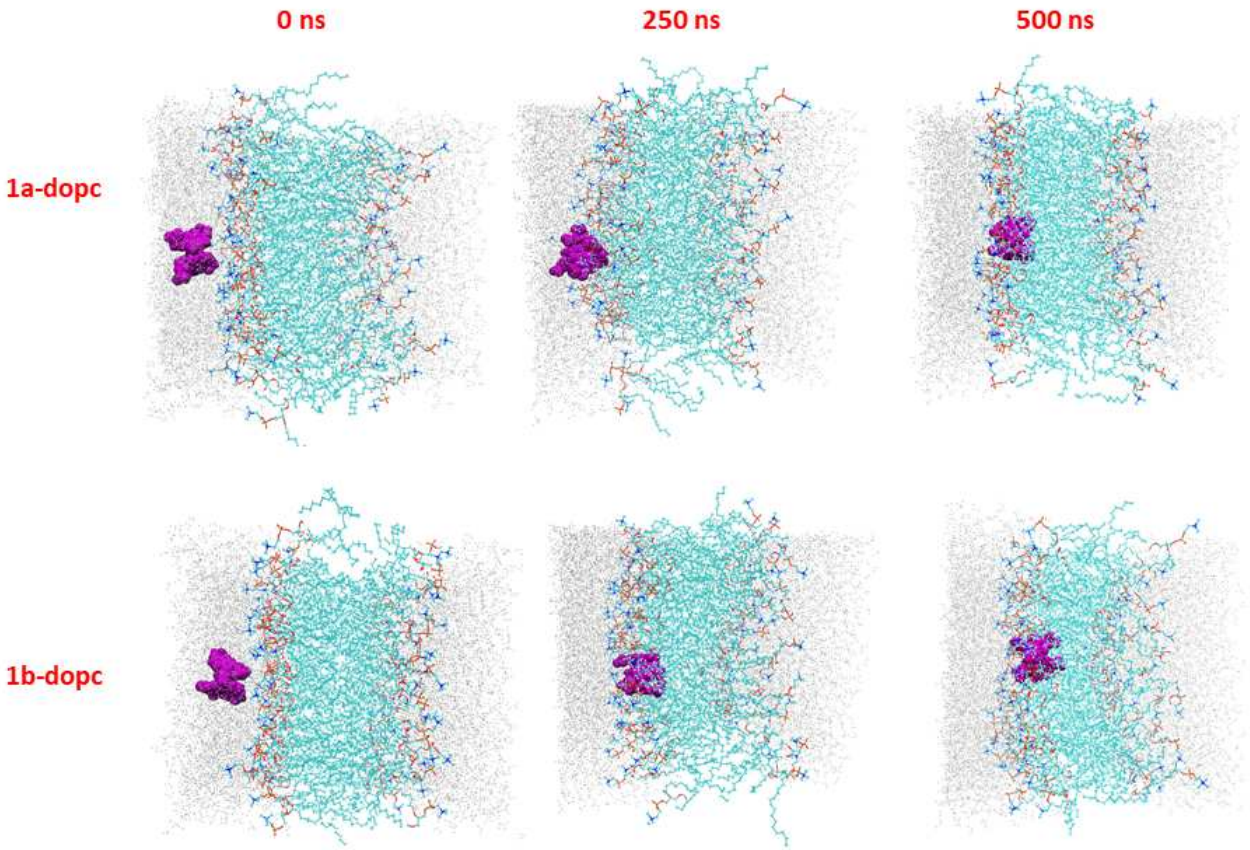

Figure 7-2. *Time evolution (0, 250, and 500 ns simulation time) of representative snapshots of 1a-dopc and 1b-dopc systems. Receptor molecules are presented in vdW representation (purple), lipid heads and tails are represented in lines, and water molecules are presented in point (silver). Ions are excluded to enhance visual clarity.*

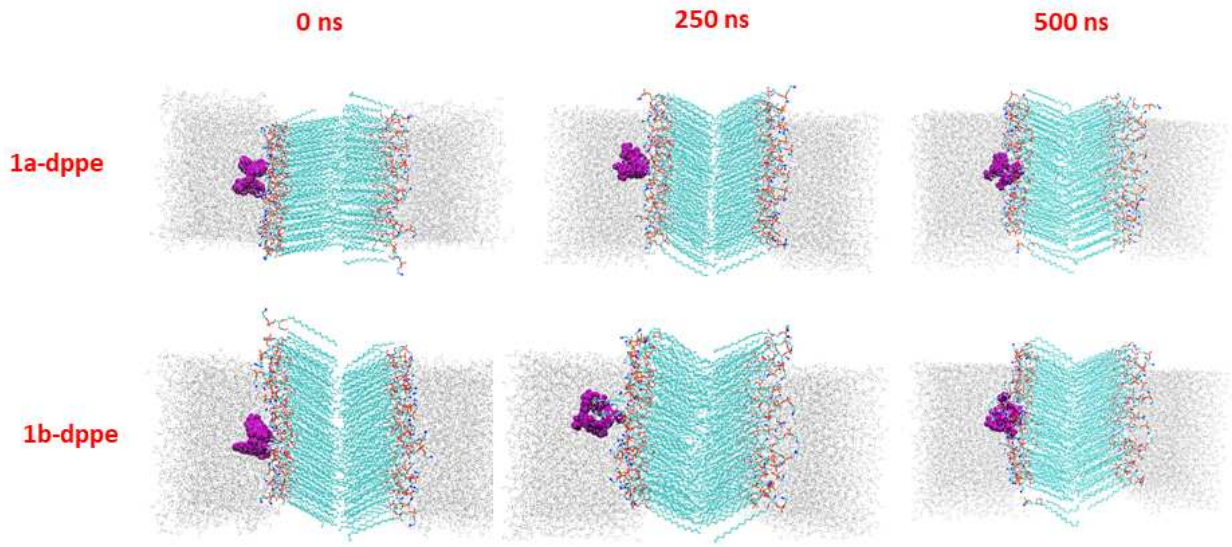

Figure 7-3. *Time evolution (0, 250, and 500 ns simulation time) of representative snapshots of 1a-dppe and 1b-dppe systems. Receptor molecules are presented in vdW representation (purple), lipid heads and tails are represented in lines, and water molecules are presented in point (silver). Ions are excluded to enhance visual clarity.*

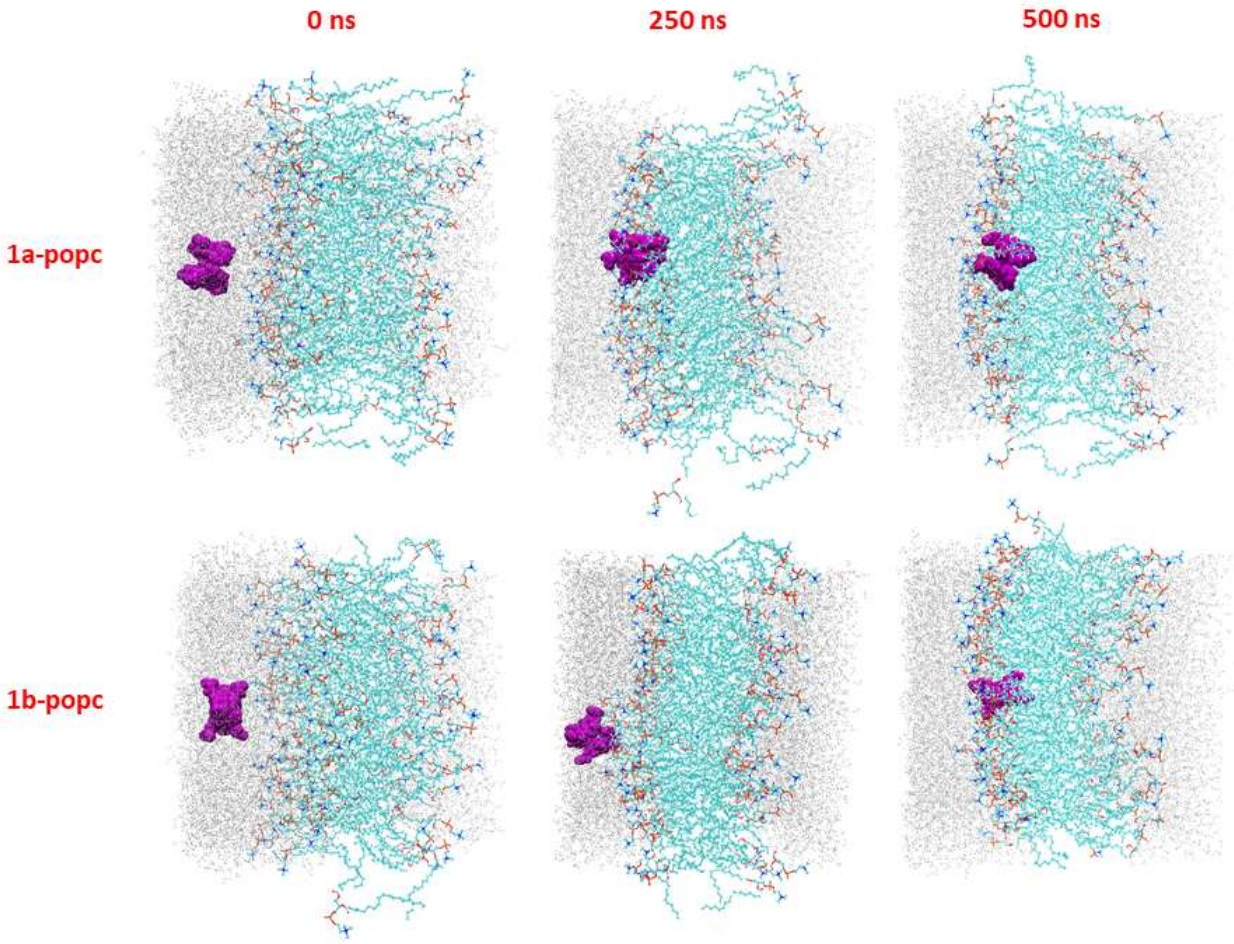

Figure 7-4. *Time evolution (0, 250, and 500 ns simulation time) of representative snapshots of 1a-popc and 1b-popc systems. Receptor molecules are presented in vdW representation (purple), lipid heads and tails are represented in lines, and water molecules are presented in point (silver). Ions are excluded to enhance visual clarity.*

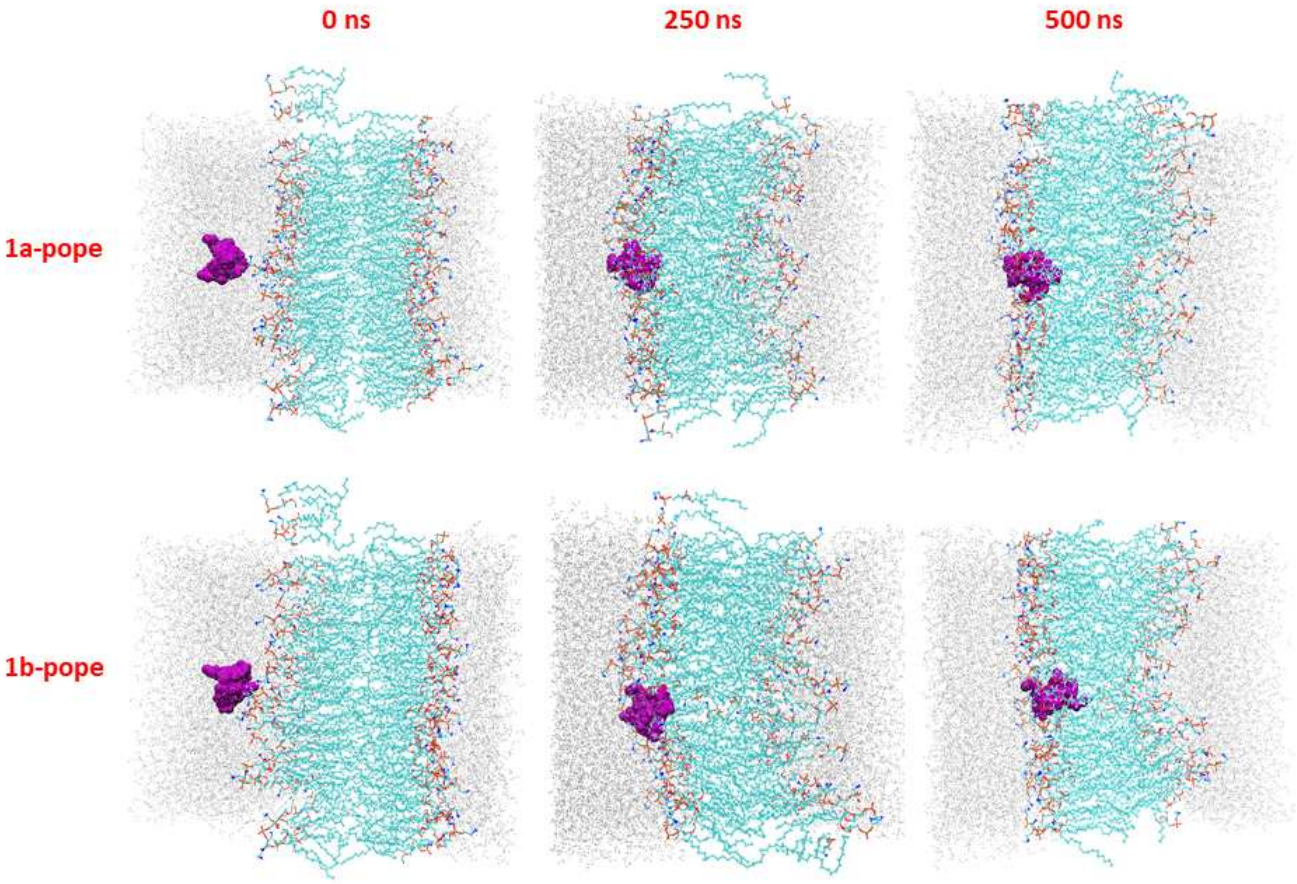

Figure 7-5. *Time evolution (0, 250, and 500 ns simulation time) of representative snapshots of 1a-pope and 1b-pope systems. Receptor molecules are presented in vdW representation (purple), lipid heads and tails are represented in lines, and water molecules are presented in point (silver). Ions are excluded to enhance visual clarity.*

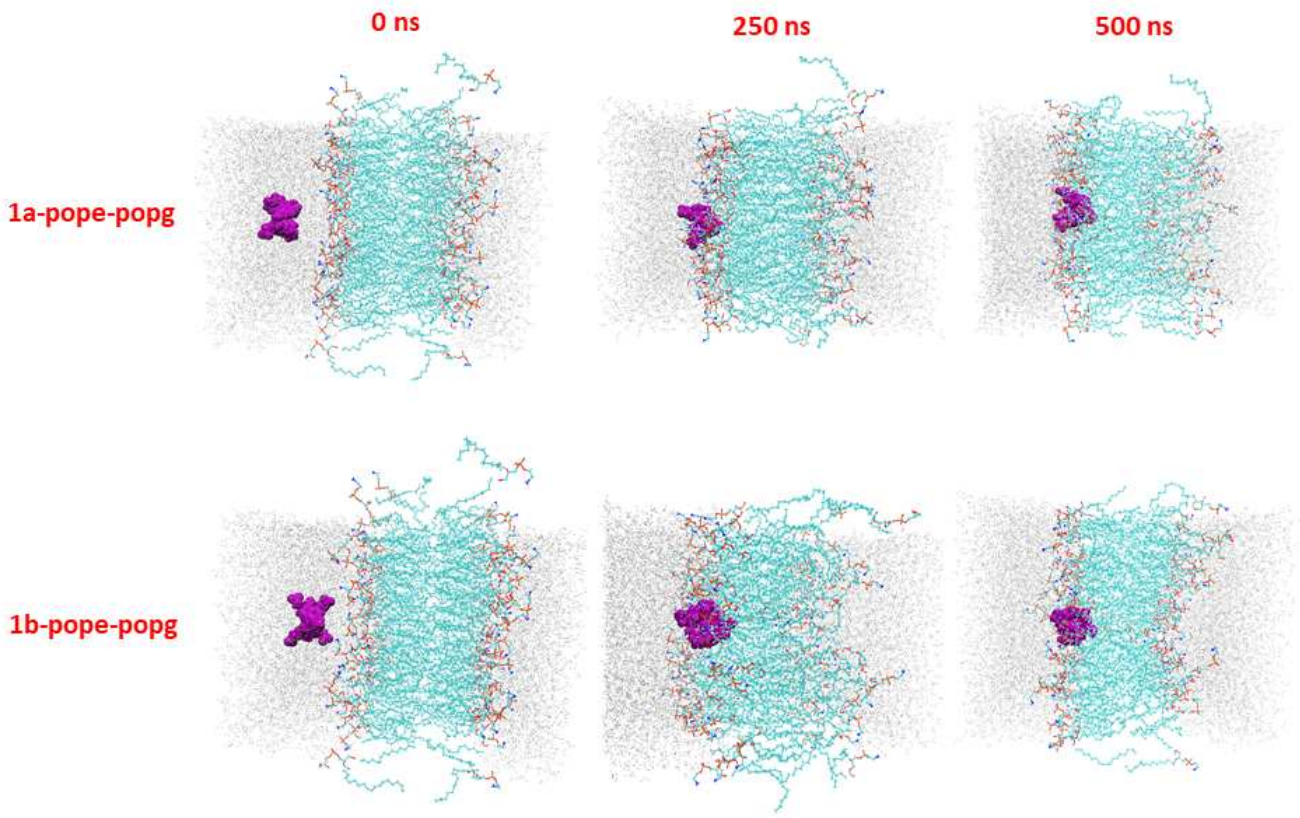

Figure 7-6. *Time evolution (0, 250, and 500 ns simulation time) of representative snapshots of 1a-pope-popg and 1b-pope-popg systems. Receptor molecules are presented in vdW representation (purple), lipid heads and tails are represented in lines, and water molecules are presented in point (silver). Ions are excluded to enhance visual clarity.*

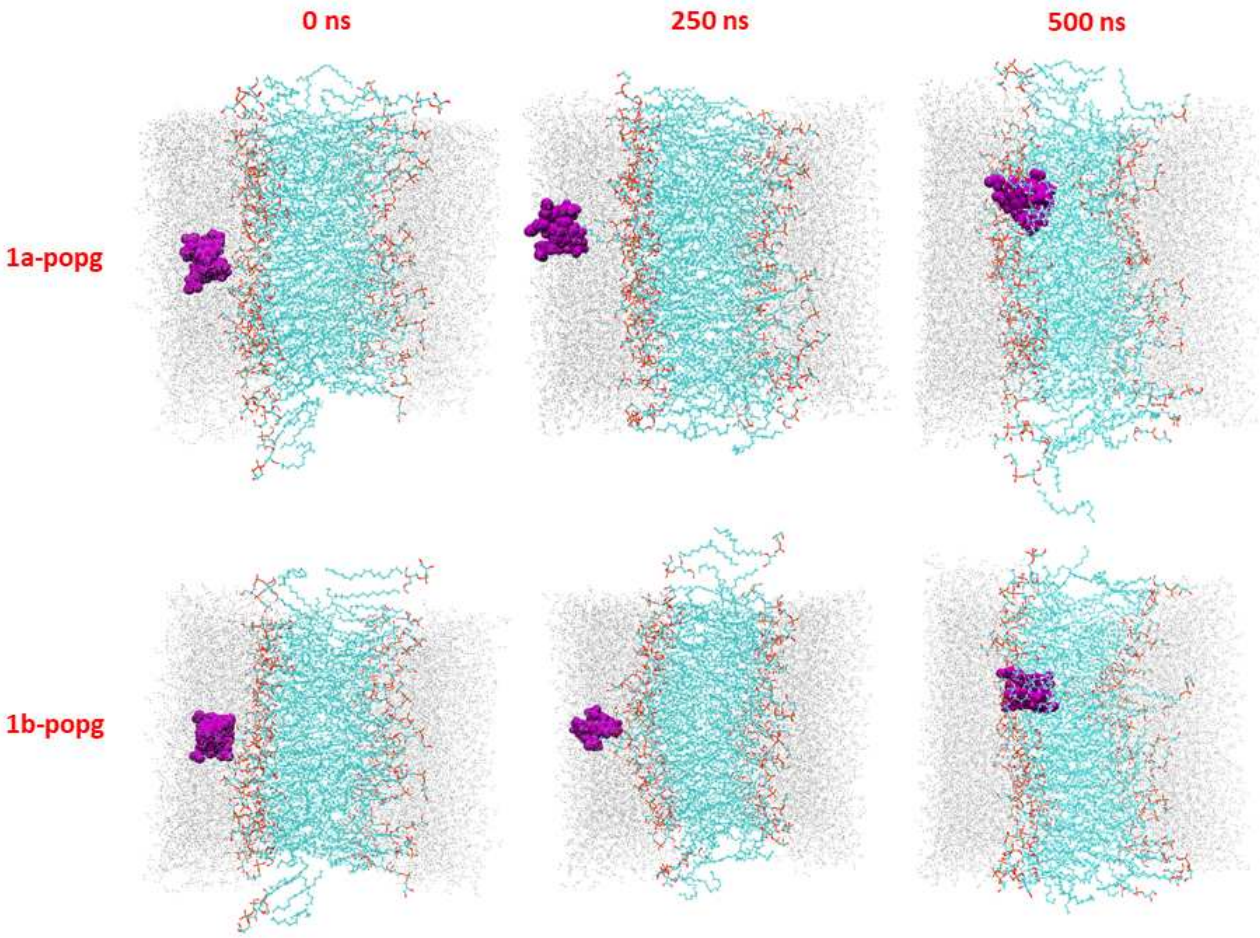

Figure 7-7. *Time evolution (0, 250, and 500 ns simulation time) of representative snapshots of 1a-popg and 1b-popg systems. Receptor molecules are presented in vdW representation (purple), lipid heads and tails are represented in lines, and water molecules are presented in point (silver). Ions are excluded to enhance visual clarity.*

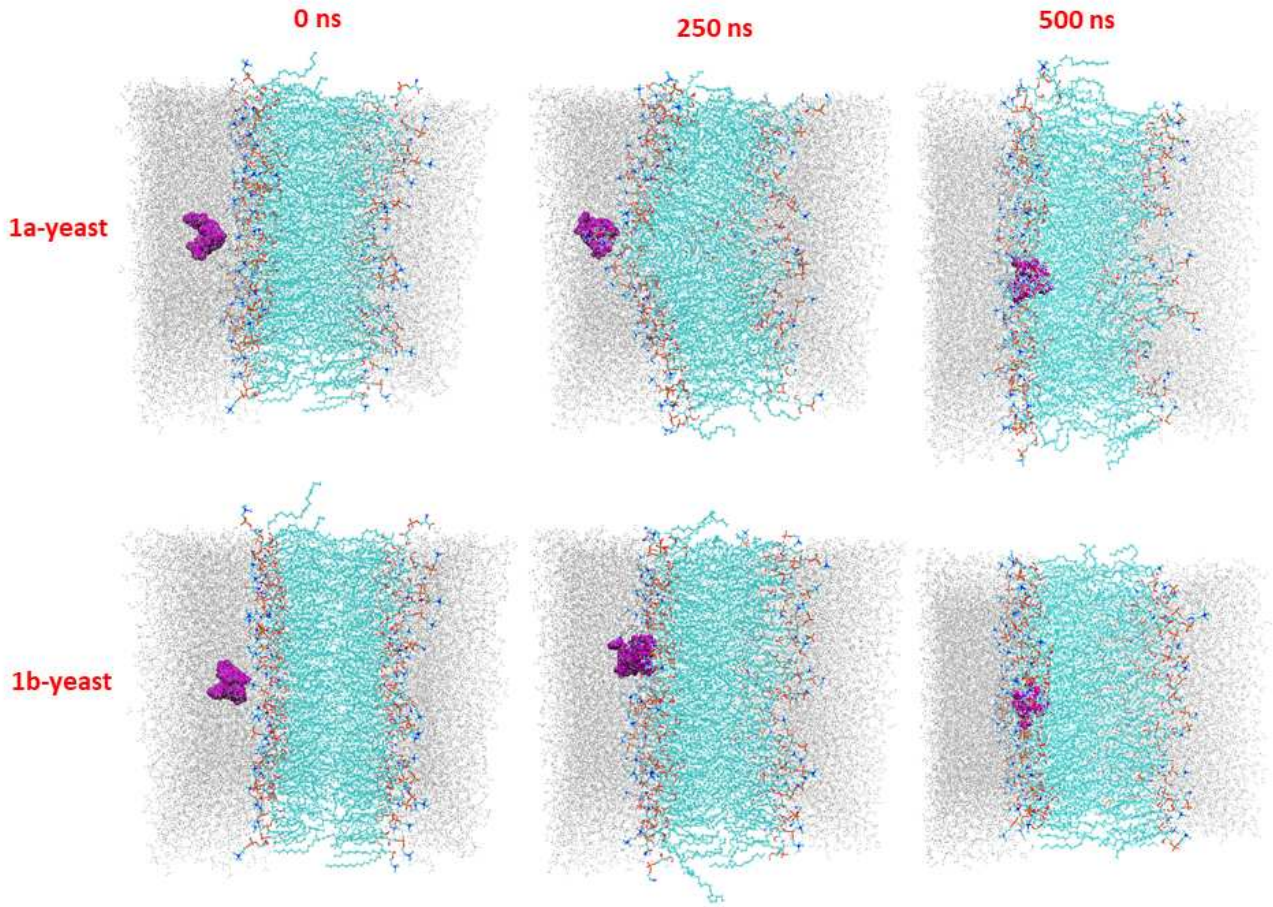

Figure 7-8. *Time evolution (0, 250, and 500 ns simulation time) of representative snapshots of 1a-yeast and 1b-yeast systems. Receptor molecules are presented in vdW representation (purple), lipid heads and tails are represented in lines, and water molecules are presented in point (silver). Ions are excluded to enhance visual clarity.*

We have analyzed the center of mass (COM) – center of mass (COM) distance between host and model lipid bilayer. The time evolution of these COM-COM distances of all the systems is displayed in Figure 7-9. Distances between lipid bilayer center and a head group of one of the leaflets (i.e., bilayer center to the head group of upper leaflet or lower leaflet) are different for different systems. These are 18.40 ± 0.71 Å for 1a-dopc, 23.40 ± 0.95 Å for 1a-dppe, 18.60 ± 0.62 Å for 1a-popc, 18.85 ± 0.75 Å for 1a-pope, 20.35 ± 0.81 Å for 1a-pope-popg, 18.95 ± 0.69 Å for 1a-popg, 21.30 ± 0.85 Å for 1a-yeast, 18.45

± 0.60 Å for 1b-dopc, 23.50 ± 0.93 Å for 1b-dppe, 18.55 ± 0.68 Å for 1b-popc, 19.55 ± 0.78 Å for 1b-pope, 20.20 ± 0.82 Å for 1b-pope-popg, 19.05 ± 0.77 Å for 1b-popg, and 21.10 ± 0.84 Å for 1b-yeast system.

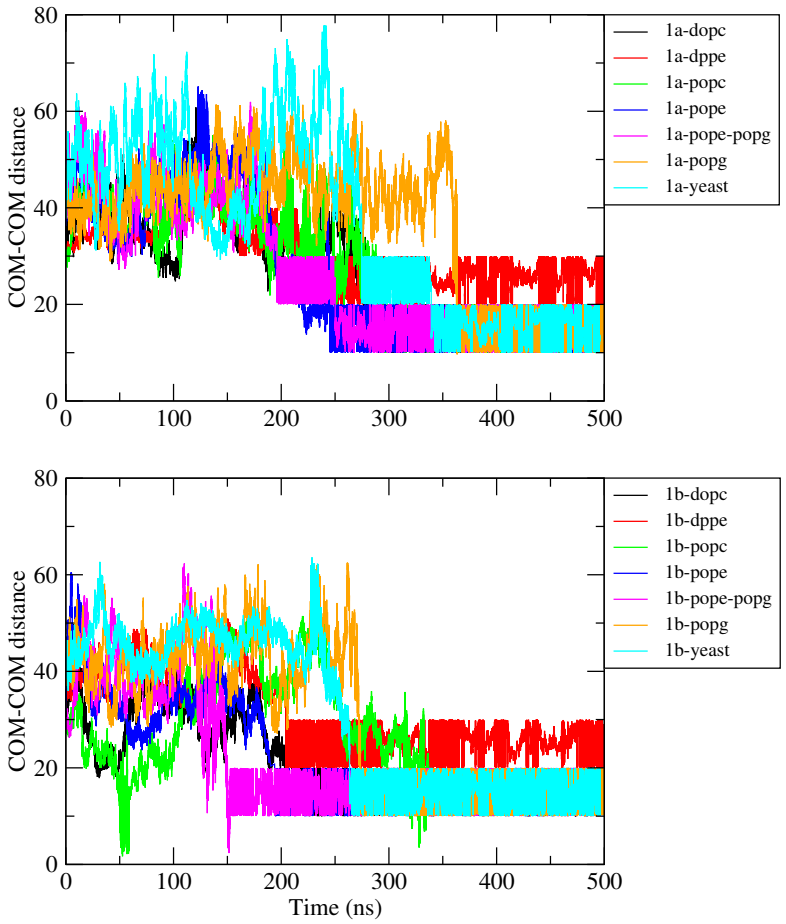

Figure 7-9. *COM-COM distance between host and lipid bilayer with simulation time for all the systems (different systems with a different color) are in this figure.*

From Figure 7-9, it is clear that initially, every system has a higher value of COM-COM distance between host and lipid bilayers. This value decreases with time and reaches a minimum value. When it reaches the minimum value, its fluctuation also becomes more restricted compared to the initial values. This signifies the strong adsorption of receptor molecules into the bilayer surface. The average COM-COM distance (after reaching the

minimum value) between receptors and lipid bilayers varies from system to system. These values are around 14.00 Å for 1a-dopc, 22.50 Å for 1a-dppe, 13.50 Å for 1a-popc, 14.50 Å for 1a-pope, 15.50 Å for 1a-pope-popg, 14.50 Å for 1a-popg, 14.00 Å for 1a-yeast, 13.60 Å for 1b-dopc, 23.50 Å for 1b-dppe, 14.00 Å for 1b-popc, 14.00 Å for 1b-pope, 14.50 Å for 1b-pope-popg, 15.00 Å for 1b-popg, and 14.50 Å for 1b-yeast system. Now, if we compare the distance between the lipid bilayer center and a head group of one of the leaflets with the average COM-COM distance of every corresponding system, it can be found that receptor molecules are adsorbed into every model lipid bilayer head region, and more insertion is portrayed in every model lipid bilayer except for DPPE bilayer containing systems. Host molecules in all systems (except for DPPE containing systems) reside at the intersection of lipid head and lipid tail regions (indicating the distance values). Thus, direct permeation of these receptors does not occur in this time scale as the mean translocation time of these components is in the mili second (ms) time scale [362].

The density distribution profiles of lipid head, lipid tail, water, and receptor molecule with model lipid bilayer z-normal may shed more light on the translocation properties of these receptors through the bilayer. These mass density profiles are calculated by taking the center of the box as z=0. The mass densities of these components are calculated in slabs of thickness 0.1 along the z-direction. These profiles of each of the systems are presented in Figure 7-10. Since every model lipid bilayer is symmetric, the mass density profile of lipid head, lipid tail, and water molecules remain symmetric at both the leaflet of the bilayers. Lipid head density is similar for every system except for DPPE bilayer containing systems. Every lipid head mass density profile shows a gaussian type curve, and in DPPE systems, it has less breadth and more height. Lipid tail density is also similar for every system (with somewhat difference in DPPE containing systems). Lipid tail density remains entirely at the central position of the lipid bilayer. Lipid head and tail have an almost similar density for every system. All the lipid head density profiles show some contacts with lipid tail region but do not spread much inside the lipid tail region. Thus, every model lipid bilayer remains structurally stable throughout the simulation. Water density profiles are outside the leaflet and show contacts with the lipid head region. Spreading of water density profile depends on the thickness of water layers at both sides of a particular model lipid bilayer. These water density profiles also signify the stability of these model bilayer structures. Now if we look into the receptor mass density profiles into these bilayers' normal.

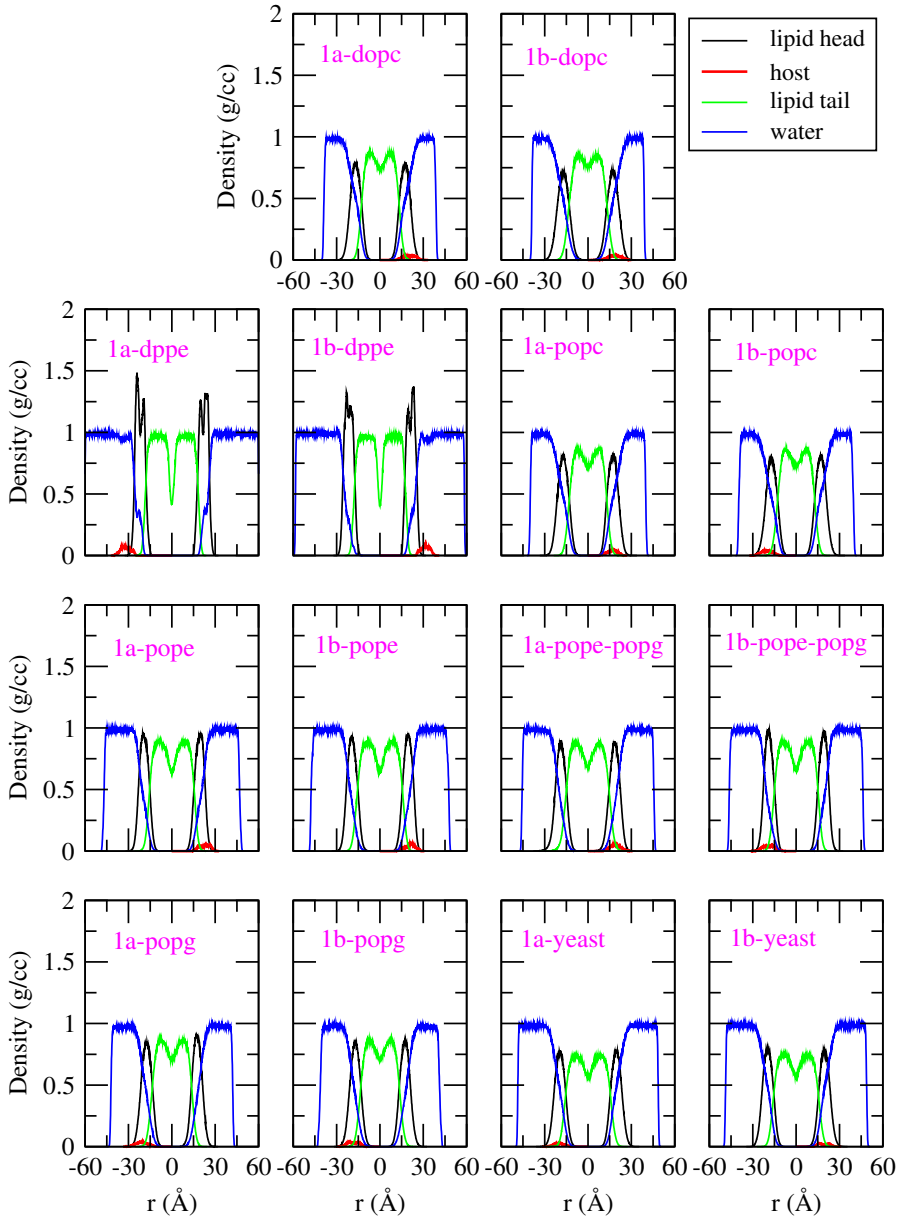

Figure 7-10. *The evolvement of mass density (in g/cc unit) of lipid head, lipid tail, water, and host molecule along the bilayer z-normal for 500 ns simulation trajectories of all the systems.*

As, only one receptor molecule is present in every system, receptor mass density is very low

compared to the other three density profiles. Receptor density resides at either lower or upper of the bilayer leaflet. All the receptor mass density profiles are wider than the DPPE containing systems. These density profiles remain almost entirely in the lipid head region. Some of its portions cross the lipid head regions and enter into the lipid tail regions except for DPPE containing systems. In DPPE systems, this receptor density profile remains entirely at the water phase, and a part of its portion enters into the lipid head region. As receptor mass density does not observe on both the leaflets, it can be said that direct permeation of these receptors does not occur in this time scale as the mean translocation time of these components is in the ms time scale [362]. After the 500 ns trajectories, receptor molecules reside at the intersection of lipid head and lipid tail except for DPPE containing systems (in which receptor molecule resides at the surface of the lipid head region). Thus, we deduce that the adhesion energy and gain in lipid tail entropy are insufficient to address the energy penalty (mechanical and surface tension) associated with membrane bending and receptor confinement because these receptors do not translocated any of these model lipid bilayers [363].

Insertion of Receptors into Model Lipid Bilayer

Here we focus on the insertion and interaction of receptors into these model lipid bilayers. We investigate the hosts' solvation properties in these model lipid bilayers and their interactions with various lipid bilayer portions and water to understand this intriguing activity. We have analyzed the radial distribution functions (RDFs) between host-lipid head, host-lipid tail, and host-water, and these are presented in Figure 7-11. As, host molecule absorbed on the lipid head region within 400 ns of simulation time (evident from COM–COM distance between host and lipid bilayer (Figure 7-9)), thus, we have taken last 100 ns trajectories for these RDF analysis. It is evident that the host molecule shows similar types of interactions with every model lipid bilayer except for the DPPE bilayer containing systems. Host molecules interact with lipid head portion within 5 Å distance with all the model lipid bilayer except for DPPE containing systems (in which host-lipid head maximum interaction is shown around 15 Å distance). Thus the absorption of host molecules into the bilayer head portion is more profound in every used model lipid bilayers systems except for DPPE containing systems. A similar trend is found in host-lipid tail interactions, but this interaction is much less compared with host-lipid head interaction and almost nil host-lipid tail interaction in the case of DPPE containing systems. This may be due to the fact that as the simulation temperature (303.15 K) is less than the DPPE bilayer

transition temperature (336.15 K), this bilayer is in the gel phase; thus, lipid tails become so rigid which does not permit the receptor to interact with the lipid tail portions [361].

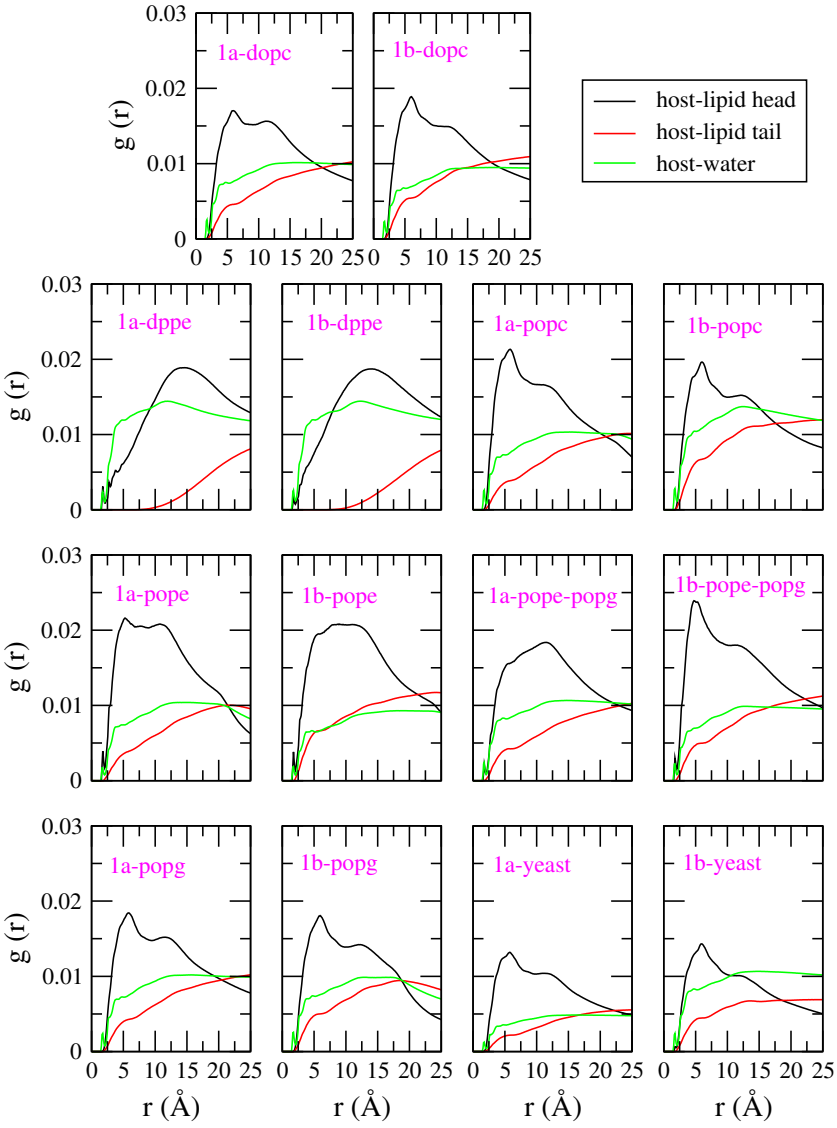

Figure 7-11. *Radial distribution function (g(r)) plots in between host-lipid head, host-lipid tail, and host-water for all the systems are presented here.*

Now, host-water interaction is somewhat higher than host-lipid tail interaction but much

lesser than the host-lipid head interaction except for DPPE containing systems. In DPPE bilayer systems, host-water interaction is almost comparable with the host-lipid head interaction. It infers that the host molecule is inserted deeper into the lipid head portion and remains at the intersection position between lipid head and tail except for DPPE bilayer systems. In DPPE bilayer systems, the host molecule is only absorbed (not inserted) into the lipid head, and most of the hosts' portion remains in the water phase.

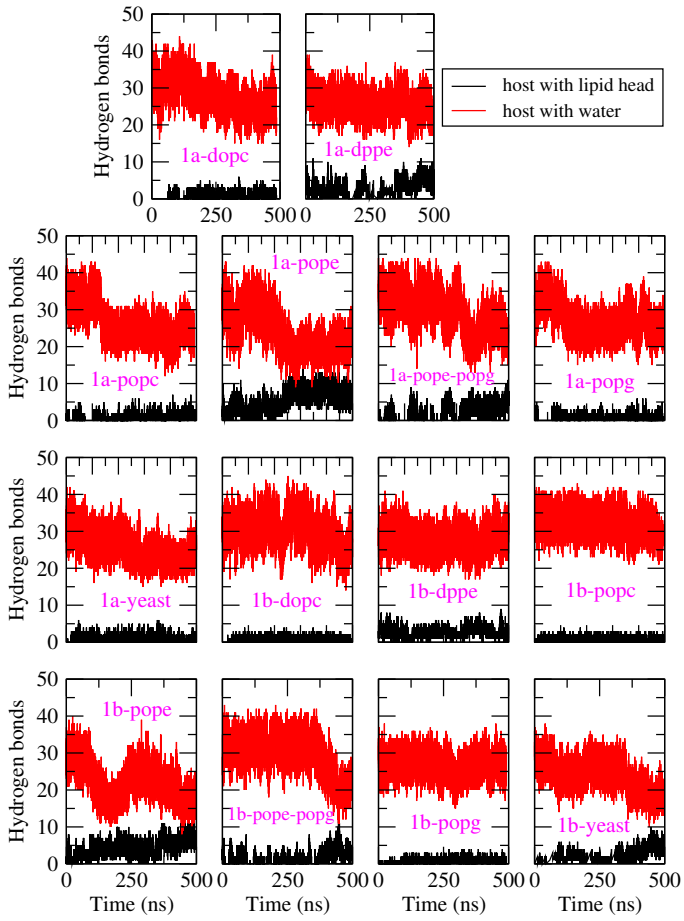

Figure 7-12. *Hydrogen bond values between host-lipid head and host-water as a function of simulation time for all the systems are pictorially drawn here.*

The RDF plots show that the host molecule interact more with the lipid head portion, followed by water molecules. Therefore, we have analyzed the time evolution of

the host-lipid head and host-water hydrogen bond, and the same are plotted in Figure 7-12. We have adopted geometric criteria for hydrogen bond analysis [109–115]. The cut-off distance (r_c) for donor-acceptor pair was chosen as $r_c \leq 3.4$ Å, and the angle (θ_c) for the donor-acceptor-hydrogen was allowed for $\theta_c \leq 45^o$. This is schematically shown in Figure 2-6 of Chapter 2. As the simulation progress, the host-water hydrogen bond value decreases for all of the systems except for DPPE bilayer-containing systems. This result confirms more and more portion of receptor molecules inserted into the lipid bilayer head region with simulation time. But for DPPE containing systems, receptor molecules just adsorbed into the lipid bilayer head region, and most of the hosts' portion remains in the water phase. The same finding is also depicted from the host-lipid head hydrogen bond value. This result also supports the findings from the RDF analysis.

Next, we will examine on the energetic aspect of different types of interactions. For the same, we have calculated the van der Waals (vdW) and electrostatic (elec) interaction energy parameters for host-lipid head, host-lipid tail, and host-water interactions. The time evolution of host-lipid head and host-lipid tail interactions is plotted in Figure 7-13 and host-water interaction is plotted in Figure 7-14. In host-lipid head interaction (Figure 7-13), elec interaction is predominant over the vdW interaction energy. The host-lipid head elec interaction energy is varied for all the systems, but vdW energy is comparably favorable for all the systems except for DPPE containing systems. In DPPE containing systems, host-lipid head vdW interaction energy is almost zero. The host-lipid tail (Figure 7-13) elec interaction energy is zero for every system, and very less favorable vdW interaction (negative value of energy) is portrayed (except for DPPE containing systems, in which host-lipid tail vdW interaction energy is also zero). For host-water interaction (Figure 7-14), elec interaction is much more predominant over the vdW interaction in all the systems. This elec interaction energy remains same or decreases with simulation time, and vdW interaction becomes unfavorable (positive energy value) as some simulation progresses. These interactions prove that receptor molecules only absorbed in DPPE containing systems (i.e., 1a-dppe and 1b-dppe), and more absorption and insertion is seen for all the other model lipid bilayer systems. All the above findings further support the adsorption and insertion of receptor molecule into the lipid bilayer head region except for DPPE model lipid bilayer (in which the only adsorption is happening).

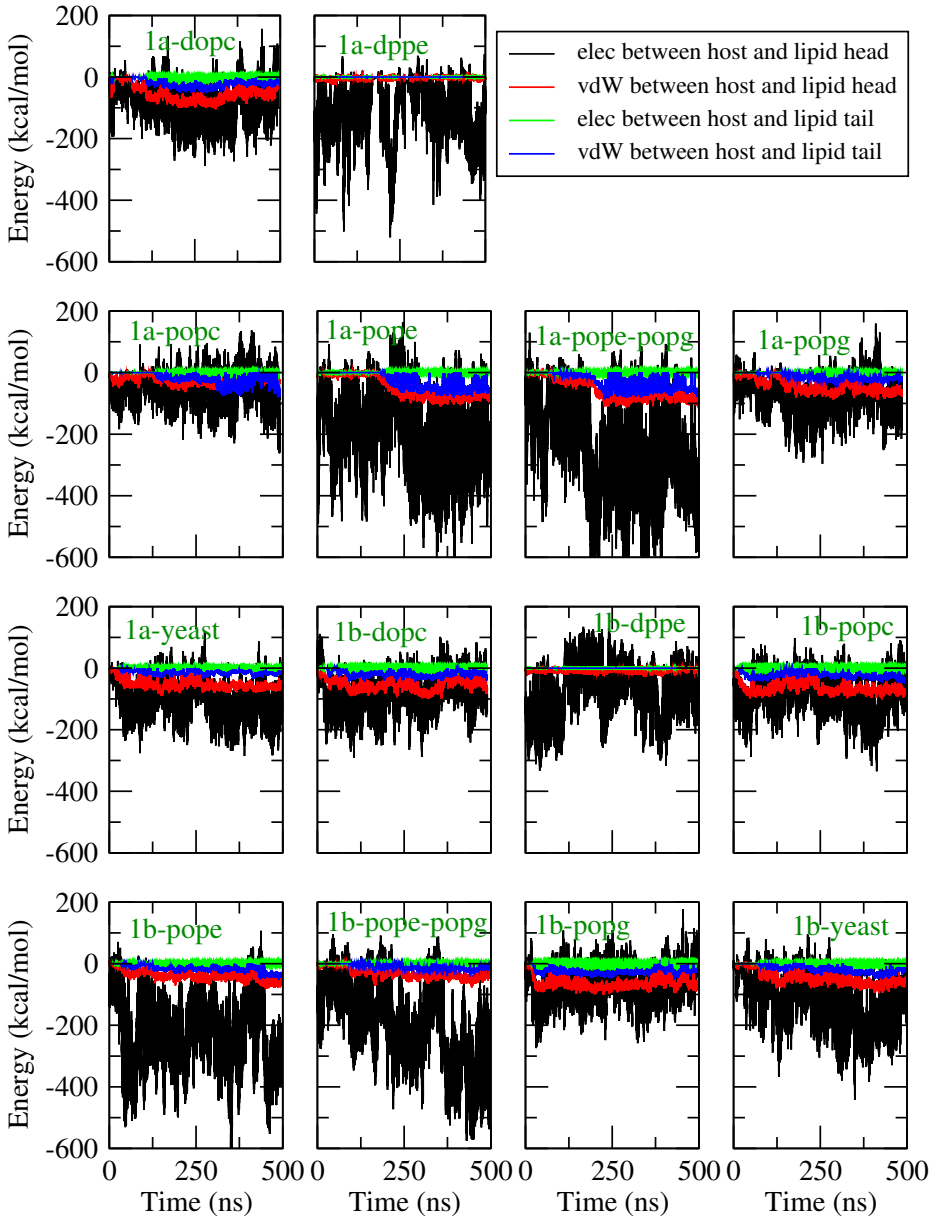

Figure 7-13. *van der Waals (vdW) and electrostatic (elec) interaction energy parameters between host-lipid head and host-lipid tail as a function of 500 ns simulation time is represented with different colors.*

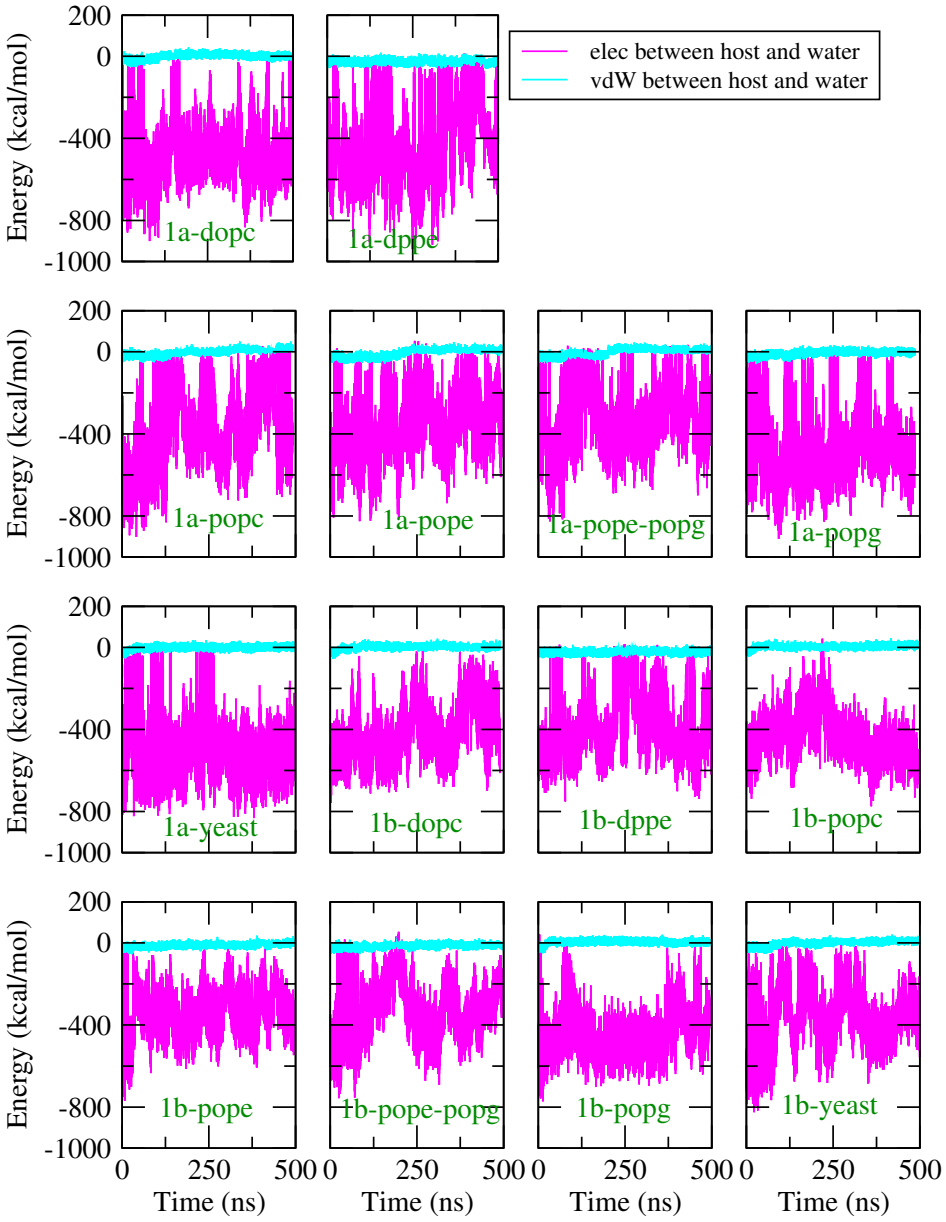

Figure 7-14. *van der Waals (vdW) and electrostatic (elec) interaction energy parameters between host-water as a function of 500 ns simulation time is represented with different colors.*

Free Energy Profiles

As direct permeation of these receptors in nanosecond time scale normal MD simulation is not possible, we have analyzed the free energy profiles of these translocation processes using the biased umbrella sampling simulation. These free energy profiles are calculated through the potential of mean force (PMF) analysis, and they are presented in Figure 7-15. Every receptor-bilayer system shows a similar type of free energy profile. Free energy values are similar in the water phase, and then it decreases until it reaches a minimum value. Thus, the interior location of the lipid bilayer is the most favorable position for these receptors. A sharp negative gradient close to the lipid head region confirms the easy translocation of these receptors inside these model lipid bilayers. After reaching the minimum free energy value, it starts to increase and reaches a maximum energy value at the center of the bilayer. Therefore, one energy barrier persists at the central position of every model lipid bilayers which may affect the active permeation of these receptors through these model lipid bilayers and may need passive permeation through model lipid bilayers. As these model bilayers are symmetric (i.e., upper and lower leaflet contains an equal number of same components), all of these free energy profiles are symmetric. The different systems show minimum energy values at a different positions inside the lipid bilayer core. These distances are ±13.0 Å (for 1a-popc and 1b-popg), ±14.0 Å (for 1a-dopc, 1b-popc, 1b-pope, 1a-popg, and 1a-yeast), ±15.0 Å (for 1b-dopc, 1a-pope, and 1b-yeast), ±16.0 Å (for 1a-pope-popg and 1b-pope-popg), ±17.0 Å (for 1a-dppe), and ±18.0 Å (for 1b-dppe). Minimum free energy values of all the systems are as follows: –26.83 (1a-dopc), –36.84 (1b-dopc), –23.23 (1a-dppe), –24.16 (1b-dppe), –40.10 (1a-popc), –45.67 (1b-popc), –28.37 (1a-pope), –34.72 (1b-pope), –20.47 (1a-pope-popg), –28.67 (1b-pope-popg), –25.98 (1a-popg), –32.94 (1b-popg), –28.42 (1a-yeast), and –34.23 (1b-yeast) kcal/mol. The energy barrier at the center of each model lipid bilayer needs to overcome to translocate through these model lipid bilayers. These barrier heights are: 17.21 (1a-dopc), 13.70 (1b-dopc), 31.26 (1a-dppe), 33.31 (1b-dppe), 9.33 (1a-popc), 7.95 (1b-popc), 17.93 (1a-pope), 15.35 (1b-pope), 11.64 (1a-pope-popg), 11.95 (1b-pope-popg), 15.82 (1a-popg), 9.94 (1b-popg), 14.19 (1a-yeast), and 10.28 (1b-yeast) kcal/mol. All the barrier heights are comparable to smaller hydrophilic molecules except for DPPE bilayer-containing systems. Distance of getting minimum free energy value from umbrella sampling simulation may vary with the final adsorption distance from normal MD simulation due to the distortion of model lipid bilayers [364].

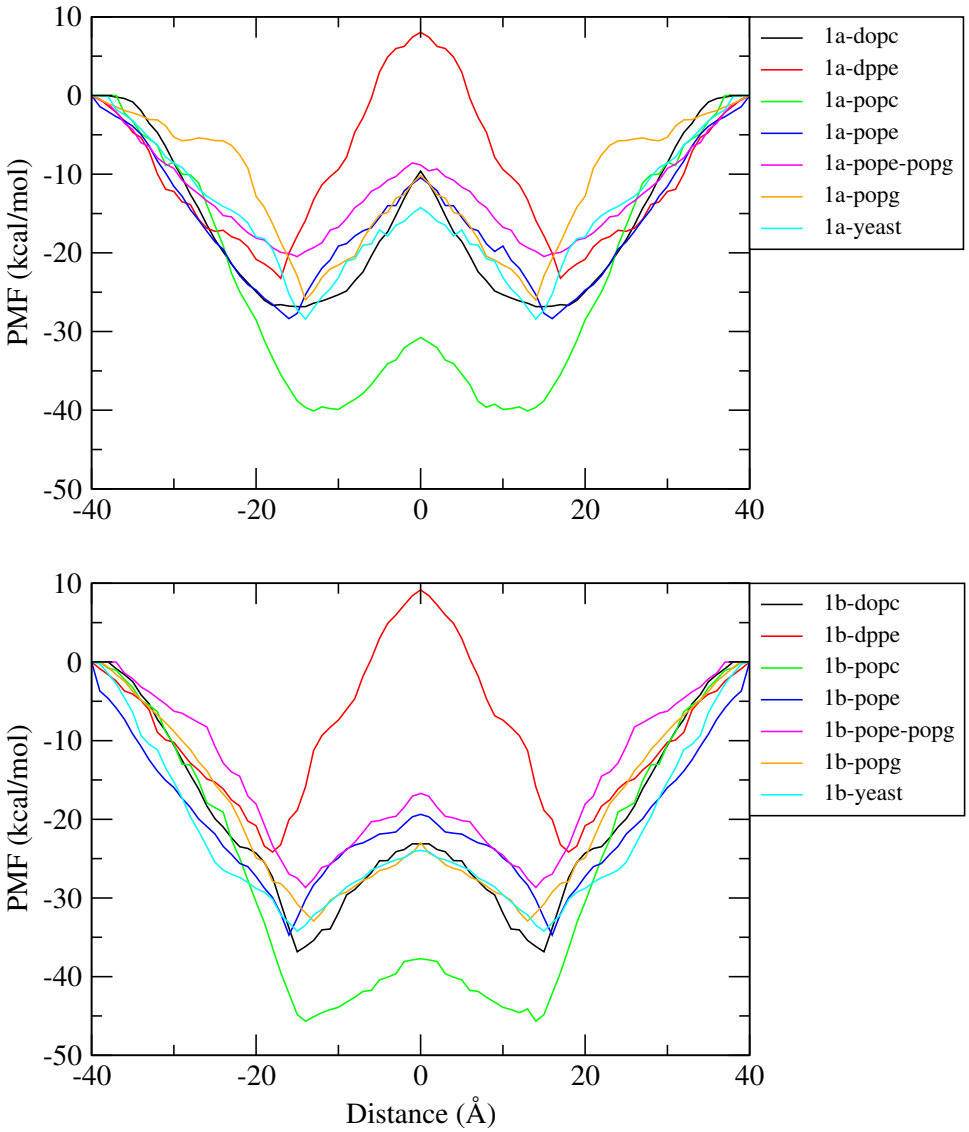

Figure 7-15. *Free energy profile for the translocation of host-1a or host-1b along with every model lipid bilayer z-normal. Reaction coordinate is the COM-COM z-distance between host and lipid bilayer molecule. The central position of the lipid bilayer is the z=0 Å in the reaction coordinate.*

Among all these systems, 1b-popc and 1a-pope-popg systems show the maximum and minimum free energy values, respectively. Again, 1b-dppe and 1b-popc systems have the

highest and lowest energy barriers, respectively. From the free energy values at the contact minimum regions, we can infer that all these receptors reside comfortably at the core of these model lipid bilayers. Also, passive transport of these receptors may be possible through these model lipid bilayers (due to the low barrier height) except for DPPE bilayer-containing systems (which have a very high energy barrier at the center).

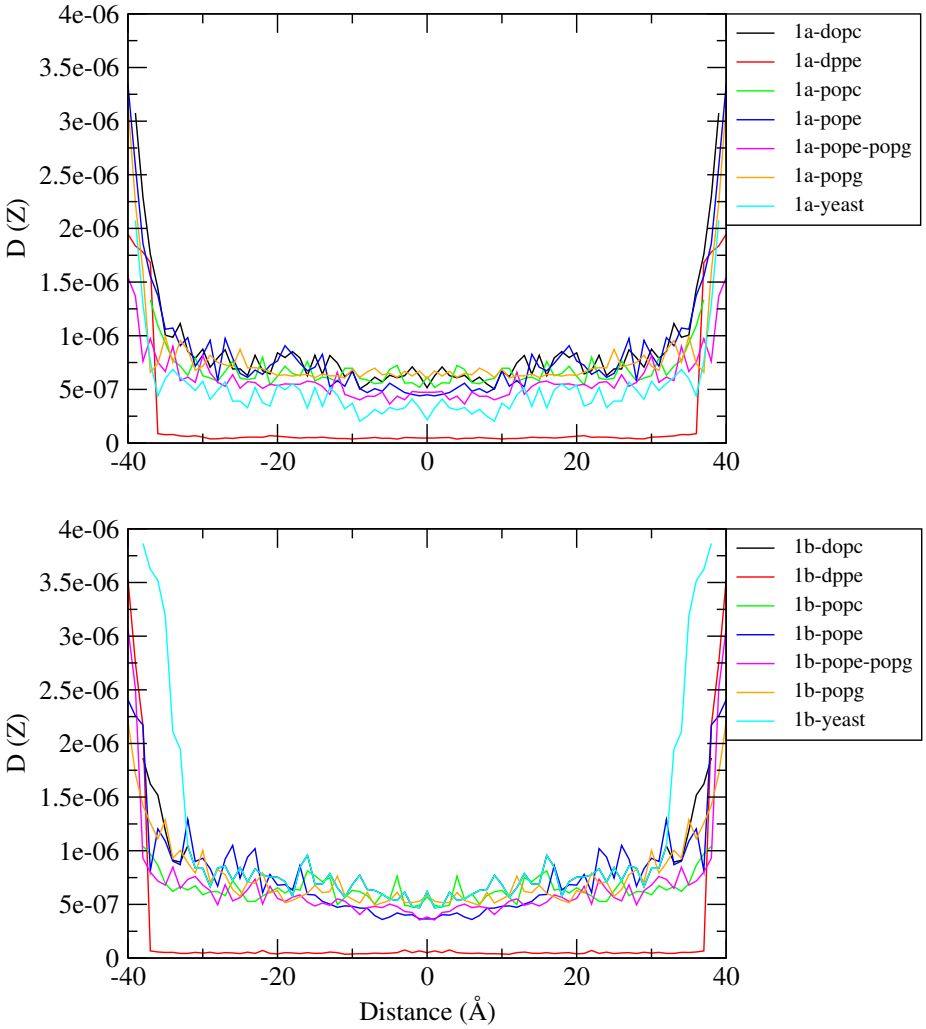

Figure 7-16. *Position dependent diffusion coefficient (D(Z)) of both the receptor molecules into the model lipid bilayer system is represented here. The central position of the lipid bilayer is the z=0 Å in the reaction coordinate. D(Z) value is in* $cm^2 s^{-1}$ *unit.*

Next, we are interested in the position-dependent diffusion coefficient (D(Z)) values of these receptors throughout the lipid bilayers, which are calculated by following the work of Gerhard Hummer [365]. These diffusion coefficient values of host-1a or host-1b along the z-normal of these model lipid bilayers are depicted in Figure 7-16. These diffusion profiles are almost similar for all the systems. D(Z) values are maximum at the water phase. But, this value decreases as we move from the water phase to the lipid phase. After reaching a minimum, D(Z) value remains constant as we further move towards the bilayer center. D(Z) values are more than 50 times higher inside the lipid bilayer core for all the systems than for both the DPPE bilayer containing systems (which have 10^{-8} order D(Z) values). Thus, it can be suggested that diffusion of these receptors through these model lipid bilayers are very slow for every system, but each system has more diffusion than that in the 1a-dppe and 1b-dppe systems.

Effect of Receptors over Bilayer Properties

We are now interested to see how these receptors insertion affects the stability of these model lipid bilayer structures during these simulation processes. For the same, we have analyzed the thickness and area per lipid (APL) of these model lipid bilayers in the absence and presence of host-1a or host-1b, and these are presented in Figure 7-17. Bilayer thickness is considered as the distance between the phosphate groups of the upper and lower leaflet. In the absence of any receptor molecule (i.e., in the case of the pure model lipid bilayer) bilayer thickness of these model lipid bilayers decreases as follows: 48.00±1.30 Å (DPPE), 43.40±0.90 Å (Yeast), 42.50±1.10 Å (POPE), 41.70±0.80 Å (POPE/POPG), 39.60±0.73 Å (DOPC), 39.30±0.84 Å (POPG), and 38.60±0.62 Å (POPC). Some of these values show good agreement with previously reported simulation and experimental results [366–370]. These model lipid bilayers show thinning effect due to the insertion of these receptors. The thickness of these bilayers in different systems are as follows: 36.80±0.86 Å (1a-dopc), 36.90±0.63 Å (1b-dopc), 46.80±0.98 Å (1a-dppe), 47.00±1.05 Å (1b-dppe), 37.20±0.85 Å (1a-popc), 37.10±0.65 Å (1b-popc), 39.70±0.69 Å (1a-pope), 39.10±0.96 Å (1b-pope), 40.70±0.87 Å (1a-pope-popg), 40.40±0.80 Å (1b-pope-popg), 37.90±0.90 Å (1a-popg), 38.10±0.64 Å (1b-popg), 42.60±0.95 Å (1a-yeast), and 42.20±0.90 Å (1b-yeast). After the insertion of receptor molecule inside these model lipid bilayers, thickness value changes very slightly. The APL values of these pure model lipid bilayers increase as follows: 43.46±0.56 $Å^2$ (DPPE), 56.43±0.72 $Å^2$ (POPE), 58.16±0.75 $Å^2$ (POPE/POPG), 65.56±0.85 $Å^2$ (POPG), 68.14±0.74 $Å^2$ (POPC), 68.42±0.96 $Å^2$

(Yeast), and 71.31±1.03 Å^2 (DOPC).

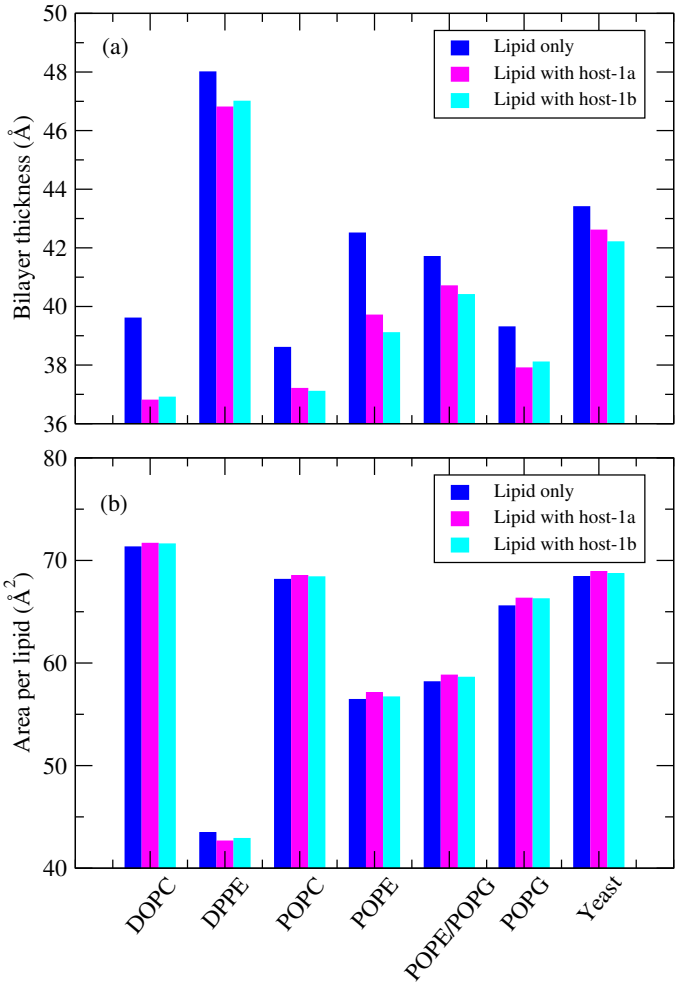

Figure 7-17. *(a) Thickness of different types of the model lipid bilayer (in Å unit) in presence and absence of receptor molecules, and (b) Area per lipid (APL) (in Å^2 unit) of all the model lipid bilayers in the absence and presence of receptor molecule.*

Note that the APL values reported in this work are in well agreement with the reported simulation and experimental results [371–375]. Receptor insertion causes APL to decrease in the case of DPPE bilayer-containing systems and increases in every other model lipid bilayer systems. After the receptor insertion, APL value for different systems are as follows: 71.66±1.10 Å^2 (1a-dopc), 71.60±0.99 Å^2 (1b-dopc), 42.63±0.52 Å^2 (1a-dppe), 42.88±0.64 Å^2 (1b-dppe), 68.52±0.75 Å^2 (1a-popc), 68.39±0.82 Å^2 (1b-popc), 57.11±0.71 Å^2 (1a-

pope), 56.68±0.73 Å^2 (1b-pope), 58.81±0.86 Å^2 (1a-pope-popg), 58.60±0.81 Å^2 (1b-pope-popg), 66.31±0.99 Å^2 (1a-popg), 66.25±0.84 Å^2 (1b-popg), 68.90±0.75 Å^2 (1a-yeast), and 68.70±0.92 Å^2 (1b-yeast). Changes in APL value after the insertion of receptor molecules into these model lipid bilayers are minor compared to pure model lipid bilayers. Thus, bilayer thickness and APL value confirms the structural stability of these model lipid membrane.

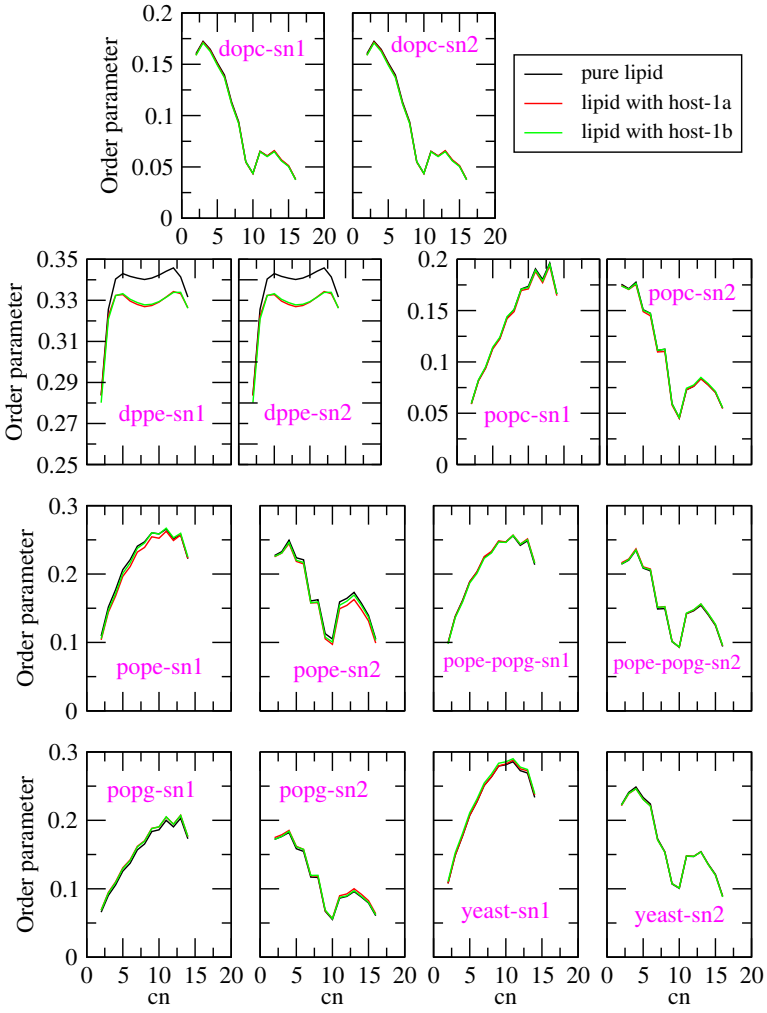

Figure 7-18. *sn1 and sn2 chain order parameters (S_{CD}) for pure model lipid bilayer and lipid bilayers in the presence of receptor molecules. cn represents the carbon number of that chain.*

Now, we focus on how the order parameters of the lipid tail of these model lipid bilayers changes compared to the pure lipid bilayers and the corresponding bilayers containing host-1a or host-1b. Order parameters are an important parameter to determine the structural stability of lipid bilayers. Every model lipid bilayer contains two lipid chains, i.e., lipid chain 1 (sn1) and lipid chain 2 (sn2). The order parameters as a function of carbon number (cn) of that particular chain are presented in Figure 7-18. In the pure model lipid bilayer, order parameters of sn1 and sn2 are the highest for DPPE, followed by Yeast, POPE, POPE/POPG, POPG, POPC, and DOPC bilayer. Receptor insertion into these model lipid bilayers decreases the sn1 and sn2 for DPPE membrane-containing systems but remains unchanged for all other model membranes. With the insertion of receptors, order parameters of both the chains of these model membranes remain essentially unchanged. Thus, We can further confirm that all the model lipid bilayers remain structurally stable during these insertion processes except for DPPE bilayer-containing systems (those become somewhat structurally disturbed during the simulation).

■ SUMMARY AND CONCLUSIONS

We have employed biased and unbiased atomistic molecular dynamics simulation to check the effects of endo-functionalized molecular tubes or naphthotubes (host-1a and host-1b) on seven different types of model lipid bilayers and permeation properties of these receptors through these model lipid bilayers. Lipid types include six model lipid bilayers (POPC, POPE, DOPC, POPG, DPPE, POPE/POPG) and one realistic membrane (Yeast). Here, we have focused on the insertion and permeation of these receptors into these model bilayers using unbiased MD simulation and the effects of an external force on the translocation of these receptors through these model lipid bilayers using biased MD simulation (umbrella sampling) techniques. We find that these receptors spontaneously translocate toward these model lipid bilayers head region and do not proceed further into these lipid bilayers tail regions (reside at the interface between lipid head and lipid tail region) except for the DPPE containing systems. In the DPPE model lipid bilayer containing systems (1a-dppe and 1b-dppe), receptor molecules are only absorbed on the bilayer surface and reside at the interface between lipid head and water. This finding is supported by the representative snapshots of the final conformation of the different model lipid bilayer and receptor molecule, COM–COM distance between host and model lipid bilayer, the density distribution profiles of lipid head, lipid tail, water, and receptor molecule with model lipid bilayer z-normal, RDFs between host-lipid head, host-lipid tail and host-water,

time evolution of the host-lipid head and host-water hydrogen bond, and the van der Waals and electrostatic interaction energy parameters between host-lipid head, host-lipid tail and host-water components. Thus, the active permeation of these receptors through these model lipid bilayers is not possible. To check the possibility of passive permeation, we have analyzed the free energy profiles and position-dependent diffusion coefficients (D(Z)) of these translocation processes. From free energy profiles, we observe that the interior location of the lipid bilayer is the most favorable position for these receptors, and passive transport of these receptors may be possible through these model lipid bilayers (due to the low barrier height) except for DPPE bilayer-containing systems (that have a very high energy barrier at the center). Further, the diffusion of these receptors through these model lipid bilayers are very slow for every system.

This research has allowed us to assess the biocompatibility of host-1a or host-1b in microscopic detail. Future research into the mechanism of drug carrier and release activity of these endo-functionalized molecular tubes of various practical lipid membranes will be driven by these findings. We hope to address this in near future.

Chapter 8

Summary and our view on the molecular recognition in water using endo-functionalized molecular tubes and uses of these receptors as drug delivery vehicles

"Everything that living things do can be understood in terms of the jigglings and wigglings of atoms."

– Richard Feynman

My doctoral thesis is directed towards the artificial receptors, molecular recognition, and uses of these artificial receptors as drug delivery vehicles. The endo-functionalized molecular tubes or naphthotubes (host-1a and host-1b in Figure 1-4 of Chapter 1) are used throughout this thesis. Most of the work of this thesis was performed using the classical MD simulation technique. Here, we have focused on the molecular recognition properties of these receptors from the aqueous medium and the application of these receptors in the biomedical field.

At first, we begin with some application of these receptors at various important fields like chiral or enantiomeric separation and drug solubilization. Initially, we begin with the chiral separation properties of these receptors in the aqueous medium. We have analyzed the structural and energetic aspect of chiral separation of some epoxide enantiomers by these molecular tubes. This study showcases atomistic details of the main stabilizing factors in these recognition processes, the structural stability of molecular tubes in water, and how we can use these molecular tubes as a CSP in chiral chromatography. Our results show that every guest-induced receptor gets a more symmetrical structure than the host molecule devoid of any guest molecule. Thus, the inclusion of guests into the host cavity provides more structural stability to endo-functionalized molecular tube molecules and facilitates the recognition of epoxide enantiomers into its cavity. Binding free energy value also suggests that host-guest hydrophobic interaction is the main contributing factor along with hydrogen bonding interaction for the complexation process, and all of these complexation processes are enthalpy driven. Our findings imply that for small epoxide enantiomers (i.e., guest molecules which have less amount of hydrophobic surface area) is not possible to precisely separate by the host molecular tubes, but for the epoxide enantiomers with a high amount of surface area may be separatable by using these endo-functionalized molecular tubes in the aqueous medium. Thus, in the chiral chromatography technique, these water-soluble endo-functionalized molecular tubes may be used as CSP in the separation of epoxide enantiomers having relatively sizeable hydrophobic surface area. Inspired by the chiral separation properties of organic epoxides, we are interested to see the stereoselective binding of peptides using these receptors is possible or not. Thus, we have computationally shown the possibility of chiral separation for the enantiomeric pairs of the two model peptides, namely, (d, l)-asparagine and (d, l)-phenylalanine in the presence of water with these two receptors. We have studied the interactions operating in the host-peptide complexes and the associated structural changes to better understand the chiral segregation process. We have also investigated the dynamics and the changes in the water structure for selected host-peptide complexes close to the receptor surface. Analysis shows that

both the host molecules are conformationally stable and less flexible, and the stability of every host-peptide system remains intact during the simulation. The presence of the host and the host-peptide complexes affect the translational diffusion and the hydrogen bond lifetime values of water molecules near the surface compared to that of bulk water. The binding free energy values obtained indicate that the formation of stable host-peptide complexes is an enthalpically favorable process. d- and l- isomers of the same peptide form complexes with a particular host molecule with an energy difference of more than 1 kcal/mole. Thus, we can say that the chiral separation of these model peptides with the help of these endo-functionalized molecular tubes may be attainable from the energy point of view. The connection so derived from our studies between the peptide stereochemistry and its influence while interacting with the host would be beneficial in designing improved supramolecular receptors with better complexation ability. The ideas obtained may be further implemented to resolve larger peptides and proteins as model systems that are conformationally more complex.

After elucidating these receptors' stereoselective or enantioselective properties, we are interested in using these receptors as a drug solubility enhancement agent for poorly water-soluble drug molecules. Therefore, we have explored the drug solubility enhancement in an aqueous medium using these two macrocyclic host molecules. They satisfy most of the conditions to be used as supramolecular receptors for drug solubilization in an aqueous medium. We have restricted our drug solubilization studies in aqueous solution, particularly as common practical problems often involve water as the solvent medium. Biomedical engagements of a supramolecular receptor commence with the formation of stable host-drug complexes with the drug molecules. Structural analysis shows that both the host molecules are conformationally stable and flexible, and the stability of every host-drug system remains intact during the simulation. The binding free energy values obtained indicate that the formation of stable host-drug complexes is an enthalpically favorable process. From every structural and energetic aspect, it is clear that both the host molecules form stable host-drug complexes with all the drug molecules. Thus, we propose that these two supramolecular receptors may be used as drug solubilizing agents, and patients will benefit from this theranostic application shortly.

All the major applications shown previously are mainly based on host-guest complexation in the aqueous medium. But the role of water molecules in the complexation of these receptors is not elucidated yet. Thus, we discuss the waters' role in the guest binding process of these small miniature receptors . We have portrayed this using classical MD sim-

ulation and grid inhomogeneous solvation theory (GIST) methodology. Trajectories from MD simulation have been utilized in GIST methodology to estimate different localized thermodynamic parameters at different regions of these receptors. The grid methodology also makes it easy to focus on regions where a high water density is present. These two receptors can encapsulate many environmentally and industrially important molecules from water. Also, to investigate the effect of electrostatic, we have used the nonpolar version of these receptors in which all the partial charges of the atomic sites of both these receptors are artificially set to zero. A high density of water molecules is present inside both the regular host molecules. Our results signify that those guest molecules form stronger interactions with these hosts than the host-water interactions, replace the water molecules, and form a strong host-guest complex. On the other hand, unfavorable water-water interaction is partly or fully balanced by favorable solute-water interactions. Every energetic and entropic solvation parameters are less perturbed for nonpolar host molecules than the corresponding regular host molecules. Therefore, the value of the free energy for removing water molecules from a particular region of purely nonpolar host molecules is more favorable than the corresponding regular host molecules. The dense torus region in both the nonpolar host molecules demonstrates that packaging contributes more to create the dense torus region. These results indicate the importance of confinement on the water structure. These small host molecules uncover the detailed solvation structure, thermodynamic pattern and offer a comprehensive insight into the formation of strong host-guest complexes. This study also proves host-1b is a better complexing agent than host-1a.

As host-1b is a better complexing agent than host-1a, thus, now we have used host-1b and find the possibility of complexation of this host with four different strongly neutral hydrophilic guest molecules namely, 1,4-dioxane (14D), acetone, DMSO, and DMF in water and the effect of the guest concentration on these complexes, stability is examined by using classical molecular dynamics simulation. All these guest molecules are neutral and hydrophilic. Selective recognition of neutral hydrophilic molecules in an aqueous solvent is challenging for artificial molecular receptors, and very few systems can do this work. The binding free energy calculations reveal host-1b/14D complexation is energetically most stable, and the synergistic host-guest hydrophobic and hydrogen bonding interactions play profound roles in the stability of these host-guest complexes. Specifically, as the host cavity contains a small hydrophilic part and a large hydrophobic part, so guest molecules having both these parts form hydrogen bonds with the hosts' hydrophilic part and make favorable hydrophobic interaction with the hydrophobic part of the host at the time of complexation.

We also examine the effect of the concentration of different guest molecules on the host-guest complexation ability by determining different types of hydrogen bond properties, preferential interaction parameters, water-inserted guest interaction energy parameters, host-guest binding free energy, and potential of mean force. From the calculated free energy values, it is revealed that as the concentration of guest decreases, the free energy becomes less favorable. In specific the complexation ability decreases as the guest concentration decreases for a particular type of guest molecule. We suspect that the idea displayed in this study can act as a guide to different synthetic receptors for the recognition of other environmentally or biologically important neutral hydrophilic molecules. We hope this process may keep water free from industrial pollution by encapsulating industrial pollutants from water mediums.

As of now, in this thesis, host-1a and host-1b are used for enantiomeric or chiral separation procedures, enhancement of poorly water-soluble drug solubilization, and encapsulation of environmentally important contaminants from the aqueous medium. As these two receptor molecules can enhance the solubility of low water-soluble drug molecules (discussed earlier), we are interested in the usefulness of these receptors as drug delivery vehicles. The first and foremost criteria for any molecules that show promising in drug delivery is to permeate lipid bilayers. For the same, we have investigated the effects of these endo-functionalized molecular tubes or naphthotubes on seven different types of model lipid bilayers and the permeation properties of these receptors through these model lipid bilayers. Lipid types include six model lipid bilayers (POPC, POPE, DOPC, POPG, DPPE, POPE/POPG) and one realistic membrane (Yeast). We find that these receptors spontaneously translocate toward these model lipid bilayers head region and do not proceed further into these lipid bilayers tail regions (reside at the interface between lipid head and lipid tail region) except for the DPPE containing systems. In the DPPE model lipid bilayer-containing systems (1a-dppe and 1b-dppe), receptor molecules are only absorbed on the bilayer surface and reside at the interface between lipid head and water. Thus, the active permeation of these receptors through these model lipid bilayers is not possible. From free energy profiles, we observe that the interior location of the lipid bilayer is the most favorable position for these receptors, and passive transport of these receptors may be possible through these model lipid bilayers (due to the low barrier height) except for DPPE bilayer-containing systems (that have a very high energy barrier at the center). This research has allowed us to assess the biocompatibility of host-1a or host-1b in microscopic detail. Future research into the mechanism of drug carrier and release activity of these

endo-functionalized molecular tubes of various practical lipid membranes will be driven by these findings. We hope to address this shortly.

In this thesis, host-guest complexation investigations indicate the driving factors behind complexation and offer insight into noncovalent interactions between the host and guest moiety. This study also provides interaction between these receptors and different model lipid bilayers to find the possibility of using these receptors as drug delivery vehicles. The expertise accumulated leads to the design of therapeutic functional compounds, such as molecular reactors for catalysis, or the advancement of structure-based drug design and their delivery in medicinal chemistry.

Bibliography

1. Lehn, J.-M. *Wiley-VCH, Weinheim*, **1995**.
2. Fischer, E.; Thierfelder, H. *Ber. Dtsch. Chem. Ges.* **1894**, *27*, 2031-2037.
3. Fischer, E. *Ber. Dtsch. Chem. Ges.* **1894**, *27*, 2985-2993.
4. van der Waals, J. D. *Leiden University, Netherlands*, **1873**.
5. Watson, J. D.; Crick, F. H. C. *Nature* **1953**, *171*, 737-738.
6. Pedersen, C. J. *J. Am. Chem. Soc.* **1967**, *89*, 2495-2496.
7. Pedersen, C. J. *J. Am. Chem. Soc.* **1967**, *89*, 7017-7036.
8. Lehn, J.-M. *Acc. Chem. Res.* **1978**, *11*, 49-57.
9. Cram, D. J.; Kaneda, T.; Helgeson, R. C.; Brown, S. B.; Knobler, C. B.; Maverick, E.; Trueblood, K. N. *J. Am. Chem. Soc.* **1985**, *107*, 3645-3657.
10. Cram, D. J.; Lein, G. M. *J. Am. Chem. Soc.* **1985**, *107*, 3657-3668.
11. Kim, D. H.; Atwood, J. L.; Davies, J. E. D.; MacNicol, D. D.; Vögtle, F. *Pergamon, Oxford, 2nd ed.*, **1996**, *4*, 503-526.
12. Calladine, C. R.; Drew, H. R.; Luisi, B.; Travers, A. *Academic Press, New York, 3rd ed.*, **2004**.
13. Cram, D. J. *Angew. Chem. Int. Ed. Engl.* **1986**, *25*, 1039-1134.
14. Cabbiness, D. K.; Margerum, D. W. *J. Am. Chem. Soc.* **1969**, *91*, 6540-6541.
15. Cram, D. J. *Angew. Chem. Int. Ed. Engl.* **1988**, *27*, 1009-1020.
16. Schneider, H.-J. *Angew. Chem. Int. Ed. Engl.* **2009**, *48*, 3924-3977.
17. Steed, J. W.; Turner, D. R.; Wallace, K. *John Wiley & Sons*, **2007**.
18. Schmidtchen, F. P. *Chem. Soc. Rev.* **2010**, *39*, 3916-3935.
19. Gokel, G. W.; Leevy, W. M.; Weber, M. E. *Chem. Rev.* **2004**, *104*, 2723-2750.

20. Zhang, Z.-J.; Liu, Y. *Synlett.* **2012**, *23*, 1733-1750.

21. Liu, Y.; Chen, Y. *Acc. Chem. Res.* **2006**, *39*, 681-691.

22. Harada, A.; Hashidzume, A.; Yamaguchi, H.; Takashima, Y. *Chem. Rev.* **2009**, *109*, 5974-6023.

23. Liu, Y.; Chen, Y. *Chem. Soc. Rev.* **2010**, *39*, 495-505.

24. Böhmer, V. *Angew. Chem. Int. Ed. Engl.* **1995**, *34*, 713-745.

25. Ikeda, A.; Shinkai, S. *Chem. Rev.* **1997**, *97*, 1713-1734.

26. Lagona, J.; Mukhopadhyay, P.; Chakrabarti, S.; Isaacs, L. *Angew. Chem., Int. Ed.* **2005**, *44*, 4844-4870.

27. Gutsche, C. D. *Stoddart, J. F. Ed.; The Royal Society of Chemistry: Cambridge*, **1989**.

28. Wieser, V.; Dieleman, C. B.; Matt, D. *Chem. Rev.* **1997**, *165*, 93-161.

29. Hardie, M. J. *Chem. Soc. Rev.* **2010**, *39*, 516-527.

30. Ogoshi, T.; Kanai, S.; Fujinami, S.; Yamagishi, T.; Nakamoto, Y. *J. Am. Chem. Soc.* **2008**, *130*, 5022-5023.

31. Wang, Y.; Ping, G.; Li, C.; Pan, F.; Yang, D. *Chem. Commun.* **2016**, *52*, 9858-9872.

32. Schmidtchen, F. P. *Org. Lett.* **2002**, *4*, 431-434.

33. Wang, M.-X.; Zhang, X.-H.; Zheng, Q.-Y. *Angew. Chem. Int. Ed.* **2004**, *43*, 838-842.

34. Chun, Y.; Singh, N. J.; Hwang, I.-C.; Lee, J. W.; Yu, S. U.; Kim, K. S. *Nat. Commun.* **2013**, *4*, 1797-1804.

35. Poh, B.-L.; Lim, C. S.; Khoo, K. S. *Tetrahedron Lett.* **1989**, *30*, 1005-1008.

36. Poh, B.-L.; Lim, C. S. *Tetrahedron* **1990**, *46*, 3651-3658.

37. Georghiou, P. E.; Valluru, G.; Schneider, C.; Liang, S.; Woolridge, K.; Mulla, K.; Adronovc, A.; Zhao, Y. *RSC Adv.* **2014**, *4*, 31614-31617.

38. Huang, G.-B.; Wang, S.-H.; Ke, H.; Yang, L.-P.; Jiang, W. *J. Am. Chem. Soc.* **2016**, *138*, 14550-14553.

39. Jia, F.; He, Z.; Yang, L.-P.; Pan, Z.-S.; Yi, M.; Jiang, R.-W.; Jiang, W. *Chem. Sci.* **2015**, *6*, 6731-6738.

40. Jia, F.; Wang, H.-Y.; Li, D.-H.; Yang, L.-P.; Jiang, W. *Chem. Commun.* **2016**, *52*, 5666-5669.

41. Xu, Z.; Jia, S.; Wang, W.; Yuan, Z.; Ravoo, B. J.; Guo, D.-J. *Nat. Chem.* **2019**, *11*, 86-93.

42. Murray, J.; Kim, K.; Ogoshi, T.; Yao, W.; Gibb, B. C. *Chem. Soc. Rev.* **2017**, *46*, 2479-2496.

43. Barrow, S. J.; Kasera, S.; Rowland, M. J.; del Barrio, J.; Scherman, O. A. *Chem. Rev.* **2015**, *115*, 12320-12406.

44. Ma, D.; Hettiarachchi, G.; Nguyen, D.; Zhang, B.; Wittenberg, J. B.; Zavalij, P. Y.; Briken, V.; Isaacs, L. *Nat. Chem.* **2012**, *4*, 503-510.

45. Bier, D.; Rose, R.; Bravo-Rodriguez, K.; Bartel, M.; Ramirez-Anguita, J. M.; Dutt, S.; Wilch, C.; Klàrner, F.-G.; Sanchez-Garcia, E.; Schrader, T.; Ottmann, C. *Nat. Chem.* **2013**, *5*, 234-239.

46. He, S.; Zhiti, A.; Barba-Bon, A.; Hennig, A.; Nau, W. M. *Front. Chem.* **2020**, *8*, 597927.

47. Nilam, M.; Collin, S.; Karmacharya, S.; Hennig, A.; Nau, W. M. *ACS Sens.* **2021**, *6*, 175-182.

48. Zappacosta, R.; Cornelio, B.; Pilato, S.; Siani, G.; Estour, F.; Aschi, M.; Fontana, A. *Molecules* **2019**, *24*, 1387.

49. Biedermann, F.; Ghale, G.; Hennig, A.; Nau, W. M. *Commun. Biol.* **2020**, *3*, 383.

50. Khuntawee, W.; Wolschann, P.; Rungrotmongkol, T.; WongEkkabut, J.; Hannongbua, S. *J. Chem. Inf. Model.* **2015**, *55*, 1894-1902.

51. Shinoda, W. *Biochim. Biophys. Acta* **2016**, *1858*, 2254-2265.

52. Loftsson, T.; Brewster, M. E. *J. Pharm. Sci.* **1996**, *85*, 1017-1025.

53. Shorthill, B. J.; Avetta, C. T.; Glass, T. E. *J. Am. Chem. Soc.* **2004**, *126*, 12732-12733.

54. Avetta, C. T.; Shorthill, B. J.; Ren, C.; Glass, T. E. *J. Org. Chem.* **2012**, *77*, 851-857.

55. Ren, C.; Lee, J. S.; Glass, T. E. *Supramol. Chem.* **2014**, *26*, 607-611.

56. Van Allan, J. A.; Giannini, D. D.; Whitesides, T. H. *J. Org. Chem.* **1982**, *47*, 820-823.

57. He, Z.; Yang, X.; Jiang, W. *Org. Lett.* **2015**, *17*, 3880-3883.

58. He, Z.; Ye, G.; Jiang, W. *Chem. Eur. J.* **2015**, *21*, 3005-3012.

59. Yang, L.-P.; Wang, X.; Yao, H.; Jiang, W. *Acc. Chem. Res.* **2020**, *53*, 198-208.

60. Yang, L.-P.; Liu, W.-E.; Jiang, W. *Tetrahedron Lett.* **2016**, *57*, 3978-3985.

61. Wereszczynski, J.; McCammon, J. A. *Quarterly Reviews of Biophysics* **2012**, *45*, 1-25.

62. Ponder, J. W.; Case, D. A. *Adv. Prot. Chem.* **2003**, *66*, 27-85.

63. Case, D. A.; Babin, V.; Berryman, J. T.; Betz, R. M.; Cai, Q.; Cerutti, D. S.; Cheatham, III, T. E.; Darden, T. A.; Duke, R. E.; Gohlke, H.; et al. *Amber14*. University of California: San Francisco, CA, **2014**.

64. Cornell, W. D.; Cieplak, P.; Bayly, C. I.; Gould, I. R.; Merz, K. M. Jr.; Ferguson, D. M.; Spellmeyer, D. C.; Fox, T.; Caldwell, J. W.; Kollman, P. A. *J. Am. Chem. Soc.* **1995**, *117*, 5179-5197.

65. Jones, J. E. *Proc. R. Soc. Lond.* **1924**, *106*, 463-477.

66. Coulomb, C. A. *Collection de ḿemoires relatifs à la physique* Gauthier-Villars, **1884**, 569-638.

67. Bayly, C. I.; Cieplak, P.; Cornell, W. D.; Kollman, P. A. *J. Phys. Chem.* **1993**, *97*, 10269-10280.

68. Cornell, W. D.; Cieplak, P.; Bayly, C. I.; Kollmann, P. A. *J. Am. Chem. Soc.* **1993**, *115*, 9620-9631.

69. Verlet, L. *Phys. Rev.* **1967**, *159*, 98-103.

70. Van Gunsteren, W. F.; Berendsen, H. J. C. *Mol. Simul.*, **1988**, *1:3*, 173-185.

71. Ryckaert, J.-P.; Ciccotti, G.; Berendsen, H. J. C. *J. Comput. Phys.* **1977**, *23*, 327-341.

72. Jorgensen, W. L.; Chandrasekhar, J.; Madura, J. D.; Impey, R. W.; Klein, M. L. *J. Chem. Phys.* **1983**, *79*, 926-935.

73. Essmann. U.; Perera. L.; Berkowitz. M. *J. Chem. Phys.* **1995**, *103*, 8577-8592.

74. Martinez, L.; Andrade, R.; Birgin, E. G.; Martinez, J. M. *J. Comput. Chem.* **2009**, *30*, 2157-2164.

75. Berendsen, H. J. C.; Postma, J. P. M.; van Gunsteren, W. F.; DiNola, A.; Haak, J. R. *J. Chem. Phys.* **1984**, *81*, 3684-3690.

76. Hunenberger, P. H. *Adv. Polym. Sci.* **2005**, *173*, 105-149.

77. Roe, D. R.; Cheatham, T. E. *J. Chem. Theory Comput.* **2013**, *9*, 3084-3095.

78. Humphrey, W.; Dalke, A.; Schulten, K. *J. Mol. Graph.* **1996**, *14*, 33-38.

79. Srinivasan, J.; Cheatham, T. E.; Cieplak, P.; Kollman, P. A.; Case, D. A. *J. Am. Chem. Soc.* **1998**, *120*, 9401-9409.

80. Miller, III. B. R.; McGee, Jr. T. D.; Swails, J. M.; Homeyer, N.; Gohlke, H.; Roitberg, A. E. *J. Chem. Theory Comput.* **2012**, *8*, 3314-3321.

81. Lee, F. S.; Chu, Z.-T.; Bolger, M. B.; Warshel, A. *Protein Eng.* **1992**, *5*, 215-228.

82. Lee, F. S.; Chu, Z. T.; Warshel, A. *J. Comput. Chem.* **1993**, *14*, 161-185.

83. Hansson, T.; Marelius, J.; Åqvist, J. *J. Comput. Aided Mol. Des.* **1998**, *12*, 27-35.

84. Hansson, T.; Åqvist, J. *Protein Eng.* **1995**, *8*, 1137-1144.

85. Hamelberg, D.; McCammon, J. A. *J. Am. Chem. Soc.* **2004**, *126*, 7683-7689.

86. Jayaram, B.; Sprous, D.; Beveridge, D. L. *J. Phys. Chem. B* **1998**, *102*, 9571-9576.

87. Kasimova, A. O.; Pavan, G. M.; Danani, A.; Mondon, K.; Cristiani, A.; Scapozza, L.; Gurny, R.; Moller, M. *J. Phys. Chem. B* **2012**, *116*, 4338-4345.

88. Sanner, M. F.; Olson, A. J.; Spehner, J. C. *Biopolymers* **1996**, *38*, 305-320.

89. Kastner, J. *WIREs Comput. Mol. Sci.* **2011**, *1*, 932-942.

90. Liu, Q.; Zuo, F.; Zhao, Z.; Chen, J.; Xu, D. *Phys. Chem. Chem. Phys.* **2017**, *19*, 23924-23933.

91. Zhang, Q.; Tu, Y.; Tian, H.; Zhao, Y.-L.; Stoddart, J. F.; Ågren, H. *J. Phys. Chem. B* **2010**, *114*, 6561-6566.

92. Kumar, S.; Rosenberg, J. M.; Bouzida, D.; Swendsen, R. H.; Kollman, P. A. *J. Comput. Chem.* **1992**, *13*, 1011-1021.

93. Souaille, M.; Roux, B. *Comput. Phys. Commun.* **2001**, *135*, 40-57.

94. Stalcup, A. M. *Annu. Rev. Anal. Chem.* **2010**, *3*, 341-363.

95. Chen, L.; Reiss, P. S.; Chong, S. Y.; Holden, D.; Jelfs, K. E.; Hasell, T.; Little, M. A.; Kewley, A.; Briggs, M. E.; Stephenson, A.; et al. *Nat. Mater.* **2014**, *13*, 954-960.

96. Dahl, S. G.; Sylte, I. *Basic Clin. Pharmacol. Toxicol.* **2005**, *96*, 151-155.

97. Shahgaldian, P.; Pieles, U. *Sensors* **2006**, *6*, 593-615.

98. Silva, B.; Fernandes, C.; Pinho, P. G.; Remiao, F. *J. Anal. Toxicol.* **2018**, *42*, 17-24.

99. Ward, T. J.; Ward, K. D. *Anal. Chem.* **2012**, *84*, 626-635.

100. Kempe, M.; Mosbach, K. *J. Chromatogr. A* **1995**, *694*, 3-13.

101. Takeuchi, T.; Haginaka, J. *J. Chromatogr. B* **1999**, *728*, 1-20.

102. Ward, T. J.; Ward, K. D. *Anal. Chem.* **2010**, *82*, 4712-4722.

103. Hammock, L.; Hammock, B.; Casid, J. E. *Bull Environ Contam Toxicol* **1974**, *12*, 759-764.

104. Fioriti, J. A.; Bentz, A. P.; Sims, R. J. *J. Am. Oil Chem. Soc.* **1966**, *43*, 37-38.

105. Wang, L.-L.; Chen, Z.; Liu, W.-E.; Ke, H.; Wang, S.-H.; Jiang, W. *J. Am. Chem. Soc.* **2017**, *139*, 8436-8439.

106. Frisch, M. J.; Trucks, G. W.; Schlegel, H. B.; Scuseria, G. E.; Robb, M. A.; Cheeseman, J. R.; Scalmani, G.; Barone, V.; Petersson, G. A.; Nakatsuji, H.; et al. *Gaussian 09, Revision A.02*, Gaussian, Inc.: Wallingford, CT, **2009**.

107. Wang, J.; Wang, W.; Kollman, P. A.; Case, D. A. *J. Mol. Graph. Model.* **2006**, *25*, 247-260.

108. Wang, J.; Wolf, R. M.; Caldwell, J. W.; Kollman, P. A.; Case, D. A. *J. Comput. Chem.* **2004**, *25*, 1157-1174.

109. Bandyopadhyay, S.; Chakraborty, S.; Bagchi, B. *J. Am. Chem. Soc.* **2005**, *127*, 16660-16667.

110. Paul, S.; Patey, G. N. *J. Am. Chem. Soc.* **2007**, *129*, 4476-4482.

111. Balasubramanian, S.; Pal, S.; Bagchi, B. *Phys. Rev. Lett.* **2002**, *89*, 115505.

112. Chandra, A. *Phys. Rev. Lett.* **2000**, *85*, 768-771.

113. Chandra, A. *J. Phys. Chem. B* **2003**, *107*, 3899-3906.

114. Bhattacharyya, K.; Bagchi, B. *J. Phys. Chem. A* **2000**, *104*, 10603-10613.

115. Nandi, N.; Bhattacharyya, K.; Bagchi, B. *Chem. Rev.* **2000**, *100*, 2013-2046.

116. Choudhury, N.; Pettitt, B. M. *J. Am. Chem. Soc.* **2005**, *127*, 3556-3567.

117. Choudhury, N. *J. Phys. Chem. B* **2008**, *112*, 6296-6300.

118. Paul, S.; Paul, S. *J. Phys. Chem. B* **2015**, *119*, 9820-9834.

119. Paul, S.; Paul, S. *J. Phys. Chem. B* **2019**, *123*, 3475-3489.

120. Altarsha, M.; Yeguas, V.; Ingrosso, F.; Lòpez, R.; Ruiz-Lòpez, M. F. *J. Phys. Chem. B* **2013**, *117*, 3091-3097.

121. Chattaraj, K. G.; Paul, S. *J. Chem. Phys.* **2019**, *150*, 064501.

122. Johnson, E. R.; Keinan, S.; Mori-Sànchez, P.; Contreras-Garcìa, J.; Cohen, A. J.; Yang, W. *J. Am. Chem. Soc.* **2010**, *132*, 6498-6506.

123. Lu, T.; Chen, F. *J. Comput. Chem.* **2011**, *33*, 580-592.

124. Zhang, X. X.; Bradshaw, J. S.; Izatt, R. M. *Chem. Rev.* **1997**, *97*, 3313-3361.

125. Cram, D. J. *Science* **1988**, *240*, 760-767.

126. Cram, D. J.; Helgeson, R. C.; Sousa, L. R.; Timko, J. M.; Newcomb, M.; Moreau, P.; de Jong, F.; Gokel, G. W.; Hoffman, D. H.; Domeier, L. A.; Peacock, S. C.; Madan, K.; Kaplan, L. *Pure Appl. Chem.* **1975**, *43*, 327-349.

127. Stoddart, J. F. *Chem. Soc. Rev.* **1979**, *8*, 85-142.

128. Joll, S. T.; Bradshaw, J. S.; Izatt, R. M. *J. Heterocycl. Chem.* **1982**, *19*, 3-19.

129. Izatt, R. M.; Zhu, C. Y.; Huszthy, P.; Bradshaw, J. S. *Cooper, S. R. Ed.; VCH Publishers: New York*, **1992**, Chapter 12.

130. Bradshaw, J. S.; Huszthy, P.; McDaniel, C. W.; Oue, M.; Zhu, C. Y.; Izatt, R. M. *J. Coord. Chem.* **1992**, *27*, 105-114.

131. Wang, T.; Bradshaw, J. S.; Izatt, R. M. *J. Heterocycl. Chem.* **1994**, *31*, 1097-1114.

132. Webb, T. H.; Wilcox, C. S. *Chem. Soc. Rev.* **1993**, *22*, 383-395.

133. Pal, S.; Bagchi, B.; Balasubramanian, S. *J. Phys. Chem. B* **2005**, *109*, 12879-12890.

134. Pal, S.; Balasubramanian, S.; Bagchi, B. *Phys. Rev. E* **2003**, *67*, 061502.

135. Sen, S.; Sukul, D.; Dutta, P.; Bhattacharyya, K. *J. Phys. Chem. A.* **2001**, *105*, 10635-10639.

136. Mondal, S. K.; Sahu, K.; Ghosh, S.; Sen, P.; Bhattacharyya, K. *J. Phys. Chem. A.* **2006**, *110*, 13646-13652.

137. Jana, M.; Bandyopadhyay, S. *J. Phys. Chem. B.* **2011**, *115*, 6347-6357.

138. Jana, M.; Bandyopadhyay, S. *J. Chem. Phys.* **2011**, *134*, 025103.

139. Maier, J. A.; Martinez, C.; Kasavajhala, K.; Wickstrom, L.; Hauser, K. E.; Simmerling, C. *J. Chem. Theory Comput.* **2015**, *11*, 3696-3713.

140. Chowdhuri, S.; Chandra, A. *Phys. Rev. E* **2002**, *66*, 041203.

141. Chandra, A. *Proc. Indian Natn. Sci. Acad.* **2003**, *49*, 49-59.

142. Guarˋdia, E.; Laria, D.; Martí, J. *J. Phys. Chem. B* **2006**, *110*, 6332-6338.

143. Bruce, C. D.; Senapati, S.; Berkowitz, M. L.; Perera, L.; Forbes, M. D. E. *J. Phys. Chem. B* **2002**, *106*, 10902-10907.

144. Senapati, S.; Berkowitz, M. L. *J. Phys. Chem. A* **2004**, *108*, 9768-10907.

145. Pizzitutti, F.; Marchi, M. *J. Phys. Chem. B* **2007**, *111*, 7584-7590.

146. Ong, E. E. S.; Liow, J.-L. *Fluid Ph. Equilibria.* **2019**, *481*, 55-65.

147. Nandi, N.; Bagchi, B. *J. Phys. Chem.* **1996**, *100*, 13914-13919.

148. Rani, P.; Biswas, P. *J. Phys. Chem. B* **2015**, *119*, 13262-13270.

149. Pal, S.; Bandyopadhyay, S. *Langmuir* **2013**, *29*, 1162-1173.

150. Pal, S.; Maiti, P. K.; Bagchi, B. *J. Chem. Phys.* **2006**, *125*, 234903.

151. Laage, D.; Elsaesser, T.; Hynes, J. T. *Chem. Rev.* **2017**, *117*, 10694-10725.

152. Stillinger, F. H. *Adv. Chem. Phys.* **1975**, *31*, 1-101.

153. Stillinger, F. H. *Science* **1980**, *209*, 451-457.

154. Luzar, A.; Chandler, D. *Nature* **1996**, *379*, 55-57.

155. Luzar, A.; Chandler, D. *Phys. Rev. Lett.* **1996**, *76*, 928-931.

156. Luzar, A. *J. Chem. Phys.* **2000**, *113*, 10663-10675.

157. Luzar, A. *Chem. Phys.* **2000**, *258*, 267-276.

158. Rapaport, D. C. *Mol. Phys.* **1983**, *50*, 1151-1162.

159. Indra, S.; Biswas, R. *Mol. Simul.* **2015**, *41*, 471-482.

160. Pal, S.; Chakraborty, K.; Khatua, P.; Bandyopadhyay, S. *J. Chem. Phys.* **2015**, *142*, 055102.

161. Chattaraj, K. G.; Paul, R.; Paul, S. *Langmuir* **2020**, *36*, 1773-1792.

162. Takagi, T.; Ramachandran, C.; Bermejo, M.; Yamashita, S.; Yu, L. X.; Amidon, G. L. *Mol. Pharm.* **2006**, *3*, 631-643.

163. Hauss, D. J. *Adv. Drug Deliv. Rev.* **2007**, *59*, 667-676.

164. Lipinski, C. A. *J. Pharmacol. Toxicol. Methods* **2000**, *44*, 235-249.

165. Porter, C. J. H.; Trevaskis, N. L.; Charman, W. N. *Nature Rev. Drug Discov.* **2007**, *6*, 231-248.

166. Allen, T. M.; Cullis, P. R. *Science* **2004**, *303*, 1818-1822.

167. Leuner, C.; Dressman, J. *Eur. J. Pharm. Biopharm.* **2000**, *50*, 47-60.

168. Muller, R. H.; Keck, C. M. *J. Biotechnol.* **2004**, *113*, 151-170.

169. Blagden, N.; de Matas, M.; Gavan, P. T.; York, P. *Adv. Drug Deliv. Rev.* **2007**, *59*, 617-630.

170. Patri, A. K.; Kukowska-Latallo, J. F.; Baker, J. R. *Adv. Drug Deliv. Rev.* **2005**, *57*, 2203-2214.

171. Serajuddin, A. T. M. *Adv. Drug Deliv. Rev.* **2007**, *59*, 603-616.

172. Stella, V. J.; Nti-Addae, K. W. *Adv. Drug Deliv. Rev.* **2007**, *59*, 677-694.

173. Chaban, V. V.; Prezhdo, O. V. *ACS Nano* **2011**, *5*, 5647-5655.

174. Chaban, V. V.; Savchenko, T. I.; Kovalenko, S. M.; Prezhdo, O. V. *J. Phys. Chem. B* **2010**, *114*, 13481-13486.

175. Chaban, V. V.; Prezhdo, V. V.; Prezhdo, O. V. *ACS Nano* **2012**, *6*, 2766-2773.

176. Szente, L.; Szejtli, J. *Adv. Drug Deliv. Rev.* **1999**, *36*, 17-28.

177. Rajewski, R. A.; Stella, V. J. *J. Pharm. Sci.* **1996**, *85*, 1142-1169.

178. Stella, V. J.; Rajewski, R. A. *Pharm. Res.* **1997**, *14*, 556-567.

179. Jeon, Y. J.; Kim, S.-Y.; Ko, Y. H.; Sakamoto, S.; Yamaguchi, K.; Kim, K. *Org. Biomol. Chem.* **2005**, *3*, 2122-2125.

180. Macartney, D. H. *Isr. J. Chem.* **2011**, *51*, 600-615.

181. Walker, S.; Oun, R.; McInnes, F. J.; Wheate, N. J. *Isr. J. Chem.* **2011**, *51*, 616-624.

182. Dong, N.; Xue, S.-F.; Zhu, Q.-J.; Tao, Z.; Yang, L.-X. *Supramol. Chem.* **2008**, *20*, 659-665.

183. Koner, A. L.; Ghosh, I.; Saleh, N.; Nau, W. M. *Can. J. Chem.* **2011**, *89*, 139-147.

184. Dong, N.; Wang, X.; Pan, J.; Tao, Z. *Acta Chim. Sinica* **2011**, *69*, 1431-1437.

185. Miskolczy, Z.; Megyesi, M.; Tarkanyi, G.; Mizsei, R.; Biczok, L. *Org. Biomol. Chem.* **2011**, *9*, 1061-1070.

186. Zhao, Y.; Buck, D. P.; Morris, D. L.; Pourgholami, M. H.; Day, A. I.; Collins, J. G. *Org. Biomol. Chem.* **2008**, *6*, 4509-4515.

187. Zhao, Y.; Pourgholami, M. H.; Morris, D. L.; Collins, J. G.; Day, A. I. *Org. Biomol. Chem.* **2010**, *8*, 3328-3337.

188. Goldoni, L.; Grugni, M.; De Munari, S.; Cassin, M.; Bernardini, R. *Chem. Lett.* **2010**, *39*, 676-677.

189. Acartùrk, F.; Kislal, Ò.; Celebi, N. *Int. J. Pharm.* **1992**, *85*, 1-6.

190. Aiassa, V.; Zoppi, A.; Albesa, I.; Longhi, M. R. *Carbohydrate Polymers* **2015**, *121*, 320-327.

191. Aiassa, V.; Zoppi, A.; Becerra, M. C.; Albesa, I.; Longhi, M. R. *Carbohydrate Polymers* **2016**, *152*, 672-678.

192. Barbosa, J. A. A.; Zoppi, A.; Quevedo, M. A.; de Melo, P. N.; de Medeiros, A. S. A.; Streck, L.; De Oliveira, A. R.; Fernandes-Pedrosa, M. F.; Longhi, M. R.; Silva-Junior, A. A. D. *Int. J. Mol. Sci.* **2014**, *15*, 17077-17099.

193. Bayomi, M. A.; Abanumay, K. A.; Al-Angary, A. A. *Int. J. Pharm.* **2002**, *243*, 107-117.

194. Beig, A.; Miller, J. M.; Dahan, A. *Eur. J. Pharm. Biopharm.* **2013**, *85*, 1293-1299.

195. Shadrack, D. M.; Swai, H. S.; Munissi, J. J. E.; Mubofu, E. B.; Nyandoro, S. S. *Molecules* **2018**, *23*, 1419.

196. González-Méndeza, I.; Aguayo-Ortizb, R.; Sorroza-Martíneza, K.; Solanoc, J. D.; Porcua, P.; Riveraa, E.; Dominguez, L. *Bioorg. Med. Chem.* **2020**, *28*, 115510.

197. Sherje, A. P.; Kulkarni, V.; Murahari, M.; Nayak, U. Y.; Bhat, P.; Suvarna, V.; Dravyakar, B. *Mol. Pharm.* **2017**, *14*, 1231-1242.

198. Cerutti, J. P.; Quevedo, M. A.; Buhlman, N.; Longhi, M. R.; Zoppi, A. *Carbohydrate Polymers* **2019**, *205*, 480-487.

199. Zhou, J.; Yu, G.; Huang, F. *Chem. Soc. Rev.* **2017**, *46*, 7021-7053.

200. Suad, K. S.; Al-Burtomani, F. O. S. *J. Inc. Phenom. Macro. Chem.* **2019**, *93*, 157-172.

201. Cho, E.; Jung, S. *Molecules* **2015**, *20*, 19620-19646.

202. Ma, X.; Zhao, Y. *Chem. Rev.* **2015**, *115*, 7794-7839.

203. Arima, H.; Hayashi, Y.; Higashi, T.; Motoyama, K. *Expert Opin. Drug Deliv.* **2015**, *12*, 1425-1441.

204. de Miranda, J. C.; Martins, T. E. A.; Veiga, F.; Ferraz, H. G. *Braz. J. Pharm. Sci.* **2011**, *47*, 665-681.

205. Passos, J. J.; Sousa, F. B. De.; Lula, I. S.; Barreto, E. A.; Lopes, J. F.; Almeida, W. B. De.; Sinisterra, R. D. *Int. J. Pharm.* **2011**, *421*, 24-33.

206. Hirayama, F.; Uekama, K. *Adv. Drug Delivery Rev.* **1999**, *36*, 125-141.

207. Choudhury, N.; Pettitt, B. M. *J. Am. Chem. Soc.* **2007**, *129*, 4847-4852.

208. Kataev, E. A.; Müller, C. *Tetrahedron* **2014**, *70*, 137-167.

209. Garcìa-Sosa, A. T. *J. Chem. Inf. Model.* **2013**, *53*, 1388-1405.

210. Ladbury, J. *Chem. Biol.* **1996**, *3*, 973-980.

211. de Beer, S. B. A.; Vermeulen, N. P. E.; Oostenbrink, C. *Curr. Top. Med. Chem.* **2010**, *10*, 55-66.

212. Li, Z.; Lazaridis, T. *Phys. Chem. Chem. Phys.* **2007**, *9*, 573-573.

213. Baron, R.; Setny, P.; Andrew McCammon, J. *J. Am. Chem. Soc.* **2010**, *132*, 12091-12097.

214. Gilson, M. K.; Honig, B. *Proteins: Struct., Funct., Genet.* **1988**, *4*, 7-18.

215. Gilson, M. K.; Honig, B. *J. Comput. Aided Mol. Des.* **1991**, *5*, 5-20.

216. Sitkoff, D.; Sharp, K.; Honig, B. *J. Phys. Chem.* **1994**, *98*, 1978-1988.

217. Qiu, D.; Shenkin, P. S.; Hollinger, F. P.; Still, W. C. *J. Phys. Chem. A* **1997**, *101*, 3005-3014.

218. Dominy, B. N.; Brooks, C. L. III. *J. Phys. Chem. B* **1999**, *103*, 3765-3773.

219. Sigalov, G.; Fenley, A.; Onufriev, A. *J. Chem. Phys.* **2006**, *124*, 124902.

220. Jorgensen, W. L.; Madura, J. D. *Mol. Phys.* **1985**, *56*, 1381-1392.

221. Berendsen, H. J. C.; Grigera, J. R.; Straatsma, T. P. *J. Phys. Chem.* **1987**, *91*, 6269-6271.

222. Ren, P.; Ponder, J. W. *J. Phys. Chem. B* **2003**, *107*, 5933-5947.

223. Swope, W. C.; Pitera, J. W.; Madura, J. D.; Dick, T. J.; Hura, G. L.; Head-Gordon, T.; Horn, H. W. *J. Chem. Phys.* **2004**, *120*, 9665-9678.

224. Abascal, J. L. F.; Vega, C. A. *J. Chem. Phys.* **2005**, *123*, 234505.

225. Young, T.; Abel, R.; Kim, B.; Berne, B. J.; Friesner, R. A. *Proc. Natl. Acad. Sci. U. S. A.* **2007**, *104*, 808-813.

226. Setny, P.; Baron, R.; McCammon, J. A. *J. Chem. Theory Comput.* **2010**, *6*, 2866-2871.

227. Biela, A.; Nasief, N. N.; Betz, M.; Heine, A.; Hangauer, D.; Klebe, G. *Angew. Chem. Int. Ed.* **2013**, *52*, 1822-1828.

228. Nguyen, C. N.; Cruz, A.; Gilson, M. K.; Kurtzman, T. *J. Chem. Theory Comput.* **2014**, *10*, 2769-2780.

229. Frank, H. S.; Evans, M. W. *J. Chem. Phys.* **1945**, *13*, 507.

230. Eisenberg, D.; Kauzmann, W. *1st ed.; Oxford University Press: New York*, **1969**.

231. Wong, S. E.; Lightstone, F. C. *Expert Opin. Drug. Discov.* **2010**, *6*, 65-74.

232. Abel, R.; Wang, L.; Friesner, R. A.; Berne, B. J. *J. Chem. Theory Comput.* **2010**, *6*, 2924-2934.

233. Garcà-Sosa, A. T.; Firth-Clark, S.; Mancera, R. L. *J. Chem. Inf. Model.* **2005**, *45*, 624-633.

234. Hummer, G. *Nat. Chem.* **2010**, *2*, 906-907.

235. Abel, R.; Young, T.; Farid, R.; Berne, B. J.; Friesner, R. A. *J. Am. Chem. Soc.* **2008**, *130*, 2817-2831.

236. Li, Z.; Lazaridis, T. *J. Am. Chem. Soc.* **2003**, *125*, 6636-6637.

237. Li, Z.; Lazaridis, T. *J. Phys. Chem. B* **2006**, *110*, 1464-1475.

238. Nettleton, R. E.; Green, M. S. *J. Chem. Phys.* **1958**, *29*, 1365.

239. Wallace, D. C. *J. Chem. Phys.* **1987**, *87*, 2282.

240. Morita, T.; Hiroike, K. *Prog. Theor. Phys.* **1961**, *25*, 537-578.

241. Lazaridis, T. *J. Phys. Chem. B* **1998**, *102*, 3531-3541.

242. Lazaridis, T. *J. Phys. Chem. B* **1998**, *102*, 3542-3550.

243. Li, Z.; Lazaridis, T. *Methods Mol. Biol.* **2012**, *819*, 393-404.

244. Huggins, D. J. *Phys. Chem. Chem. Phys.* **2012**, *14*, 15106.

245. Huggins, D. J. *J. Comput. Chem.* **2012**, *33*, 1383-1392.

246. Haider, K.; Huggins, D. J. *J. Chem. Inf. Model.* **2013**, *53*, 2571-2586.

247. Nguyen, C.; Gilson, M. K.; Young, T. *arXiv:1108.4876*, **2011**.

248. Nguyen, C. N.; Kurtzman Young, T.; Gilson, M. K. *J. Chem. Phys.* **2012**, *137*, 044101.

249. Raman, E. P.; MacKerell, A. D. Jr. *J. Chem. Phys.* **2013**, *139*, 055105.

250. Nguyen, C. N.; Kurtzman, T.; Gilson, M. K. *J. Chem. Theory Comput.* **2016**, *12*, 414-429.

251. Singh, H.; Misra, S.; Hnizdo, V.; Fedorowicz, A.; Demchuk, E. *Am. J. Math. Manage. Sci.* **2003**, *23*, 301-321.

252. Hnizdo, V.; Darian, E.; Fedorowicz, A.; Demchuk, E.; Li, S.; Singh, H. *J. Comput. Chem.* **2007**, *28*, 655-668.

253. Yao, H.; Ke, H.; Zhang, X.; Pan, S.-J.; Li, M.-S.; Yang, L.-P.; Schreckenbach, G.; Jiang, W. *J. Am. Chem. Soc.* **2018**, *140*, 13466-13477.

254. Liu, W.-E.; Chen, Z.; Yang, L.-P.; Jiang, W. *Chem. Commun.* **2019**, *55*, 9797-9800.

255. Ke, H.; Yang, L.-P.; Xie, M.; Chen, Z.; Yao, H.; Jiang, W. *Nat. Chem.* **2019**, *11*, 470-477.

256. Paul, R.; Paul, S. *J. Chem. Inf. Model.* **2020**, *60*, 212-225.

257. Nakano, M.; Tateishi-Karimata, H.; Tanaka, S.; Tama, F.; Miyashita, O.; Nakano, S.-I.; Sugimoto, N. *Nucleic Acids Res.* **2015**, *43*, 10114-10125.

258. Ramsey, S.; Nguyen, C.; Salomon-Ferrer, R.; Walker, R. C.; Gilson, M. K.; Kurtzman, T. *J. Comput. Chem.* **2016**, *37*, 2029-2037.

259. Weeks, J. D.; Chandler, D.; Andersen, H. C. *J. Chem. Phys.* **1971**, *54*, 5237-5247.

260. Hagler, A. T.; Moult, J. *Nature* **1978**, *272*, 222226.

261. Li, Z.; Lazaridis, T. *J. Phys. Chem. B* **2005**, *109*, 662-670.

262. Abel, R.; Salam, N. K.; Shelley, J.; Farid, R.; Friesner, R. A.; Sherman, W. *Chem. Med. Chem.* **2011**, *6*, 1049-1066.

263. Snyder, P. W.; Mecinovic, J.; Moustakas, D. T.; Thomas, S. W.; Harder, M.; Mack, E. T.; Lockett, M. R.; Hèroux, A.; Sherman, W.; Whitesides, G. M. *Proc. Natl. Acad. Sci. U.S.A.* **2011**, *108*, 17889-17894.

264. Young, T.; Hua, L.; Huang, X.; Abel, R.; Friesner, R.; Berne, B. J. *Proteins: Struct., Funct., Bioinf.* **2010**, *78*, 1856-1869.

265. Moghaddam, S.; Inoue, Y.; Gilson, M. *J. Am. Chem. Soc.* **2009**, *131*, 4012-4021.

266. Chang, C. A.; Chen, W.; Gilson, M. K. *Proc. Natl. Acad. Sci. U.S.A.* **2007**, *104*, 1534-1539.

267. Adriaenssens, L.; Ballester, P. *Chem. Soc. Rev.* **2013**, *42*, 3261-3277.

268. Anslyn, E. V.; Dougherty, D. A. *University Science Books: Sausalito, CA*, **2006**, 230-232.

269. Schneider, H.-J.; Yatsimirsky, A. K. *Chem. Soc. Rev.* **2008**, *37*, 263-277.

270. Smith, B. D. *Royal Society of Chemistry: Cambridge, UK*, **2015**.

271. Lee, H. H. L.; Lee, J. W.; Jang, Y.; Ko, Y. H.; Kim, K.; Kim, H. I. *Angew. Chem. Int. Ed.* **2016**, *55*, 8249-8253.

272. Carcanague, D. R.; Knobler, C. B.; Diederich, F. *J. Am. Chem. Soc.* **1992**, *114*, 1515-1517.

273. Kato, Y.; Conn, M. M.; Rebek, J. Jr. *J. Am. Chem. Soc.* **1994**, *116*, 3279-3284.

274. Torneiro, M.; Still, W. C. *J. Am. Chem. Soc.* **1995**, *117*, 5887-5888.

275. Allott, C.; Adams, H.; Hunter, C. A.; Rotger, C.; Thomas, J. A.; Bernad, P. L. Jr.; Rotger, C. *Chem. Commun.* **1998**, 2449-2450.

276. Butterfield, S. M.; Rebek, J. Jr. *J. Am. Chem. Soc.* **2006**, *128*, 15366-15367.

277. Ferrand, Y.; Crump, M. P.; Davis, A. P. *Science* **2007**, *318*, 619-622.

278. Verdejo, B.; Gil-Ramrez, G.; Ballester, P. *J. Am. Chem. Soc.* **2009**, *131*, 3178-3179.

279. Ke, C.; Destecroix, H.; Crump, M. P.; Davis, A. P. *Nat. Chem.* **2012**, *4*, 718-723.

280. Peck, E. M.; Liu, W.; Spence, G. T.; Shaw, S. K.; Davis, A. P.; Destecroix, H.; Smith, B. D. *J. Am. Chem. Soc.* **2015**, *137*, 8668-8671.

281. Mooibroek, T. J.; Casas-Solvas, J. M.; Harniman, R. L.; Renney, C. M.; Carter, T. S.; Crump, M. P.; Davis, A. P. *Nat. Chem.* **2016**, *8*, 69-74.

282. Rios, P.; Carter, T. S.; Mooibroek, T. J.; Crump, M. P.; Lisbjerg, M.; Pittelkow, M.; Supekar, N. T.; Boons, G.-J.; Davis, A. P. *Angew. Chem. Int. Ed.* **2016**, *55*, 3387-3392.

283. Cecioni, S.; Imberty, A.; Vidal, S. *Chem. Rev.* **2015**, *115*, 525-561.

284. Zhang, Y.-M.; Yang, Z.-X.; Chen, Y.; Ding, F.; Liu, Y. *Cryst. Growth Des.* **2012**, *12*, 1370-1377.

285. Jorgensen, W. L.; Maxwell, D. S.; Tirado-Rives, J. *J. Am. Chem. Soc.* **1996**, *118*, 11225-11236.

286. Nagy, P. I.; Völgyi, G.; Takàcs-Novàk, K. *J. Phys. Chem. B* **2008**, *112*, 2085-2094.

287. Lago, N. F.; Albert, M.; Lombardi, A.; Pirani, F. *Theor. Chem. Acc.* **2016**, *135*, 161.

288. Almeida, G. G.; Cordeiro, J. M. M. *J. Braz. Chem. Soc.* **2011**, *22*, 2178-2185.

289. Mushrif, S. H.; Caratzoulas, S.; Vlachos, D. G. *Phys. Chem. Chem. Phys.* **2012**, *14*, 2637-2644.

290. Vasudevan, V.; Mushrif, S. H. *J. Mol. Liq.* **2015**, *206*, 338-342.

291. Jia, G.-Z.; Huang, K.-M.; Yang, L.-J.; Yang, X.-Q. *Int. J. Mol. Sci.* **2009**, *10*, 1590-1600.

292. Larson, J. W.; McMahon, T. B. *Inorg. Chem.* **1984**, *23*, 2029-2033.

293. Emsley, J. *Chem. Soc. Rev.* **1980**, *9*, 91-124.

294. Das, S.; Paul, S. *J. Chem. Inf. Model.* **2017**, *57*, 1461-1473.

295. Leavitt, S.; Freire, E. *Curr. Opin. Struct. Biol.* **2001**, *11*, 560-566.

296. Bouchemal, K.; Mazzaferro, S. *Drug Discovery Today* **2012**, *17*, 623-629.

297. Davis, F.; Higson, S. *Wiley: Chichester*, **2011**.

298. Steed, J. W.; Atwood, J. L. *Wiley: Chichester*, **2009**.

299. EI-Barghouthi, M. I.; Assaf, K. I.; Rawasdeh, A. M. M. *J. Chem. Theory Comput.* **2010**, *6*, 984-992.

300. Kirkwood, J. G.; Buff, F. P. *J. Chem. Phys.* **1951**, *19*, 774-777.

301. Matteoli, E.; Mansoori, G. A. *Taylor and Francis, New York*, **1990**.

302. Ben-Naim, A. *Plenum Press, New York*, **1992**.

303. Ben-Naim, A. *Oxford University Press, New York*, **2006**.

304. Smith, P. E. *J. Phys. Chem. B* **2006**, *110*, 2862-2868.

305. Smith, P. E. *Biophys. J.* **2006**, *91*, 849-856.

306. Sharma, B.; Paul, S. *J. Mol. Liq.* **2016**, *224*, 930-939.

307. Sugano, K.; Kansy, M.; Artursson, P.; Avdeef, A.; Bendels, S.; Di, L.; Ecker, G. F.; Faller, B.; Fischer, H.; Gerebtzoff, G.; Lennernaes, H.; Senner, F. *Nat. Rev. Drug Discov.* **2010**, *9*, 597-614.

308. Dobson, P. D.; Kell, D. B. *Nat. Rev. Drug Discov.* **2008**, *7*, 205-220.

309. Seydel, J. K.; Wiese, M. *Wiley-VCH Verlag GmbH*, **2002**.

310. Ouyang, D.; Smith, S. C. *John Wiley & Sons Ltd.*, West Sussex, UK, **2015**.

311. Rapoport, T. A. *Nature* **2007**, *450*, 663-669.

312. Xiang, T.-X.; Anderson, B. D. *Adv. Drug Deliv. Rev.* **2006**, *58*, 1357-1378.

313. Loverde, S. M. *J. Phys. Chem. Lett.* **2014**, *5*, 1659-1665.

314. Hollingsworth, S. A.; Dror, R. O. *Neuron* **2018**, *99*, 1129-1143.

315. Tieleman, D. P. *Clin. Exp. Pharmacol. Physiol.* **2006**, *33*, 893-903.

316. Ercan, N. I.; Stroeve, P.; Tringe, J. W.; Faller, R. *Langmuir* **2018**, *34*, 4314-4323.

317. Khadka, N. K.; Cheng, X.; Ho, C. S.; Katsaras, J.; Pan, J. *Biophys. J.* **2015**, *108*, 2492-2501.

318. Ercan, N. I.; Stroeve, P.; Tringe, J. W.; Faller, R. *Langmuir* **2016**, *32*, 10026-10033.

319. Ercan, N. I. *J. Chem. Inf. Model.* **2019**, *59*, 4413-4426.

320. Lee, B. L.; Kuczera, K.; Middaugh, R.; Jas, G. S. *J. Chem. Phys.* **2016**, *144*, 245103.

321. Carpenter, T. S.; Kirshner, D. A.; Lau, E. Y.; Wong, S. E.; Nilmeier, J. P.; Lightstone, F. C. *Biophys. J.* **2014**, *107*, 630-641.

322. Ulander, J.; Haymet, A. *Biophys. J.* **2003**, *85*, 3475-3484.

323. Khakbaz, P.; Klauda, J. B. *Chem. Phys. Lipids* **2015**, *192*, 12-22.

324. Wan, G.; Dai, X.; Yin, Q.; Shi, X.; Qiao, Y. *J. Mol. Graphics Modell.* **2015**, *60*, 98-107.

325. Gupta, R.; Rai, B. *Langmuir* **2018**, *34*, 5860-5870.

326. Hansen, F. Y.; Peters, G. H.; Taub, H.; Miskowiec, A. *J. Chem. Phys.* **2012**, *137*, 204910.

327. Wei, T.; Huang, T.; Qiao, B.; Zhang, M.; Ma, H.; Zhang, L. *J. Phys. Chem. B* **2014**, *118*, 13202-13209.

328. Comer, J.; Schulten, K.; Chipot, C. *J. Chem. Theory Comput.* **2014**, *10*, 2710-2718.

329. Orsi, M.; Sanderson, W. E.; Essex, J. W. *J. Phys. Chem. B* **2009**, *113*, 12019-12029.

330. Riahi, S.; Rowley, C. N. *J. Am. Chem. Soc.* **2014**, *136*, 15111-15113.

331. Wang, Y.; Hu, D.; Wei, D. *J. Chem. Theory Comput.* **2014**, *10*, 1717-1726.

332. Martin, L. J.; Chao, R.; Corry, B. *Biophys. Chem.* **2014**, *185*, 98-107.

333. Bemporad, D.; Essex, J. W. *J. Phys. Chem. B* **2004**, *108*, 4875-4884.

334. Orsi, M.; Essex, J. W. *Soft Matter* **2010**, *6*, 3797-3808.

335. Porasso, R. D.; Drew Bennett, W. F.; Oliveira-Costa, S. D.; Lòpez Cascales, J. J. *J. Phys. Chem. B* **2009**, *113*, 9988-9994.

336. dos Santos, D. J. V. A.; Eriksson, L. A. *Biophys. J.* **2006**, *91*, 2464-2474.

337. Hotarat, W.; Nutho, B.; Wolschann, P.; Rungrotmongkol, T.; Hannongbua, S. *Molecules* **2020**, *25*, 2532.

338. Kyrychenko, A.; Sevriukov, I. Y.; Syzova, Z. A.; Ladokhin, A. S.; Doroshenko, A. O. *Biophys. Chem.* **2011**, *154*, 8-17.

339. Wei, C.; Pohorille, A. *J. Phys. Chem. B* **2014**, *118*, 12919-12926.

340. Xiang, T.-X.; Jiang, Z.-Q.; Song, L.; Anderson, B. D. *Mol. Pharmaceutics* **2006**, *3*, 589-600.

341. Oroskar, P. A.; Jameson, C. J.; Murad, S. *Langmuir* **2015**, *31*, 1074-1085.

342. Fiedler, S. L.; Violi, A. *Biophys. J.* **2010**, *99*, 144-152.

343. Erimban, S.; Daschakraborty, S. *Phys. Chem. Chem. Phys.* **2020**, *22*, 6335-6350.

344. Gupta, R.; Rai, B. *J. Phys. Chem. B* **2016**, *120*, 7133-7142.

345. Bedrov, D.; Smith, G. D.; Davande, H.; Li, L. *J. Phys. Chem. B* **2008**, *112*, 2078-2084.

346. Bozdaganyan, M. E.; Orekhov, P. S.; Shaytan, A. K.; Shaitan, K. V. *Plos One* **2014**, *9*, e102487.

347. Gupta, R.; Badhe, Y.; Mitragotri, S.; Rai, B. *Nanoscale* **2020**, *12*, 6318-6333.

348. Aranha, M. P.; Mukherjee, D.; Petridis, L.; Khomami, B. *Langmuir* **2020**, *36*, 1043-1052.

349. Casalegno, M.; Raos, G.; Sello, G. *Phys. Chem. Chem. Phys.* **2015**, *17*, 2344-2348.

350. Herce, H. D.; Garcia, A. E. *J. Biol. Phys.* **2007**, *33*, 345-356.

351. Herce, H. D.; Garcia, A. E. *Proc. Natl. Acad. Sci. U. S. A.* **2007**, *104*, 20805-20810.

352. Khajeh, A.; Modarress, H. *Biophys. Chem.* **2014**, *187-188*, 43-50.

353. Söderhäll, J. A.; Laaksonen, A. *J. Phys. Chem. B* **2001**, *105*, 9308-9315.

354. Silvius, J. R. *John Wiley & Sons, Inc.: New York*, **1982**, *2*, 239-281.

355. Balliano, L. C.; Milla, P.; Rocco, F.; Conzelmann, A.; Vionnet, C.; Kelly, D. E.; Kelly, S.; Schweizer, E.; Schu, H.-J.; Ller, U. H.; et al. *Yeast* **1999**, *15*, 601-614.

356. Jo, S.; Lim, J. B.; Klauda, J. B.; Im, W. *Biophys. J.* **2009**, *97*, 50-58.

357. Wu, E. L.; Cheng, X.; Jo, S.; Rui, H.; Song, K. C.; Dávila-Contreras, E. M.; Qi, Y.; Lee, J.; Monje-Galvan, V.; Venable, R. M.; et al. *J. Comput. Chem.* **2014**, *35*, 1997-2004.

358. Case, D. A.; Ben-Shalom, I. Y.; Brozell, S. R.; Cerutti, D. S.; Cheatham, T. E.; Cruzeiro, V. W. D.; Darden, T. A.; Duke, R. E.; Ghoreishi, D.; Gilson, M. K.; et al. *AMBER 2018*; University of California: San Francisco, CA, **2018**.

359. Gould, I. R.; Skjevik, A. A.; Dickson, C. J.; Madej, B. D.; Walker, R. C. *in preparation*, **2018**.

360. Joung, I. S.; Cheatham III, T. E. *J. Phys. Chem. B* **2008**, *112*, 9020-9041.

361. Lyu, Y.; Xiang, N.; Mondal, J.; Zhu, X.; Narsimhan, G. *J. Phys. Chem. B* **2018**, *122*, 2341-2354.

362. Qiao, R. *Nano. Lett.* **2007**, *7*, 614-619.

363. Contini, C.; Schneemilch, M.; Gaisford, S.; Quirke, N. *J. Exp. Nanosci.* **2018**, *13*, 62-81.

364. Li, L.; Devande, H.; Bedrov, D.; Smith, G. D. *J. Phys. Chem. B* **2007**, *111*, 4067-4072.

365. Hummer, G. *New J. Phys.* **2005**, *7*, 34.

366. Lee, J.; Cheng, X.; Swails, J. M.; Yeom, M. S.; Eastman, P. K.; Lemkul, J. A.; Wei, S.; Buckner, J.; Jeong, J. C.; Qi, Y.; et al. *J. Chem. Theory Comput.* **2016**, *12*, 405-413.

367. Venable, R. M.; Brown, F. L. H.; Pastor, R. W. *Chem. Phys. Lipids* **2015**, *192*, 60-74.

368. Pluhackova, K.; Kirsch, S. A.; Han, J.; Sun, L.; Jiang, Z.; Unruh, T.; Bö ckmann, R. A. *J. Phys. Chem. B* **2016**, *120*, 3888-3903.

369. Kuĉerka, N.; Nieh, M.-P.; Katsaras, J. *Biochim. Biophys. Acta, Biomembr.* **2011**, *1808*, 2761-2771.

370. Kuĉerka, N.; van Oosten, B.; Pan, J.; Heberle, F. A.; Harroun, T. A.; Katsaras, J. *J. Phys. Chem. B* **2015**, *119*, 1947-1956.

371. Kuĉerka, N.; Nagle, J. F.; Sachs, J. N.; Feller, S. E.; Pencer, J.; Jackson, A.; Katsaras, J. *Biophys. J.* **2008**, *95*, 2356-2367.

372. Kuĉerka, N.; Tristram-Nagle, S.; Nagle, J. F. *J. Membr. Biol.* **2006**, *208*, 193-202.

373. Rappolt, M.; Hickel, A.; Bringezu, F.; Lohner, K. *Biophys. J.* **2003**, *84*, 3111-3122.

374. Skjevik, Å. A.; Madej, B. D.; Dickson, C. J.; Lin, C.; Teigen, K.; Walker, R. C.; Gould, I. R. *Phys. Chem. Chem. Phys.* **2016**, *18*, 10573-10584.

375. Mukherjee, S.; Kar, R. K.; Nanga, R. P. R.; Mroue, K. H.; Ramamoorthy, A.; Bhunia, A. *Phys. Chem. Chem. Phys.* **2017**, *19*, 19289-19299.

List of publications

1. **Paul, R.**; Paul, S. Synergistic Host-Guest Hydrophobic and Hydrogen Bonding Interactions in the Complexation Between Endo-Functionalized Molecular Tube and Strongly Hydrophilic Guest Molecules in Aqueous Solution. *Phys. Chem. Chem. Phys.* **2018**, *20*, 16540-16550.

2. **Paul, R.**; Paul, S. How Does the Complexation Ability Between Host Endo-Functionalized Molecular Tube and Strongly Hydrophilic Guest Molecules in Water Depend on Guest Concentration? *J. Mol. Liq.* **2019**, *283*, 507-514.

3. **Paul, R.**; Paul, S. Computational Study of Encapsulation of Polyaromatic Hydrocarbons by Endo-Functionalized Receptors in Nonpolar Medium. *J. Chem. Inf. Model.* **2020**, *60*, 212-225.

4. **Paul, R.**; Paul, S. Tuning the Trapping of Epoxides by Endo-Functionalized Molecular Tubes in an Aqueous Medium: A Computational Study. *J. Phys. Chem. C* **2020**, *124*, 3589-3600.

5. Chattaraj, K. G.; **Paul, R.**; Paul, S. Switching of Self-Assembly to Solvent-Assisted Assembly of Molecular Motor: Unveiling the Mechanisms of Dynamic Control on Solvent Exchange. *Langmuir* **2020**, *36*, 1773-1792. (Chattaraj, K. G. and **Paul, R.** contributed equally)

6. **Paul, R.**; Chattaraj, K. G.; Paul, S. Role of Hydrotropes in Sparingly Soluble Drug Solubilization: Insight from a Molecular Dynamics Simulation and Experimental Perspectives. *Langmuir* **2021**, *37*, 4745-4762. (**Paul, R.** and Chattaraj, K. G. contributed equally)

7. **Paul, R.**; Paul, S. Prediction of Local Thermodynamics of Water In and Around Endo-Functionalized Molecular Tube Receptors: An Approach Using Grid Inhomogeneous Solvation Theory. *J. Mol. Liq.* **2021**, *334*, 116338.

8. **Paul, R.**; Mitra, A.; Paul, S. Phase Separation Property of a Hydrophobic Deep Eutectic Solvent-Water Binary Mixture: A Molecular Dynamics Simulation Study. *J. Chem. Phys.* **2021**, *154*, 244504. (**Paul, R.** and Mitra, A. contributed equally)

9. **Paul, R.**; Paul, S. Exploration on the Drug Solubility Enhancement in Aqueous Medium with the Help of Endo-Functionalized Molecular Tubes: A Computational Approach. *Phys. Chem. Chem. Phys.* **2021**, *23*, 18999-19010.

10. **Paul, R.**; Paul, S. Translocation of Endo-Functionalized Molecular Tubes Across Different Lipid Bilayers: Atomistic Molecular Dynamics Simulation Study. *Langmuir* **2021**, *37*, 10376-10387.

11. **Paul, R.**; Mitra, A.; Paul, S. A Computational Approach on the Stereoselective Binding of Peptides from Aqueous Medium with Endo-Functionalized Molecular Tubes. *Phys. Chem. Chem. Phys.* **2021**, *23*, 22703-22717.

12. **Paul, R.**; Sawoo, D.; Paul, S. Inhibitory Action of Indanone-Carbamate Hybrid Molecules on the Aggregation of Aβ_{16-22} Peptides and their Translocation across POPC Lipid Bilayer: A Molecular Dynamics Simulation Study. (Manuscript under revision). (**Paul, R.** and Sawoo, D. contributed equally)

13. **Paul, R.**; Bera, S.; Paul, S. Small Molecules on the Inhibition of Aβ_{16-22} Peptides Aggregation and Permeation of these Molecules through POPC Lipid Bilayer: An Insights from Molecular Dynamics Simulation Study. (Manuscript under revision). (**Paul, R.** and Bera, S. contributed equally)

14. Pal, T.; **Paul, R.**; Paul, S. Phenylpropanoids on the Inhibition of β-Amyloid Aggregation and the Movement of these Molecules through the POPC Lipid Bilayer. (Manuscript under revision). (Pal, T. and **Paul, R.** contributed equally)

Conferences/Workshops attended

1. Presented a poster entitled "Molecular Dynamics Study of Complexes between Endo-Functionalized Molecular Tube and Strongly Hydrophilic Guest Molecules in Aqueous Solution" in the workshop "Sorbonne-JNCASR School for Advanced Computational Materials Science (SJSACMS 2018)' held at JNCASR, Bengaluru, Karnataka, India.

2. Presented a poster entitled "Complexation Between Endo-Functionalized Molecular Tube and Strongly Hydrophilic Guest Molecules in Aqueous Solution and Its Concentration Dependency" in the conference "Frontiers in Chemical Sciences (FICS-2018)" held at IIT Guwahati, Assam, India.

3. Presented a poster entitled "Synergistic Host-Guest Hydrophobic and Hydrogen Bonding Interactions in the Complexation Between Endo-Functionalized Molecular Tube and Strongly Hydrophilic Guest Molecules in Aqueous Solution " in the conference "Theoretical Chemistry Symposium (TCS-2019)" held at BITS Pilani, Pilani, Rajasthan, India.

4. Attended a workshop "FREE ENERGY CALCULATIONS FOR CHEMICAL AND BIOLOGICAL SYSTEMS (FECCBS-2019)" held at IIT Kanpur, Kanpur, Uttar Pradesh, India.